Método Quiral No Perturbativo para el Estudio de la Dinámica Fuerte Mesón-Mesón, su Espectroscopía y Aplicaciones Afines

Departamento de Física Teórica

Universidad de Valencia

– Estudi General –

Tesis Doctoral

presentada por

José Antonio Oller Berber

Junio 1999

D. Eulogi Osset Bàguena, Catedràtic de Física Teòrica de la Universitat de València,

CERTIFIQUE: Que la present Memòria *Método Quiral No Perturbativo para el Estudio de la Dinámica Fuerte Mesón-Mesón, su Espectroscopía y Aplicaciones Afines* ha sigut realitzada sota la meua direcció al Departament de Física Teòrica de la Universitat de València per D. José Antonio Oller Berber.

I per a que així conste es presenta la referida Memòria, signant el present certificat.

València, 28 de juny de 1999

Signat: Eulogi Osset Bàguena

Espero que el presente trabajo sirva de humilde agradecimiento para todas aquellas personas que a lo largo de mi vida me hayan alentado y ayudado a seguir hacia adelante con ilusión y confianza.

Agradezco a mi director de tesis Eulogio Oset, la cantidad de tiempo tan enorme que me ha dedicado para discutir todas estas cuestiones que se presentan en la memoria. También quisiera agradecerle la confianza que siempre ha mantenido hacia mis iniciativas a las que se ha adherido con ilusión y espíritu crítico.

También agradezco a mis colaboradores ciéntificos: J. R. Peláez, F. Guerrero, S. Kamalov, H. Lee, A. Ramos y M. J. Vicente, con los que he pasado gratos y fructíferos momentos.

A Antonio Pich, que aunque siempre ha andado un tanto ocupado, a lo largo de los años he aprendido mucho de él y de sus reports.

Y por supuesto al resto de miembros del Departamento, especialmente a A. Gil, L. Alvarez, J. Reyes, L. Cabral y J. C. Nacher por la gran ayuda que me han prestado ante mis diversas dudas informáticas. Como también agradecimientos para mi buen amigo ya de muchos años, Pedro Navarro.

A mi mujer María José, la gran sacrificada de esta tesis, para que mantenga siempre la ilusión y no decaiga por muy lejos que estemos de Valencia. A mi hija María José, con la que en los últimos meses he mantenido largas y muy interesantes discusiones sobre aspectos diversos.

Agradezco también a mi familia, en especial a mi padre J.A. Oller, el no haber nunca escatimado esfuerzos para ayudarme en lo que hayan podido.

Finalmente, agradecimientos para el Colegio Mayor San Juan de Ribera y a sus colegiales de ayer y hoy, donde tanto he aprendido a ser un poco más persona.

A todos

Gracias

Contents

Introducción

Hoy en día se considera a la **Cromodinámica Cuántica** (QCD) [1] como la teoría que describe las interacciones fuertes. Dicha teoría utiliza los quarks como grados de libertad. Esta elección de grados de libertad resulta útil para el régimen de altas energías donde, debido al fenómeno de la libertad asintótica, los quarks se manifiestan como estructuras puntuales que interactúan débilmente. De hecho, ésta es la única situación en la que se sabe resolver QCD dado que se pueden emplear técnicas perturbativas.

Sin embargo, para energías < 2 GeV, las que se van a considerar en esta tesis, los grados de libertad relevantes son los hadrones: mesones y baryones. Para pasar de quarks a hadrones mediante QCD se tendría que saber resolver el problema del confinamiento de los quarks. Sin embargo, en la actualidad permance incluso como un enigma si QCD es confinante.

Se podría pensar en construir una teoría que tuviese como grados de libertad directamente los hadrones, sin embargo, esta solución resulta tanto o más complicada que el problema mismo que se pretende resolver dada la superabundancia de hadrones en el espectro. No obstante en los años 60 se dieron pasos en esta dirección a través de la hipótesis del *bootstrap* [2]. Dicha hipótesis establecía que todos los hadrones procederían de las fuerzas de interacambio originados por ellos mismos. Las técnicas utilizadas serían las de la Matriz-S complementadas con la hipótesis de que las interacciones fuertes sean lo más fuerte posible respetando los principios de unitariedad y analiticidad de la Matriz-S. De este modo todas las partículas observadas se apoyarían unas a otras para conseguir tal objetivo y se fijarían las constantes de acoplo que fuesen apareciendo. El *bootstrap* falló dado que pretendía que todas las resonancias que iban apareciendo se puediesen interpretar como resonancias hadrónicas. Sin embargo, hoy en día sabemos que ésta no es la situación general. Bien al contrario, en términos de quarks, existen muchos estados que son $q\bar{q}$ o qqq y su existencia puede ser entendida en una primera aproximación a partir de las interacciones entre los quarks sin relación alguna con las amplitudes de scattering entre los hadrones. Por otra parte, en large N_c QCD toda la física de loops, en la que se basa el *bootstrap*, es subleading y desaparecería en dicho límite mientras que la masa de la mayoría de los hadrones es $\mathcal{O}(1)$, por ejemplo de aquellos que se pueden clasificar como $q\bar{q}$ or qqq.

En el espectro de QCD existe un hecho remarcable, como es la aparición de un triplete de isospín con una masa mucho más pequeña que el resto de las masas del espectro hadrónico. Se trata de los piones, π. Esta situación se puede extender a $SU(3)$ dando lugar al octete de pseudoscalares π, K y η_8. Desde el punto de vista de QCD, esta característica del

espectro puede ser entendida a partir del hecho de que dicha teoría presenta una simetria quiral global $SU(3)_L \otimes SU(3)_R$ que espontaneamente se rompería a $SU(3)_{R+L} \equiv SU(3)_V$. Los ocho generadores correspondientes a la simetría rota $SU(3)_{R-L} \equiv SU(3)_A$, por el teorema de Goldstone, darían lugar a un octete de partículas pseudoscalares de masa nula, los bosones de Goldstone, que se identificarían con el octet de piones, kaones y etas. Sin emargo, todavía no se ha demostrado que QCD tenga ruptura espontánea de simetría quiral, aunque, contenga las simetrías correctas.[1]

El hueco anteriormente aludido en el espectro de QCD, entre los pseudo-bosones de Goldstone y las resonances más pesadas, se puede aprovechar para construir un Lagrangiano efectivo en función de los bosones de Goldstone en el que las partículas masivas desaparecerían como grados explícitos de libertad. Su presencia repercutiría en el valor final de los contratérminos a ordenes superiores. Este esquema ha sido realizado dando lugar a **Chiral Perturbation Theory** (χPT) [4, 5], que es por tanto, el Lagrangiano efectivo de QCD para bajas energías. Dicha teoría permite calcular de un **modo sistemático** cualquier función de Green en una serie de potencias sobre los momentos externos de los bosones de Goldstone. La escala sobre la que se realiza dicha expansión, $\Lambda_{\chi PT}$, viene a corresponder con las masas de los estados masivos más próximos, lo que implica que $\Lambda_{\chi PT} \approx 1$ GeV.

Junto a sus grandes virtudes χPT presenta también obvias limitaciones. En primer lugar a partir de esta teoría no se pueden generar los estados masivos ya que precisamente han sido integrados para dar origen a dicha teoría efectiva. Dicho de otro modo, a partir de una expansión en potencias no se puede generar polos, los cuales están ligados a tales estados masivos. Por otro lado, hay correcciones quirales de orden superior que también limitan dicha expansión. De hecho a partir de las correcciones introducidas por los loops se puede llegar a la conclusión de que $\Lambda_{\chi PT} \leq 1.2$ GeV [6]. Estos hechos hacen que típicamente una expansión quiral sólo sea válida hasta energías del orden de unos 500 MeV. Por otra parte, el número de parámetros libres presentes en los lagrangianos quirales aumenta rápidamente con el orden en el que se calcula. Así, mientras que el lagrangiano quiral de orden más bajo viene dado únicamente en términos de masas y de f_π, la constante de desintegración del pion, el orden siguiente requiere de 10 nuevos parámetros libres y el siguiente orden al anterior requiere algo más de 100 nuevas constantes. Es decir, el poder predictivo de la teoría se pierde rápidamente con el orden en que se calcula.

Por lo tanto parece obvio el interés que pueden suscitar técnicas no perturbativas capaces de llevar a cabo una resumación de la expansión quiral a energías superiores manteniendo el poder predictivo de la teoría.

Para conseguir tal objetivo se harán uso de resultados muy generales procedentes de la Teoría de la Matrix-S que serán presentados en el capítulo primero.

En el segundo capítulo se llevará a cabo un repaso somero de χPT [4, 5] haciendo hin-

[1] Existe no obstante un teorema que remite la solución de este problema a demostrar que QCD es confinante en el límite quiral. Designando por N_f el número de sabores de quark sin masa en el Lagrangiano de QCD y por N_c el número de colores, el teorema puede ser enunciado como sigue: *Si* $N_f \geq 3$, $N_c \geq 3$ *y supuesto que los quarks estén confinaddos (no hay objetos físicos con color), la simetría quiral* $SU(N_f)_L \times SU(N_f)_R \times U_V(1)$ *se rompe necesariamente a su subgrupo diagonal* $U_V(N_f)$ *generado por las corrientes vectoriales [3]*

capié en aquellos aspectos que se utilizarán a lo largo del trabajo, como son los lagrangianos quirales $\mathcal{L}_2$ y $\mathcal{L}_4$ así como la introducción explícita de resonancias con spin$\leq$1 siguiendo el trabajo ref. [7]. Un aspecto muy interesante en la anterior referencia es la saturación por parte de las resonancias de los contratérminos que aparecen en $\mathcal{L}_4$. Dicho concepto, anticipando resultados del capítulo 6, se discutirá prestando atención especial al caso de las resonancias escalares. Se verá que las resonancias escalares que conducen a dicha saturación de los contratérminos quirales no son las más ligeras sino las que corresponden a las del siguiente nonete que aparece con una masa estimada de 1.2 GeV. También se discutirá cómo el primer nonete escalar, con una masa $\leq$ 1 GeV, tiene un origen dinámico, fruto esencialmente de la unitarización de las amplitudes chirales de orden más bajo. Con ello se pone de manifiesto la importancia que las correcciones de unitariedad tendrán para la onda S con isospin(I) 0, 1 y 1/2. Así quedaría resuelto un problema cuyo origen tiene mucho que ver con el Modelo Sigma Lineal. Este es un modelo particular de realización de la simetría quiral en el que junto a los piones se introduce una particula escalar, σ, con el mismo nivel de "elementariedad" que los piones. Dicha partícula presenta una masa reducida, de unos 500 MeV, difícil de entender a partir de su repercusión en los contratérminos quirales y de otros modelos inspirados en QCD, los cuales predicen una masa para la primera resonancia escalar de alrededor de 1 GeV [8]. Veremos, que dicho mesón σ, típicamente reclamado por los modelos de potencial N-N y en análisis de los desfasajes de $\pi\pi$, no es la sigma del Modelo Sigma Lineal. En contra, se trata de una resonancia pión ica y que por tanto no tiene el mismo nivel de "elementariedad" que los piones.

En el capítulo tercero se discuten ciertos aspectos generales con respecto al concepto de resonancia. Tras introducir el concepto de una Breit-Wigner se discuten algunas de sus limitaciones que surgen cuando hay presente un background significativo o cuando la resonancia se acopla con un canal cuyo threshold está muy próximo a la masa de la resonancia. Todos estos aspectos tienen una realización práctica en el controvertido sector escalar.

En el cuarto capítulo se discute el Método de la Amplitud Inversa (IAM), comenzando propiamente con el material original de esta memoria. Dicho método se basa en el desarrollo de la inversa de la Matriz-T a partir del desarrollo quiral de dicha matriz. Este procedimiento presenta la ventaja de que cuando la amplitud T tiene un polo su inversa sólo tiene un cero que obviamente no presenta ningún problema para un desarrollo en serie. También tiene la ventaja de que dicho método es unitario a todos los órdenes en el desarrollo quiral. Estas técnicas se aplicarán a una amplísima gama de procesos de colisión de dos mesones describiéndolos con notable éxito hasta una energía de unos 1.2 GeV. También se verá como dicho método es capaz de generar las resonancias observadas experimentalmente como son: $f_0(980)$, $a_0(980)$, ρ, K^*, σ, κ y una singularidad próxima al mesón ϕ. Seguidamente, se estudiarán las posiciones de los polos asociados a las anteriores resonancias y las anchuras parciales de desintegración de las mismas.

En los dos siguientes capítulos se emplea el método N/D [9] para llegar a una amplitud unitarizada a partir de χPT y su extensión para incluir campos resonantes explícitos. En el capítulo quinto se introduce el método N/D y se aplica para discutir tanto los canales vectoriales con I=1 y 1/2 como los escalares con I=0, 1, 1/2. Para la onda P se llega a las

bien conocidas conclusiones de VMD. En el caso de la onda S el estudio es especialmente valioso para la zona de energías menores que 1.2 GeV donde se incluyen todos los canales relevantes. Se observa la aparición, como se ha discutido arriba, de un primer nonete escalar que englobaría las resonancias σ, κ, $a_0(980)$ y una importante contribución a la $f_0(980)$. El estudio se forzó hasta energías de unos 1.4 GeV observándose la aparición de un segundo nonete que consistiría de un octete alrededor de 1.4 GeV y de un singlete alrededor de 1 GeV que da contribución a la resonancia $f_0(980)$. Sin embargo, el estudio detallado del octete escalar con una masa de unos 1.4 GeV requeriría de la inclusión de más canales como son los 4π para $I = 0$ y el canal de $K\eta'$ para $I = 1/2$.

Este es uno de los objetivos planteados en el siguiente capítulo donde se estudiarán la onda S con $I = 3/2$ y $1/2$ introduciéndose en este último caso, junto a $K\pi$ el canal de $K\eta'$. Asimismo se ampliará el estudio llevado a cabo en el capítulo quinto para permitir la inclusión de forma perturbativa de los cortes no físicos a $\mathcal{O}(p^4)$. Este estudio corrobora al anterior pues da lugar a la aparición de un meson κ en una posición semejante a la obtenida en capítulo quinto y a la necesidad de una resonancia K_0^* perteneciente a un octete escalar con una masa desnuda entre 1.3-1.4 GeV. Por otro lado, las constantes de dicho octete escalar y su masa son tales que conducen al concepto de saturación de los contratérminos quirales de $\mathcal{L}_4$ en acuerdo cualitativo con la ref. [7]. Cualitativo porque en dicho trabajo se abogaba por un nonete escalar con una masa de un 1 GeV que incluyese la $a_0(980)$ que sería algo así como la ρ para el nonete escalar. Veremos que esta prescripción no es la correcta sino que la $a_0(980)$ pertenece a un nonete escalar subleading en large N_c mientras que el nonete escalar que se mantendría en large N_c tendría una masa de unos 1.2 GeV. En este capítulo se fija el valor de las constantes de acoplo del nonete escalar en large N_c a partir de la anulación de los factores de forma escalares de $K\pi$, $K\eta$ y $K\eta'$ en el infinito dando un valor adecuado también desde el punto de vista fenomenológico tal y como se ha discutido.

Finalmente en el capítulo siete se abordan ciertos procesos electromagnéticos en los que las correcciones de interacción de estado final resultan decisivas. Se discuten los factores de forma escalares y vectoriales de $\pi\pi$ haciendo uso de la ecuación de Omnès y de los resultados del capítulo 4. También se aborda de una forma original el problema de $\gamma\gamma \to$meson-meson con un excelente acuerdo con la experiencia. Utilizando el mismo tipo de aproximación se estudian diversos procesos de desintegración del mesón ϕ relevantes para la física que se pretende detectar en DAPHNE y con el detector SND en Novosibirsk. Este estudio se ha visto corrobado por recientes medidas llevadas a cabo por este último grupo experimental.

Para mayores detalles se presenta el siguiente material.

Chapter 1

Elements of the S-Matrix Theory of Strong Interactions.

In preparing this chapter I have made extensive use of three very nice and good books [10], [11] and [12]. Further details on any particular subject can be found in these references.

1.1 Free particle states.

From the beginning we are going to consider just the scattering of hadrons without spin, mesons. Let $|m, \vec{p}>$ denote the free state of one meson with three-momentum $\vec{p}$ and mass m. The relativistic invariant scalar product of two such states is

$$< \vec{p}', m|m, \vec{p} >= (2\pi)^3 \delta^{(3)}(\vec{p} - \vec{p}')2p^0 \tag{1.1}$$

where

$$p^0 = \sqrt{m^2 + \vec{p}^2} \tag{1.2}$$

is the energy of the particle.

From these mono-particle states we can construct multi-particle ones just by doing the direct product of the former states

$$|m_1, \vec{p}_1;\, m_2, \vec{p}_2;\, ...\, m_n, \vec{p}_n >= |m_1, \vec{p}_1 > \otimes |m_2, \vec{p}_2 > \otimes ... \, |m_n, \vec{p}_n > \tag{1.3}$$

In this way, we generate a n free particle state such that the i_{th} particle has mass m_i and three-momentum $\vec{p}_i$. Eq. (1.1) fixes the scalar product of the multiparticle states, eq. (1.3), to be

$$< m_n, \vec{p}\,'_n;\, ...\, m_2, \vec{p}\,'_2;\, m_1, \vec{p}\,'_n|m_1, \vec{p}_1;\, m_2, \vec{p}_2;\, ...\, m_n \vec{p_n} >= \prod_{i=1}^{n} (2\pi)^3 2\, p_i^0\, \delta^{(3)}(\vec{p}_i - \vec{p}\,'_i) \tag{1.4}$$

In the case of two particles, it is interesting to work out explicitly eq. (1.4) by noting that

$$(2\pi)^6\, 4\, p_1^0\, p_2^0\, \delta^{(3)}(\vec{p}_1-\vec{p}\,'_1)\, \delta^{(3)}(\vec{p}_2-\vec{p}\,'_2) = (2\pi)^4 \delta^{(4)}(\mathcal{P}-\mathcal{P}')\, (2\pi)^2\, 4\, W^0\, |\vec{p}|^{\,-1}\, \delta(\Omega-\Omega') \quad (1.5)$$

where $\mathcal{P}$ and $\mathcal{P}'$ are the total four-momenta of the states $|m_1, \vec{p}_1;\, m_2, \vec{p}_2>$ and $|m_1, \vec{p}\,'_1;\, m_2, \vec{p}\,'_2>$ respectively, W is the total energy in the center of mass frame(c.m.), $|\vec{p}|$ is the modulus of the three momentum of the particles in the c.m. and Ω, Ω' are the polar angles of the three-momenta $\vec{p}_1$ and $\vec{p}\,'_1$ in the same frame.

From eq. (1.5) the standard separation between the free motion of the c.m. and the rest of variables attached to the relative motion of the particles can be seen. This separation is in fact independent of the number of particles and gives rise to the concept of **phase space**. For the state $|m_1, \vec{p}_1;\, m_2, \vec{p}_2;\, ...\, m_n, \vec{p_n}>$ it is given by

$$d\mathcal{Q} = \int \prod_{i=1}^{n} \frac{d^3 p_i}{(2\pi)^3 2p_i^0} (2\pi)^4 \delta^{(4)}(\mathcal{P} - \sum_{i=1}^{n} p_i) \quad (1.6)$$

where the integration is done with respect the total four-momentum $\sum_{i=1}^{n} p_i$ and $d\mathcal{Q}$ represents an infinitesimal of phase space.

From eq. (1.5), the phase space for a two particle state results:

$$d\mathcal{Q} = \frac{d\Omega}{4W} \frac{|\vec{p}|}{4\pi^2} \quad (1.7)$$

in terms of the c.m. variables.

In the following we will omit the mass m of a particle in the labelling of its state. It will be understood that the state $|\vec{p}_i>$ will have a mass m_i.

1.2 The S-Matrix and the T-Matrix. Unitarity (I).

Let us consider the scattering process of the ingoing free state $|i>$ to the outgoing one $|f>$. The probability amplitude will be

$$<f|S|i> \equiv S_{if} \quad (1.8)$$

where S is the evolution operator. Due to the Lorentz invariance, the matrix element S_{if}, regarded as a function of the states $|i>$ and $|f>$, is a scalar under Lorentz transformations. On the other hand, since the total probability of finding the state $|i>$ in any possible final state $|f>$ must be 1, the S-operator must be unitary. Thus,

$$S\, S^\dagger = S^\dagger\, S = I \quad (1.9)$$

Because of translation invariance, the scattering process does not affect the total c.m. motion. In this way, one can write the matrix element S_{if} as

$$< f|S|i >= (2\pi)^4 \delta^{(4)}(\mathcal{P}_f - \mathcal{P}_i) < \alpha_f|S_{\mathcal{P}}|\alpha_i > \tag{1.10}$$

where $|\alpha_i >$ and $|\alpha_f >$ refer to the states $|i >$ and $|f >$ after eliminating the global c.m. motion. A short way to write eq. (1.10) is by expressing the S-matrix as the direct product

$$S = I \otimes S_{\mathcal{P}} \tag{1.11}$$

and then eq. (1.9) also implies that

$$S_{\mathcal{P}}\, S_{\mathcal{P}}^{\dagger} = S_{\mathcal{P}}^{\dagger}\, S_{\mathcal{P}} = I \tag{1.12}$$

for the evolution operator $S_{\mathcal{P}}$ which only connects states $|\alpha >$ with the same total four-momentum.

The process $|i > \rightarrow |f >$ will have in general two ways of occur: with or without interaction. To make explicit such separation, the T-matrix is defined as:

$$S = I - i\,T \tag{1.13}$$

From eq. (1.11), T may also be written as the direct product:

$$T = I \otimes T_{\mathcal{P}} \tag{1.14}$$

and then

$$S_{\mathcal{P}} = I - i\,T_{\mathcal{P}} \tag{1.15}$$

The unitarity requirements given by eqs. (1.9) and (1.12), when applied to T and $T_{\mathcal{P}}$, respectively, imply

$$\begin{aligned} T - T^{\dagger} &= -i\,T^{\dagger}\,T \\ T_{\mathcal{P}} - T_{\mathcal{P}}^{\dagger} &= -i\,T_{\mathcal{P}}^{\dagger}\,T_{\mathcal{P}} \end{aligned} \tag{1.16}$$

Including a resolution of the identity among $T^{\dagger}$ and T in the right hand side (R.H.S) of the first of eqs. (1.16), we have

$$< f|T|i > - < f|T^{\dagger}|i >= -i \sum_a \int \left[\prod_{i=1}^{n_a} \frac{d^3 p_i}{2p_i^0 (2\pi)^3} \right] < f|T^{\dagger}|a >< a|T|i > \tag{1.17}$$

with n_a the number of particles in the intermediate state $|a >$. Each one of these states $|a >$, which have the same quantum numbers than the final or initial ones, is called a **channel**. After removing a common factor $(2\pi)^4 \delta^{(4)}(\mathcal{P}_f - \mathcal{P}_i)$ in both sides of eq. (1.17), one finds

$$< \alpha_f|T_{\mathcal{P}}|\alpha_i > - < \alpha_f|T_{\mathcal{P}}^{\dagger}|\alpha_i >= -i\sum_a \int d\mathcal{Q}_a < \alpha_f|T_{\mathcal{P}}^{\dagger}|\alpha_a >< \alpha_a|T_{\mathcal{P}}|\alpha_i > \qquad (1.18)$$

where $d\mathcal{Q}_a$ is the phase space for the state $|a>$, eq. (1.6). In the former equation it is sufficient to sum over those states $|a>$ whose threshold is lower than $\mathcal{P}^0$, otherwise $d\mathcal{Q}_a$ will be zero because of the $\delta(\mathcal{P}^0 - \sum_{i=1}^{n_a} p_i^0)$ in eq. (1.6).

1.3 Partial wave amplitudes. Unitarity (II).

We can represent the scattering of two mesons, both in the final and initial states, as:

$$a(p_1) + b(p_2) \to c(p_3) + d(p_4) \qquad (1.19)$$

with p_i the four-momentum for the i_{th} particle. If the three-momenta of the initial particles are given, there will be six degrees of freedom for the former process corresponding to the final three-momenta, $\vec{p}_3$ and $\vec{p}_4$ (we assume that all the masses are known). However, because of the conservation of the total four-momenta, the number of degrees of freedom is reduced just to two, for instance, the angles (θ, ϕ) defining the c.m. direction of the three-momentum of particle c. On the other hand, taking the z-axis along the initial c.m. three-momentum of particle a, rotational invariance requires that $T_{\mathcal{P}}$ will not depend on ϕ. To see this, note that

$$\begin{aligned} |\alpha_f > &\equiv |\theta, \phi >= \mathcal{R}_z(\phi)|\theta, 0 > \\ |\alpha_i > &= |0, 0 > \end{aligned} \qquad (1.20)$$

with $\mathcal{R}(\phi)$ a rotation around the z-axis. Thus,

$$\begin{aligned} T_{\mathcal{P}}(\theta, \phi)_{if} &= < \theta, \phi|T_{\mathcal{P}}|0, 0 >=< \theta, 0|\mathcal{R}_z^{\dagger}(\phi)T_{\mathcal{P}}|0, 0 >=< \theta, 0|\mathcal{R}_z^{\dagger}(\phi)T_{\mathcal{P}}\mathcal{R}_z(\phi)|0 >= \\ &= < \theta, 0|T_{\mathcal{P}}|0, 0 >= T_{\mathcal{P}}(\theta, 0)_{if} \end{aligned} \qquad (1.21)$$

where we have used the rotational invariance requirement

$$\mathcal{R}_z^{\dagger}(\phi)T_{\mathcal{P}}\mathcal{R}_z(\phi) = T_{\mathcal{P}} \qquad (1.22)$$

In eq. (1.21) we have written the full expression $T_{\mathcal{P}}(\theta, \phi)_{if}$ to distinguish from the operator $T_{\mathcal{P}}$ itself. In the following, we will not have such possible source of ambiguity and then we will denote simply by $T_{\mathcal{P}}(\theta)$ the matrix element among two states of two mesons, which only depends on θ because of eq. (1.21).

Making an expansion of $T_{\mathcal{P}}(\theta)$ in terms of the Legendre polynomials $P_L(\theta)$, we have:

$$T_{\mathcal{P}}(\theta) = \sum_{L=0}^{\infty} (2L+1) P_L(\cos\theta) T_L(s) \tag{1.23}$$

where $T_L(s)$ is called the partial wave amplitude with angular momentum L, and $s = \mathcal{P}^2 = W^2$, which is the only scalar we can form from $\mathcal{P}$.

The inverse of eq. (1.23) is:

$$T_L(s) = \frac{1}{2} \int_{-1}^{1} d\cos\theta P_L(\cos\theta) T_{\mathcal{P}}(\theta) \tag{1.24}$$

The unitarity requirements upon a partial wave amplitude $T_L(s)$ follows from a partial wave decomposition of both sides of eq. (1.18). In this way, below the threshold of intermediate states with more than two particles, one has, using also eq. (1.7):

$$T_L(s)_{if} - T_L^*(s)_{if} = -i \sum_a T_L(s)_{ia} T_L^*(s)_{fa} \frac{\vec{p}_a}{4\pi W} \tag{1.25}$$

where $|\vec{p}_a|$ is the modulus of the c.m. three-momentum for the state $|a>$. Due to time reversal invariance, $T_L(s)_{\alpha\beta} = T_L(s)_{\beta\alpha}$, (see for instance pag. 231 of ref. [11]). Thus,

$$\mathrm{Im}\, T_L(s) = -\sum_a T_L(s)_{ia} T_L^*(s)_{af} \frac{|\vec{p}_a|}{8\pi W} \tag{1.26}$$

In a matrix notation, eq. (1.26) can be written as

$$\mathrm{Im}\, T_L(s) = -T_L^\dagger(s) \rho(s) T_L(s) \tag{1.27}$$

with $\rho(s)$ a diagonal matrix with elements

$$\rho(s)_{ij} = \frac{|\vec{p}_i|}{8\pi W} \delta_{ij} \tag{1.28}$$

If we isolate $\rho(s)$ from eq. (1.27), taking into account that $\mathrm{Im}\, T_L = (T_L - T_L^\dagger)/(2i)$, one has

$$-\rho = \frac{1}{2i} (T_L^\dagger)^{-1} \cdot \left[T_L - T_L^\dagger \right] \cdot (T_L)^{-1} = \frac{1}{2i} \left[(T_L^\dagger)^{-1} - (T_L)^{-1} \right] \tag{1.29}$$

From where a well known and important result follows,

$$\mathrm{Im}\, T_L^{-1}(s) = \rho(s) \tag{1.30}$$

This result establishes that all the dynamics of a scattering process of two particles, both in the initial and final states, is contained in the real part of the inverse of the partial wave amplitudes, since the imaginary part is fixed by unitarity. This is the basis for the K-matrix approach, which is usually defined as:

$$T_L = \left[K^{-1} + i\rho\right]^{-1} \tag{1.31}$$

hence,

$$K^{-1} = \mathrm{Re}\,(T_L^{-1}) \tag{1.32}$$

For energies below the first inelastic threshold, the sum in eq. (1.26) reduces only to the elastic term, and then

$$\mathrm{Im}\, T_L^{-1} = \frac{|\vec{p}|}{8\pi W} \tag{1.33}$$

If we write

$$T_L(s) = -\frac{8\pi W}{|\vec{p}|} e^{i\delta(s)_L} \sin\delta(s)_L \tag{1.34}$$

eq. (1.33) follows immediately. The quantity $\delta(s)_L$ is known as **phase shift** for the corresponding partial wave amplitude. The magnitude S_L is usually defined as

$$S_L = 1 - i\frac{|\vec{p}|}{4\pi W} T_L = e^{2i\delta_L} \tag{1.35}$$

and then $S_L\, S_L^* = 1$.

The above formulae can be easily generalized to the case of several coupled channels. As before, we use a matrix notation. Requiring the matrix S_L to be symmetric, because of time reversal, one has

$$S_L = I - 2i\rho^{1/2} T_L \rho^{1/2} \tag{1.36}$$

From eq. (1.27), it follows that

$$S_L \cdot S_L^\dagger = S_L^\dagger \cdot S_L = I \tag{1.37}$$

Just another way to state unitarity for partial waves amplitudes.

On the other hand, the matrix element $(S_L S_L^\dagger)_{ii}$ is given by:

$$|(S_L)_{i1}|^2 + |(S_L)_{i2}|^2 + ... + |(S_L)_{ii}|^2 + ... + |(S_L)_{in}|^2 = 1 \tag{1.38}$$

Then, $|(S_L)_{ii}| \leq 1$, so that, in general,

$$(S_L)_{ii} = \eta_i e^{2i\delta_i} \tag{1.39}$$

where we have suppressed the subindex L in δ because it is clear to which partial wave we are referring. For the elastic case, eq. (1.35), $\eta = 1$.

For a two channel process, imposing eq. (1.37), the matrix S_L can be written as:

$$S_L \;=\; \begin{pmatrix} \eta e^{2i\delta_1} & i(1-\eta^2)^{1/2} e^{i(\delta_1+\delta_2)} \\ i(1-\eta^2)^{1/2} e^{i(\delta_1+\delta_2)} & \eta e^{2i\delta_2} \end{pmatrix} \tag{1.40}$$

Eqs. (1.36), (1.39) and (1.40) will be used to extract phase shifts and inelasticities in terms of the T-matrix.

To end this section let us see the modifications to eq. (1.25) when some of the states correspond to identical particles, for instance, $\pi^0\pi^0$, $\eta\eta$ or two pions in the isospin formalism. The differences arise because the phase space for such identical particles states must be divided by two since a direction (θ, ϕ) cannot be distinguished of its inverse, $(\pi - \theta, \phi + \pi)$. Hence, for these states instead of the phase space factor $p_a/(8\pi W)$ we will have $p_a/(16\pi W)$. An important aspect to realize about eq. (1.25) is that an intermediate state appears in two amplitudes at the same time in the sum of this equation. Hence, we can maintain the same phase space for all the states but dividing by $(\sqrt{2})^\alpha$ each partial wave, with α the number of identical particle states that appear in the amplitude. For instance, $\alpha = 2$ for the scattering of $\pi\pi \to \pi\pi$, $\alpha = 1$ for $\pi\pi \to K\bar{K}$, $\alpha = 0$ for $K\pi \to K\pi$ and so on. Another advantage of considering this normalization is that all the formulae relating phase shifts and inelasticities to the T-matrix will be the same since they are direct consequence of unitarity and the normalization of the states, which have remained the same both for identical/non-identical particle states. However, one has to keep in mind such normalization factor when comparing with other experimental data in order to remove it, if it is necessary. In this way eq. (1.24) transforms to

$$T_L(s) = \frac{1}{2\,(\sqrt{2})^\alpha} \int_{-1}^{1} d\cos\theta\, P_L(\cos\theta)\, T_{\mathcal{P}}(\theta) \tag{1.41}$$

1.4 Crossing and Analyticity.

Let us consider once again the scattering of two-meson states, given by eq. (1.19). Taking into account that $p_i^2 = m_i^2$ and the conservation of the total four-momentum, we can form only three Lorentz scalars from the momenta p_i. These are the well known Mandelstam variables s, t and u, given by:

$$\begin{aligned} s &= (p_1 + p_2)^2 = (p_3 + p_4)^2 \\ t &= (p_1 - p_3)^2 = (p_2 - p_4)^2 \\ u &= (p_1 - p_4)^2 = (p_2 - p_3)^2 \end{aligned} \tag{1.42}$$

the variable s was introduced already after eq. (1.23).

Thus, the T-matrix, which is just a Lorentz scalar, will be a function of these variables. However, only two of the three Mandelstam variables are independent since:

$$s + t + u = \sum_{i=1}^{4} m_i^2 \tag{1.43}$$

The process in eq. (1.19) is called the s-channel because the s Mandelstam variable is the square of the total energy in the c.m., as we have already seen.

In order to introduce the concept of crossing, it is worth representing the scattering in eq. (1.19) by Fig. 1.1:

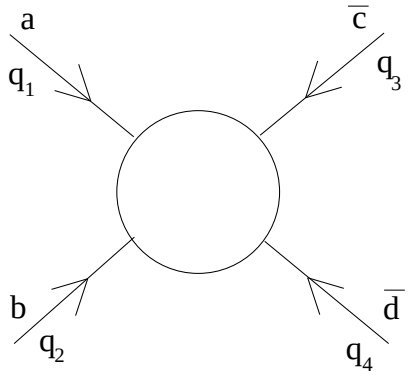

Figure 1.1: Crossing symmetric diagram for a two particle scattering.

where all the momenta are ingoing and the bars indicate that the antiparticle has to be considered, in order to obtain the quantum numbers of the vacuum. We redefine the Mandelstam variables as

$$\begin{aligned} s &= (q_1+q_2)^2 \\ t &= (q_1+q_3)^2 \\ u &= (q_1+q_4)^2 \end{aligned} \tag{1.44}$$

We now take the convention that the four-momentum for the outgoing particles is the same but with opposite sign than the one of their antiparticles in Fig. 1.1. The four-momentum of the ingoing particles will be the same than in Fig. 1.1. As a consequence, eqs. (1.42) and (1.44) are equivalent, since $q_1 = p_1$, $q_2 = p_2$, $q_3 = -p_3$ and $q_4 = -p_4$.

We can also consider the particles b and $\bar{d}$ in Fig. 1.1 as outgoing ones, so that we will have the process:

$$a(p_1) + \bar{c}(-p_3) \to \bar{b}(-p_2) + d(p_4) \tag{1.45}$$

but now

$$\begin{aligned} s &= (p_1-p_2)^2 \\ t &= (p_1+p_3)^2 \\ u &= (p_1-p_4)^2 \end{aligned} \tag{1.46}$$

Hence, s, t, u plays for the process (1.45) the same role than t, s, u in the process (1.19). Since for (1.45), the square of the total c.m. energy corresponds to the t variable this process is called the t-channel.

In analogous way, the u-channel process is given when considering particles c and $\bar{b}$ as the outgoing ones.

$$a(p_1) + \bar{d}(-p_4) \rightarrow c(p_3) + \bar{b}(-p_2) \tag{1.47}$$

with

$$\begin{aligned} s &= (p_1 - p_2)^2 \\ t &= (p_1 - p_3)^2 \\ u &= (p_1 + p_4)^2 \end{aligned} \tag{1.48}$$

As a consequence of eqs. (1.42), (1.46) and (1.48), the Mandelstam variables s, t and u will have a different range of values in the physical region of the s-, t- or u-channels. The physical region for each channel will correspond to

$$\begin{aligned} W_x &\geq m_{x1} + m_{x2} \\ -1 &\leq \cos\theta_x \leq 1 \end{aligned} \tag{1.49}$$

with the subindex x indicating any of the three channels.

Since the three physical regions are non-overlapping there is no reason why we cannot refer to the three physical amplitudes as a single amplitude $T(s,t,u)$ which is now defined over all three physical regions and which takes the appropriate values in each one. This is just a question of convention or terminology. But it becomes full of physical significance when we introduce the hypothesis that this amplitude $T(s,t,u)$, initially defined on the three disjoint physical regions, permits an analytic continuation which apart from certain specific singularities allows it to be defined over the whole of the s, t and u complex planes. This is the content of the so called **Mandelstam Hypothesis** [13]. To accomplish this, one requires a knowledge of the singularities of $T(s,t,u)$ as a function of two complex variables. These singularities appear always that one of the variables s, t or u are greater than the threshold of an intermediate state. If this state is multiparticle, the singularity will be a branch point or a simple pole if the state is monoparticle. For certain mass ratios one encounters anomalous singularities, that is, branch points not determined simply by the masses of the intermediate states ref. [14]. All the problems discussed in this work are believed to have normal singularities, consistently with the information obtained from the use of the effective Lagrangians.

The Mandelstam Hypothesis has not been derived from a clear set of physical principles coming from Quantum Field Theory. However, all the Feynman diagrams analyzed so far, fulfill the Mandelstam representation.

For partial wave amplitudes the situation is essentially the same than for the full amplitude since the former ones are obtained by projecting the latter over a certain partial wave, eq. (1.24). Hence, a partial wave amplitude will have, for $s > (m_{s1} + m_{s2})^2$, the 'physical cut' also called 'right hand cut' or 'unitarity cut', due to the presence of intermediate states with the same quantum number than the s-channel. It has also poles coming from

resonances or bound states and the 'unphysical cuts' which appear from the projection of the physical cuts in the crossed channels, that is, t- or u-channels. For instance, for the elastic $\pi\pi$ scattering it is easy to see that the unphysical cut appears for $s < 0$. This is a general feature of the unphysical cut for the scattering of particles with equal mass, that is, it appears for $s < s_L$. This is why, in this situation, the unphysical cut is also called 'left hand cut'. As a consequence of the Mandelstam Hypothesis it follows that the partial wave amplitudes must satisfy hermitian analyticity, that is, $T_L(s) = T_L^*(s^*)$. This is so, because in the real s-axis there is a segment where $T_L(s)$ has not cuts. For the $\pi\pi$ scattering this happens for $0 < s < 4m_\pi^2$, with m_π the mass of the pion in the isospin limit. Thus, the hermitian analyticity follows as a consequence of the Schwartz theorem for analytic functions of one complex variable.

From eq. (1.30) it is clear that a partial wave amplitude must have several Riemann sheets as a function of s due to the multivalued relation among p and s. For a two meson state, with masses m_1 and m_2, this relation is:

$$|\vec{p}| = \pm \frac{\sqrt{(s-(m_1+m_2)^2)(s-(m_1-m_2)^2)}}{2\sqrt{s}} \tag{1.50}$$

and we have a cut for $0 \leq s \leq (m_1 - m_2)^2$ and $s \geq (m_1 + m_2)^2$. For a two particles with the same mass only the last cut survives. The physical sheet corresponds to the plus sign in front of eq. (1.50). When the sign changes we are in an unphysical sheet.

In the physical region, there can be only poles along the real axis and below the lightest threshold (bound states). Note that a pole on the real axis and above the first threshold violates unitarity, eq. (1.27), since it would imply the equality $\infty = \infty^2$ which is not possible. In the unphysical sheets there can be poles above/below threshold. If the pole is above a threshold it will be unstable and will have also an imaginary part due to its width. A simple picture of why poles off the real axis must be on the unphysical sheets can be obtained from the inverse of the propagator of a resonance present in a Breit-Wigner representation, which is valid for energies close to the mass of the state:

$$s - M_R^2 + iM_R\Gamma(s) \tag{1.51}$$

with $\Gamma(s)$ the width of the resonance for $s = M_R^2$. It is important to note that $\Gamma \propto p^{2J+1}$, where J is the spin of the resonance. If $s \to M_R^2 \pm i\epsilon$, with $\epsilon > 0$, the term $iM_R\Gamma$ develops an imaginary part in the physical sheet which goes as $\pm iM_R\Gamma(M_R^2)$, so that it cannot cancel the imaginary part of s since both have the same sign. Only if we are in the unphysical sheet, the sign is opposite and the cancellation is possible.

Chapter 2

Effective Chiral Lagrangians.

In this chapter we want to give a general overview over some aspects of Chiral Perturbation Theory(χPT) [4, 5] and the extension of the formalism to the intermediate energy region by including explicit resonance fields with spin ≤ 1, ref. [7]. In preparing this chapter I have made large use of the report [15].

2.1 Chiral Symmetry.

The QCD Lagrangian with massless u, d and s quarks coupled to several external sources reads:

$$\mathcal{L}_{QCD} = \mathcal{L}^0_{QCD} + i\bar{q}D^\mu\gamma_\mu q + \bar{q}\gamma^\mu(v_\mu + \gamma_5 a_\mu)q - \bar{q}(s - i\gamma_5 p)q \tag{2.1}$$

where $\mathcal{L}^0_{QCD}$ is the part of the QCD Lagrangian for the heavier quarks c, b and t and gluons, v_μ, a_μ, s and p are the vector, axial, scalar and pseudoscalar external sources, D_μ is the covariant derivative for the $SU(3)$-color gauge symmetry and

$$q = \begin{pmatrix} u \\ d \\ s \end{pmatrix} \tag{2.2}$$

is a vector in the three dimensional flavour space.

The Lagrangian eq. (2.1) exhibits a local $SU(3)_L \otimes SU(3)_R$ flavour symmetry under the following transformation rules

$$\begin{aligned} q &\rightarrow g_R\frac{1}{2}(1+\gamma_5)q + g_L\frac{1}{2}(1-\gamma_5)q \\ v_\mu \pm a_\mu &\rightarrow g_{R,L}(v_\mu \pm a_\mu)g^\dagger_{R,L} + i\, g_{R,L}\partial_\mu\, g^\dagger_{R,L} \\ s + ip &\rightarrow g_R(s+ip)g^\dagger_L \\ g_{R,L} &\in SU(3)_{R,L} \end{aligned} \tag{2.3}$$

This chiral symmetry, which should be rather good in the light quark sector, is not seen in the hadronic spectrum. Although hadrons can be classified in $SU(3)_V \equiv SU(3)_{R+L}$ representations, degenerate multiplets with opposite parity are not observed. Moreover, the octet of the lightest pseudoscalar mesons (π, K, η) can be understood if the chiral $SU(3)_L \otimes SU(3)_R$ symmetry spontaneously breaks down to $SU(3)_V$. Then, according to the Goldstone theorem [16] an octet of pseudoscalar massless bosons appear in the theory, since they will have the same quantum numbers as the broken generators of $SU(3)_A = SU(3)_{R-L}$. One thus expects that (π, K, η) are to be identified with this octet of Goldstone bosons.

Furthermore, Chiral Symmetry is also explicitly broken by a mass term in eq. (2.1)

$$-\bar{q} M_q q \tag{2.4}$$

when fixing the scalar source $s(x) = M = diag(m_u, m_d, m_s)$. Because of this term the Goldstone bosons acquire a small mass. On the other hand $SU(3)_V$ in the hadronic spectrum is an approximate symmetry because m_s is much larger than m_u or m_d.

2.2 Chiral Perturbation Theory.

To take advantage of the mass gap separating the lightest pseudoscalar octet from the rest of the hadronic spectrum we build an effective field theory containing only the Goldstone modes. We collect the Goldstone fields in a traceless $SU(3)$ matrix

$$\Phi = \frac{\vec{\lambda}}{\sqrt{2}}\,\vec{\phi} = \begin{pmatrix} \frac{1}{\sqrt{2}}\pi^0 + \frac{1}{\sqrt{6}}\eta_8 & \pi^+ & K^+ \\ \pi^- & -\frac{1}{\sqrt{2}}\pi^0 + \frac{1}{\sqrt{6}}\eta_8 & K^0 \\ K^- & \bar{K}^0 & -\frac{2}{\sqrt{6}}\eta_8 \end{pmatrix} \tag{2.5}$$

where λ_i are the Gell-Mann's matrices with $\mathrm{Tr}(\lambda_i \lambda_j) = 2\delta_{ij}$. From this matrix one has a non linear realization of the chiral symmetry through $U(\phi) = e^{i\sqrt{2}\Phi/f}$, with f a constant. This matrix transforms linearly under $SU(3)_L \otimes SU(3)_R$ as:

$$U(\phi) \to g_R U(\phi) g_L^\dagger \tag{2.6}$$

and hence, the Goldstone boson fields ϕ transform in a non-linear form.

The effective Lagrangian will be constructed as a power expansion series in terms of the external Goldstone momenta and the quark matrix mass. The lowest order chiral Lagrangian invariant under Lorentz transformations, parity and charge conjugation with only two derivatives and linear in the quark masses is [5]

$$\mathcal{L}_2 = \frac{f^2}{4} < D_\mu U^\dagger\, D^\mu U + U^\dagger\, \mathcal{M} + \mathcal{M}^\dagger\, U > \tag{2.7}$$

where $<>$ means $SU(3)$-flavour trace and

$$\mathcal{M} = 2B_0(s + ip) \tag{2.8}$$

with B_0 a constant and the covariant derivative

$$D_\mu U = \partial_\mu U - i r_\mu U + i U l_\mu \tag{2.9}$$

where $r_\mu(l_\mu) = v_\mu + (-)a_\mu$, respectively.

Fixing $s(x) = M$ and $p(x) = 0$, the $\mathcal{M}$ term in eq. (2.7) gives rise to a quadratic pseudoscalar mass term plus additional interactions proportional to the quark masses. This is the reason why in χPT the quark masses are considered as $\mathcal{O}(p^2)$. In the isospin limit with $\hat{m} = \frac{m_u + m_d}{2}$, the following relations arise

$$\begin{aligned} m_\pi^2 &= 2\hat{m}B_0 \\ m_K^2 &= (\hat{m} + m_s)B_0 \\ m_{\eta_8}^2 &= \frac{2}{3}(\hat{m} + 2m_s)B_0 \end{aligned} \tag{2.10}$$

satisfying the Gell-Mann[17]-Okubo[18] mass relation.

$$3\, m_{\eta_8}^2 = 4\, m_K^2 - m_\pi^2 \tag{2.11}$$

The meaning of the constant f can be achieved when calculating from the lowest order Lagrangian, eq. (2.7), the axial current. Then f results to be the pion decay constant in the chiral limit, that is,

$$f = f_\pi + \mathcal{O}(m_q) \tag{2.12}$$

The next to leading order Lagrangian, $\mathcal{L}_4$, is constructed with the same building blocks than $\mathcal{L}_2$, namely, eqs. (2.3), (2.5), (2.6) and (2.9). Preserving Lorentz invariant, parity and charge conjugation one has:

$$\begin{aligned} \mathcal{L}_4 = {} & L_1 \left\langle \partial_\mu U^\dagger \partial^\mu U \right\rangle^2 + L_2 \left\langle \partial_\mu U^\dagger \partial_\nu U \right\rangle \left\langle \partial^\mu U^\dagger \partial^\nu U \right\rangle \\ & + L_3 \left\langle \partial_\mu U^\dagger \partial^\mu U \partial_\nu U^\dagger \partial^\nu U \right\rangle + L_4 \left\langle \partial_\mu U^\dagger \partial^\mu U \right\rangle \left\langle U^\dagger \mathcal{M} + \mathcal{M}^\dagger U \right\rangle \\ & + L_5 \left\langle \partial_\mu U^\dagger \partial^\mu U \left(U^\dagger \mathcal{M} + \mathcal{M}^\dagger U \right) \right\rangle + L_6 \left\langle U^\dagger \mathcal{M} + \mathcal{M}^\dagger U \right\rangle^2 \\ & + L_7 \left\langle U^\dagger \mathcal{M} - \mathcal{M}^\dagger U \right\rangle^2 + L_8 \left\langle \mathcal{M}^\dagger U \mathcal{M}^\dagger U + U^\dagger \mathcal{M} U^\dagger \mathcal{M} \right\rangle \\ & + H_1 \left\langle F_{R\,\mu\nu} F_R^{\mu\nu} + F_{L\,\mu\nu} F_L^{\mu\nu} \right\rangle + H_2 \left\langle \mathcal{M}^\dagger \mathcal{M} \right\rangle \end{aligned} \tag{2.13}$$

In $\mathcal{L}_4$ there is also the anomalous term [21, 22]. We will come back to this point in **chapter 6**.

In the former equation we have also included the strength tensor:

$$\begin{aligned} F_L^{\mu\,\nu} &= \partial^\mu\,\ell^\nu - \partial^\nu\,\ell^\mu - i[\ell^\mu,\ell^\nu] \\ F_R^{\mu\,\nu} &= \partial^\mu\,r^\nu - \partial^\nu\,r^\mu - i[r^\mu,r^\nu] \end{aligned} \tag{2.14}$$

In the $\mathcal{L}_4$ the terms proportional to H_1 and H_2 do not contain the pseudoscalar fields and are therefore not directly measurable. Thus, at $\mathcal{O}(p^4)$ we need ten additional coupling constants L_i to determine the low-energy behaviour of the Green functions. These couplings have an infinite plus a finite part. The infinite part cancels with the infinities from loops, so that at the end only the finite parts, L_i^r, remain. In χPT the $\overline{MS}$-1 scheme is the usual renormalization scheme. At the present time these L_i^r constants have to be fitted to the phenomenology. In general, the number of free parameters increases drastically with the order of the chiral expansion so that for $\mathcal{L}_6$ there are more than one hundred free couplings. This implies that the predictive power of the theory is rapidly lost with higher orders.

On the other hand, the convergence of the χPT series is restricted to low energies, typically for $\sqrt{s} < 500$ MeV, although this upper limit depends strongly on the process to be considered. Note that the lightest well established resonance, the $\rho(770)$ has a mass of 770 MeV. This resonance introduces a pole in the T-matrix which cannot be reproduced by a power expansion. Thus, the masses of the heavier states not included in eq. (2.5), put a clear upper limit to the χPT series and also give us the scale $\Lambda_{\chi PT}$ over which the χPT power series is constructed

$$\frac{\mathcal{O}(p^4)}{\mathcal{O}(p^2)} \sim \frac{p^2}{\Lambda^2_{\chi PT}} \tag{2.15}$$

with $\Lambda_{\chi PT} \approx M_\rho \approx 1$ GeV.

One can also obtain an estimation of $\Lambda_{\chi PT}$ by taking into account those contributions coming from loops when allowing a change in the regularization scale by a factor of $\mathcal{O}(1)$ [6]. The result is that

$$\Lambda_{\chi PT} \leq 4\pi f_\pi \approx 1.2 \text{ GeV} \tag{2.16}$$

In the next section we discuss how to include explicit resonance fields compatible with chiral symmetry and its breaking. Their contributions to the low energy constants L_i is also discussed.

2.3 Resonances and Chiral Symmetry.

Following ref. [7] we include heavier hadron states than the lightest pseudoscalar mesons (π, K, η). The former states will comprise vector (V), axial (A), scalar (S) and pseudoscalar (P) octets and scalar (S_1) and pseudoscalar (P_1) singlets. The exchange of these resonances between the Goldstone bosons contains the resonance propagators which for $p^2 << M_R^2$ can be expanded as

$$\frac{1}{p^2 - M_R^2} = \frac{-1}{M_R^2}\left(1 + \frac{p^2}{M_R^2} + \left(\frac{p^2}{M_R^2}\right)^2 + ...\right) \tag{2.17}$$

giving rise to contributions which should be embodied in the χPT counterterms. However, from the equation above it is obvious that a resummation to all orders of such local contributions is obtained including the explicit resonance fields.

The interaction Lagrangian of the octets and singlets of resonances with spin$\leq$1 to lowest order in the chiral expansion are given by [7]:

Vector Octet, $\mathbf{J^{PC} = 1^{--}}$

$$\frac{F_V}{2\sqrt{2}} < V_{\mu\nu} f_+^{\mu\nu} > + \frac{iG_V}{\sqrt{2}} < V_{\mu\nu} u^\mu u^\nu > \tag{2.18}$$

Axial Octet, $\mathbf{J^{PC} = 1^{++}}$

$$\frac{F_A}{2\sqrt{2}} < A_{\mu\nu} f_-^{\mu\nu} > \tag{2.19}$$

Pseudosalar Octet, $\mathbf{J^{PC} = 0^{-+}}$

$$i\, d_m \; < P\, \chi_- > \tag{2.20}$$

Scalar Octet, $\mathbf{J^{PC} = 0^{++}}$

$$c_d \; < S\, u_\mu u^\mu > + c_m \; < S\, \chi_+ > \tag{2.21}$$

Scalar Singlet, $\mathbf{J^{PC} = 0^{++}}$

$$\widetilde{c}_d\, S_1 \; < u_\mu u^\mu > + \widetilde{c}_m\, S_1 \; < \chi_+ > \tag{2.22}$$

Pseudoscalar Singlet, $\mathbf{J^{PC} = 0^{-+}}$

$$i\, \widetilde{d}_m\, P_1 \; < \chi_- > \tag{2.23}$$

In matrix notation

$$V_{\mu\nu} = \begin{pmatrix} \frac{\rho^0}{\sqrt{2}} + \frac{w_8}{\sqrt{6}} & \rho^+ & K^{*\,+} \\ \rho^- & \frac{-\rho^0}{\sqrt{2}} + \frac{w_8}{\sqrt{6}} & K^{*\,0} \\ K^{*\,-} & \bar{K}^{*\,0} & \frac{-2\,w_8}{\sqrt{6}} \end{pmatrix}_{\mu\nu} \tag{2.24}$$

and similarly for the rest of the octets. From eq. (2.18) and (2.19) the V and A resonances only couple at lowest order as octets. In the former equations the vector and axial octets are included as antisymmetric tensor fields, such that if $|W, p>$ represents a vector or axial resonance with momentum p and mass M, then

$$< 0|W_{\mu\nu}|W, p >= i\, M^{-1}\, [p_\mu\, \epsilon_\nu(p) - p_\nu\, \epsilon_\mu(p)] \tag{2.25}$$

with $\epsilon_\mu(p)$ the polarization vector of the resonance state. The propagator is given by:

$$\frac{M^{-2}}{M^2 - p^2 - i\epsilon}\, \left[g_{\mu\rho}\, g_{\nu\sigma}\, (M^2 - p^2) + g_{\mu\rho}\, p_\nu\, p_\sigma - g_{\mu\sigma}\, p_\nu\, p_\rho - (\mu \leftrightarrow \nu)\right] \tag{2.26}$$

In the Lagrangians given above we have also used:

$$\begin{aligned} u_\mu &= i u^\dagger D_\mu U u^\dagger = u_\mu^\dagger \\ \chi_\pm &= u^\dagger \mathcal{M} u^\dagger \pm u \mathcal{M}^\dagger u \\ f_\pm^{\mu\nu} &= u F_L^{\mu\nu} u^\dagger \pm u^\dagger F_R^{\mu\nu} u \end{aligned} \tag{2.27}$$

In ref. [7] the $\mathcal{O}(p^4)$ contributions which appear through the exchange of the above resonances are also studied. Note that this is the first order to which resonance exchange contributes to the χPT series since their couplings to the Goldstone fields are $\mathcal{O}(p^2)$.

At $\mathcal{O}(p^4)$ the resonance exchange gives contribution to all the terms of $\mathcal{L}_4$ in eq. (2.13).

The V exchange generates contributions to L_1, L_2, L_3, L_9 and L_{10}, while A exchange contributes to L_{10}:

$$\begin{aligned} L_1^V &= \frac{G_V^2}{8\, M_V^2} & L_2^V &= 2\, L_1^V \\ L_9^V &= \frac{F_V\, G_V}{2\, M_V^2} & L_3^V &= -6\, L_1^V \\ L_{10}^{V+A} &= -\frac{F_V^2}{4\, M_V^2} + \frac{F_A^2}{4\, M_A^2} \end{aligned} \tag{2.28}$$

with M_V the V octet mass in the chiral limit which is approximately given by the mass of the ρ [7]. F_V and G_V are obtained from the decay $\rho \to e^+\, e^-$ and the electromagnetic radius of the pion [7], respectively. F_A and M_A are deduced from the Weinberg's sum rules [23]. The values are $F_V = 154$ MeV, $G_V = 53$ MeV, $M_V = M_\rho = 770$ MeV, $F_A = 123$ MeV and $M_A = 968$ MeV.

The resulting values of the L_i couplings [7] are summarized in Table 2.1, which compares the different resonance exchange contributions with the phenomenologically determined values of the $L_i^r(M_\rho)$ at the scale $\mu = M_\rho$. The results shown in the table establish a chiral version of vector (and axial-vector) meson dominance: whenever they can contribute at

all, V and A exchanges seem to completely dominate the relevant coupling constants, as it is clear when summing columns three and four of the former table and comparing with the experimental values.

Making use of additional QCD inspired assumptions of high-energy behaviour, such as unsubtracted dispersion relations for the pion electromagnetic form factor, the V couplings can be expressed in terms of f_π [24]:

$$\begin{aligned} F_V &= \sqrt{2}\, f_\pi \\ G_V &= \frac{f_\pi}{\sqrt{2}} \end{aligned} \tag{2.29}$$

The former relations are calculated without loop contributions as it should be in large N_c QCD, where N_c means number of colours. Applying the Weinberg's sum rules we obtain from the equation above the parameters of the axial resonances

$$\begin{aligned} F_A &= f_\pi \\ M_A &= \sqrt{2}\, M_V \end{aligned} \tag{2.30}$$

Note that the deviation between the values in eqs. (2.29) and (2.30) and the values given above are about a $20-25\%$. This is the kind of deviations one can expect in values given from large N_c QCD. The values of the L_i couplings using eqs. (2.29) and (2.30) are shown in the last column of Table 2.1.

The situation for the scalar sector is much more complicated. In fact, there is not even a consensus neither upon which states form the lightest scalar nonet nor how many states there are below 1 GeV. One of the aims of this thesis is trying to bring light into this problem. As we will see in **section 6**, the contributions from the scalar resonances to the different L_i couplings are those needed to saturate the values of the $L_i^r(M_\rho)$, as claimed in [7]. However, the scalar nonet which is used in [7], with a mass around 1 GeV and containing the $a_0(980)$ resonance, is not the proper one. The right scalar octet appears with a mass of around 1.2 GeV and couplings which can be determined in large N_c from the vanishing of the scalar $K\pi$, $K\eta$ and $K\eta'$ form factors at infinite [103]. The values are:

$$c_d = c_m = \frac{f_\pi}{\sqrt{2}} \approx 46.2 \text{ MeV} \tag{2.31}$$

The scalar octet considered in [7], with the $a_0(980)$ resonance, originates now from the interactions between the pseudoscalar mesons, that is, it corresponds to dynamically generated resonances from a certain set of strengths, see **sections 3.1 and 5.4**. In this way, this octet disappears in the large N_c limit.

The contribution of $S{+}S_1$ to the L_i^r are:

$$\begin{aligned} &L_1^{S+S_1} = -\tfrac{c_d^2}{6\,M_S^2} + \tfrac{\widetilde{c}_d^{\,2}}{2\,M_{S_1}^2} \quad L_3^S = \tfrac{c_d^2}{2\,M_S^2} \quad L_4^{S+S_1} = -\tfrac{c_d\,c_m}{3\,M_S^2} + \tfrac{\widetilde{c}_d\,\widetilde{c}_m}{M_{S_1}^2} \quad L_5^S = \tfrac{c_d\,c_m}{M_S^2} \\ &L_6^{S+S_1} = -\tfrac{c_m^2}{6\,M_S^2} + \tfrac{\widetilde{c}_m^{\,2}}{2\,M_{S_1}^2} \quad L_8^S = -\tfrac{c_m^2}{2\,M_S^2} \end{aligned} \tag{2.32}$$

Table 2.1: V, A, S, S_1 and η_1 contributions to the coupling constants L_i^r in units of 10^{-3}. The Total^2 column comes from eqs. (2.29) and (2.30) as explained in the text.

i	$L_i^r(M_\rho)$	V	A	S	S_1	η_1	Total	Total^2
1	0.4 ± 0.3	0.6	0	-0.2	0.2	0	0.6	0.9
2	1.4 ± 0.3	1.2	0	0	0	0	1.2	1.8
3	-3.5 ± 1.1	-3.6	0	0.6	0	0	-3.0	-4.9
4	-0.3 ± 0.5	0	0	-0.5	0.5	0	0	0
5	1.4 ± 0.5	0	0	1.5	0	0	1.5	1.5
6	-0.2 ± 0.3	0	0	-0.2	0.2	0	0	0
7	-0.4 ± 0.2	0	0	0	0	-0.3	-0.3	-0.3
8	0.9 ± 0.3	0	0	0.7	0	0	0.7	0.7
9	6.9 ± 0.7	6.9	0	0	0	0	6.9	7.3
10	-5.5 ± 0.7	-10.0	4.0	0	0	0	-6.0	-5.5

The couplings of S_1, $\widetilde{c}_{d,m}$ and its mass, can be determined through large N$_c$ argumentation, following [7]. In order to guarantee that for instance, L_4 or L_6 become zero in this limit, since they are subleading constants, one needs:

$$\widetilde{c}_d = \epsilon\,\frac{c_d}{\sqrt{3}} \quad \widetilde{c}_m = \epsilon\,\frac{c_m}{\sqrt{3}} \quad M_1 = M_8 \tag{2.33}$$

with $\epsilon = \pm 1$ and c_d, m given in eq. (2.31).

In **section 5.4** the parameters of the scalar singlet are fitted to data and the values obtained are compatible with the above ones, taking into account the level of precision expected in a large N$_c$ estimation as already commented before.

The scalar contributions to the $L_i^r(M_\rho)$ from eqs. (2.31), (2.32) and (2.33) are given in the fifth and sith columns of Table 2.1 with a mass of 1.2 GeV, see **section 6.5**. It is worth to remark that these values have been determined with only one free parameter, the mass M_S of the scalar octet fitted to data in **section 6.5**, since the couplings have been fixed by eq. (2.31). The conclusions about the scalar contributions to the L_i^r in [7] can be maintained although, when taking also into account the findings of **chapter 5**, the scalar nonet there proposed is incorrect.

The exchange of the η_1 meson generates a sizeable contribution to L_7 [5, 7]:

$$L_7^{\eta_1} = -\frac{\widetilde{d}_m{}^2}{2\,M_{\eta_1}^2} \tag{2.34}$$

The magnitude of this contribution can be calculated from the quark-mass expansion of m_η^2 and $m_{\eta'}^2$, which fixes the η_1 parameters in the large N$_c$ limit [7]: $m_{\eta_1} = 804$ MeV, $|\widetilde{d}_m| = 20$ MeV. The final result for L_7 is in close agreement with its phenomenological value as can be seen in the seventh column of Table 2.1.

Chapter 3

Some Aspects about Resonances.

As it was explained in **section 2**, χPT is unable to reproduce resonances which, on the other hand, are an essential characteristic of the strong interactions in the intermediate energy region, $\sqrt{s} \geq 0.8$ GeV. To overcome this difficulty two ways will be presented in the following chapters:

1) In one of the methods one generates poles from the χPT expansion of the inverse of the T-matrix instead of the T-matrix itself. This will give rise to the Inverse Amplitude Method [25] generalized to coupled channels in [26].

2) The second one consists of the inclusion of explicit resonance fields as given in [7] but at the same time developing a suitable unitarization method in order to compare directly with data from the meson-meson scattering. This will be accomplished making use of the N/D method [9, 27].

In both cases unitarity is fulfill to all orders in the chiral expansion. This is also an important source for higher order corrections in the χPT series, especially for the S-wave meson-meson scattering, as we will see along this thesis.

3.1 Resonances.

A striking feature of the experimental data is the frequent occurrence of peaks, bumps or dips when the various cross sections are displayed as a function of energy. The most familiar way to interpret these situations, is to suppose that each peak is due to a resonance in a single partial wave, since resonances have well defined spin, and that the resonant phase shift δ_L increases rapidly through an odd-integral multiple of $\frac{\pi}{2}$ at the resonance energy (or mass). Clearly, for an elastic resonance this gives the required peak in the cross section

$$\sigma_{tot} \approx \frac{4\pi}{\vec{p}^2} \sin^2 \delta_L \tag{3.1}$$

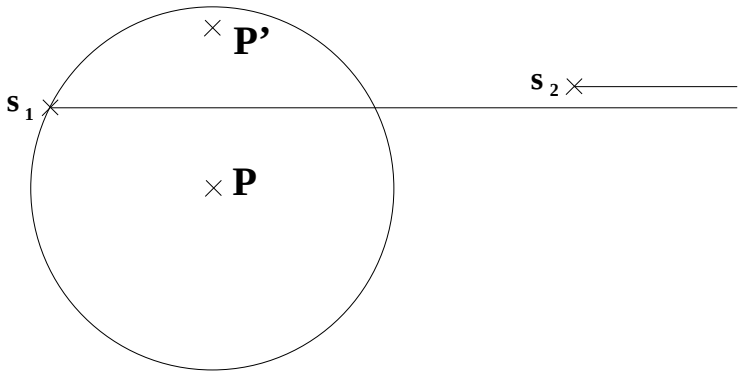

Figure 3.1: s_1 and s_2 are threshold branch points. P, P' are resonance pole positions on the unphysical sheet reached by crossing the cut from s_1. Notice that the circle of convergence of the series of eq. (3.3) includes a region of the physical sheet.

However, in many cases there is a significant amount of background which causes that this description is over-simplified. For instance, in the case of the I=0 $\pi\pi$ scattering one has a dip instead of a peak in the cross section. In fact, the cross section almost vanishes at the mass of the $f_0(980)$ resonance. This can be easily understood from eq. (3.1) taking into account that the $f_0(980)$ appears over a soft and large background. The background phase shift is around $\frac{\pi}{2}$ which must be summed to the resonant phase shift, also $\frac{\pi}{2}$. The sum is around π radians, which according to eq. (3.1) gives a very small cross section.

From the point of view of Quantum Field Theory there is no fundamental difference between a bound state and a resonance, other than the matter of stability. In both cases they correspond to simple poles. However, as indicated at the end of **section 1.4**, while bound states appear below the lowest threshold over the real axis in the physical sheet, resonances are associated with simple poles in the unphysical sheets. Furthermore, since partial wave amplitudes satisfy hermitian analyticity, $T_L(s) = T_L^*(s^*)$, as we also saw in **section 1.4**, poles in the complex plane occur in complex conjugate positions.

Consider a resonance of spin J associated with poles P, P' on the unphysical sheet (sheet II). The positions P, P' are shown on Fig. 3.1, although the diagram actually represents the physical sheet, sheet II is reached by crossing the cut originating from the threshold branch point s_1. Since below the inelastic threshold $T_L(s + i\epsilon) = T_L^{II}(s - i\epsilon)$, where the supraindex II means that the amplitude is considered in the second sheet, the pole P is much closer to the physical region which corresponds to $s + i\epsilon$, with $\epsilon > 0$. In this way, we disregard the conjugate pole P'. We denote the pole position by $s_P = s_R - i\gamma$ where γ is real an positive. To consider the physical effect of this pole we expand the product

$$h(s) = (s - s_P)\, T_L(s) \tag{3.2}$$

in a power series about the pole position $s = s_P$.

$$h(s) = h(s_P) + (s - s_P)h'(s_P) + ... \tag{3.3}$$

This series converges in the circle centered on s_P that passes through the next nearest singularity of $T_L(s)$, which in the case shown in Fig. 3.1 is the threshold branch point s_1. The circle encloses part of the physical region and for γ small enough we may assume that

$$h(s) \approx h(s_P) \tag{3.4}$$

for physical s near s_R. This approximation leads to the Breit-Wigner resonance formula

$$T_L(s) \approx \frac{h(s_P)}{s - s_R + i\gamma} \tag{3.5}$$

Since,

$$|T_L(s)|^2 = \frac{|h(s_P)|^2}{(E - E_R)^2(E + E_R)^2 + \gamma^2} \approx \frac{1}{4}\,\frac{|h(s_P)|^2/s_R}{(E - E_R)^2 + \Gamma^2/4} \tag{3.6}$$

with

$$\Gamma = \frac{\gamma}{s_R^{1/2}} \tag{3.7}$$

the width of the resonance which corresponds also to the width of the peak at half maximum. Also from (3.5) it is clear that δ_L,

$$\delta_L = \tan^{-1}\frac{\mathrm{Im}\, T_L}{\mathrm{Re}\, T_L} \tag{3.8}$$

passes through an odd multiple of $\frac{\pi}{2}$ as s increases through s_R.

So far we agreed with our original simple resonance picture. However, the fitting of a narrow peak with a Breit-Wigner formula corresponds to the simplest extrapolation from the physical region to the nearby unphysical pole. The extrapolation can be improved by keeping more terms in the expansion of eq. (3.3). These terms correspond to the so called **background** of the resonance. When the background is appreciable the actual observed width of the cross section peak need not be Γ, and the phase shift need not pass through an odd multiple of $\frac{\pi}{2}$ at precisely the resonance energy. This last situation is the corresponding one to the σ resonance in the $\pi\pi$ scattering, see Table 5.1 in **section 5.4**. The width of this resonance is as large as its mass and then there are many terms in eq. (3.3). In fact, while the σ pole is around $500 + i250$ MeV, the $\pi\pi$ phase shifts reach 90^0 around $\sqrt{s} \approx 900$ MeV as can be seen in Fig. 4.5.

Another fact which distorts the simple Breit-Wigner picture is the presence of a close threshold to which the resonance couples strongly. To see how this effect arises let us consider a single two particle channel. Then from eq. (1.31) we see that all the dynamics is contained in the K-matrix. Since the branch point at s_1 is associated to the phase space ρ, which is explicitly separated, the K-matrix does not contain this branching point. On the other hand, the K-matrix contains the unphysical cuts of T_L and the threshold singularities of the other channels with higher threshold. If we used coupled channels, the K-matrix would not have these later singularities. Provided that the unphysical cuts are

sufficiently distant, K^{-1} can be approximated by a few terms of a power series expansion about $s = s_1$.

$$|\vec{p}|^L K^{-1} |\vec{p}|^L = a^{-1} + \frac{1}{2} r \vec{p}^{\,2} + ... \tag{3.9}$$

This is called an **effective range expansion** (e.r.a), with $a/(8\pi\sqrt{s})$ the scattering length and $-8\pi\sqrt{s}\, r$ the effective range. The factor $|\vec{p}|^{2L}$ on the left hand side (L.H.S), allows for the threshold behaviour of T_L. It follows from eqs. (1.31) and (3.9) that the effective range approximation for the amplitude is

$$T_L = \frac{|\vec{p}|^{2L}}{a^{-1} + \frac{1}{2} r \vec{p}^{\,2} + i\rho\, |\vec{p}|^{2L}} \tag{3.10}$$

The resonance situation happens for $a < 0$ and $r > 0$. Indeed let us rewrite the former equation as

$$T_L = \frac{2}{r}\, \frac{|\vec{p}|^{2L}}{\vec{p}^{\,2} - \vec{p}_R{}^2 + i\rho\, |\vec{p}|^{2L}\, 2/r} \tag{3.11}$$

with

$$\vec{p}_R{}^2 = \frac{-2a^{-1}}{r} = \frac{(M_R^2 - (m_1 + m_2)^2)(M_R^2 - (m_1 - m_2)^2)}{4\, M_R^2} \tag{3.12}$$

the square of the c.m. three-momentum of the particles in the mass of the resonance. Solving eq. (3.12) one obtains the resonance mass, M_R. Expanding $\vec{p}^{\,2}$ around $s = M_R^2$ up to order $s - M_R^2$, we have

$$\vec{p}^{\,2} = \vec{p}_R{}^2 + \frac{s - M_R^2}{4\, M_R^4}(M_R^4 - (m_1^2 - m_2^2)^2) + ... \tag{3.13}$$

Substituting this in eq. (3.11), after elementary algebraic manipulations:

$$T_L = \frac{8\, |\vec{p}|^{2L}\, M_R^4/(M_R^4 - (m_1^2 - m_2^2)^2) r}{s - M_R^2 + i\rho\, |\vec{p}|^{2L}\, 8\, M_R^4/(M_R^4 - (m_1^2 - m_2^2)^2) r} \tag{3.14}$$

Comparing with eqs. (3.5) and (3.7) we see that

$$\Gamma(s) = \rho\, |\vec{p}|^{2L}\, 8 M_R^3/(M_R^4 - (m_1^2 - m_2^2)^2) r \tag{3.15}$$

Note that we need $r > 0$ for Γ positive and $a < 0$ to have $\vec{p}_R{}^2$ in eq. (3.12) also greater than zero.

If the resonance is close to threshold the $|\vec{p}|^{2L+1}$ dependence in the width, recall the $|\vec{p}|$ factor in ρ, makes it to be skewed towards higher energies. In particular, note that below threshold $i\rho$ in the former equation, is purely real and negative so that the above equation behaves like a function close to a real pole. But when the threshold is open $i\rho$ is purely imaginary and it behaves like a Breit-Wigner with a width strongly energy dependent.

These aspects where discussed for the $a_0(980)$ resonance in [28]. Note that the former resonance appears very close to the $K\bar{K}$ threshold to which it couples strongly.

In the generation of a resonance from eq. (3.10), we have only required that $a < 0$ and $r > 0$. The dynamical reasons why this actually happens can be very different. Generally speaking, one can distinguish two cases.

A) Presence of a preexisting resonance before unitarization.

As an example, consider the ρ meson. From [7] we can calculate easily the contribution of the $\mathcal{O}(p^2)$ plus the exchange in the s-channel of the ρ meson in the $I = L = 1$ $\pi\pi$ scattering, Fig. 3.2.

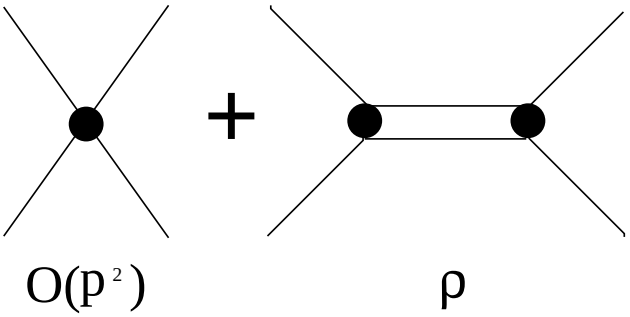

Figure 3.2: Lowest order χPT plus the exchange of the ρ meson in the s-channel.

We can identify the former real contributions as the K-matrix in eq. (1.31). Thus, we have:

$$K = -\frac{2}{3}\frac{\vec{p}^{\,2}}{f_\pi^2} + g_v^2 \frac{2}{3\,f_\pi^2}\frac{s\,\vec{p}^{\,2}}{s - M_\rho^2} \tag{3.16}$$

with $f_\pi = 92.4$ MeV, the pion decay constant and $M_\rho = 770$ MeV, the mass of the ρ meson. The KSFR relation [29] establishes that from vector meson dominance (VMD) and chiral symmetry:

$$g_v^2 \approx 1 \tag{3.17}$$

Then the K-matrix for the former process simplifies to

$$K = \frac{2\,\vec{p}^{\,2}}{3\,f_\pi^2}\frac{M_\rho^2}{s - M_\rho^2} \tag{3.18}$$

Doing an effective range approximation of the former result, one has:

$$\begin{aligned} a^{-1} &= -\frac{3\,f_\pi^2}{2}(1 - \frac{4\,m_\pi^2}{M_\rho^2}) \\ r &= \frac{12\,f_\pi^2}{M_\rho^2} \end{aligned} \tag{3.19}$$

Note that in this case the e.r.a is exact. It is also interesting to see that the χPT value at $\mathcal{O}(p^2)$ for a^{-1} is

$$a^{-1} = -\frac{3\, f_\pi^2}{2} \tag{3.20}$$

Then it receives from the ρ meson a correction of around $\frac{4m_\pi^2}{M_\rho^2} \sim 13\%$. Hence, the χPT series works very well for quantities around the threshold of pions. It is interesting to note that in this case the effective range approximation, eq. (3.10), with the values of eq. (3.19) gives rise to a resonance with a width, which is the preexisting one included in eq. (3.16). Note that if the input resonance disappears(i.e. $M_\rho \to \infty$), it also fades away in the e.r.a. since $r \to 0$.

B) Resonances generated by forces between mesons.

The typical example of application of eq. (3.10) is the deuteron pole below threshold in the $I = L{=}0$ $p - n$ interaction. In this case $a < 0$ but $r < 0$ so that $\vec{p}_R{}^2 < 0$ and hence a bound state appears. This deuteron pole can be well described in terms of one pion exchange between the nucleons. In more general terms, this problem was addressed in [30] arriving to the same conclusion, that is, the deuteron is a bound state not an 'elementary' particle as the nucleons.

We will see in **chapter 5** of the present work, that for the meson-meson scalar sector one can find both types of resonances: preexisting and generated from a given set of forces. In the first case, we will have the first scalar octet around 1.4 GeV and a singlet around 1 GeV and in the second case one has the σ, κ and $a_0(980)$ resonances.

Finally, it is interesting to note that the term proportional to i in the denominator of eq. (3.14), comes from the imaginary part of the diagram given in Fig. 3.3.

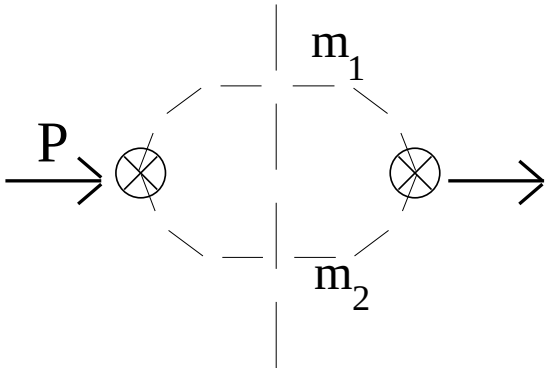

Figure 3.3: Loop function with two meson propagators.

However, this diagram has also a real part which can have great importance in the final mass of the resonance because it dresses the bare mass M_R present in eq. (3.14). These effects have been found to be crucial in the S-wave resonances, see for instance ref. [31, 32]. This is also telling us that unitarity corrections will play an important role in the scalar sector.

Chapter 4

The Inverse Amplitude Method (IAM).

The effective chiral Lagrangian techniques have become a widespread tool to address the problem of the low energy interactions of Goldstone bosons [4, 5]. We have presented in **section 2**, the χPT formalism [4, 5] which is the low energy effective theory of the strong interactions (QCD). Another example is the standard model strongly interacting symmetry breaking sector (SISBS) [33] or the effective chiral Lagrangians in solid-state physics for high-T_c superconductors [34]. In all the cases, the chiral symmetry constraints are a powerful tool to determine the low energy matrix elements in a systematic way.

These Lagrangians consist of an expansion on the powers of the external momenta of the Goldstone bosons over some typical scale, Λ, which is related to the masses of the heavier particles. For instance in χPT, resonances appear for $\sqrt{s} \approx 0.8$ GeV, so that $\Lambda_{\chi PT} \approx 1$ GeV. Of course, when a resonance appears, there is no way to reproduce it form the expansion since it is associated to a pole. Furthermore, as explained in **section 2.2**, there are also higher order corrections, as chiral loops, which make that $\Lambda_{\chi PT} < 4\,\pi\, f_\pi \approx 1.2$ GeV [6]. These facts make that the χPT expansion is typically valid up to energies around 500 GeV. Nevertheless, the constraints imposed by chiral symmetry breaking are rather powerful and not restricted to the region where χPT is meant to converge [35].

Another drawback of the effective chiral theories, is the appearance of a fast increasing number of free parameters (not fixed by the symmetry) as one increases the order of the calculation. At $\mathcal{O}(p^2)$ the χPT Lagrangian only contains the masses of pions, kaons and etas and f_π. At $\mathcal{O}(p^4)$ several new free parameters appear; for instance in χPT there are 12 parameters and in the SISBS one needs 13. At $\mathcal{O}(p^6)$ in χPT there are more than 100 new parameters. That is, the predictive power of the theory is lost as we go higher in order.

Because of the former reasons, nonperturbative schemes become necessary in order to go to higher energies and to maintain the predictive power of the theory.

An attempt to extend the ideas of chiral symmetry to the non-perturbative regime, constructing a unitary T-matrix, is the Inverse Amplitude Method (IAM)[25]. This approach proved efficient in reproducing low energy data and produced poles in the amplitudes asso-

ciated to the ρ and K^* in the vector channel as well as the σ in the scalar one. It has also been applied to study the SISBS resonances that could appear at LHC [36]. Since only elastic unitarity was imposed in the IAM, multichannel problems could not be addressed. As a consequence, neither the f_0 and a_0 resonances, nor the inelasticities could be obtained. A similar problem with coupled channels could also appear in the SISBS if the top quark couples strongly to longitudinal gauge bosons.

The treatment of coupled channels has proved to be crucial in order to reproduce the basic features of the f_0 and a_0 resonances [37, 38] and in general for all the scalar sector with $I = 0, 1, 1/2$ [31].

4.1 The IAM with Coupled Channels.

The generalization of the IAM to coupled channels was given in [26]. The results can be applied to any system whose low energy dynamics is given by effective $\mathcal{O}(p^2)$ and $\mathcal{O}(p^4)$ chiral Lagrangians. The free parameters will be those of the $\mathcal{O}(p^4)$ Lagrangian. The method will be applied to the meson-meson interactions, giving a remarkable agreement with phenomenology as we will see in the next sections. Let us go first with the derivation.

The idea is to exploit eqs. (1.30), (1.31) and (1.32) with the information contained in χPT up to $\mathcal{O}(p^4)$. As it is clear from the former formulas, the dynamical information is contained in the inverse of the partial wave amplitude under consideration, the K-matrix. Furthermore, while the standard χPT series fails close to a resonance pole, the inverse of T_L will have only a **zero**. As a consequence, one might try to calculate the expansion of T_L^{-1}, which will have zeros at the poles of T_L, and in principle does not present convergence problems in this case. Note also that making use of this method, the final partial wave amplitude will be unitary and hence we also reproduce the loop corrections coming from unitarity.

In the following, in order to simplify the notation, we will denote just by T a partial wave amplitude with definite isospin (I) and angular momentum (L).

Expanding T^{-1} in powers of p^2, as one would do for T using χPT, one has:

$$T \simeq T_2 + T_4 + ...$$

$$T^{-1} \simeq T_2^{-1} \cdot [1 + T_4 \cdot T_2^{-1} ...]^{-1} \simeq T_2^{-1} \cdot [1 - T_4 \cdot T_2^{-1} ...] \tag{4.1}$$

where T_2 is lowest order χPT amplitude and T_4 the next to leading one.

This expression requires the inversion of T_2 which might not be invertible, as it happens, for instance in the $(I, L) = (1, 1)$ channel. In order to avoid the use of T_2^{-1} we modify eq. (1.31) by formally multiplying by $T_2 \cdot T_2^{-1}$ on the right and $T_2^{-1} \cdot T_2$ on the left. All the steps are justified using the continuity of the functions involved in the derivation, starting from a matrix close to T_2, which can be inverted. Thus, eq. (1.31) can be rewritten as

$$T = T_2 \cdot [T_2 \cdot \mathrm{Re}\, T^{-1} \cdot T_2 + i T_2 \cdot \rho \cdot T_2]^{-1} \cdot T_2 \tag{4.2}$$

Now, using the expansion for T^{-1} of eq. (4.1) we find

$$T_2 \cdot \mathrm{Re}\, T^{-1} \cdot T_2 \simeq T_2 - \mathrm{Re}\, T_4 + ... \tag{4.3}$$

and recalling that

$$\mathrm{Im}\, T_4 = -T_2 \cdot \rho \cdot T_2 \tag{4.4}$$

we finally obtain, within the $\mathcal{O}(p^4)$ approximation

$$T = T_2 \cdot [T_2 - T_4]^{-1} \cdot T_2 \tag{4.5}$$

From eq. (1.32) and (4.3) we also obtain the expression for the K-matrix

$$K = T_2 \cdot [T_2 - \mathrm{Re}\, T_4]^{-1} \cdot T_2 \tag{4.6}$$

which is very similar to eq. (4.5) but using $\mathrm{Re}\, T_4$ instead of T_4, which appears in the T matrix formula.

Note, as it is clear from eq. (4.2), that what we are expanding is actually $T_2 \cdot \mathrm{Re}\, T^{-1} \cdot T_2$, which is also convergent for low energies.

In another context, the above equation can also be derived using Padé approximants [39]. This equation is a generalization to multiple coupled channels of the IAM of ref. [25]. It makes the method more general and powerful and also allows one to evaluate transition cross sections as well as inelasticities.

The coupled channel result has additional virtues with respect to the single channel IAM. Indeed, in this latter case the expansion of eq. (4.1) is meaningless if $|T_2| < |T_4|$ or $T_2 = 0$ [40]. In particular, if T_2 vanishes, eq. (4.5) yields $T = T_2^2 \cdot T_4^{-1}$, which has a *double* zero, whereas the correct result would be $T \simeq T_4$. This indeed occurs in the $L = 0$ partial waves below threshold (Adler zeros). However, within the coupled channel formalism, if a matrix element, say $(T_2)_{11}$, vanishes, it is sufficient that $(T_2)_{12} \neq 0$, since then eq. (4.5) gives $(T)_{11} \simeq (T_4)_{11}$, which is the correct result. In conclusion, while the single channel IAM gives a *double* zero whenever $T_2 = 0$, the coupled channel method leads to *single* zeros close to the zeros of T_2. Of course, our formalism does not improve the χPT result for partial waves with $L \geq 2$ since T_2 is identically zero for all the channels.

The single channel IAM has another related problem, since close to the Adler zero it presents an spurious pole when $T_2 = T_4$. The coupled channel method also avoids this problem, although it runs into a similar one when the determinant of the $T_2 - T_4$ matrix vanishes below threshold. This happens indeed for $L = 0$, $I = 0$ around $\sqrt{s} \simeq 120$ MeV. Excluding the neighborhood of this zero of the determinant, we can still recover from eq. (4.5) the usual χPT expansion, $T \simeq T_2 + T_4 + ...$ valid for low energies. In any case we concentrate here on results above the two pion threshold.

4.2 The IAM and Vector Meson Dominance (VMD).

Let us consider the example given in **section 3.1.A**. From eq. (3.16) we can calculate T_2 and $\mathrm{Re}\, T_4$. Taking into account that at $\mathcal{O}(p^2)$ and $\mathcal{O}(p^4)$ $T_2 = K_2$ and $\mathrm{Re}\, T_4 = K_4$, where K_2 and K_4 are the $\mathcal{O}(p^2)$ and $\mathcal{O}(p^4)$ terms of the chiral expansion of K, respectively, the results are:

$$\begin{aligned} T_2 &= -\frac{2}{3}\frac{\vec{p}^{\,2}}{f_\pi^2} \\ \mathrm{Re}\, T_4 &= -g_v^2 \frac{2}{3}\frac{\vec{p}^{\,2}}{f_\pi^2}\frac{s}{M_\rho^2} \end{aligned} \tag{4.7}$$

Then, after applying eq. (4.6) one has:

$$K = -\frac{2}{3}\frac{\vec{p}^{\,2}}{f_\pi^2}\frac{M_\rho^2}{M_\rho^2 - g_v^2\, s} \tag{4.8}$$

Chiral Symmetry plus VMD require $g_v^2 = 1$, the well known KSFR relation [29], which gives the coupling of the vector mesons ρ or K^*, in terms of f_π as can be seen from eq. (3.16) for the ρ meson. If this is the case, which phenomenologically is well established, then the reproduction of the vectors mesons ρ or K^* through the IAM is a fact, compare eq. (4.8) with eq. (3.18). This explains the success of the IAM for the vector channels. This close relation among the IAM and VMD was already realized in [41].

However, in a general scenario with g_v^2 very different form 1 one cannot guarantee the applicability of the IAM. This point should be considered when making use of the IAM in other situations beyond QCD, as the ESBS [36].

Note that the IAM has come from an expansion of the inverse of the K-matrix, as was also the case for an e.r.a. eq. (3.9). The difference is that the IAM relies on a chiral expansion in powers of p^2, where p^2 can be a linar combination of masses squared, s, t or u, while the e.r.a. involves powers of $\vec{p}^{\,2}$. On the other hand, the input for the e.r.a., a and r, is experimental while in the IAM the input comes from the chiral Lagrangians of $\mathcal{O}(p^2)$ and $\mathcal{O}(p^4)$.

4.3 Unitarization of $\pi\pi$ and $K\bar{K}$.

In this section we are going to present the results of applying the IAM to the study of the $\pi\pi$ partial wave amplitudes with (I, L)=(0,0), (1,1) and (2,0). The pions couple with the $K\bar{K}$ channel in the waves (0,0) and (1,1), although, as we will see below, this coupling is negligible in the (1,1) case. This study was developed in [42]. However, in this work, instead of the minus sign in front of the T-matrix in eq. (1.13) a plus sign was chosen. Hence, the sign of the T-matrix must be changed when using all the equations above for this section.

In order to apply eq. (4.5) we need the $\mathcal{O}(p^4)$ χPT amplitudes. For $\pi\pi \to \pi\pi$ this calculation was done in [5] for the $SU(2)$ case and extended to $SU(3)$ in [43]. The $\pi\pi \to K\bar{K}$ amplitude can be obtained by crossing from the $K\pi \to K\pi$ one calculated in [43]. However, the $K\bar{K} \to K\bar{K}$ was not calculated before we did it in [42].

In principle, this calculation seems to be unreasonable since the $K\bar{K}$ threshold is almost 1 GeV, and furthermore, for I=0,1 at this energy the $f_0(980), a_0(980)$ resonances appear which couple strongly to the $K\bar{K}$ channel. In fact, after making this $\mathcal{O}(p^4)$ calculation, we will see that, at this energy, the $\mathcal{O}(p^4)$ result is larger than the $\mathcal{O}(p^2)$ one. Obviously, what all this is telling us is that one cannot rely in the perturbative chiral expansion at these energies. This implies that one cannot compare the predictions directly with the experiment, using the $\mathcal{O}(p^2)$ plus $\mathcal{O}(p^4)$ ChPT amplitudes, and hence, one needs to use some nonperturbative method in order to obtain a proper resummation of the χPT series.

4.3.1 The $K\bar{K} \to K\bar{K}$ scattering amplitude at $\mathcal{O}(p^4)$ in χPT.

In order to calculate the $K\bar{K}$ amplitude, one needs to consider two isospin amplitudes, I=0 and 1, which cannot be connected by crossing symmetry because they have different absolute values for the strangeness. This is opposite to what happens in $K\pi$ scattering with $I = 3/2$ and $1/2$.

We calculate the amplitudes $K^+K^- \to K^+K^-$ and $K^+K^- \to K^0\bar{K}^0$ which we denote by T_{cc} and T_{cn} respectively.

The scattering amplitudes with definite isospin $T^{(I)}$ can be written in terms of T_{cc} and T_{cn} in the following way:

$$\begin{aligned} T^{(0)}(s,t,u) = &\quad T_{cc}(s,t,u) + T_{cn}(s,t,u) \\ T^{(1)}(s,t,u) = &\quad T_{cc}(s,t,u) - T_{cn}(s,t,u) \end{aligned} \tag{4.9}$$

We now proceed to describe the calculation scheme for these amplitudes up to $\mathcal{O}(p^4)$.

At lowest order one has the ChPT lagrangian at $\mathcal{O}(p^2)$

$$\mathcal{L}_2 = \frac{f^2}{4} \left\langle \partial_\mu U^\dagger \partial^\mu U + \mathcal{M} \left(U + U^\dagger \right) \right\rangle \tag{4.10}$$

where $\langle\rangle$ stands for the trace of the 3×3 matrices built from $U(\Phi)$ and $\mathcal{M}$,

$$U(\Phi) = \exp\left(\frac{i\sqrt{2}}{f} \Phi \right) \tag{4.11}$$

where Φ is expressed in terms of the Goldstone boson fields as

$$\Phi(x) = \begin{bmatrix} \frac{1}{\sqrt{2}}\pi^0 + \frac{1}{\sqrt{6}}\eta & \pi^+ & K^+ \\ \pi^- & -\frac{1}{\sqrt{2}}\pi^0 + \frac{1}{\sqrt{6}}\eta & K^0 \\ K^- & \bar{K}^0 & -\frac{2}{\sqrt{6}}\eta \end{bmatrix} \tag{4.12}$$

The mass matrix $\mathcal{M}$ is given by

$$\mathcal{M} = \begin{bmatrix} \hat{m}_\pi^2 & 0 & 0 \\ 0 & \hat{m}_\pi^2 & 0 \\ 0 & 0 & 2\hat{m}_K^2 - \hat{m}_\pi^2 \end{bmatrix} \tag{4.13}$$

in the isospin limit. Where $\hat{m}$ means bare masses.

From this lagrangian we can evaluate the lowest order contribution to the $K\bar{K}$ scattering amplitudes

$$\begin{aligned} T_{cc,2}(s,t,u) &= \frac{1}{f^2}\left[\frac{2}{3}\hat{m}_K^2 + \frac{4}{3}m_K^2 - u\right] \\ T_{cn,2}(s,t,u) &= \frac{1}{2f^2}\left[\frac{2}{3}\hat{m}_K^2 + \frac{4}{3}m_K^2 - u\right] \end{aligned} \tag{4.14}$$

where the subindex 2 means $\mathcal{O}(p^2)$.

At $\mathcal{O}(p^2)$ $f \approx f_\pi = 92.4$ MeV and $\hat{m}_K = m_K = 495.7$ MeV. But when we go to next order these equalities do not hold. This is the reason why we keep the distinction between bare and physical masses.

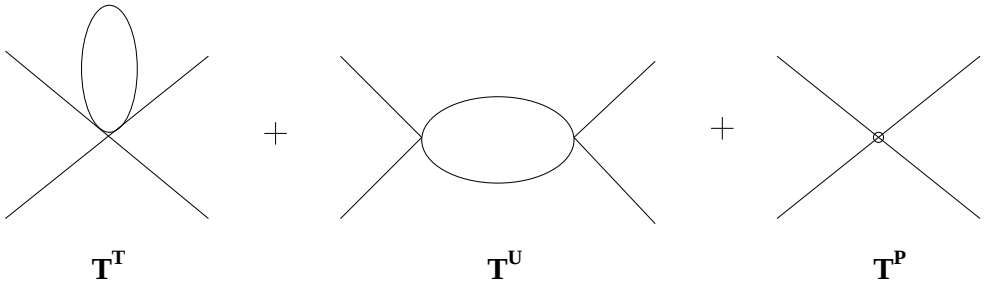

Figure 4.1: Diagrams at $\mathcal{O}(p^4)$

At $\mathcal{O}(p^4)$ one has to calculate the diagrams schematically shown in Fig. 4.1. T_4^T represents contributions coming from the $\mathcal{L}_2$ ChPT lagrangian with six fields and a tadpole loop. The T_4^U represents the loops constructed from the $\mathcal{L}_2$ amplitudes with four fields appearing in the vertices of the loop. We will call this contribution unitarity loops because it makes the amplitude unitary at $\mathcal{O}(p^4)$. These loops include contributions from loops in the s,t and u channels, as shown in Fig. 4.2.

Finally the T_4^P amounts for the $\mathcal{O}(p^4)$ polynomial contribution coming for the $\mathcal{L}_4$ ChPT lagrangian, which can be written as,

$$\begin{aligned} \mathcal{L}_4 = L_1 \left\langle \partial_\mu U^\dagger \partial^\mu U \right\rangle^2 + L_2 \left\langle \partial_\mu U^\dagger \partial_\nu U \right\rangle \left\langle \partial^\mu U^\dagger \partial^\nu U \right\rangle \\ + L_3 \left\langle \partial_\mu U^\dagger \partial^\mu U \partial_\nu U^\dagger \partial^\nu U \right\rangle + L_4 \left\langle \partial_\mu U^\dagger \partial^\mu U \right\rangle \left\langle U^\dagger \mathcal{M} + \mathcal{M}^\dagger U \right\rangle \\ + L_5 \left\langle \partial_\mu U^\dagger \partial^\mu U \left(U^\dagger \mathcal{M} + \mathcal{M}^\dagger U \right) \right\rangle + L_6 \left\langle U^\dagger \mathcal{M} + \mathcal{M}^\dagger U \right\rangle^2 \end{aligned} \tag{4.15}$$

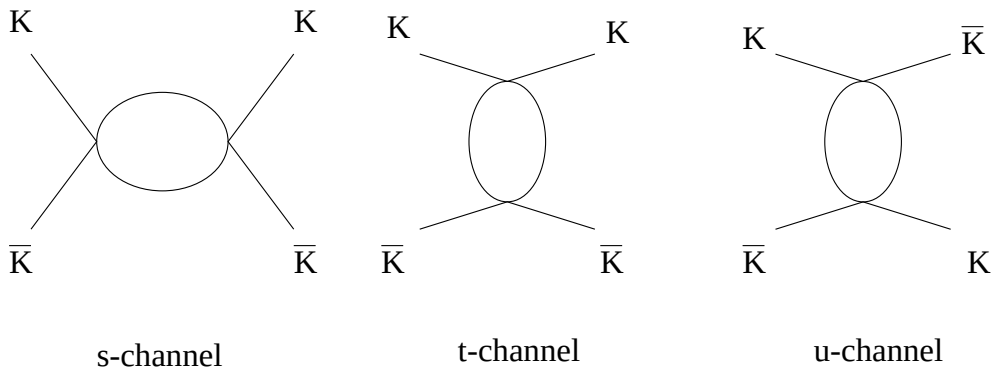

Figure 4.2: Diagrams for the s, t and u channels

$$+L_7 \left\langle U^\dagger \mathcal{M} - \mathcal{M}^\dagger U \right\rangle^2 + L_8 \left\langle \mathcal{M}^\dagger U \mathcal{M}^\dagger U + U^\dagger \mathcal{M} U^\dagger \mathcal{M} \right\rangle$$

When taking into account the wave function renormalization, Fig. 4.3, and the relation between bare and physical masses and decay constants in the lowest order amplitudes, other $\mathcal{O}(p^4)$ contributions appear.

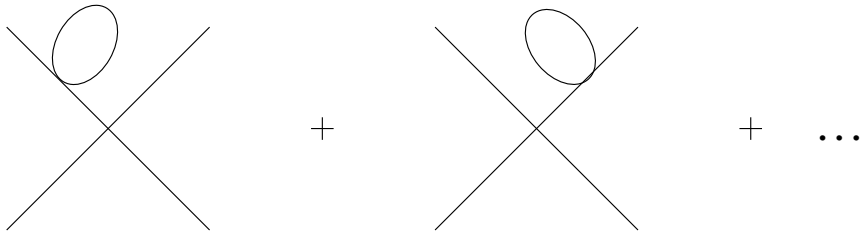

Figure 4.3: Wave function renormalization

The relation between m_K and $\hat{m}_K$ and the one between f and f_π at $\mathcal{O}(p^4)$ can be obtained from [5].

The final amplitude up to next to leading order is then obtained summing all the former contributions. We express it divided in four parts: T_2, T_4^T, T_4^U and T_4^P where the subindices indicate the order in powers of momentum.

In T_4^T and T_4^P we have also included, in addition to the one coming from Fig. 4.1, the $\mathcal{O}(p^4)$ contributions from the renormalization of the wave function, masses and decay constants. The ones with L_i parameters are included in T_4^P and the rest, of tadpole type, in T_4^T.

The amplitude for $K^+K^- \to K^+K^-$ is:

$$T_{cc,2}(s,t,u) = \frac{2m_K^2 - u}{f_\pi^2} \tag{4.16}$$

$$T_{cc,4}^T = \frac{A_\pi^r}{288 f_\pi^4 \pi^2}(8m_K^2 + m_\pi^2 - 3u) + \frac{A_K^r}{288 f_\pi^4 \pi^2}(8m_K^2 + 3u)$$

$$+\frac{A_\eta^r}{288 f_\pi^4\pi^2}(20m_K^2-m_\pi^2-6u) \tag{4.17}$$

$$\begin{aligned}
T^U_{cc,4} &= \frac{-20m_K^4-2s^2-2su+u(3m_\pi^2+u)+m_K^2(8s+11u-4m_\pi^2)}{192 f_\pi^4\pi^2}\\
&+\frac{A_\pi^r}{288 f_\pi^4\pi^2}(13m_K^2-m_\pi^2-6u)+\frac{A_K^r}{576 f_\pi^4\pi^2}(32m_K^2-15u)\\
&+\frac{A_\eta^r}{576 f_\pi^4\pi^2}(22m_K^2+2m_\pi^2-15u)\\
&+\left\{\frac{B_\pi^r(s)}{1536 f_\pi^4\pi^2}\left[8m_K^2(s-4m_\pi^2)+s(7s-4u)+8m_\pi^2(s+2u)\right]\right.\\
&+\frac{B_K^r(s)}{384 f_\pi^4\pi^2}5(8m_K^4+s(s-u)-4m_K^2t)\\
&+\frac{B_\eta^r(s)}{4608 f_\pi^4\pi^2}(8m_K^2-9s)^2\\
&\left.+\frac{B_{\pi\eta}^r(s)}{768 f_\pi^4\pi^2}(4m_K^2-3s)^2+\ \ s\leftrightarrow t\right\}+\frac{B_K^r(u)}{32 f_\pi^4\pi^2}(u-2m_K^2)^2
\end{aligned} \tag{4.18}$$

$$\begin{aligned}
T^P_{cc,4} &= L_1\frac{8}{f_\pi^4}(-8m_K^4+s^2+t^2+4m_K^2u)\\
&+L_2\frac{4}{f_\pi^4}(s^2+t^2+2u^2-4m_K^2u)\\
&+L_3\frac{4}{f_\pi^4}(-8m_K^4+s^2+t^2+4m_K^2u)\\
&-L_4\frac{16m_K^2u}{f_\pi^4}-L_5\frac{8m_K^2u}{f_\pi^4}+(2L_6+L_8)\frac{32m_K^4}{f_\pi^4}
\end{aligned} \tag{4.19}$$

The amplitude for $K^+K^-\to K^0\bar{K}^0$ is

$$T_{cn,2}=\frac{2m_K^2-u}{2f_\pi^2} \tag{4.20}$$

$$\begin{aligned}
T^T_{cn,4} &= \frac{A_\pi^r}{576 f_\pi^4\pi^2}(-4m_K^2+m_\pi^2+6t)+\frac{A_K^r}{288 f_\pi^4\pi^2}(10m_K^2-3t)\\
&+\frac{A_\eta^r}{576 f_\pi^4\pi^2}(20m_K^2-m_\pi^2-6u)
\end{aligned} \tag{4.21}$$

$$T^U_{cn,4} = \frac{24m_K^4-6m_\pi^2s-2s^2-2su+u^2+2m_K^2(4m_\pi^2-7t)}{384 f_\pi^4\pi^2}$$

$$
\begin{aligned}
&+\frac{A_\pi^r}{1152 f_\pi^4\pi^2}(38m_K^2-2m_\pi^2-6s-15u)\\
&+\frac{A_K^r}{576 f_\pi^4\pi^2}(10m_K^2+3s-6u)+\frac{A_\eta^r}{1152 f_\pi^4\pi^2}(22m_K^2+2m_\pi^2-15u)\\
&+\frac{B_\pi^r(s)}{1536 f_\pi^4\pi^2}(8m_K^2(s-4m_\pi^2)+s(7s-4t)+8m_\pi^2(s+2t))\\
&+\frac{B_\pi^r(t)}{384 f_\pi^4\pi^2}(s-u)(t-4m_\pi^2)+\frac{B_K^r(s)}{96 f_\pi^4\pi^2}(-8m_K^2+s(s-u)+4m_K^2(s+u))\\
&+\frac{B_K^r(t)}{384 f_\pi^4\pi^2}(-8m_K^2+t(t-u)+4m_K^2(t+u))+\frac{B_K^r(u)}{64 f_\pi^4\pi^2}(u-2m_K^2)^2\\
&+\frac{B_\eta^r(s)}{4608 f_\pi^4\pi^2}(8m_K^2-9s)^2-\frac{B_{\pi\eta}^r(s)}{768 f_\pi^4\pi^2}(3s-4m_K^2)^2\\
&+\frac{B_{\pi\eta}^r(t)}{384 f_\pi^4\pi^2}(3t-4m_K^2)^2
\end{aligned}
\tag{4.22}
$$

$$
\begin{aligned}
T_{cn,4}^P &= L_1\frac{8}{f_\pi^4}(s-2m_K^2)^2\\
&+L_2\frac{4}{f_\pi^4}(-8m_K^4+t^2+u^2+4m_K^2 s)\\
&+L_3\frac{2}{f_\pi^4}(-8m_K^4+s^2+t^2+4m_K^2 u)\\
&+L_4\frac{4}{3f_\pi^4}(-24m_K^4+12m_K^2 s)-L_5\frac{4m_K^2 u}{f_\pi^4}\\
&+(2L_6+L_8)\frac{16m_K^4}{f_\pi^4}
\end{aligned}
\tag{4.23}
$$

In the above formulas we have used the quantities

$$
A_P^r=-m_P^2\left[-1+\ln\left(\frac{m_P^2}{\mu^2}\right)\right] \tag{4.24}
$$

$$
\begin{aligned}
B_{PQ}^r(s) &= \frac{\lambda^{1/2}(s,m_P^2,m_Q^2)}{2s}\ln\left(\frac{m_P^2+m_Q^2-s+\lambda^{1/2}(s,m_P^2,m_Q^2)}{m_P^2+m_Q^2-s-\lambda^{1/2}(s,m_P^2,m_Q^2)}\right)\\
&+2-\ln\left(\frac{m_Q^2}{\mu^2}\right)+\frac{m_P^2-m_Q^2+s}{2s}\ln\left(\frac{m_Q^2}{m_P^2}\right)
\end{aligned}
\tag{4.25}
$$

In the equal mass limit (4.25) reduces to

$$
B_P^r(s)=2-\ln\left(\frac{m_P^2}{\mu^2}\right)-\sigma(m_P^2,s)\ln\left(\frac{\sigma(m_P^2,s)+1}{\sigma(m_P^2,s)-1}\right) \tag{4.26}
$$

where

$$\begin{aligned}\lambda(s,m_P^2,m_Q^2) &= [s-(m_P+m_Q)^2][s-(m_P-m_Q)^2]\\ \sigma(m_P^2,s) &= \sqrt{1-\frac{4m_P^2}{s}}\end{aligned} \tag{4.27}$$

The functions (4.24) and (4.25) come from the Passarino-Veltman integrals with one and two propagators [44].

It is interesting to note that L_7 does not appear in T_4^P. This also happens in $\pi\pi\to\pi\pi$ and $K\pi\to K\pi$ $\mathcal{O}(p^4)$ scattering amplitudes. L_6 and L_8 appear in the combination $2L_6+L_8$ as a consequence of the Kaplan and Manohar symmetry [45].

As it was stated before, the corrections coming from the $\mathcal{O}(p^4)$ calculation are, at least, as large as the lowest order contribution itself. For example in the $K\bar{K}$ threshold:

$$T_{cc,2} = 56.5$$
$$T_{cc,4} = 73.6 + i\,36.74$$

Unambiguously this means that a perturbative calculation is useless in this region and that some non perturbative scheme should be used in order to compare with the experimental phenomenology.

4.3.2 Results: Fit, Phase Shifts and Inelasticities.

Once, we have calculated the $\mathcal{O}(p^4)$ χPT amplitude and using the elastic $\pi\pi$ and $K\pi$ ones, given in [43] we can now apply eq. (4.5). Taking into account the normalization introduced in eq. (1.41), we will have $\alpha=2$ for $\pi\pi\to\pi\pi$, $\alpha=1$ for $\pi\pi\to K\bar{K}$ and $\alpha=0$ for $K\bar{K}\to K\bar{K}$.

With this normalization, for the different (I,L) partial waves amplitudes, unitarity reads, from eq. (1.26)

For (I,L)=(0,0)

$$4m_\pi^2 < s < 4m_K^2: \qquad \mathrm{Im}\,T_{11} = \rho(m_\pi^2,s)\,|T_{11}|^2 \tag{4.28}$$

$$\begin{aligned}4m_K^2 < s < 4m_\eta^2: \qquad \mathrm{Im}\,T_{12} &= \rho(m_\pi^2,s)\,T_{11}T_{12}^* + \rho(m_K^2,s)\,T_{12}T_{22}^*\\ \mathrm{Im}\,T_{22} &= \rho(m_\pi^2,s)\,|T_{12}|^2 + \rho(m_K^2,s)\,|T_{22}|^2\\ \mathrm{Im}\,T_{11} &= \rho(m_\pi^2,s)\,|T_{11}|^2 + \rho(m_K^2,s)\,|T_{12}|^2\end{aligned} \tag{4.29}$$

For (I,L)=(1,1)

$$4m_\pi^2 < s < 4m_K^2: \qquad \mathrm{Im}\,T_{11} = \rho(m_\pi^2,s)\,|T_{11}|^2 \tag{4.30}$$

$$\begin{aligned}4m_K^2 < s: \qquad \mathrm{Im}\,T_{12} &= \rho(m_\pi^2,s)\,T_{11}T_{12}^* + \rho(m_K^2,s)\,T_{12}T_{22}^*\\ \mathrm{Im}\,T_{22} &= \rho(m_\pi^2,s)\,|T_{12}|^2 + \rho(m_K^2,s)\,|T_{22}|^2\\ \mathrm{Im}\,T_{11} &= \rho(m_\pi^2,s)\,|T_{11}|^2 + \rho(m_K^2,s)\,|T_{12}|^2\end{aligned} \tag{4.31}$$

And for (I, L)=(2,0)

$$4m_\pi^2 < s: \qquad \mathrm{Im}\, T_{11} = \rho(m_\pi^2, s)\, |T_{11}|^2 \tag{4.32}$$

with $\rho(m^2, s)$ given by eq. (1.28), where m is the mass of the particle to be used in evaluating the three-momentum in this equation.

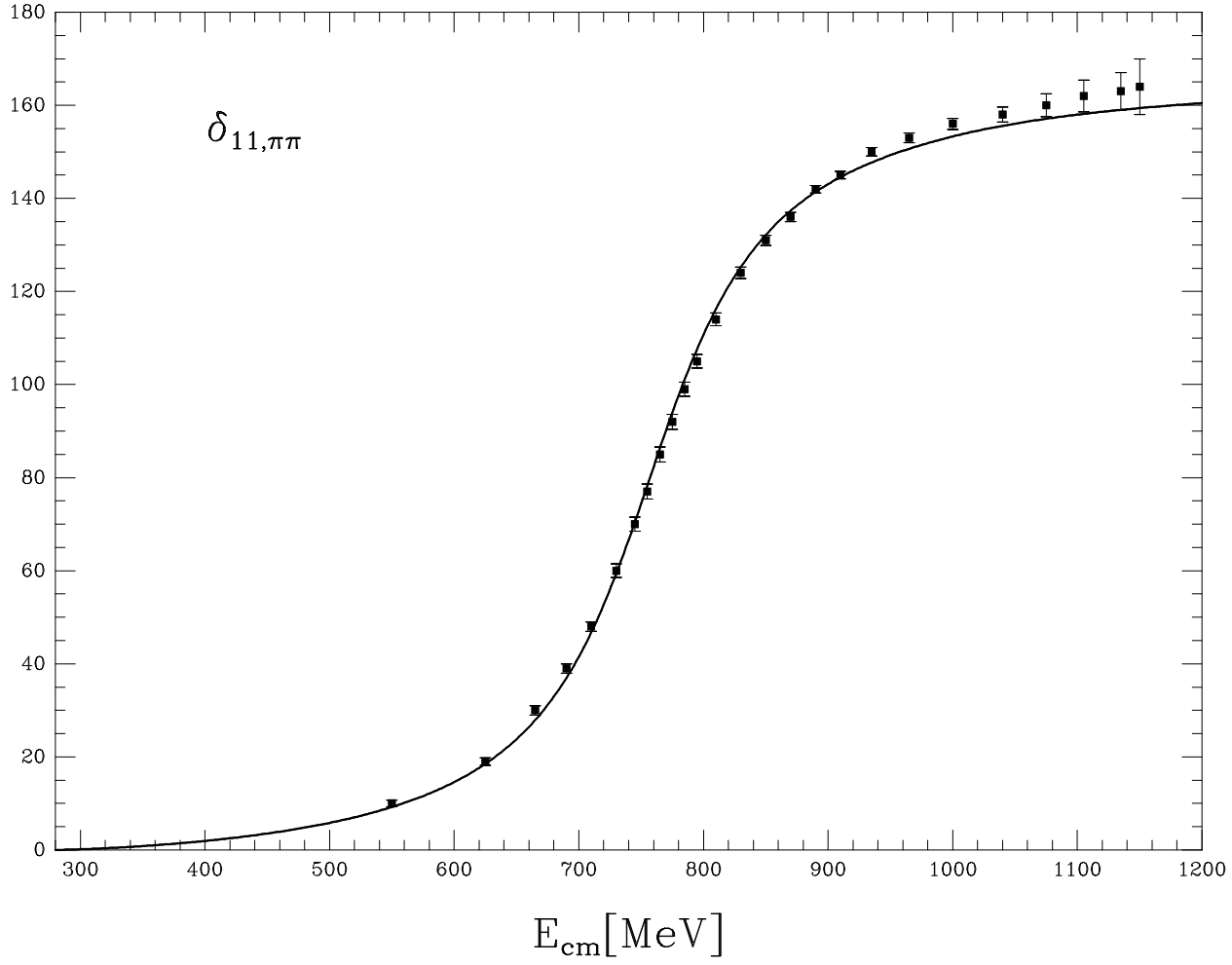

Figure 4.4: Phase shift for $\pi\pi \to \pi\pi$ in $I = L = 1$. Data: [50].

In deriving (4.5) one was concerned essentially with the right hand cut, responsible for unitarity in the corresponding channel. As a result, the imaginary part of the amplitudes to be used in (4.5), above the lightest threshold (in our case the $\pi\pi$ one, $s = 4m_\pi^2$) and below the highest one ($s = 4m_K^2$), was restricted to come only from unitarity, (4.29), neglecting the left hand cut contribution to the imaginary part that appears in $T_{cc,4}$ and $T_{cn,4}$ for $s < 4m_K^2 - 4m_\pi^2$. However, we have maintained the left hand cut contribution to the imaginary part of $T_{cc,4}$ and $T_{cn,4}$ below the $K\bar{K}$ threshold. One way to see how large is the resulting deviation from unitarity is to check the value of the inelasticity in the energy

region $4m_\pi^2 < s < 4m_K^2$ for (I,L)= (0,0) and (1,1) where two channels appear. In both cases the deviation from 1 is smaller than 1%.

The $\eta\eta$ intermediate state has been included in the $\mathcal{O}(p^4)$ ChPT amplitudes. However, for the (0,0) channel for $\sqrt{s} > 2m_\eta$ this state gives further contribution to the imaginary part of our amplitudes in addition to the one expressed in (4.29). This means that eq. (4.5) with only the $\pi\pi$ and $K\overline{K}$ states does not fulfill unitarity strictly for $\sqrt{s} > 2m_\eta \simeq$ 1.1 GeV. The influence of the $\eta\eta$ state is particularly significative in the $K\overline{K} \to \pi\pi$ S-wave phase shifts, Fig. 4.6. We will come back to this point later.

From eqs. (1.36) and (1.40) we obtain the phase shifts for $\pi\pi \to \pi\pi$ (δ_1) and $\pi\pi \to K\bar{K}$ ($\delta_1 + \delta_2$) for $(I,L) = (0,0)$ and $(1,1)$. For (I,L)=(2,0) only the $\pi\pi$ channel is necessary, when omitting multipion states. In this case, it is sufficient to take eq. (1.39) with $\eta = 1$.

In ChPT the experimental values for the L_i coefficients come from $\mathcal{O}(p^4)$ fits to low energy experimental data. Here we fit the L_i constants to experiment in a much broader energy interval and with an expression valid to all orders. Hence, differences are expected between our fitted L_i parameters and the values quoted from ChPT.

Furthermore, our approach is not cross symmetric. This implies that contributions from the left hand cut of order higher than $\mathcal{O}(p^4)$ are effectively reabsorbed in the values of our L_i coefficients. This point has been studied in [40] with the conclusion that the value of the L_i obtained from a non cross symmetric method are influenced by this reabsorption procedure of the left hand cut. In this way, the value we quote for our L_i constants has to be taken with care when comparing with the values of the L_i from ChPT.

We have used simultaneously the phase shifts of the $\pi\pi \to \pi\pi$ with $I = 0$ and 1, Figs. 4.4 and 4.5, to fit the value of our free parameters: L_1, L_2, L_3, L_4, L_5 and $2L_6 + L_8$. The fit has been done using MINUIT. In the energy region $\sqrt{s} =$ 500-950 MeV the data from different experiments for S-wave $\pi\pi$ phase shifts are incompatible. Given that situation, we have taken as central value for each energy the mean value between the different experimental results [44–48]. For $\sqrt{s} =$ 0.95-1 GeV, the mean value comes from [47, 49]. In both cases the error is the maximum between the experimental errors and the largest distance between the experimental points and the average value.

The quoted errors in the value we have obtained for the L_i coefficients is just the statistical one.

The fit is pretty good, as can be seen in Figs. 4.4 and 4.5, with a $\chi^2 = 1.3$ per degree of freedom. The values we obtain at the M_ρ scale and in units of 10^{-3} are

$$\begin{aligned} L_1 &= 0.72^{+0.03}_{-0.02} \\ L_2 &= 1.36^{+0.02}_{-0.05} \\ L_3 &= -3.24 \pm 0.04 \\ L_4 &= 0.20 \pm 0.10 \\ L_5 &= 0.0^{+0.8}_{-0.4} \\ 2L_6 + L_8 &= 0.00^{+0.26}_{-0.20} \end{aligned} \tag{4.33}$$

The small errors for L_1, L_2 and L_3 are due to the strong constraints imposed by the small

errors in the experimental data of the $\delta_{11,\pi\pi}$ phase shift, Fig. 4.4.

The values of ChPT are

$$\begin{aligned} L_1 &= 0.4 \pm 0.3 \\ L_2 &= 1.4 \pm 0.3 \\ L_3 &= -3.5 \pm 1.1 \\ L_4 &= -0.3 \pm 0.5 \\ L_5 &= 1.4 \pm 0.5 \\ 2L_6 + L_8 &= 0.5 \pm 0.7 \end{aligned} \tag{4.34}$$

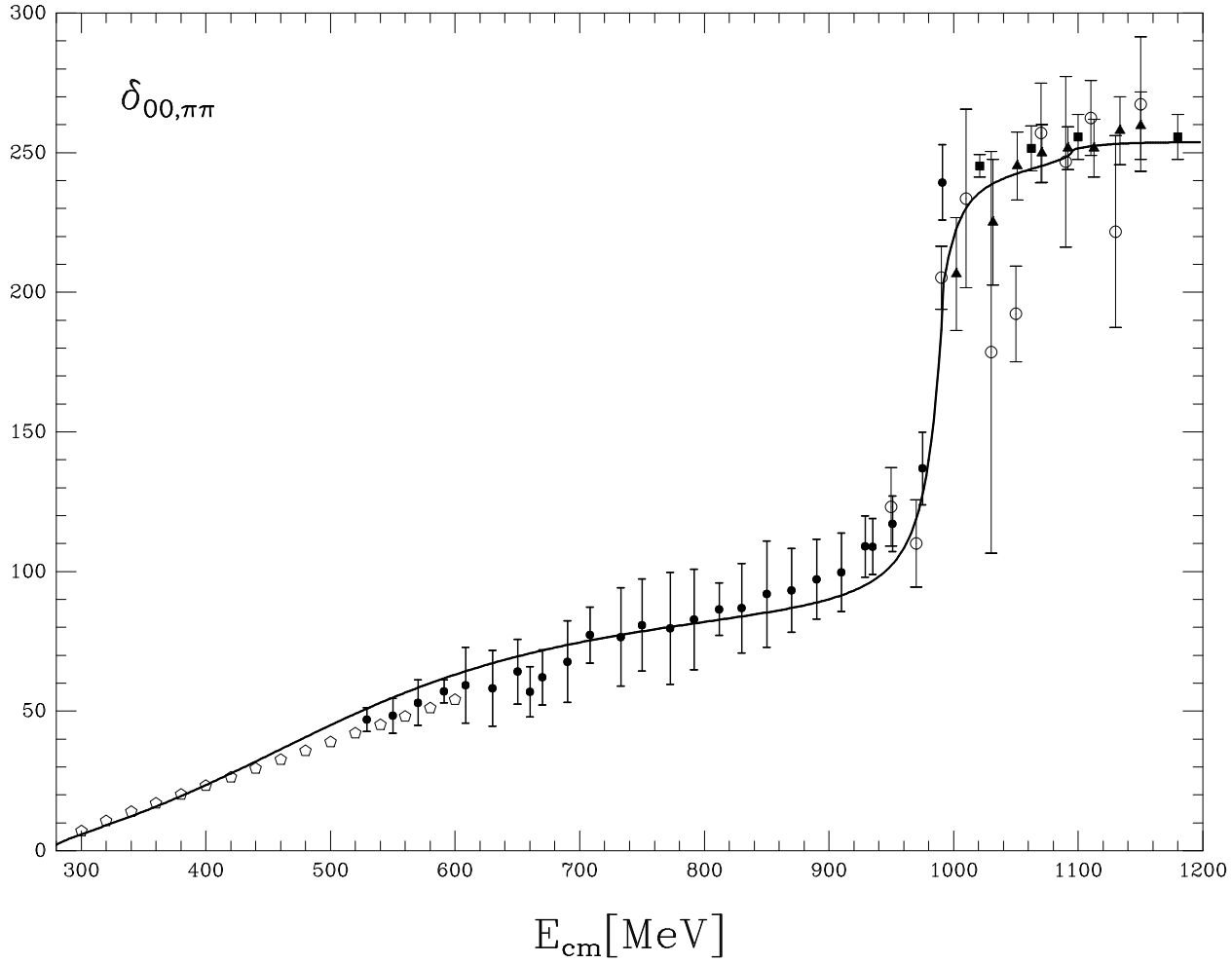

Figure 4.5: Phase shift for $\pi\pi \to \pi\pi$ in $I = L = 0$. Data: Empty pentagon [51]; empty circle [46]; full square [49]; full triangle [47]; full circle represents the average explained above.

We can see that our values, taking errors into account, are compatible with those from ChPT, and then we can guarantee a good behaviour at low energies for our predictions.

Using these values for L_i we also describe correctly phase shifts, scattering lengths and form factors for the $I = L = 0$ and $I = L = 1$ channels, as we will see later.

In Fig. 4.4 we show our fitted δ_1 for $I = L = 1$, from the two pion threshold up to 1.2 GeV and we see a good agreement with the experimental data which are dominated by the presence of the $\rho(770)$ that we reproduce nicely. In this channel we obtain that the influence of the $K\bar{K}$ channel coupled to $\pi\pi$ is negligible.

In Fig. 4.5 we show δ_1 for $I = L = 0$, also from two pion threshold to 1.2 GeV. The agreement with experiment is quite satisfactory showing clearly the presence of the $f_0(980)$ resonance as a strong jump in the phase shift around 1 GeV. To get this resonance it is essential to include the kaons, and then to unitarize with coupled channel as we do. In this figure we also have plotted data from [51], but since no error is quoted we have not included this data in the fit.

Now, once we have fixed the L_i from the fit we predict other magnitudes.

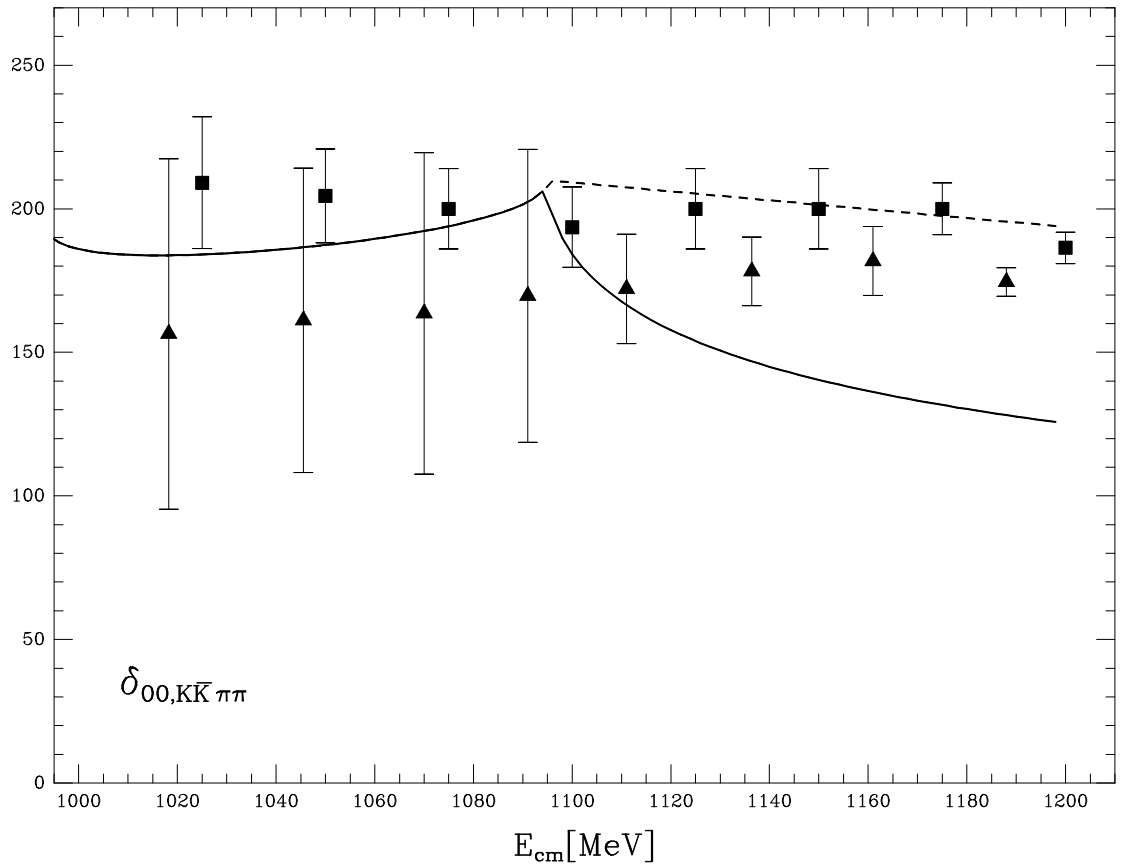

Figure 4.6: Phase shift for $\pi\pi \to K\bar{K}$ in $I = L = 0$. Data: full square [52], full triangle [53].

In Fig. 4.6 the phase shift for the $K\bar{K} \to \pi\pi$ scattering, $\delta_1 + \delta_2$, is shown for $I = L = 0$.

In this figure one sees clearly the $\eta\eta$ threshold. This process is the most sensible to the $\eta\eta$ intermediate state, contrary to what happens with the $\pi\pi$ phase shifts, Fig. 4.5, where its inclusion is almost negligible. One way to realize the influence of this channel in the former phase shifts is to cancel the imaginary part to T_4 coming from the intermediate $\eta\eta$ s-channel loop for $\sqrt{s} > 2m_\eta \simeq 1.1$ GeV. In this way the dashed line curve in Fig. 4.6 is obtained, which agrees very well with data. This is telling us that the inclusion of the $\eta\eta$ channel in the unitarization procedure for the (0,0) channel is important for studying the $K\bar{K} \to \pi\pi$ scattering. In any case, as explained above, the threshold is very close to 1.2 GeV where other intermediate states, as four pions, are also important and should be included as well. Hence, we think that the inclusion of the $\eta\eta$ threshold in eq. (4.5) should be done when going to higher energy, that is, when extending the model for energies higher than 1.2 GeV.

In Fig. 4.7, $(1-(\eta_{00})^2)/4$ is shown. Our results display the same tendency as the experimental data, particularly when taking into account the large experimental errors.

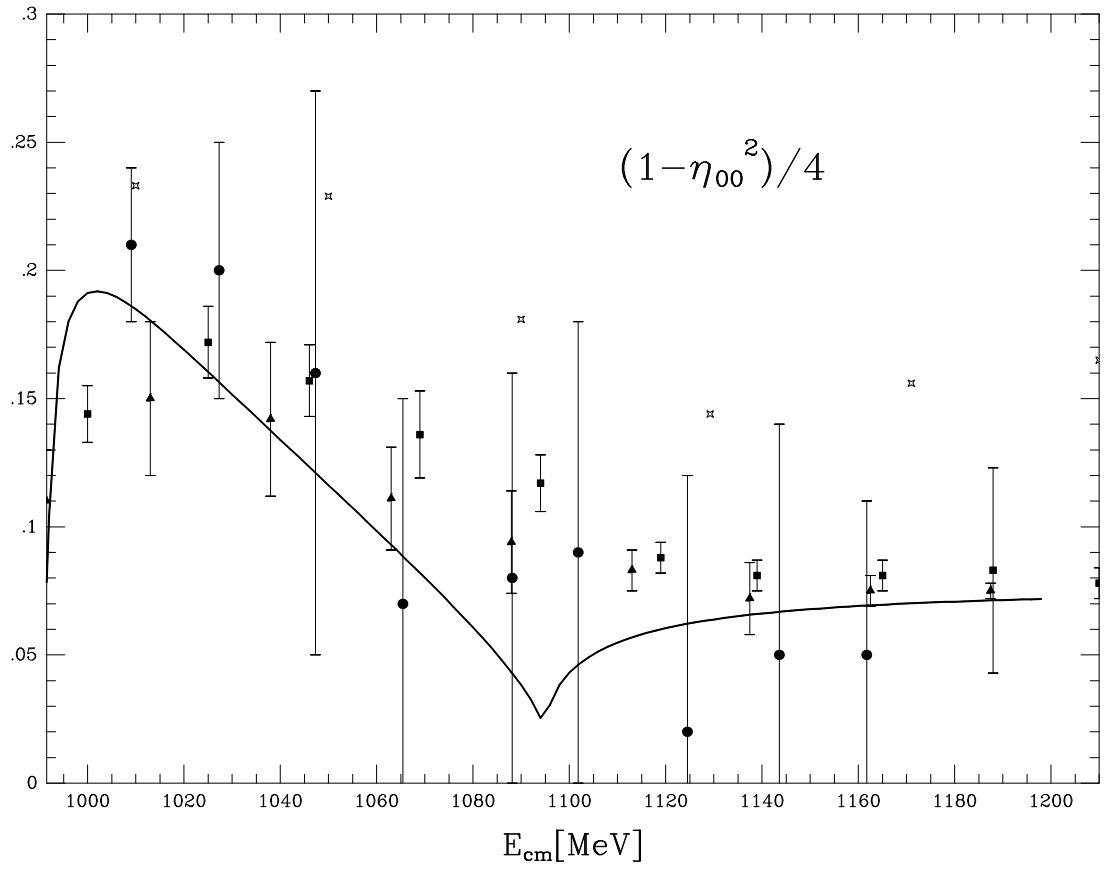

Figure 4.7: $(1-(\eta_{00})^2)/4$, where η_{00} is the inelasticity in $I = L = 0$. Data: starred square [51], full square [52], full triangle [53], full circle [54].

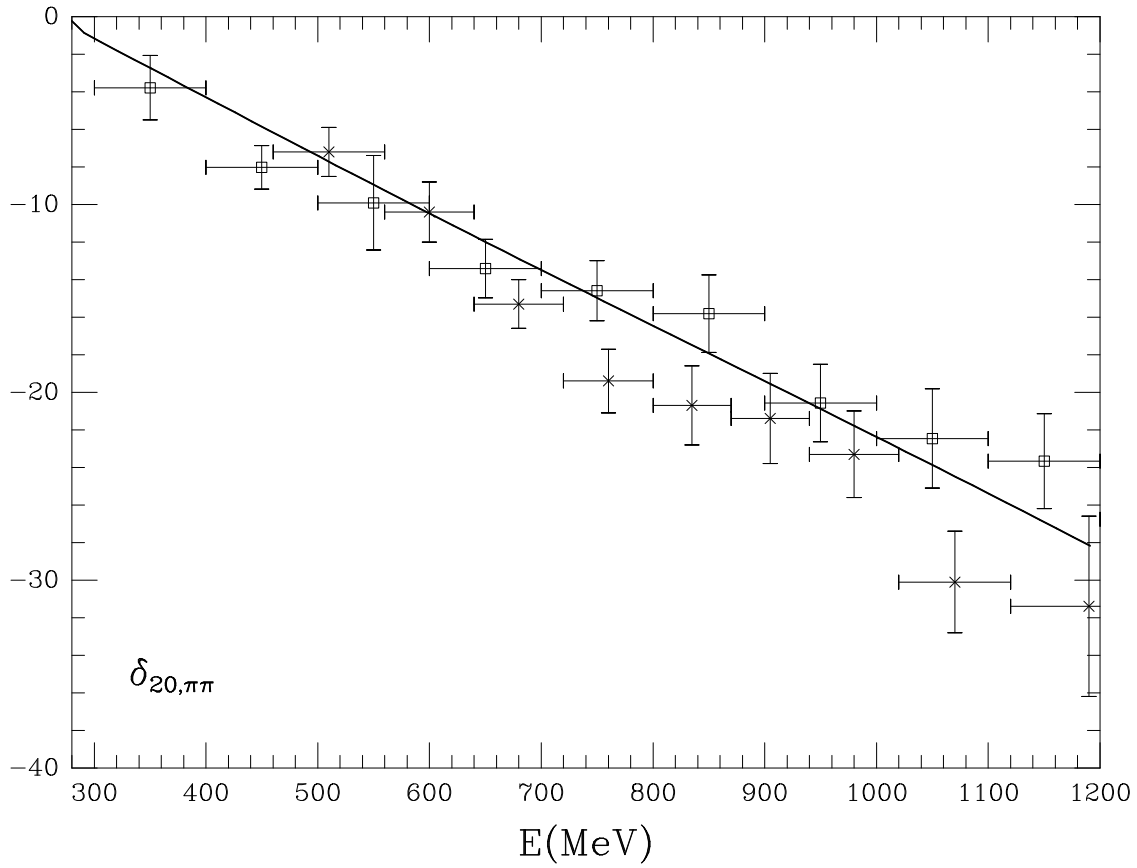

Figure 4.8: Phase shift for $\pi\pi \to \pi\pi$ in $I = 2, L = 0$. Data: cross [55], empty square [56].

In Fig. 4.8 we show the $\pi\pi$ phase shift with I=2, L=0. The agreement with experimental data is fair. Contrary to the other channels that we have shown, in this case no resonances appear and there is only the $\pi\pi$ channel. So, in this case our result (apart of differences on the L_i values) is the same than in the IAM [25].

We have also calculated the scattering lengths for the three channels unitarized in this work, (I, L)=(0,0), (1,1) and (2,0). We denote them by a_L^I. In Table 4.1 we show the value we obtain for a_L^I together with the experimental and the ChPT values to $\mathcal{O}(p^4)$. We see in this table that a good agreement with experiment is accomplished. Our values are also close to the ones from ChPT as one should expect because for low energies we recover the chiral expansion.

4.4 Two-meson scattering below 1.2 GeV.

In the former section the IAM with coupled channels was applied with the full $\mathcal{O}(p^4)$ χPT amplitudes. This calculation is rather involved and it is not done in all two-meson

Table 4.1: Comparison of scattering lengths in different channels

a_L^I	ChPT	Our results	Experiment
a_0^0	0.20 ± 0.01	0.210 ± 0.002	0.26 ± 0.05
a_1^1	0.037 ± 0.002	0.0356 ± 0.0008	0.038 ± 0.002
a_0^2	-0.041 ± 0.004	-0.040 ± 0.001	-0.028 ± 0.012

channels, for instance, in those channels with the η meson. In this section, following the work done in ref. [57], we are going to present an approximation to calculate the full $\mathcal{O}(p^4)$ amplitude which turns out to be technically much simpler and rather accurate at the phenomenological level. We also come back to the sign of the T-matrix given in eq. (1.13)

In **section 4.2** and in the former one, we have already seen the tight relation between the vector mesons and the counterterms present in the $\mathcal{O}(p^4)$ chiral Lagrangian, and how the vector resonances can be reproduced from the $\mathcal{O}(p^4)$ χPT Lagrangian through the IAM due to VMD. This is complementary to what we have commented in **section 2.3** with respect to ref. [7], where they show the chiral version of VMD, that is, those L_i to which vector resonances contribute are saturated by such contributions.

For the scalar sector it is not phenomenologically clear if a Scalar Meson Dominance exists nor to which states should be applied. In fact, in the following chapters we will try to address this problem. There, **sections 5.2** and **5.4**, we will see that the unitarization of the lowest order χPT amplitudes in this sector is an extremely important contribution.

We can take into account both factors, counterterms for the vectors channels and unitarity of the $\mathcal{O}(p^2)$ for the scalar ones, by approximating the $\mathcal{O}(p^4)$ χPT amplitude as:

$$\text{Re } T_4 \simeq T_4^P + T_2 \cdot \text{Re } G(s) \cdot T_2 \tag{4.35}$$

where T_2 is the lowest order χPT amplitude, T_4^P is the polynomial tree level contribution from the $\mathcal{O}(p^4)$ Lagrangian and $G(s)$ is a diagonal matrix corresponding to the loop integral with two meson propagators, given by:

$$G_{nn}(s) = i \int \frac{d^4q}{(2\pi)^4} \frac{1}{q^2 - m_{1n}^2 + i\epsilon} \frac{1}{(P-q)^2 - m_{2n}^2 + i\epsilon} \tag{4.36}$$

where P is the total initial four-momentum of the two meson system. This G matrix has the property

$$\text{Im } G_{nn}(s) = -\rho_{nn}(s) \tag{4.37}$$

as can be easily checked.

The real part of $G(s)$ is divergent and requires regularization. We evaluate it making use of a cut-off regularization with a maximum value, q_{max}, for the modulus of the three-

momentum in the integral. An analytical expression for $G_{nn}(s)$ is given in Appendix A, where we also connect with the Dimensional Regularization Scheme.

The K-matrix corresponding to eq. (4.35) follows immediately from eq. (4.6)

$$K = T_2 \cdot [T_2 - T_4^P - T_2 \cdot \mathrm{Re}\, G \cdot T_2]^{-1} \cdot T_2 \tag{4.38}$$

The polynomial T_4^P is given in terms of the L_i coefficients of the $\mathcal{O}(p^4)$ Lagrangian. Within our approach, these coefficients will be fitted to data and denoted by $\hat{L}_i$ since they do not have to coincide with those used in χPT, as we shall see. Actually, the L_i coefficients depend on a regularization scale (μ). In our scheme this scale dependence appears through the cut-off.

In addition, there are also differences between our renormalization scheme and that of standard χPT. Indeed, our approach considers the iteration of loop diagrams in the s-channel, but neglects loops in the u or t channels. However, the smooth structure of these terms for the physical s-channel, since we are far away from the associated singularities, allows them to be approximately reabsorbed when fitting the $\hat{L}_i$ coefficients. Concerning tadpoles, they would be exactly reabsorbed in the $\hat{L}_i$ in the equal mass case. Therefore, when masses are different, we are omitting terms proportional to differences between the actual masses squared and an average mass squared. In fact, in eq. (4.35) we have factorized out of the loop integral the vertices T_2 with their on-shell value. In doing this, see ref. [58] and **section 4.2**, we are also neglecting tadpole contributions which always go to renormalize physical masses and couplings of the lowest order amplitude, when calculating such tadpoles terms at next to leading order. Thus, all these contributions will make the $\hat{L}_i$ differ from the L_i, although we expect them to be of the same order.

This way of dealing with tadpoles has an additional advantage. Apart from the usual tadpole diagrams that would also appear in standard χPT there are some additional tadpole terms. They come from the determinant of the $SU(3)$ metric that should be included in the path integral measure in order to make the generating functional $SU(3)$ covariant [59]. With dimensional regularization such contributions vanish, but that is not the case when using a cutoff regularization [60]. Nevertheless, we have just described how tadpoles are absorbed within our approximation and thus we do not have to calculate them.

With these approximations our calculations have been considerably simplified at the expense of losing some precision at low energies with respect to the full $\mathcal{O}(p^4)$ χPT calculation. As far as we are mostly interested in resonance behavior as well as higher energies this is not very relevant. Nevertheless, if the complete $\mathcal{O}(p^4)$ calculations were available, we could directly use eq. (4.5), and have both an accurate low energy description and a good coupled channel unitarity behavior, as we have already done in the former section.

Using eq. (4.5), the formula for the T matrix in this section is given by

$$T = T_2 \cdot [T_2 - T_4^P - T_2 \cdot G \cdot T_2]^{-1} \cdot T_2 \tag{4.39}$$

The calculation of T_2 and T_4^P is done making use of the Lagrangians $\mathcal{L}_2$ and $\mathcal{L}_4$ given in **section 4.3.1**.

The states with definite isospin, with the phases $|\pi^+\rangle = -|1,1\rangle$, $|K^-\rangle = -|1/2\,-1/2\rangle$, are given by

$$\mathbf{I=0},$$
$$|K\bar{K}\rangle = -\frac{1}{\sqrt{2}}|K^+(\vec{q})K^-(-\vec{q}) + K^0(\vec{q})\bar{K}^{\,0}(-\vec{q})\rangle$$
$$|\pi\pi\rangle = -\frac{1}{\sqrt{3}}|\pi^+(\vec{q})\pi^-(-\vec{q}) + \pi^-(\vec{q})\pi^+(-\vec{q}) + \pi^0(\vec{q})\pi^0(-\vec{q})\rangle$$

$$\mathbf{I=1, I_3=0},$$
$$|K\bar{K}\rangle = -\frac{1}{\sqrt{2}}|K^+(\vec{q})K^-(-\vec{q}) - K^0(\vec{q})\bar{K}^{\,0}(-\vec{q})\rangle$$
$$|\pi\eta\rangle = |\pi^0(\vec{q})\eta(-\vec{q})\rangle$$
$$|\pi\pi\rangle = -\frac{1}{\sqrt{2}}|\pi^+(\vec{q})\pi^-(-\vec{q}) - \pi^-(\vec{q})\pi^+(-\vec{q})\rangle$$

$$\mathbf{I=2, I_3=2},$$
$$|\pi\pi\rangle = |\pi^+(\vec{q})\pi^+(-\vec{q})\rangle$$

$$\mathbf{I=1/2, I_3=1/2},$$
$$|K\pi\rangle = -|\frac{\sqrt{2}}{3}\pi^+(\vec{q})K^0(-\vec{q}) + \frac{1}{\sqrt{3}}\pi^0(\vec{q})K^+(-\vec{q})\rangle$$
$$|K\eta\rangle = |K^+(\vec{q})\eta(-\vec{q})\rangle$$

$$I=3/2, I_3=3/2,$$
$$|K\pi\rangle = -|K^+(\vec{q})\pi^+(-\vec{q})\rangle$$

The resulting amplitudes which we obtain are compiled in Appendix B.

4.4.1 Results

We have carried out a fit to the data, which is shown in Figs. 4.9 to 4.16, using as free parameters the $\hat{L}_i$ with $i = 1,2,3,4,5,7$ and $2\hat{L}_6 + \hat{L}_8$. In Table 4.2 the different channels which appear in each partial wave amplitude are shown. The cut-off is fixed to $q_{max} = 1.02$ GeV. The values that we obtain for the $\hat{L}_i$ are shown in Table 4.3 (after Fig. 4.16). We compare them with the standard values for the L_i coefficients obtained in χPT at the scale $\mu = 2\,q_{max}/\sqrt{e}$ (see appendix A.2) and we see that they are of the same order.

Table 4.2: Channels used in the different I, J channels

	I=0	I=1/2	I=1	I=3/2	I=2
J=0	$\pi\pi$ $K\bar{K}$	$K\pi$ $K\eta$	$\pi\eta$ $K\bar{K}$	$K\pi$	$\pi\pi$
J=1	$K\bar{K}$	$K\pi$ $K\eta$	$\pi\pi$ $K\bar{K}$		

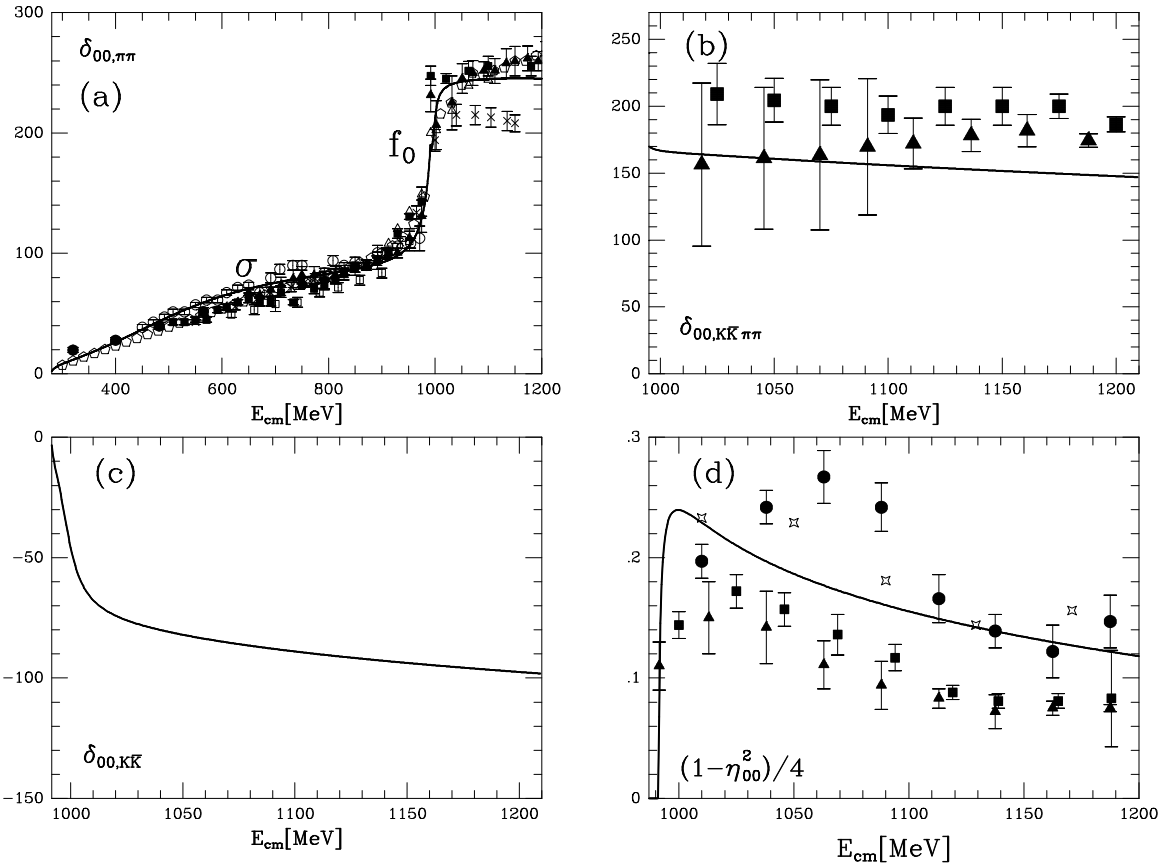

Figure 4.9: Results in the $I = L = 0$ channel. (a) phase shifts for $\pi\pi \to \pi\pi$ as a fraction of the c.m. energy of the meson pair: full triangle [47], open circle [48], full square [49], open triangle [61], open square [62] (all these are analysis of the same experiment [63]), cross [50], full circle [64], empty pentagon [51]. (b) phase shifts for $K\bar{K} \to \pi\pi$: full square [52] , full triangle [53]. (c) Phase shifts for $K\bar{K} \to K\bar{K}$. (d) Inelasticity: results and data for $(1 - \eta^2)/4$: starred square [51], full square [52] , full triangle [53], full circle [65].

We show first the results on phase shifts and inelasticities in the different channels and later on we discuss about the pole positions, widths and partial decay widths.

4.4.2 Phase shifts and inelasticities

We will now go in detail through the results in each (I, L) channel.

Channel (0,0)

As we can see in eq. (1.40) we have three independent magnitudes δ_1, δ_2 and η. In Figs.(4.9.a) and (4.9.c) we show the δ_1 and δ_2 corresponding to $\pi\pi \to \pi\pi$ and $K\bar{K} \to K\bar{K}$ elastic scattering. In Fig.(4.9.b) we plot the phase shift for $K\bar{K} \to \pi\pi$. This is actually $\delta_1 + \delta_2$, which is therefore redundant information. However, there are data for this process but not for elastic $K\bar{K}$, and that is why we are plotting $\delta_1 + \delta_2$. The agreement with experiment is good, with small discrepancies in the $K\bar{K} \to \pi\pi$ phase shifts. In Fig.(4.9.a) we see a bump around 600 MeV which is due to the σ resonance, whose associated pole appears around $442 - i225$ MeV, as we shall see below. The fast raise in the phase shift at 1 GeV is caused by the f_0 pole around $980 - i14$ MeV, which translates in an apparent mass of $\simeq 980$ MeV and a 30 MeV width. Small discrepancies with data start showing up around 1.2 GeV. The omission of the $\eta\eta$ and four meson states should limit the validity of the approach at high energies since then these channels start being relevant.

Channel (1,1)

In Fig.(4.10.a) we display the $\pi\pi \to \pi\pi$ phase shifts which clearly show the ρ meson. The perfect coincidence of the results with the very precise data indicate that both the position and the width of the ρ are very well described. In Fig.(4.10.c) we show the phase shifts for $K\bar{K} \to K\bar{K}$ scattering, for which there are no data. As we can see, they are very small, which implies a weak $K\bar{K}$ interaction. Therefore the $\delta_1 + \delta_2$ phase shift of $K\bar{K} \to \pi\pi$ is essentially that of $\pi\pi \to \pi\pi$. The fact that the inelasticity is practically one, indicates that there is almost no mixture of $\pi\pi$ and $K\bar{K}$. This feature makes the ρ to behave as a pure $\pi\pi$ elastic resonance. That is why the single channel IAM gave essentially the same results as obtained here [25].

Channel (2,0)

The $I = 2$ $\pi\pi$ scattering contains only one state as shown in Table 4.2. In Fig.(4.11) we show the resulting phase shifts, whose agreement with experimental data is remarkably good up to 1.2 GeV

Channel (1,0)

In Fig.(4.12.a) the $\pi\eta \to \pi\eta$ phase shifts are shown. Those of $K\bar{K} \to \pi\eta$ are plotted in Fig.(4.12.c) and the inelasticities in Fig.(4.12.d). In the latter, it can be seen that there is an appreciable mixture between $\pi\eta$ and $K\bar{K}$ above $K\bar{K}$ threshold. In Fig.(4.12.b) we compare a mass distribution for $\pi\eta$ around the region of the a_0 resonance. The data are

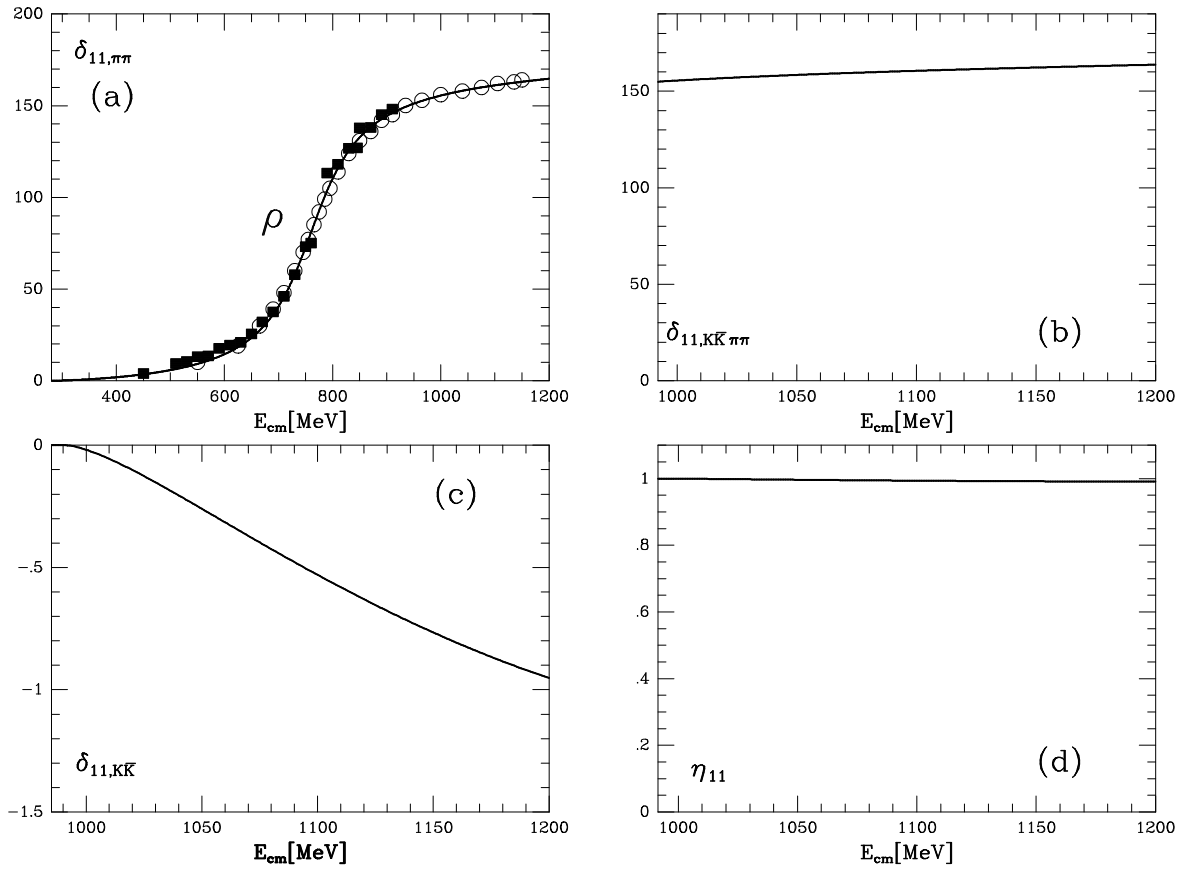

Figure 4.10: Results in the $I = L = 1$ channel. (a) phase shifts for $\pi\pi \to \pi\pi$. Data: open circle [50], black square [48]. (b), (c) same as in Fig. 4.9. (d) inelasticity.

obtained from [67] using the $K^- p \to \Sigma^+(1385)\pi\eta$ reaction, whose cross section (following [28]) can be written as

$$\frac{d\sigma}{dm} = C|T|^2 q \tag{4.40}$$

where m is the $\pi^-\eta$ invariant mass, q the π momentum in the $\pi^-\eta$ c.m. frame, T the $\pi^-\eta \to \pi^-\eta$ scattering amplitude and C a normalization constant. We observe a fairly good agreement with the experimental numbers.

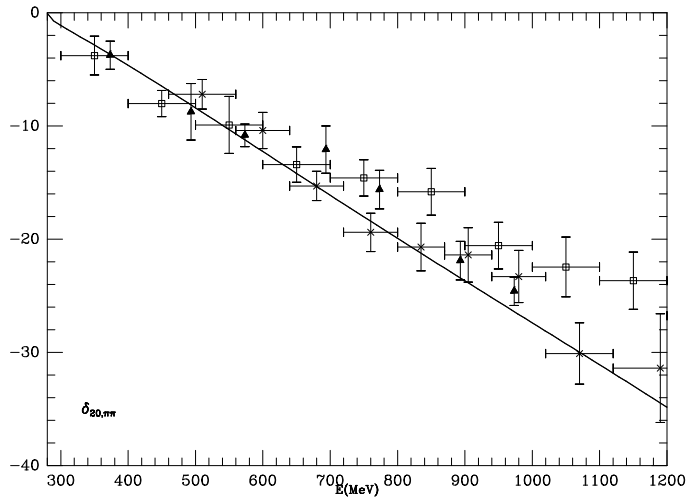

Figure 4.11: Phase shifts for $\pi\pi \to \pi\pi$ in the $I = 2$, $L = 0$ channel. Data: cross [55], empty square [56], full triangle [38].

Channel (1/2,0)

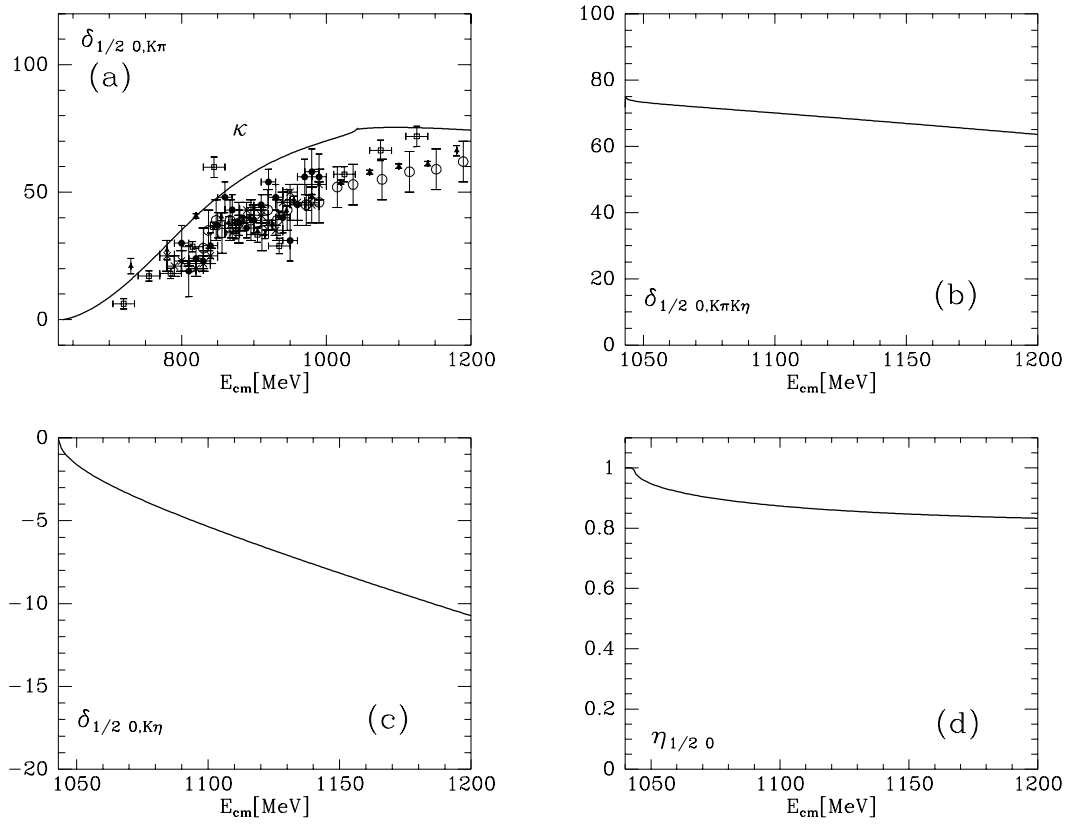

Figure 4.13: Results in the $I = 1/2$, $L = 0$ channel. (a) phase shifts for $K\pi \to K\pi$. Data: full circle [68], cross [69] , open square [70], full triangle [71], open circle [72]. (b) phase shifts for $K\pi \to K\eta$. (c) phase shifts for $K\eta \to K\eta$. (d) inelasticity.

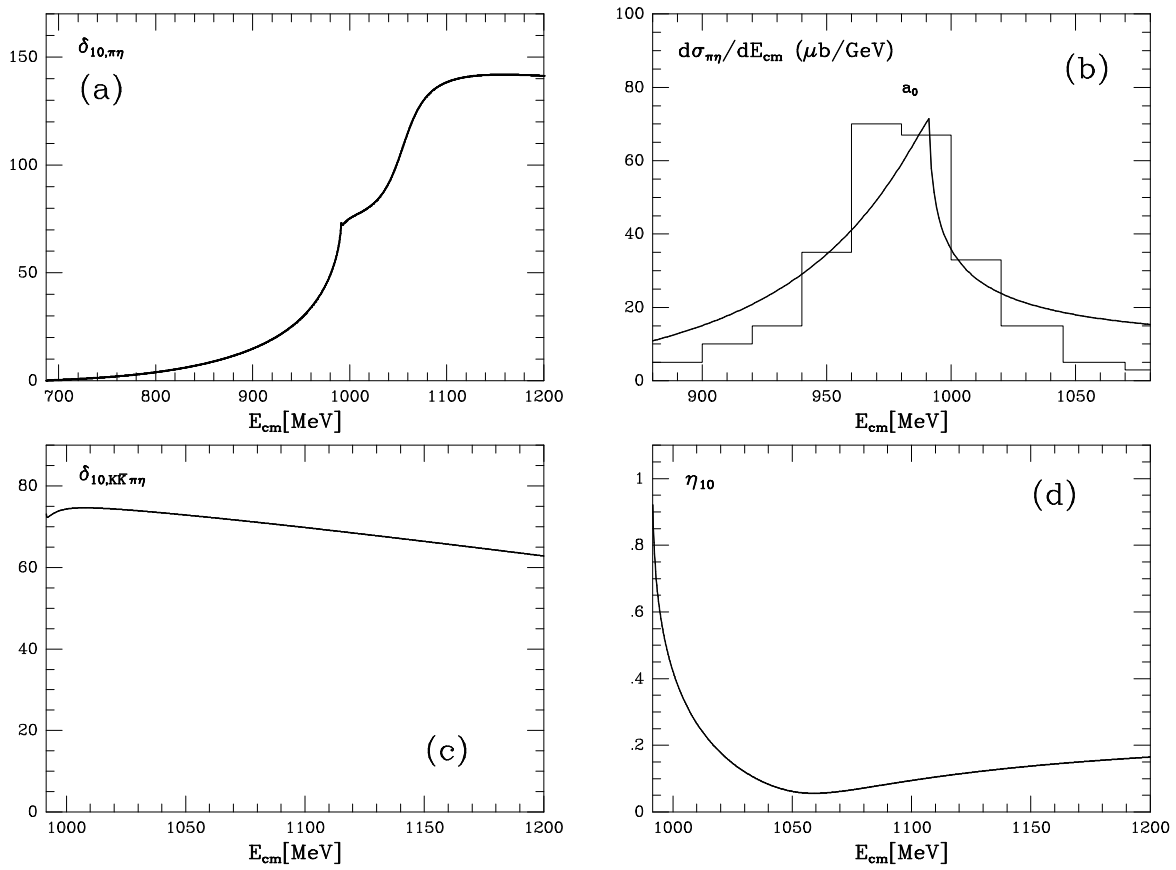

Figure 4.12: Results in the $I = 1$, $L = 0$ channel. (a) phase shifts for $\pi\eta \to \pi\eta$. (b) Invariant mass distribution for $\pi\eta$ data from [67]. (c) Phase shifts for $K\bar{K} \to \pi\eta$. (d) inelasticity.

The two coupled states are now $K\pi$ and $K\eta$. In Fig.(4.13.a) we plot the phase shifts for $K\pi \to K\pi$. The theoretical curve follows the same trend as the experimental data, although it lies a bit above them. The results and the data show a broad bump, which is related to the presence of a pole which appears around $770 - i250$ MeV. Such a resonance, whose existence has been claimed in a recent data analysis [73], is predicted in quark models of $q^2\bar{q}^2$ systems [74] and is usually denoted by $\kappa(900)$ from this last reference. This resonance bears some similarity with the σ in the (0,0) $\pi\pi$ elastic scattering channel, which is also very broad. Finally, the $K\eta \to K\eta$ phase shifts are small as shown in Fig.(4.13.c) and the inelasticities given in Fig.(4.13.d) are not distant from unity. This fact indicates a small mixture of $K\pi$ with $K\eta$.

Channel (1/2,1)

In this case we also find a resonance in Fig.(4.14.a), analogous to the ρ, but in the $K\pi$ system. This resonant state, known as the $K^*(892)$, is as clean as the ρ, and the agreement of our results with the data is remarkably good over the whole range of energies up to 1.2

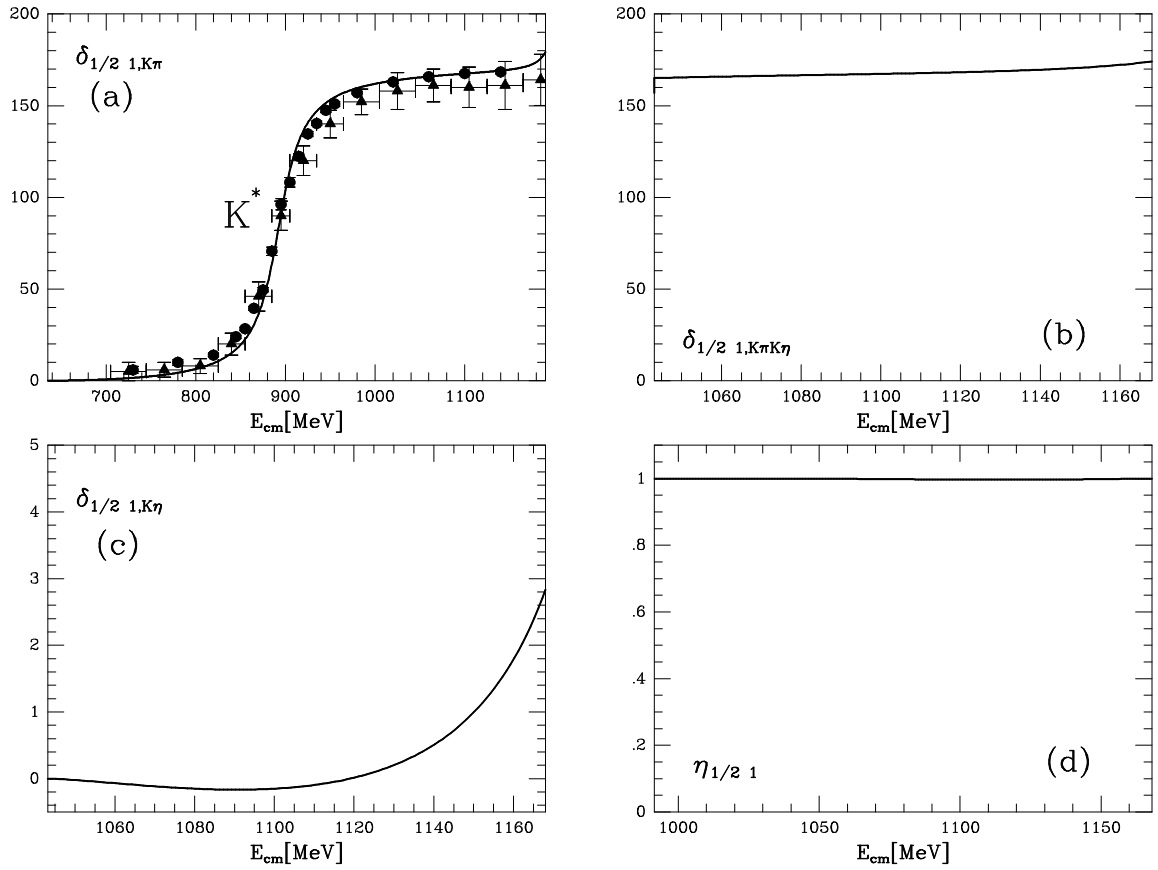

Figure 4.14: Results in the $I = 1/2$, $L = 1$ channel. (a) phase shifts for $K\pi \to K\pi$. Data: full triangle [68], open circle [71]. (b) phase shifts for $K\pi \to K\eta$. (c) phase shifts for $K\eta \to K\eta$. (d) inelasticity.

GeV. In Fig.(4.14.c) we plot the $K\eta \to K\eta$ phase shifts, which are very small. Finally, in Fig.(4.14.d) we can notice that $\eta \approx 1$ which means that there is practically no mixture of $K\pi$ and $K\eta$ in this channel. This justifies the success of [25] reproducing this resonance using only the $K\pi$ state and elastic unitarity.

Channel (3/2,0)

In Fig.(4.15) we show the $K\pi$ phase shifts. As we can see in the figure, the agreement with the data is quite good up to about 1.2 GeV.

The channel (3/2,1) in $K\pi$ (see Table 4.2) is such that $T_2 = 0$, since there is only S-wave there. In this case our method cannot be applied, as discussed above, and we should just take the T_4 contribution. That also happens for the $L = 2$ channels, since the structure of T_2, which is $\mathcal{O}(p^2)$, is a linear combination of s, t, u and squared masses. Therefore there is only $L = 0, 1$ in T_2, but not $L = 2$. Hence, the lowest contribution can only be obtained from the T_4 terms and our method has nothing to improve there with respect to

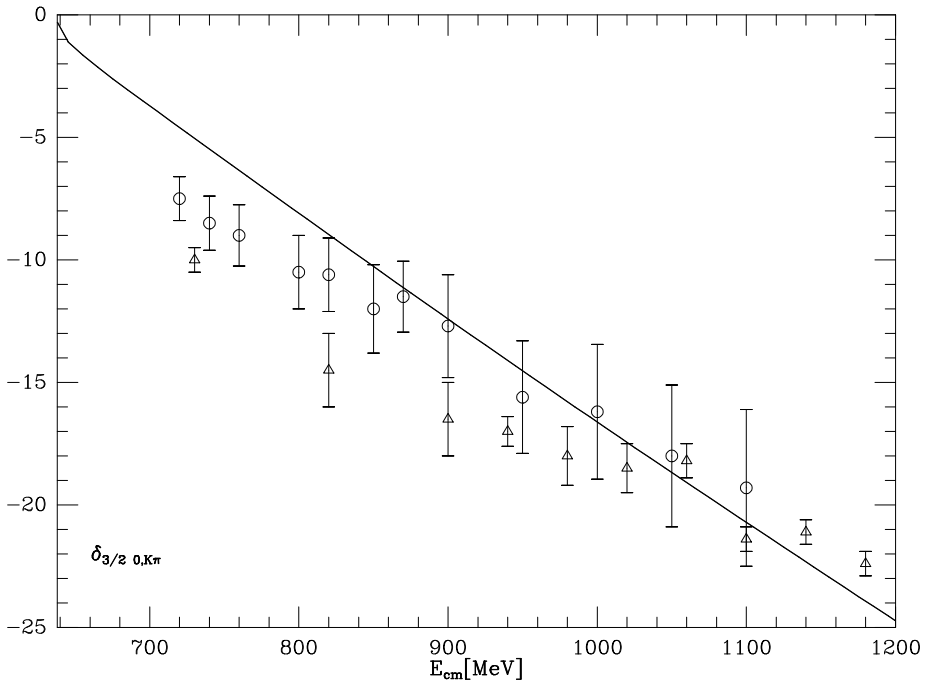

Figure 4.15: Phase shifts for $K\pi \to K\pi$ in the $I = 3/2$, $L = 0$ channel. Data: open triangle [71], open circle [75].

χPT. The phase shifts in these channels are small and have been discussed in [25]. Hence we omit any further discussion, simply mentioning that the agreement with data found in [25] is fairly good.

There is another interesting result in the (0,1), channel which is the appearance of a pole around 990 MeV, that we show in Fig.(4.16). Below 1.2 GeV there are two resonances with such quantum numbers. They are the ω and the ϕ, which fit well within the $q\bar{q}$ scheme, with practically ideal mixing, as $\frac{1}{\sqrt{2}}(u\bar{u} + d\bar{d})$ and $s\bar{s}$, respectively. In the limit of exact SU(3) symmetry these resonances manifest as one antisymmetric octet state and a symmetric singlet state. Since the spatial function of the $K\bar{K}$ state is antisymmetric its SU(3) wave function does also have to be antisymmetric and therefore it only couples to the antysimmetric octet resonance. Of course, our Lagrangians do contain some SU(3) breaking, but, in this channel we are only dealing with the $K\bar{K}$ state, neglecting states with other mesons (like the three pion channel) and, hence, our formulae for this process do not contain any SU(3) symmetry breaking term. Thus, we just see one pole, corresponding to the antisymmetric octet state of the exact SU(3) limit. Because the ideal mixing angle is around 20 degrees the pole we obtain should be closer to the physical $\phi(1020)$ than to the physical $\omega(782)$. This is in fact what happens since we obtain a mass of 990 MeV. It seems then plausible that the small coupling to three pions (an OZI suppressed coupling of third class) which we are not taking into account, could be enough to bring our pure octet state to the physical ϕ resonance.

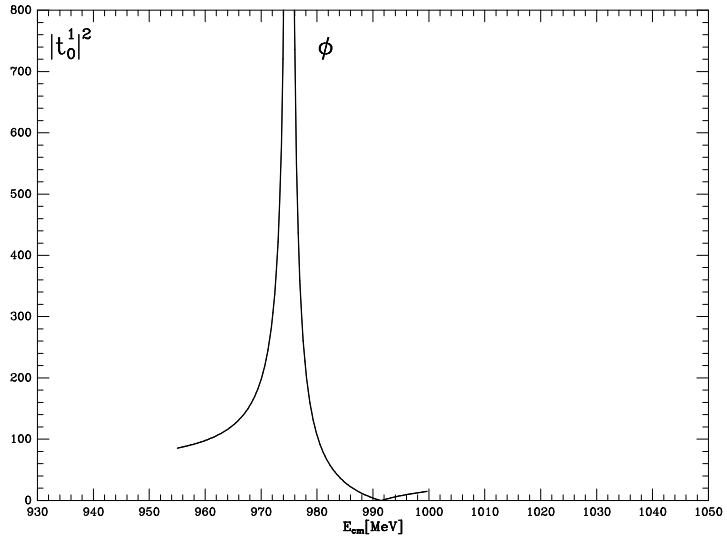

Figure 4.16: $(|T_{IJ=01}|)^2$ for $K\bar{K} \to K\bar{K}$ showing a singularity corresponding to a resonance belonging to the antysimmetric vector octet. Due to the smallness of the mixing angle between the ϕ and the ω this singularity is much closer to the ϕ meson.

Table 4.3: Fit parameters $\hat{L}_i \cdot 10^3$ and comparison with the $L_i^r \cdot 10^3$ of χPT

$q_{max} = 1.02$ GeV	$\hat{L}_1$	$\hat{L}_2$	$\hat{L}_3$	$\hat{L}_4$	$\hat{L}_5$	$2\hat{L}_6 + \hat{L}_8$	$\hat{L}_7$
	0.5	1.0	-3.2	-0.6	1.7	0.8	0.2
$\mu = 1.2$ GeV	L_1^r	L_2^r	L_3	L_4^r	L_5^r	$2L_6^r + L_8^r$	L_7
	0.1 ± 0.3	0.9 ± 0.3	-3.5 ± 1.1	-0.7 ± 0.5	0.4 ± 0.5	0.0 ± 0.3	-0.4 ± 0.2

4.4.3 Pole positions, widths and partial decay widths.

We will now look for the poles of the T matrix in the complex plane, that should appear in the unphysical Riemann sheets. The notation for the different sheets is the following:

$$\begin{array}{lll} \text{Sheet I:} & \text{Im } p_1 > 0, & \text{Im } p_2 > 0 \\ \text{Sheet II:} & \text{Im } p_1 > 0, & \text{Im } p_2 < 0 \\ \text{Sheet III:} & \text{Im } p_1 < 0, & \text{Im } p_2 < 0 \\ \text{Sheet IV:} & \text{Im } p_1 < 0, & \text{Im } p_2 > 0 \end{array} \tag{4.41}$$

where the labels $1, 2$ stand for $K\bar{K}$, $\pi\pi$ in the $I = 0$ case and $K\bar{K}$, $\pi\eta$ for the $I = 1$.

Let us remember that the mass and the width of a Breit-Wigner resonance are defined from the position of its complex pole by $\sqrt{s_{pole}} \simeq M - i\Gamma/2$. However, the phenomenologically seen mass and width of a resonance depend on the process under consideration. In Table 4.4 we give the results for the pole positions as well as the apparent or "effective" masses and widths that can be estimated from phase shifts and mass distributions in scattering processes.

We shall make differentiation between the ρ and K^*, which are clean elastic Breit-Wigner resonances, and the rest. For the ρ and K^* their mass is given by the energy at which $\delta = 90^0$ and the width is taken from the phase shifts slope around $\delta = 90^0$, by means of

$$\Gamma_R = \frac{M_R^2 - s}{M_R} \tan\delta(s) \tag{4.42}$$

We also saw that, in practice, the ρ and K^* only couple to $\pi\pi$ and $K\pi$, respectively. The σ decays only to $\pi\pi$ and the κ only to $K\pi$ due to phase space and dynamical suppression of other channels (see Fig.(4.13d)). The case of the f_0 and a_0 is different, since they can decay either to $\pi\pi$ or $K\bar{K}$ (the f_0), and $\pi\eta$ or $K\bar{K}$ (the a_0). In order to determine the partial decay widths of these resonances we follow the procedure of [58], where we show that, assuming a Breit Wigner shape for the amplitudes around the resonance pole, the partial decay widths are given by

$$\begin{aligned} \Gamma_{R,1} &= -\frac{1}{16\pi^2} \int_{E_{min}}^{E_{max}} dE \frac{q}{E^2} 4 M_R \text{Im}\, T_{11} \\ \Gamma_{R,2} &= -\frac{1}{16\pi^2} \int_{E_{min}}^{E_{max}} dE \frac{q}{E^2} 4 M_R \frac{(\text{Im}\, T_{21})^2}{\text{Im}\, T_{11}} \end{aligned} \tag{4.43}$$

where E stands for the total c.m. energy of the meson-meson system, q is the momentum of one meson in the c.m.. The masses of the final mesons are m_1, m_2. The upper limit in the integral, E_{max}, is $\simeq M_R + \Gamma_R$ where Γ_R is the total width [58] and $E_{min} = M_R - \Gamma_R$, unless the threshold energy $(m_1 + m_2)$ for the decay is bigger than that quantity, in which case $E_{min} = m_1 + m_2$. In this way we largely avoid the contribution of the backgrounds in the amplitudes. One caveat must be raised concerning eq. (4.43), which was already pointed out in the study of the $f_0 \to \gamma\gamma$ decay [76]. The subtlety is that the background phase shifts around this resonance, coming from the broad σ pole, are about 90^0, see Fig. 4.9a. This background makes the $f_0 \to \pi\pi$ coupling constant to appear effectively multiplied by a $\pi/2$ phase (i factor) and in this way the T_{12} amplitude around the f_0 looks like an

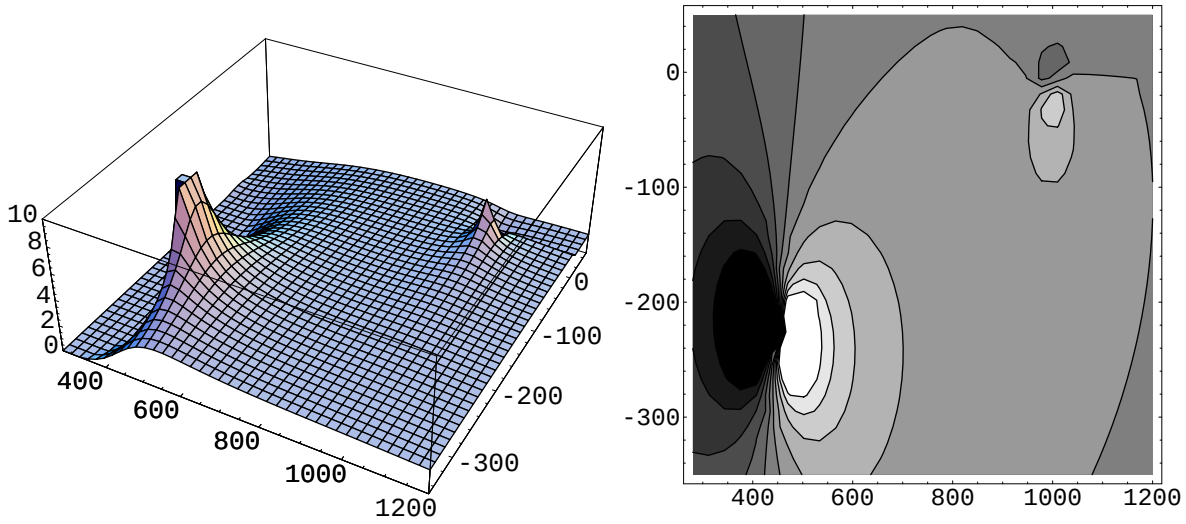

Figure 4.17: Imaginary part of the $\pi\pi$ amplitude in the (I, L)=(0,0) channel in the second Riemann sheet. On the left we show a three dimensional plot were we can observe the different structure of the σ and f_0 poles. On the right we show a contour plot of the lower half plane of the second sheet. The σ pole is very far away from the real (physical) axis and its lines of maximum gradient are parallel to it, in contrast with the f_0. That is why the effect of both poles in the phase shifts (Fig. 4.9) is so different.

ordinary Breit Wigner multiplied by i. This means that the real part has a peak around the resonance and the imaginary part changes sign. In this case the arguments used in [58] and [76] lead to a trivial modification in $\Gamma_{R,2}$, where $\mathrm{Im}\, T_{12}$ should be substituted by $\mathrm{Re}\, T_{12}$.

It is also very instructing to see the representation of the poles in a three dimensional plot. In Fig.(4.17) we are showing on the left the imaginary part of the (0,0) $\pi\pi \to \pi\pi$ scattering amplitude on the second Riemann sheet. It is possible to see very clearly the appearance of two poles that correspond to the σ and the f_0 resonances. The former is located at $442 - i227$ and thus is very far away from the real axis, which implies a huge effective width. In contrast, the other pole is located at $994 - i14$ MeV accordingly to the narrow width of the f_0 resonance.

Apart from the position of the poles, there is an additional piece of information which also determines the observed shape of a resonance. It also explains some of the differences between the "effective" masses and the real part of the pole position. On the right of Fig.(4.17) we give a contour plot, again of the imaginary part of the (0,0) amplitude in the second Riemann sheet. Notice that both poles are oriented differently, almost transversally, on the complex plane. On the one hand, the f_0 pole is oriented almost perpendicularly to the real axis, which is the relevant one in this work. As a consequence, in the positive real axis, the imaginary part of the amplitude first grows rapidly and then drops very fast again, giving rise to the dramatic variation of the phase shift typical of resonances. A similar orientation is found for the ρ, K^* and a_0 resonances too. On the other hand, the σ

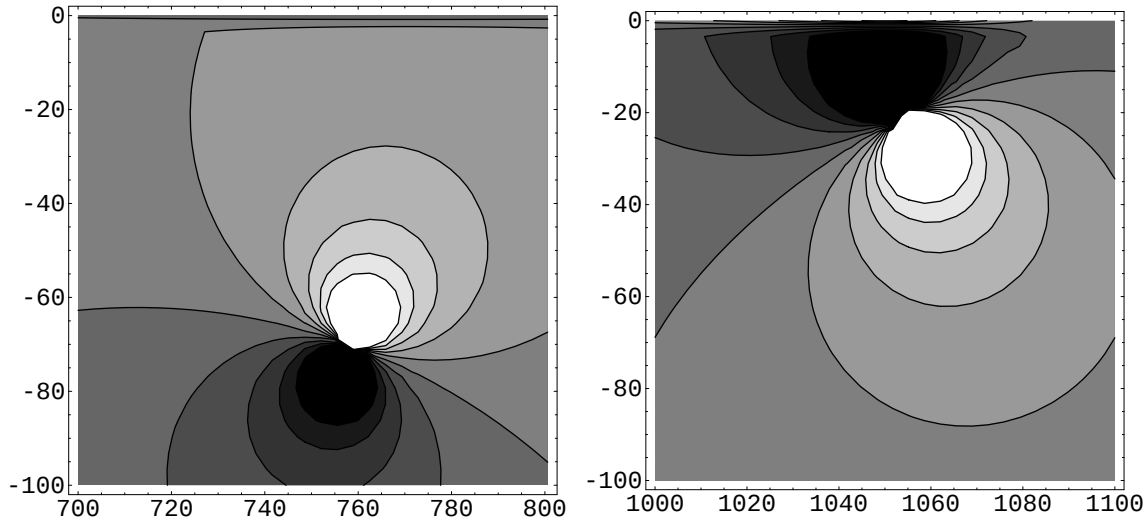

Figure 4.18: The poles associated to the ρ (left) and a_0 (right) are oriented differently. The ρ mass seen on the (I, L)=(1,1) phase shifts is slightly bigger than the real part of the position of the ρ pole, whereas the peak of the mass distribution where the a_0 is observed (see Figure 4.12) is smaller than the real part of the a_0 pole. Concerning the widths, they are obtained as twice the imaginary part of the associated pole position.

pole is oriented so that in the real axis we only see a slow and smooth increase, but almost no decrease, of the imaginary part. That is also the case of the κ resonance. This feature, together with the fact that both the σ and the κ are very far from the real axis explains why it is so hard to establish firmly their existence and their physical parameters.

Finally, in Fig.(4.18) we present a very detailed contour plot of the ρ and a_0 poles. Both of them are almost perpendicular to the real axis, but the former is tilted clockwise, whereas the latter is tilted anti-clockwise. Let us now remember that the real part of the pole position, roughly, should give us the apparent mass of the resonance. However, the lines of maximum gradient of each pole cross the real axis at a point which is slightly different from the real part of its position. Therefore, those poles rotated clockwise, as the ρ or the K^*, have an apparent mass a little bit higher than that given by the pole position. In contrast those tilted anti-clockwise, yield a resonance whose mass is somewhat lower that the one obtained from the pole. That is the case of the f_0 and the a_0.

4.5 Conclusions.

We have used a coupled channel unitary approach, together with the dynamical information contained in the $\mathcal{O}(p^2)$ and $\mathcal{O}(p^4)$ chiral amplitudes, which allows us to study the meson-meson interaction up to about $\sqrt{s} = 1.2$ GeV. This non-perturbative method generates poles in the complex plane corresponding to physical resonances. With the $\mathcal{O}(p^4)$ χPT counterterms as degrees of freedom we are able to fit, up to 1.2 GeV, all the exper-

Table 4.4: Masses and partial widths in MeV

Channel (I,J)	Resonance	Mass from pole	Width from pole	Mass effective	Width effective	Partial Widths
$(0,0)$	σ	442	454	≈ 600	*very large*	$\pi\pi - 100\%$
$(0,0)$	$f_0(980)$	994	28	≈ 980	≈ 30	$\pi\pi - 65\%$ $K\bar{K} - 35\%$
$(0,1)$	$\phi(1020)$	980	0	980	0	
$(1/2,0)$	κ	770	500	≈ 850	*very large*	$K\pi - 100\%$
$(1/2,1)$	$K^*(890)$	892	42	895	42	$K\pi - 100\%$
$(1,0)$	$a_0(980)$	1055	42	980	40	$\pi\eta - 50\%$ $K\bar{K} - 50\%$
$(1,1)$	$\rho(770)$	759	141	771	147	$\pi\pi - 100\%$

imental information in seven meson-meson channels. Moreover, in our results, we obtain the position and widths, partial decay widths, etc.... of all the resonances that appear in those channels below 1.2 GeV. Apart from the standard f_0, a_0, ρ, K^* resonances, we find poles in the T matrix for the σ in the $\pi\pi$ $I = L = 0$ channel and for κ in the (1/2,0) channel, both of them very broad.

The method has proved very efficient to extend the ideas of chiral symmetry at energies beyond the realm of applicability of χPT. However, at energies higher than 1.2 GeV, the limitations of the model show up, since, among other things, we have restricted ourselves only to two meson states. The restrictions in the space of states precluded the appearance of the ω resonance which couples dominantly to three pions.

One of the weakness of the approach is that it is not crossed symmetric. In practice, the effect of the unphysical cuts has been reabsorbed in the fit of the $\mathcal{O}(p^4)$ parameters, whose values can then be altered by those contributions.

Applications of the method to other physical problems are also in order. Indeed, it can be easily extended to deal with processes where meson pairs appear in the initial or final state, like meson pair photoproduction [76]. It looks likely that it could also prove useful describing the meson-nucleon interaction [77] complemented with Heavy Baryon Chiral Perturbation Theory. In addition, the method, non perturbative in nature, is equally well suited to study the meson-meson interaction in a nuclear medium where there has been some speculation about the appearance of bound $\pi\pi$ pairs [78].

Finally the approach could be extended to the effective chiral Lagrangian description of the Standard Model Strongly Interacting Symmetry Breaking Sector, where the single channel approach has already been applied [36].

Chapter 5

The N/D method and Chiral Symmetry.

In this section we are going to discuss a method to unitarize χPT supplied with the exchange of resonances which we introduce following [7]. In this section we follow the work ref. [27]. In this work the same convention for the T-matrix than in ref. [42] was used. Hence, as in **section 4.3**, to use the equations introduced in the former chapters the sign of the T-matrix must be changed. This will be also the case for the next chapter.

In ref. [7], the question surrounding the meson-meson dynamics was not considered. In ref. [79] the elastic $\pi\pi$ and $K\pi$ scattering is studied, although the authors use a naive "unitarization" method, based in the relation

$$\delta_L(s) = tan^{-1}\left(\frac{2\,q}{\sqrt{s}}\text{Re } T_L(s)\right) \tag{5.1}$$

which strictly only holds up to $\mathcal{O}(p^4)$, while in the resonance region, considered also in [79], all orders are needed. As the authors of [79] say in their work, a more thorough investigation of loop effects to generate imaginary parts is needed. This is precisely the aim of this chapter.

Another interesting point which we want to discuss is the problemmatic situation of the scalar sector which is still so controversial that there is not even a consensus about how many low lying states (with masses $\leq$1 GeV) are there. The main difficulties which appear in this sector are: First, the possible presence of large width resonances, as the $f_0(400-1200) \equiv \sigma$ in $\pi\pi$ scattering or the $K_0^*(900) \equiv \kappa$ in the I=1/2 $K\pi$ amplitude, which cannot be easily distinguished from background contributions. Second, the existence of some resonances which appear just in the opening of an important channel with which they couple strongly, as for example the $f_0(980)$ or the $a_0(980)$ with the $K\bar{K}$ threshold around 1 GeV. All these aspects make that, for instance, it is not clear how many states are present, which is their nature and why simple parameterization of the scalar physical amplitudes in terms of standard Breit-Wigner resonances are not adequate, as stressed in several works [31, 80, 81] and also discussed in **section 3.1**.

The conflictive situation for the scalar sector contrasts with the much better understood vector channels. In this latter case, one can achieve a sound understanding of the physics involved just from first principles [82], namely, chiral symmetry, unitarity and relations coming from the QCD limit of infinity numbers of colors (large N_c QCD). This is accomplished thanks to the leading role of the $\rho(770)$ and $K^*(890)$ resonances, in accordance with vector meson dominance, very well established from particle and nuclear physics phenomenology. The issue is whether such a basic understanding for the scalar sector is possible, and, at the same time, is able to reproduce the associated phenomenology. Connected with the former, it should be also interesting to see if some kind of scalar meson dominance remains, in analogy with the above mentioned vector meson dominance.

There have been many studies of the scalar sector but none in the basic lines we outlined before. These studies have led to a variety of models dealing with the scalar meson-meson interaction and its associated low energy spectroscopy. The low energy scalar states have been ascribed [83] to conventional $q\bar{q}$ mesons [31, 84], $q^2\bar{q}^2$ states [74, 85], $K\bar{K}$ molecules [37, 38], glueballs [86] and/or hybrids [87].

One can think in two possible ways in order to avoid the former explicit model dependence for the scalar sector, apart, of course, of solving QCD in four dimensions for low energies which, nowadays, is not affordable.

One way to proceed is to make use only of general principles that the physical amplitudes must fulfill, as unitarity and analyticity. There are a series of works by Pennington, Morgan et al. [80, 88] which fit nicely the experimental data available for the scalar-isoscalar sector and try to obtain also some understanding of the associated spectroscopy. Another work in this line is presented in [89]. However, these approaches have also problems as, for example, the specific way in which the amplitudes are parametrized and the lack of enough precision in the experimental data in order to discard other possible solutions.

Another alternative is the use of effective field theories which embody and exploit the symmetries of the underlying dynamics, in this case QCD. In this sense, χPT [4, 5] is the effective field theory of QCD with the lightest three quark flavors. This approach has been extensively used in the last years for the meson sector and allows to calculate any physical amplitude in a systematic power momentum expansion. A brief summatry of χPT was given in **chapter 2**.

This latter point of view will be the one adopted here. First, we will derive, making use of the N/D method [9], the most general structure for an arbitrary partial wave amplitude when the unphysical cuts are neglected. In this way, our method can be seen as the zero order approach to a partial wave when treating the unphysical cuts in a perturbative sense. After neglecting the unphysical cuts we then match the general structure we obtain from the N/D method with the lowest order χPT Lagrangian, $\mathcal{O}(p^2)$ [5], and its extension to include heavier meson states with spin ≤ 1 [7], beyond the lightest pseudoscalars (π, K, η). Making use of this final formalism, we will study the scalar sector with I=0, 1 and 1/2, being able to reproduce the experimental data up to about $\sqrt{s} \leq 1.4$ GeV. In order to say something for higher energies, more channels, apart from the ones taken here, should be added. This is not considered in this work, although it can be done in a straightforward way, albeit cumbersome, in terms of the present formalism. We will come back to this

point in **chapter 6**. We also study the vector $\pi\pi$ and $K\pi(I{=}1/2)$ scattering and compare it with the scalar sector to illustrate some important differences between both cases.

Some words about the unphysical cuts are in order. We expect they can be considered small in those partial wave amplitudes which are dominated by unitarity and the presence of resonances in the s-channel with the same quantum numbers of the partial wave amplitude. For example, the case of the ρ and K^* resonances in the P-wave $\pi\pi$ and $K\pi$ scattering respectively or the scalar channels with isospin 0, 1/2 or 1, where several resonances appear. In fact, for the $\rho(K^*)$ meson-meson channels, at least up to $\sqrt{s} = 1.2$ GeV, one can describe accurately the associated $\pi\pi(K\pi)$ phase shifts just in terms of simple Breit-Wigner parameterizations with the coupling of the $\rho(K^*)$ with $\pi\pi(K\pi)$ given by the KSFR relation [29] and their masses taken directly by experiment. In this way one has a free parameter description for these processes without the unphysical cuts, since it only has the physical or right hand one as required by unitarity. Thus, one can deduce that for these processes the contribution from the unphysical cuts is certainly much smaller than the one coming from the exchange of these resonances in the s-channel and from unitarity. Otherwise, a free parameter reproduction of these channels with only the right hand cut could not be possible. This type of description for the ρ and K^* meson-meson channels is given below in **section 3.3** and it was also given in ref. [82] for the case of the ρ. For the scalar channels with I=0,1 and 1/2 there have been a number of previous studies [31, 57, 58, 81, 85] which neglect the contribution from the unphysical cuts establishing clearly the great importance of unitarity for the scalar sector. In particular, in the work of ref. [58] the I=0,1 S-wave channels were described in terms of just one free parameter up to $\sqrt{s} \approx 1.2$ GeV, indicating that the contribution from the unphysical cuts should be small enough to be reabsorbed in this free parameter. The connection between the work of ref. [58] and the present one is discussed in **section 3.2**. It is also interesting to indicate that in [25, 42] the S-wave scattering was also studied including the unphysical cuts up to $\mathcal{O}(p^4)$ in χPT and the results obtained were very similar to the ones of the former works, refs. [57, 58], without any unphysical cuts at all. Apart from these considerations, we approach in the last section the influence of the unphysical cuts from χPT and the exchange of resonances in crossed channels taking into account the results of ref. [79]. In this reference, the $\pi\pi$ and $K\pi$ elastic amplitudes are calculated up to one loop including explicit resonance fields [7]. In this way the range of applicability of χPT is extended up to $\sqrt{s} \approx 700 - 800$ MeV. The loops are calculated as in χPT at $\mathcal{O}(p^4)$. We conclude that the contributions of the unphysical cuts are small and soft enough to be reabsorbed in our free parameters in a convergent way when treating the unphysical cuts in a perturbative way. It is important to indicate that such a small value for the influence of the unphysical cuts, as can be seen in Table 5.3, is due to a cancellation between the contributions coming from the loops and the exchange of resonances in crossed channels. In **chapter 6** we will enlarge the formalism to include also up to $\mathcal{O}(p^4)$ the unphysical cuts making use of the loops calculated in [43, 79] at $\mathcal{O}(p^4)$.

The main conclusion of this chapter is that one can obtain a rather accurate description of the scalar sector compared to experiment, in a way consistent with χPT and large N_c QCD [90], if the tree level structures coming from large N_c QCD for the meson-meson

scattering are introduced in a way consistent with χPT and then are properly unitarized in the way we show here. Contrary to what happens for the vector channels, where the tree level contributions determine the states which appear in the scattering, we will see that for the scalar sector the unitarization of the $\mathcal{O}(p^2)$ χPT amplitude is strong enough to produce meson-meson states, as for example, the $\sigma(500)$, $a_0(980)$, $\kappa(900)$ and a strong contribution to the $f_0(980)$. All these states, except the $f_0(980)$, disappear for large N_c QCD because they originate from effects which are subleading in $1/N_c$ counting rules (loops in the s-channel). We will see below that the origin for such a different behavior between the ρ and the σ will be just a numerical factor 1/6 between the P and S-wave $\mathcal{O}(p^2)$ χPT amplitude. Note that in a n-loop calculation this gives rise to a relative suppression factor of $1/6^{n+1}$ of the P-wave loops with respect to the S-wave ones.

5.1 Formalism.

Let us consider in the first place the elastic case, corresponding to the scattering of two particles of masses m_1 and m_2 respectively. We will also allow for several coupled channels at the end of the section.

Let $\mathrm{T}_L^I(s)$ be a partial wave amplitude with isospin I and angular momentum L. Since we are dealing with π, K and η as asymptotic particles, which have zero spin, L will also be the total spin of the partial wave. The projection in a definite angular momentum is given by eq. (1.41).

A $\mathrm{T}_L^I(s)$ partial wave amplitude has two kinds of cuts. The right hand cut required by unitarity and the unphysical cuts from crossing symmetry. In our chosen normalization, the right hand cut leads to the equation (in the following discussions we omit the superindex I, although, it should be kept in mind that we always refer to a definite isospin):

$$\mathrm{Im}\ \mathrm{T}_L^{-1} \quad = \quad -\rho(s) \tag{5.2}$$

for $s > s_{threshold} \equiv s_{th}$. In the case of two particle scattering, the one we are concerned about, $s_{th} = (m_1 + m_2)^2$ and $\rho(s)$ is given by:

$$\rho(s) = \frac{p}{8\pi\sqrt{s}} \tag{5.3}$$

with

$$p = \frac{\sqrt{(s-(m_1+m_2)^2)(s-(m_1-m_2)^2)}}{2\sqrt{s}} \equiv \frac{\lambda^{1/2}(s,m_1^2,m_2^2)}{2\sqrt{s}} \tag{5.4}$$

the c.m. three momentum of the two meson system.

The unphysical cuts comprise two types of cuts in the complex s-plane. For processes of the type $a+a \to a+a$ with $m_1 = m_2 = m_a$, there is only a left hand cut for $s < s_{Left}$. However for those ones of the type $a+b \to a+b$ with $m_1 = m_a$ and $m_2 = m_b$, apart from a left hand cut there is also a circular cut in the complex s-plane for $|s| = m_2^2 - m_1^2$, where we have taken $m_2 > m_1$. In the rest of this section, for simplicity in the formalism, we

will just refer to the left hand cut as if it were the full set of unphysical cuts. This will be enough for our purposes in this section. In any case, if we worked in the complex p^2-plane all the cuts will be linear cuts and then only the left hand cut will appear in this variable.

The left hand cut, for $s < s_{Left}$, reads:

$$\mathrm{T}_L(s+i\epsilon) - \mathrm{T}_L(s-i\epsilon) = 2i\mathrm{Im}\ \mathrm{T}_L(s) \tag{5.5}$$

The standard way of solving eqs. (5.2) and (5.5) is the N/D method [9]. In this method a T_L(s) partial wave is expressed as a quotient of two functions,

$$\mathrm{T}_L(s) = \frac{\mathrm{N}_L(s)}{\mathrm{D}_L(s)} \tag{5.6}$$

with the denominator function $\mathrm{D}_L(s)$, bearing the right hand cut and the numerator function $\mathrm{N}_L(s)$, the unphysical cuts.

In order to take explicitly into account the behavior of a partial wave amplitude near threshold, which vanishes like $p^{2L} \equiv \nu^L$, we consider the new quantity, T'_L, given by:

$$\mathrm{T}'_L(s) = \frac{\mathrm{T}_L(s)}{\nu^L} \tag{5.7}$$

which also satisfy relations of the type of eqs. (5.2) and (5.5). So that we can write:

$$\mathrm{T}'_L(s) = \frac{\mathrm{N}'_L(s)}{\mathrm{D}'_L(s)} \tag{5.8}$$

From eqs. (5.2), (5.5) and (5.7), $\mathrm{N}'_L(s)$ and $\mathrm{D}'_L(s)$ will obey the following equations:

$$\begin{array}{ll} \mathrm{Im}\ \mathrm{D}'_L = \mathrm{Im}\ \mathrm{T}'^{-1}_L\ \mathrm{N}'_L = -\rho(s)\mathrm{N}'_L\nu^L, & s > s_{th} \\ \mathrm{Im}\ \mathrm{D}'_L = 0, & s < s_{th} \end{array} \tag{5.9}$$

$$\begin{array}{ll} \mathrm{Im}\ \mathrm{N}'_L = \mathrm{Im}\ \mathrm{T}'_L\ \mathrm{D}'_L, & s < s_{Left} \\ \mathrm{Im}\ \mathrm{N}'_L = 0, & s > s_{Left} \end{array} \tag{5.10}$$

Since N'_L and D'_L can be simultaneously multiplied by any arbitrary real analytic function without changing its ratio, T'_L, nor eqs. (5.9) and (5.10), we will consider in the following that N'_L is free of poles and thus, the poles of a partial wave amplitude will correspond to the zeros of D'_L.

Using dispersion relations for $\mathrm{D}'_L(s)$ and $\mathrm{N}'_L(s)$, we write from eqs. (5.9) and (5.10):

$$\mathrm{D}'_L(s) = -\frac{(s-s_0)^n}{\pi}\int_{s_{th}}^{\infty} ds' \frac{\nu(s')^L\rho(s')\mathrm{N}'_L(s')}{(s'-s)(s'-s_0)^n} + \sum_{m=0}^{n-1} \overline{a}_m s^m \tag{5.11}$$

where n is the number of subtractions needed such that

$$\lim_{s\to\infty} \frac{\mathrm{N}'_L(s)}{s^{n-L}} = 0 \tag{5.12}$$

since, from eq. (5.3)

$$\lim_{s\to\infty}\frac{\nu^L\rho(s)}{s^L}=\frac{1}{4^{L+2}\pi} \tag{5.13}$$

On the other hand, from eqs. (5.5) and (5.7), consistently with eq. (5.12)

$$\mathrm{N}'_L(s)=\frac{(s-s_0)^{n-L}}{\pi}\int_{-\infty}^{s_{Left}}ds'\frac{\mathrm{Im}\ \mathrm{T}_L(s')\mathrm{D}'_L(s')}{\nu(s')^L(s'-s_0)^{n-L}(s'-s)}+\sum_{m=0}^{n-L-1}\overline{a}'_m s^m \tag{5.14}$$

Eqs. (5.11) and (5.14) constitute a system of integral equations the input of which is given by Im $\mathrm{T}_L(s)$ along the left hand cut.

However, eqs. (5.11) and (5.14) are not the most general solution to eqs. (5.9) and (5.10) because of the possible presence of zeros of T_L which do not originate when solving those equations. These zeros have to be included explicitly and we choose to include them through poles in D'_L (CDD poles after ref. [91]). Following this last reference, let us write along the real axis

$$\mathrm{Im}\ \mathrm{D}'_L(s)=\frac{d\lambda(s)}{ds} \tag{5.15}$$

Then by eq. (5.9),

$$\begin{aligned}\frac{d\lambda}{ds}&=-\rho(s)\nu^L\mathrm{N}'_L, \quad s>s_{th}\\ \frac{d\lambda}{ds}&=0, \qquad\qquad\quad s<s_{th}\end{aligned} \tag{5.16}$$

Let s_i be the points along the real axis where $\mathrm{T}'_L(s_i)=0$. Between two consecutive points, s_i and s_{i+1}, we will have from eq. (5.16)

$$\lambda(s)=-\int_{s_i}^{s}\nu(s')^L\rho(s')\mathrm{N}'_L(s')ds'+\lambda(s_i) \tag{5.17}$$

with $\lambda(s_i)$ unknown because the inverse of $\mathrm{T}'_L(s_i)$ is not defined. Thus, we may write

$$\lambda(s)=-\int_{s_{th}}^{s}\nu(s')^L\rho(s')\mathrm{N}'_L(s')ds'+\sum_i\lambda(s_i)\theta(s-s_i) \tag{5.18}$$

with $\theta(s)$ the usual Heaviside function.

From eqs. (5.15) and (5.18), it follows that

$$\begin{aligned}\mathrm{D}'_L(s) &= \frac{(s-s_0)^n}{\pi}\int_{s_{th}}^{\infty}\frac{\mathrm{Im}\ \mathrm{D}'_L(s')ds'}{(s'-s)(s'-s_0)^n}+\sum_{m=0}^{n-1}\overline{a}_m s^m=\sum_{m=0}^{n-1}\overline{a}_m s^m\\ &- \frac{(s-s_0)^n}{\pi}\int_{s_{th}}^{\infty}\frac{\nu(s')^L\rho(s')\mathrm{N}'_L(s')}{(s'-s)(s'-s_0)^n}ds'+\frac{(s-s_0)^n}{\pi}\int_{s_{th}}^{\infty}\frac{\sum_i\lambda(s_i)\delta(s'-s_i)}{(s'-s)(s'-s_0)^n}ds'\end{aligned}$$

$$
\begin{aligned}
&= -\frac{(s-s_0)^n}{\pi}\int_{s_{th}}^{\infty}\frac{\nu(s')^L\rho(s')\mathrm{N}'_L(s')}{(s'-s)(s'-s_0)^n}ds' + \sum_{m=0}^{n-1}\overline{a}_m s^m \\
&+ \sum_i \frac{\lambda(s_i)}{\pi(s_i-s_0)^n}\frac{(s-s_0)^n}{s_i-s}
\end{aligned}
\tag{5.19}
$$

Eq. (5.19) can also be obtained from eq. (5.9) and use of the Cauchy theorem for complex integration and allowing for the presence of poles of D'_L (zeros of T'_L) inside and along the integration contour, which is given by a circle in the infinity deformed to engulf the real axis along the right hand cut, $s_{th} < s' < \infty$. In this way one can also consider the possibility of there being higher order zeros and that some of the s_i could have non-vanishing imaginary part (because of the Schwartz theorem, s_i^* will be another zero of $\mathrm{T}'_L(s)$). However, as we will see below for $L \leq 1$, when considering chiral symmetry in the large N_c QCD limit, the zeros will appear on the real axis and also as simple zeros. In general, using T'_L instead of T_L, we avoid working with L^{th} order poles of D_L at threshold in the dispersion relation given by eq. (5.19).

The last term in the right hand side of eq. (5.19) can also be written in a more convenient way avoiding the presence of the subtraction point s_0. To see this, note that

$$
\begin{aligned}
\frac{(s-s_0)^n}{s-s_i} &= (s-s_0)^{n-1}\frac{s-s_i+s_i-s_0}{s-s_i} \\
&= (s-s_0)^{n-1}(1+\frac{s_i-s_0}{s-s_i}) = (s-s_0)^{n-1} + (s_i-s_0)\frac{(s-s_0)^{n-1}}{s-s_i} \\
&= \sum_{i=0}^{n-1}(s-s_0)^{n-1-i}(s_i-s_0)^i + \frac{(s_i-s_0)^n}{s-s_i}
\end{aligned}
\tag{5.20}
$$

The terms

$$\sum_{i=0}^{n-1}(s-s_0)^{n-1-i}(s_i-s_0)^i$$

can be reabsorbed in

$$\sum_{m=0}^{n-1}\overline{a}_m s^m$$

As a result we can write

$$\mathrm{D}'_L(s) = -\frac{(s-s_0)^n}{\pi}\int_{s_{th}}^{\infty}\frac{\nu(s')^L\rho(s')\mathrm{N}'_L(s')}{(s'-s)(s'-s_0)^n} + \sum_{m=0}^{n-1}\widetilde{a}_m s^m + \sum_i\frac{\widetilde{\gamma}_i}{s-s_i} \tag{5.21}$$

with $\widetilde{a}_m$ $(n-1 \geq m \geq 0)$ and $\widetilde{\gamma}_i$, s_i $(i \geq 0)$, arbitrary parameters. However, if some of the s_i is complex there will be another s_j such that $s_j{=}s_i^*$ and $\widetilde{\gamma}_j = \widetilde{\gamma}_i^*$, as we explained above. Each term of the last sum in eq. (5.21) is referred as a CDD pole after [91]. Note that in

principle one can have an arbitrary number of CDD poles in eq. (5.21) for a given Im T_L along the left hand cut. This is why the CDD poles are also called CDD ambiguites.

Eqs. (5.21) and (5.14) stand for the general integral equations for D'_L and N'_L, respectively. Next we do the approximation of neglecting the left hand cut, that is, we set Im $\mathrm{T}_L(s) = 0$ in eq. (5.14). Thus one has:

$$\mathrm{N}'_L(s) = \sum_{m=0}^{n-L-1} \widetilde{a}'_m s^m \tag{5.22}$$

As a result, $\mathrm{N}'_L(s)$ is just a polynomial of degree $\leq n - L - 1$ [1] . So we can write,

$$\mathrm{N}'_L(s) = \mathcal{C} \prod_{j=1}^{n-L-1} (s - s_j) \tag{5.23}$$

In eq. (5.23) it is understood that if $n - L - 1$ is zero N'_L is just a constant. Thus, the only effect of N'_L will be, apart from the normalization constant $\mathcal{C}$, the inclusion, at most, of $n - L - 1$ zeros to $\mathrm{T}'_L(s)$. But we can always divide N'_L and D'_L by eq. (5.23). The net result is that, when the left hand cut is neglected, it is always possible to take $\mathrm{N}'_L(s) = 1$ and all the zeros of $\mathrm{T}'_L(s)$ will be CDD poles of the denominator function. In this way,

$$\begin{aligned}
\mathrm{T}'_L(s) &= \frac{1}{\mathrm{D}'_L(s)} \\
\mathrm{N}'_L(s) &= 1 \\
\mathrm{D}'_L(s) &= -\frac{(s-s_0)^{L+1}}{\pi} \int_{s_{th}}^{\infty} ds' \frac{\nu(s')^L \rho(s')}{(s'-s)(s'-s_0)^{L+1}} + \sum_{m=0}^{L} a_m s^m + \sum_{i}^{M_L} \frac{R_i}{s - s_i}
\end{aligned} \tag{5.24}$$

The number of free parameters present in eq. (5.24) is $L + 1 + 2\varrho$, where ϱ is the number of CDD poles, M_L, minus the number of complex conjugate pairs of s_i. These free parameters have a clear physical interpretation. Consider first the term 2ϱ which comes from the presence of CDD poles in $\mathrm{D}'_L(s)$, eq. (5.24). In [92] the presence of CDD poles was linked to the possibility of there being elementary particles with the same quantum numbers as those of the partial wave amplitude, that is, particles which are not originated from a given 'potential' or exchange forces between the scattering states. One can think that given a $\mathrm{D}'_L(s)$ we can add a CDD pole and adjust its two parameters in order to get a zero of the real part of the new $\mathrm{D}'_L(s)$ with the right position and residue, having a resonance/bound state with the desired mass and coupling. In this way, the arbitrary parameters that come with a CDD pole can be related with the coupling constant and mass of the resulting particle. This is one possible interpretation of the presence of CDD poles. However, as we are going to see below, these poles can also enter just to ensure the presence of zeros required by the underlying theory, in this case QCD, as the Adler zeros

[1] One can always make that $n \geq L + 1$ just by multiplying N'_L and D'_L by s^k with k large enough.

for the S-wave meson-meson interaction. The derivative of the partial wave amplitude at the zero will fix the other CDD parameter, $\widetilde{\gamma}_i$. With respect to the contribution $L+1$ to the number of free parameters coming from the angular momentum L, it appears just because we have explicitly established the behavior of a partial wave amplitude close to threshold, vanishing as ν^L. This is required by the centrifugal barrier effect, well known from Quantum Mechanics.

It should be stressed that eq. (5.24) is the most general structure that an elastic partial wave amplitude, with arbitrary L, has when the left hand cut is neglected. The free parameters that appear there are fitted to the experiment or calculated from the basic underlying theory. In our case the basic dynamics is expected to be QCD, but eq. (5.24) could also be applied to other scenarios beyond QCD as the Electroweak Symmetry Breaking Sector (which also has the symmetries [93] used to derived eq. (5.24), as far as it is known).

Let us come back to QCD and split the subtraction constants a_m of eq. (5.24) in two pieces

$$a_m = a_m^L + a_m^{SL}(s_0) \tag{5.25}$$

The term a_m^L will go as N_c, because in the $N_c \to \infty$ limit, the meson-meson amplitudes go as N_c^{-1} [90]. Since the integral in eq. (5.24) is $\mathcal{O}(1)$ in this counting, the subleading term $a_m^{SL}(s_0)$ is of the same order and depends on the subtraction point s_0. This implies that eq. (5.24), when $N_c \to \infty$, will become

$$\mathrm{D}'_L(s) \equiv \mathrm{D}'^{\infty}_L(s) = \sum_{m=0}^{L} a_m^L s^m + \sum_{i}^{M_L^\infty} \frac{R_i^\infty}{s - s_i} \tag{5.26}$$

where R_i^∞ is the leading part of R_i and M_L^∞ counts the number of leading CDD poles.

Clearly eq. (5.26) represents tree level structures, contact and pole terms, which have nothing to do with any kind of potential scattering, which in large N_c QCD is suppressed.

In order to determine eq. (5.26) we will make use of χPT [5] and of the paper [7]. In this latter work it is shown the way to include resonances with spin ≤ 1 consistent with chiral symmetry at lowest order in the chiral power counting. It is also seen that, when integrating out the resonance fields, the contributions of the exchange of these resonances essentially saturate the next to leading χPT Lagrangian. We will make use of this result in order to state that in the inverse of eq. (5.26) the contact terms come just from the lowest order χPT Lagrangian and the pole terms from the exchange of resonances in the s-channel in the way given by [7] (consistently with our approximation of neglecting the left hand cut the exchange of resonances in crossed channels is not considered). In the latter statement it is assumed that the result of [7] at $\mathcal{O}(p^4)$ is also applicable to higher orders. That is, local terms appearing in χPT and from eq. (5.26) of order higher than $\mathcal{O}(p^4)$ are also saturated from the exchange of resonances for $N_c >> 1$, where loops are suppressed.

Let us prove that eq. (5.26) can accommodate the tree level amplitudes coming from

lowest order χPT [5] and the Lagrangian given in [7] for the coupling of resonances (with spin ≤ 1) with the lightest pseudoscalars (π, K and η).

Following [7], one can write the exchange of a resonance (with spin ≤ 1) divided by ν^L as:

$$\begin{array}{rl} \dfrac{(c_i s + c_i' m^2)^2}{M_i^2 - s} & ;\ \mathrm{L}=0 \\ \dfrac{d_i s}{M_i^2 - s} & ;\ \mathrm{L}=1 \end{array} \tag{5.27}$$

where M_i is the mass of the i^{th} resonance, m^2 is some combination of squared masses of the lightest pseudoscalars and c_i, c_i' and d_i are arbitrary constants with $d_i \geq 0$.

The lowest order χPT partial wave amplitude ($L \leq 1$), divided again by ν^L, can be written schematically as:

$$\begin{array}{rl} as + a'\hat{m}^2 & ;\ \mathrm{L}=0 \\ b & ;\ \mathrm{L}=1 \end{array} \tag{5.28}$$

with $\hat{m}^2$ another combination of squared masses of the lightest pseudoscalars.

Thus, in large N_c QCD, the partial wave amplitudes will have the following structure, after omitting the exchange of resonances in crossed channels and contact terms of order higher than $\mathcal{O}(p^2)$

$$\begin{aligned} \mathrm{T}_0'(s) \equiv \mathrm{T}_0'^{\infty}(s) &= as + a'\hat{m}^2 + \sum_{i=1}^{R_0} \frac{(c_i s + c_i' m^2)^2}{M_i^2 - s} \\ \mathrm{T}_1'(s) \equiv \mathrm{T}_1'^{\infty}(s) &= b + \sum_{i=1}^{R_1} \frac{d_i s}{M_i^2 - s} \end{aligned} \tag{5.29}$$

In the former equation it is understood that if $R_L = 0$ the sum does not appear.

Let us now study the inverse of eq. (5.29) in order to connect with $\mathrm{D}_L'^{\infty}$. With ξ_L, the number of zeros of $\mathrm{T}_L'^{\infty}$, we can write:

$$\frac{1}{\mathrm{T}_L'^{\infty}(s)} = \mathcal{A}_L \frac{\prod_{i=1}^{R_L}(s - M_i^2)}{\prod_{r=1}^{\xi_L}(s - s_r)} \tag{5.30}$$

In the former equation, if $R_L = 0$ or $\xi_L = 0$, the corresponding product must be substituted by 1. $\mathcal{A}_L$ is just a constant. Note that from eqs. (5.29) $\xi_0 \leq R_0 + 1$ and $\xi_1 \leq R_1$, from simple counting of the degree of the polynomials that appear in the numerators after writing eqs. (5.29) as rational functions.

On the other hand, note from eqs. (5.27) that, for $s \geq 0$, the amplitude from the exchange of resonances, both for $L = 0$ and 1, is positive below the mass of the resonance

and negative above it. This implies that in the interval, $M_{i+1}^2 \geq s \geq M_i^2$, by continuity, there will be a zero of $\mathrm{T}_L'^{\infty}$. In this way,

$$\xi_L \geq R_L - 1 \tag{5.31}$$

For $L = 0$, apart from the zeros between resonances, one has also the requirement from chiral symmetry of the presence of the Adler zero, along the real axis and below threshold. Thus, $\xi_0 \geq R_0$ and we can write

$$R_L - L + 1 \geq \xi_L \geq R_L - L \tag{5.32}$$

Note that since the $R_L - L$ zeros of T_L^{∞} are real, the possible single additional zero from the upper limit of eq. (5.32) must be also real, since a complex one would imply its conjugate too. This is so because all the coefficients in eq. (5.29) are real.

Let us do the counting of zeros and resonances from eq. (5.26). The number of zeros of $\mathrm{T}_L'^{\infty}$ is equal to the number of CDD poles of $\mathrm{D}_L'^{\infty}$, M_L^{∞}. Hence

$$\xi_L = M_L^{\infty} \tag{5.33}$$

On the other hand the number of poles of $\mathrm{T}_L'^{\infty}$ is equal to the number of zeros of $\mathrm{D}_L'^{\infty}$ which has the following upper limit

$$R_L \leq M_L^{\infty} + L \equiv \xi_L + L \tag{5.34}$$

Thus,

$$\xi_L \geq R_L - L \tag{5.35}$$

which gives the same lower limit as in eq. (5.32). Let us recall that the zeros of eq. (5.30) are real, as discussed above. This, together with the requirement of $\mathrm{T}_L'^{\infty}(s)$ being a real function on the real axis, forces all parameters in eq. (5.26) to be real. Then the number of free parameters in eq. (5.26) are $2M_L^{\infty} + L + 1 = 2\xi_L + L + 1$. When fixing the s_i parameters in eq. (5.26) to the s_r parameters in eq. (5.30) this reduces in ξ_L the number of free parameters in eq. (5.26). By fixing the arbitrary constant $\mathcal{A}_L$ of eq. (5.30) this leaves us with $\xi_L + L$ free parameters in eq. (5.26). Imposing now the position of the R_L resonances of eq. (5.30) to be at M_i^2 we have R_L additional constraints. Hence we should have

$$\xi_L + L - R_L \geq 0 \tag{5.36}$$

which actually holds, as seen above in eq. (5.35). As a consequence eqs. (5.29) can always be cast in the form of eq. (5.26)

Let us define the function $g_L(s)$ by

$$g_L(s)\nu^L = \sum_{m=0}^{L} a_m^{SL}(s_0)s^m - \frac{(s-s_0)^{L+1}}{\pi}\int_{s_{th}}^{\infty} ds' \frac{\nu(s')^L \rho(s')}{(s'-s)(s'-s_0)^{L+1}} \tag{5.37}$$

and using the notation

$$\mathrm{T}_L^\infty(s) = \nu^L [\sum_{m=0}^{L} a_m^L s^m + \sum_{i=1}^{M_L} \frac{R_i}{s - s_i}]^{-1} \tag{5.38}$$

results that from eq. (5.24) one has

$$\mathrm{T}_L(s) = [1/\mathrm{T}_L^\infty(s) + g_L(s)]^{-1} \tag{5.39}$$

The physical meaning of Eq. (5.39) is clear. The T_L^∞ amplitudes correspond to the tree level structures present before unitarization. The unitarization is then accomplished through the function $g_L(s)$. It is interesting at this point to connect with the most popular K-matrix formalism to obtain unitarized amplitudes. In this case one writes:

$$T_L(s) = [K_L(s)^{-1} - i\rho(s)]^{-1} \tag{5.40}$$

we see that the former equation is analogous to eq. (5.39) with $\mathrm{T}_L^{\infty\,-1}(s) + \mathrm{Re}\, g_L(s) = K_L(s)^{-1}$.

From the former comments it should be obvious the generalization of eq. (5.39) to coupled channels. In this case, $\mathrm{T}_L^\infty(s)$ is a matrix determined by the tree level partial wave amplitudes given by the lowest order χPT Lagrangian [5] and the exchange of resonances [7]. For instance, $[T_L^\infty(s)]_{11} = T_{11}^{(2)} + T_{11}^R$, $[T_L^\infty(s)]_{12} = T_{12}^{(2)} + T_{12}^R$ and so on. Where $T^{(2)}$ is the matrix of the $\mathcal{O}(p^2)$, χPT partial wave amplitudes [5] and T^R the corresponding one from the exchange of resonances [7] in the s-channel. Once we have $\mathrm{T}_L^\infty(s)$ its inverse is the one which enters in eq. (5.39). Because $\mathrm{N}_L'(s)$ is proportional to the identity, $g_L(s)$ will be a diagonal matrix, accounting for the right hand cut, as in the elastic case. In this way, unitarity, which in coupled channels reads (above the thresholds of the channels i and j)

$$[\mathrm{Im}\ \mathrm{T}_L^{-1}]_{ij} = -\rho_{ii}(s)\delta_{ij} = \mathrm{Im}\ \mathrm{g}_L(s)_{ii}\delta_{ij} \tag{5.41}$$

is fulfilled. The matrix element $g_L(s)_{ii}$ obeys eq. (5.37) with the right masses corresponding to the channel i and its own subtraction constants $a_i^{SL}(s_0)$.

In the present work the coupling constants and resonance masses contained in $\mathrm{T}_L^\infty(s)$ are fitted to the experiment. The same happens with the a_i^{SL} although, as we will discuss below, they are related by $SU(3)$ considerations.

In Appendix C the already stated coupled channel version of eq. (5.39) is deduced directly from the N/D method in coupled channels [94].

5.2 Reinterpretation of the results of ref. [58].

The most simple application of eq. (5.39) occurs when one only includes the lowest order χPT amplitudes and forgets about explicit resonance fields. This was the situation considered in ref. [58] for $L = 0$, although there we arrived to the same eq. (5.39) by a different argumentation. This work was already reported in my master's thesis.

Let us note that we are not including any explicit resonance and hence we are in the situation described in **section 3.1.B**. Thus, let us change momentarily the notation and instead of T_L^∞ we take the symbol V, which usually denotes a potential. In this way, eq. (5.39) can also be written as:

$$\mathrm{T}_0(s) = \mathrm{V}(s) + \mathrm{V}(s) \cdot (-g(s)) \cdot \mathrm{T}_0(s) \tag{5.42}$$

which is like a Lippmann-Schwinger(LS) equation but with relativistic propagators. However, while eq. (5.42) is an algebraic equation a LS equation is an integral one. The point is that in eq. (5.42) $\mathrm{V}(s)$ and $\mathrm{T}_0(s)$ are factorized and simply multiply the loop function $-g(s)$. In a LS equation one should have instead the following integral

$$(\mathrm{V}(-g)\mathrm{T}_L)_{\alpha\beta} = \int \frac{d^4q}{(2\pi)^4} V(k,p;q)_{\alpha i} \frac{i}{(q^2 - m_{1i}^2)\left((P-q)^2 - m_{2i}^2\right)} \mathrm{T}_0(q;k',p')_{i\beta} \tag{5.43}$$

where P is the total momentum, k and p represent the inital momenta of the ingoing mesons and k' and p' the final momenta of the outgoing ones. Only when V and T_L are factorized outside the integral eq. (5.42) and a LS equation are equivalent.

In ref. [58], it was discussed that this was in fact the case. Writting

$$\mathrm{V} = \mathrm{V}_{on-shell} + \mathrm{V}_{off-shell} \tag{5.44}$$

the $\mathrm{V}_{on-shell}(p_i)$ part, with $p_i^2 = m_i^2$, factorizes out of the integral in eq. (5.43) since it only depends of the Mandelstam variable s. For $\mathrm{V}_{off-shell}$ it was realized that it only gives rise to tadpole like contributions which can be reabsorbed in the physical values of masses and decay constants. So that, at the end, one only needs $\mathrm{V}_{on-shell}$ and hence, eq. (5.42) follows.

This result is clear from the formalism developed in the former section, since one needs the physical values for the positions and residues of the CDD poles and the constant a_0, eq. (5.24).

Other works that also use LS equations are [95] in the meson-baryon system and [96] in the meson-meson one. In fact, the former reference inspired our work [58].

In ref. [58] the $g_0(s)$ function was calculated making use of a cut-off regularization. In **appendix A** the relation between cut-off and dimensional regularization is given. The cut-off, Λ, was fixed to reproduce the experimental points, or in other words, to give the right value for the substraction constant a_0^{SL} in eq. (5.37). In Fig. 5.1 we show the results compared with data. The agreement is rather good and surprising. In this work we also found poles corresponding to the $f_0(980)$, $a_0(980)$ and $\sigma(500)$ resonances. Their masses, partial and total decay widths were in agreement with the experimental values [19].

Hence, we see that for the scalar sector with I=0,1 the unitarization of the lowest order χPT amplitudes plays a very important role and also that the resonances which appear there with masses $\leq$1 GeV will have a large meson-meson component in their nature. The same results are expected to hold in the I=1/2 S-wave amplitude by $SU(3)$ symmetry. We will investigate further these points in **section 5.4** where we will also have the presence of explicit scalar resonances.

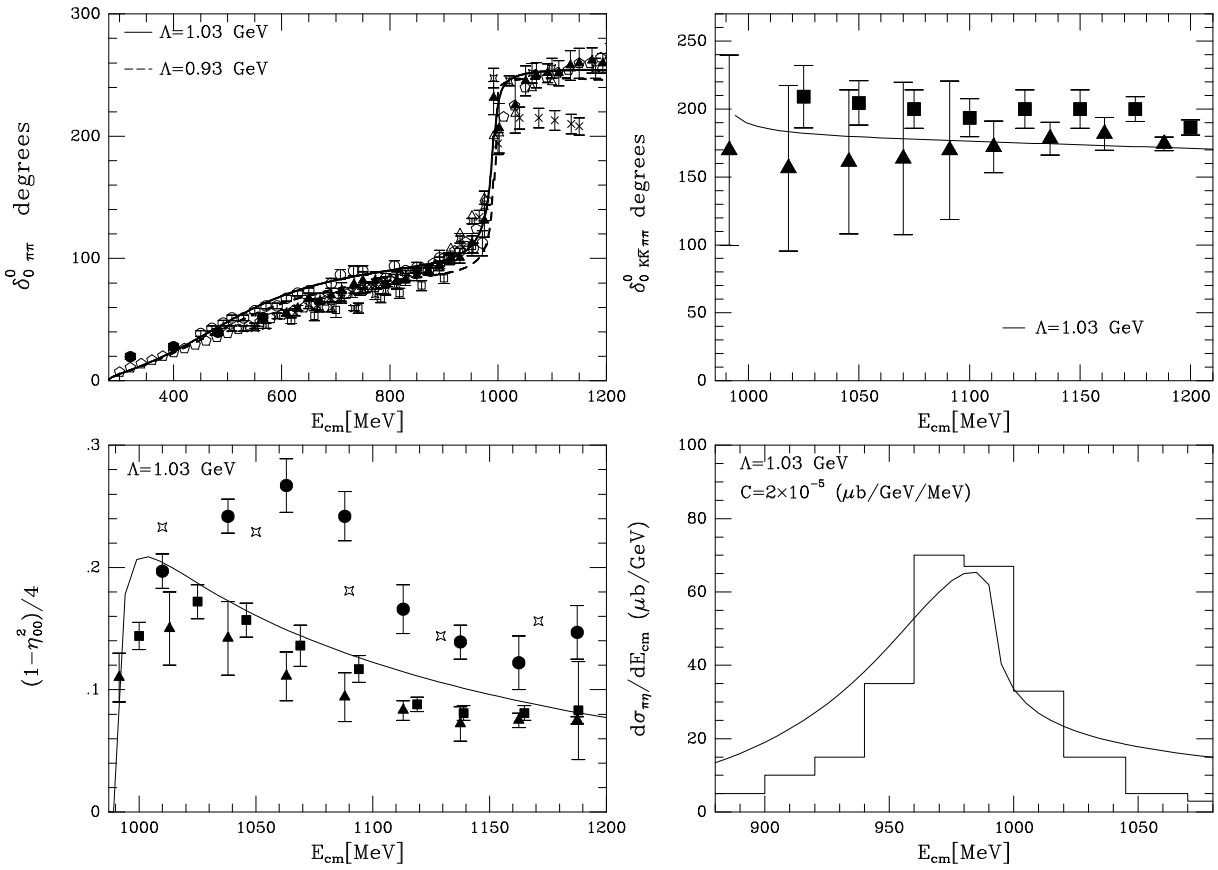

Figure 5.1: Results from [58]. References to experimental papers are also given in this paper.

5.3 The ideal case: elastic vector channels.

In this section we are going to study the $\pi\pi$ and $K\pi$ scattering with I=L=1 and I=1/2,L=1, respectively. It will be shown, as mentioned in the introduction, that these reactions can be understood just by invoking:

1) Chiral Symmetry
2) large N_c QCD
3) Unitarity

A priori, one could think that relations coming from the $N_c \to \infty$ limit should work rather accurately at the phenomenological level in these channels due to the predominant role of the ρ and K^* poles over subleading effects in $1/N_c$, as unitarity loops.

Since the zero at threshold is a simple zero for L=1, we will use, instead of eq. (5.24), the slightly modified formula:

$$\mathrm{D}_1(s) = \sum_i \frac{\gamma_i}{s - s_i} + a - \frac{s - s_0}{\pi} \int_{s_{th}}^{\infty} ds' \frac{\rho(s')}{(s' - s)(s' - s_0)} \tag{5.45}$$

where the threshold zero has passed to poles in the denominator function, D_1. This equation can be derived as eq. (5.24) but working directly with T_1 rather than T_1'. Another advantage of using eq. (5.45) instead of eq. (5.24) is that the comparison with the scalar sector will be more straightforward, because the dispersive integral will be the same.

The integral in eq. (5.45) will be evaluated making use of dimensional regularization. It can be identified up to a constant to the loop represented in Fig. 5.2. This identification is consequence of the fact that both the integral in eq. (5.45) and the loop given in Fig. 5.2 have the same cut and the same imaginary part along this cut, as it can be easily checked.

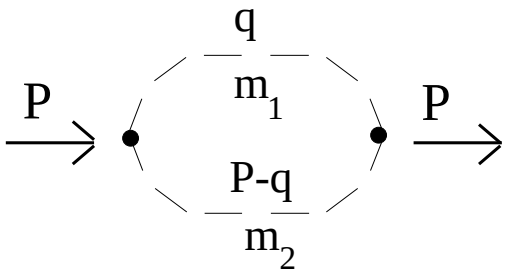

Figure 5.2: Loop giving rise to the g_0 function.

Following eq. (5.37) we define

$$\begin{aligned} g_0(s) &= a^{SL}(s_0) - \frac{s-s_0}{\pi}\int_{s_{th}}^{\infty} ds' \frac{\rho(s')}{(s'-s)(s'-s_0)} \\ &= \frac{1}{(4\pi)^2}\left[\tilde{a}^{SL}(\mu) + \log\frac{m_2^2}{\mu^2} - \frac{m_1^2-m_2^2+s}{2s}\log\frac{m_2^2}{m_1^2} - \frac{\lambda^{1/2}(s,m_1^2,m_2^2)}{2s}\cdot\right. \\ &\quad \left.\cdot\log\left(\frac{m_1^2+m_2^2-s+\lambda^{1/2}(s,m_1^2,m_2^2)}{m_1^2+m_2^2-s-\lambda^{1/2}(s,m_1^2,m_2^2)}\right)\right] \end{aligned} \tag{5.46}$$

for $s \geq s_{th}$. For $s < s_{th}$ or s complex one has the analytic continuation of eq. (5.46). The function $\lambda^{1/2}(s,m_1^2,m_2^2)$ was already introduced in eq. (5.4). The regularization scale μ, appearing in the last formula of eq. (5.46), plays a similar role than the arbitrary subtraction point s_0 in the first formula of eq. (5.46). This similarity is consequence of the fact that both μ and s_0 can have any arbitrary value but the resulting function $g_0(s)$ is independent of this particular value because of the change in the subtraction constant, $\tilde{a}^{SL}(\mu)$ for dimensional regularization or $a^{SL}(s_0)$ for the dispersion integral. The $\tilde{a}^{SL}(\mu)$ 'constant' will change under a variation of the scale μ to other one μ' as

$$\tilde{a}^{SL}(\mu') = \tilde{a}^{SL}(\mu) + \log\frac{\mu'^2}{\mu^2} \tag{5.47}$$

in order to have $g_0(s)$ invariant under changes of the regularization scale. We will take $\mu = M_\rho = 770$ MeV [19]. The function $g_0(s)$ is also symmetric under the exchange $m_1 \leftrightarrow m_2$ and for the equal mass limit it reduces to

$$g_0(s) = \frac{1}{(4\pi)^2}\Big[\tilde{a}^{SL}(\mu) + \log\frac{m_1^2}{\mu^2} + \sigma(s)\log\frac{\sigma(s)+1}{\sigma(s)-1}\Big] \tag{5.48}$$

with

$$\sigma(s) = \sqrt{1 - \frac{4m_1^2}{s}} \tag{5.49}$$

After this preamble, let us consider in first place the $\pi\pi$ scattering with I=L=1. As can be seen from Fig. 5.3 this process is dominated by the ρ exchange. From eq. (5.45) one has

$$\mathrm{T}_1^{\pi\pi}(s) = \Big[\frac{\gamma_1^{\pi\pi}}{s-4m_\pi^2} + \tilde{a}^L_{\pi\pi} + g_0^{\pi\pi}(s) + \sum_{i=2}\frac{\gamma_i}{s-s_i}\Big]^{-1} \tag{5.50}$$

The first term in the R.H.S of the last equation fixes the zero at threshold for a P-wave amplitude.

The tree level part of $T_1^{\pi\pi}(s)$ from ref. [7] and lowest order χPT [5], in the way explained in the last section, is given by:

$$\mathrm{T}_1^{\pi\pi\,\infty}(s) = \frac{2}{3}\frac{p_{\pi\pi}^2}{f^2} + g_v^2\frac{2}{3}\frac{p_{\pi\pi}^2}{f^2}\frac{s}{M_\rho^2 - s} \tag{5.51}$$

with $p_{\pi\pi}^2$ the three-momentum squared of the pions in the c.m., $f = 87.3$ MeV the pion decay constant in the chiral limit [5]. The deviation of g_v^2 with respect to unity measures the variation of the value of the ρ coupling to two pions with respect to the KSFR relation [29], $g_v^2 = 1$. In [24] this KSFR relation is justified making use of large N_c QCD (neglecting loop contributions) and an unsubtracted dispersion relation for the pion electromagnetic form factor (a QCD inspired high-energy behavior).

Comparing eqs. (5.50) and (5.51), one needs only one additional CDD pole apart from the one at threshold and we obtain

$$\begin{aligned}
\tilde{a}^L &= 0 \\
\gamma_1^{\pi\pi} &= \frac{6f^2(M_\rho^2 - 4m_\pi^2)}{(M_\rho^2 - 4m_\pi^2(1-g_v^2))} \\
\gamma_2^{\pi\pi} &= \frac{6f^2}{1-g_v^2}\,\frac{g_v^2 M_\rho^2}{M_\rho^2 - (1-g_v^2)4m_\pi^2} \\
s_2 &= \frac{M_\rho^2}{1-g_v^2}
\end{aligned} \tag{5.52}$$

Thus, we can write our final formula for the isovector $\pi\pi$ scattering in the following way

$$\mathrm{T}_1^{\pi\pi}(s) = \Big[\frac{\gamma_1^{\pi\pi}}{s-4m_\pi^2} + \frac{\gamma_2^{\pi\pi}}{s-s_2} + g_0^{\pi\pi}(s)\Big]^{-1} \tag{5.53}$$

in terms of the parameters g_v^2 and $\tilde{a}^{SL}(\mu)$. Since g_v^2 is expected to be close to unity as discussed above, it is useful to consider the limit when $g_v^2 \to 1$, in which case $s_2 \to \infty$ such that

$$\frac{\gamma_2^{\pi\pi}}{s-s_2} \to -\frac{6f^2}{M_\rho^2} \equiv \tilde{a}'^{L}_{\pi\pi} \tag{5.54}$$

in which case the second CDD pole in eq. (5.53), at s_2, moves to infinity and the CDD pole contribution gives rise to a constant term, $\tilde{a}'^{L}_{\pi\pi}$. In this limit we can write

$$\mathrm{T}_1^{\pi\pi}(s) = [\frac{\gamma_1^{\pi\pi}}{s-4m_\pi^2} + \tilde{a}'^{L}_{\pi\pi} + g_0^{\pi\pi}(s)]^{-1} \tag{5.55}$$

Our calculated phase shifts for the vector $\pi\pi$ scattering are represented in the dashed line of Fig. 5.3, when g_v^2 is taken equal to one and $\tilde{a}^{SL} = 0$. The agreement with the experimental data is rather good. If we had just taken the imaginary part of $g_0^{\pi\pi}(s)$ in the former equation we would have obtained basically the same curve. This last case corresponds just to the Breit Wigner amplitude

$$\begin{aligned} &\frac{2}{3}\frac{p_{\pi\pi}^2}{f^2}\,\frac{M_\rho^2}{M_\rho^2 - s - \mathrm{i}M_\rho\Gamma_\rho(s)} \\ &\Gamma_\rho(s) = \frac{p_{\pi\pi}^3}{12\pi f^2}\frac{M_\rho}{\sqrt{s}} \end{aligned} \tag{5.56}$$

For the I=1/2, L=1 $K\pi$ scattering, the tree level amplitude $\mathrm{T}_1^{K\pi\,\infty}$, is just given by multiplying eq. (5.51) by 3/4 and substituting $p_{\pi\pi}^2$ by $p_{K\pi}^2 = \dfrac{\lambda(s,m_\pi^2,m_K^2)}{4s}$ and M_ρ by M_K^*=896 MeV [19], the mass of the neutral $K^*(890)$. Now m_K is the mass of the kaon, 495.7 MeV [19]. On the other hand, since $m_K \neq m_\pi$ instead of having just a single pole in the denominator function, as in eq. (5.50), for the zero at threshold, one has two simple poles

$$\frac{\gamma_1^{K\pi}}{4p_{K\pi}^2} = \frac{\gamma_1^{K\pi}}{s_+ - s_-}\Big[\frac{s_+}{s-s_+} - \frac{s_-}{s-s_-}\Big] \tag{5.57}$$

with $s_+ = (m_K + m_\pi)^2$ and $s_- = (m_K - m_\pi)^2$. That is, we will have two CDD poles but both entering with just one parameter because the behavior at threshold is proportional to $p_{K\pi}^2$. In our notation

$$\lim_{s\to s_{th}} \frac{\mathrm{T}_1^{K\pi}(s)}{p_{K\pi}^2} = \frac{4}{\gamma_1^{K\pi}}$$

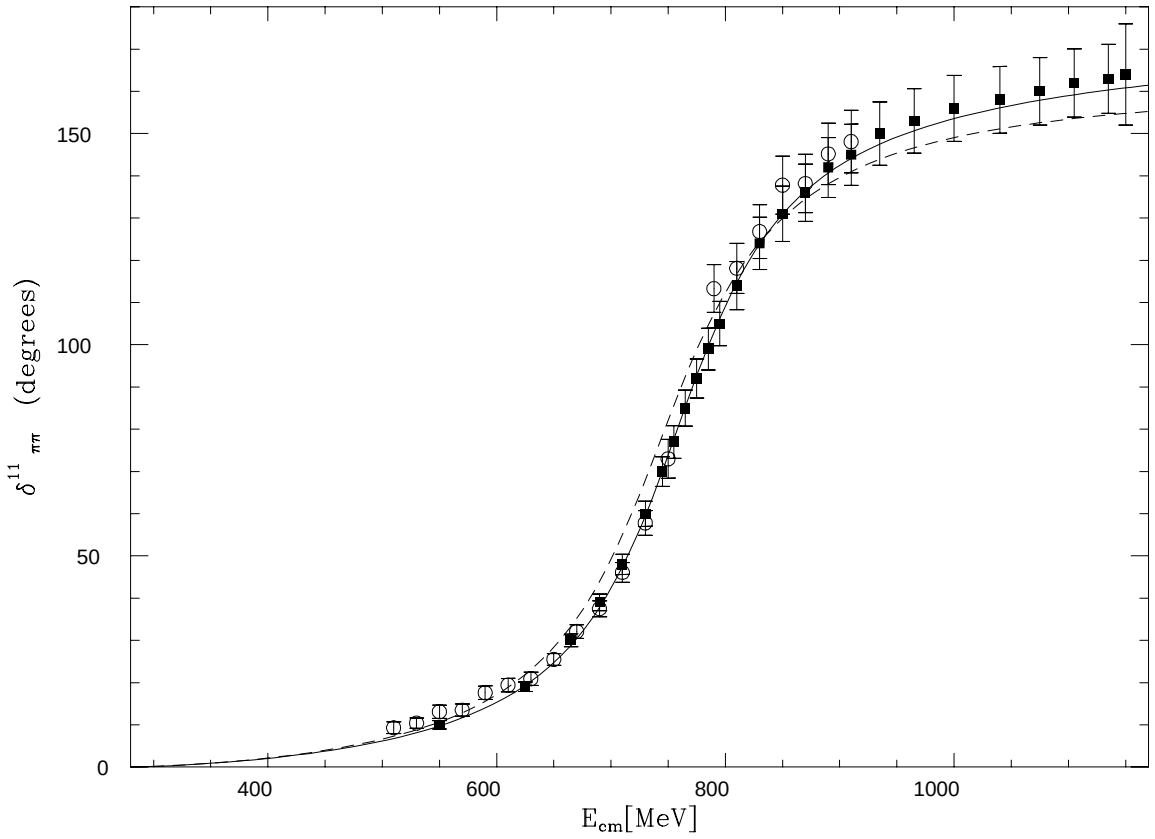

Figure 5.3: Isovector $\pi\pi$ elastic phase shifts from threshold up to $\sqrt{s} \leq 1.2$ GeV. The dashed line corresponds to taking $g_v^2 = 1$ and $\tilde{a}^{SL} = 0$. The continuum line corresponds to the simultaneous fit to the ρ and K^* channels, given by eq. (5.61). Data: circles [65], squares [66]

For the simple and realistic case, $g_v^2 = 1$, we have, analogously to the case of the ρ,

$$\mathrm{T}_1^{K\pi}(s) = [\frac{\gamma_1^{K\pi}}{4p_{K\pi}^2} + \tilde{a}'^L_{K\pi} + g_0^{K\pi}(s)]^{-1} \tag{5.58}$$

with

$$\begin{aligned} \gamma_1^{K\pi} &= \frac{8f^2(M_{K^*}^2 - (m_K + m_\pi)^2)}{M_{K^*}^2} \\ \tilde{a}^L_{K\pi} &= -\frac{8f^2}{M_{K^*}^2} \end{aligned} \tag{5.59}$$

In the general case when $g_v^2 \neq 1$, one proceeds in the same way as for the ρ introducing an extra CDD, but we shall omit the details here and the evaluations are done directly using the final formula

$$\mathrm{T}_1^{K\pi} = [\frac{1}{1/T_1^{K\pi\,\infty} + g_0^{K\pi}(s)}]^{-1} \tag{5.60}$$

with $T_1^{K\pi\,\infty}$ evaluated as mentioned above.

In Fig. 5.4, the calculated phase shifts for the I=1/2, P-wave $K\pi$ scattering are shown in the dashed curve for $g_v^2 = 1$ and $\tilde{a}^{SL} = 0$. The same remarks, as done before for the ρ when commenting Fig. 5.3, are also valid for the K^*. It is worth stressing that the dashed lines of Fig. 5.3 and 5.4 have no free parameters at all, and depend only on f and the masses of the resonances K^* and ρ.

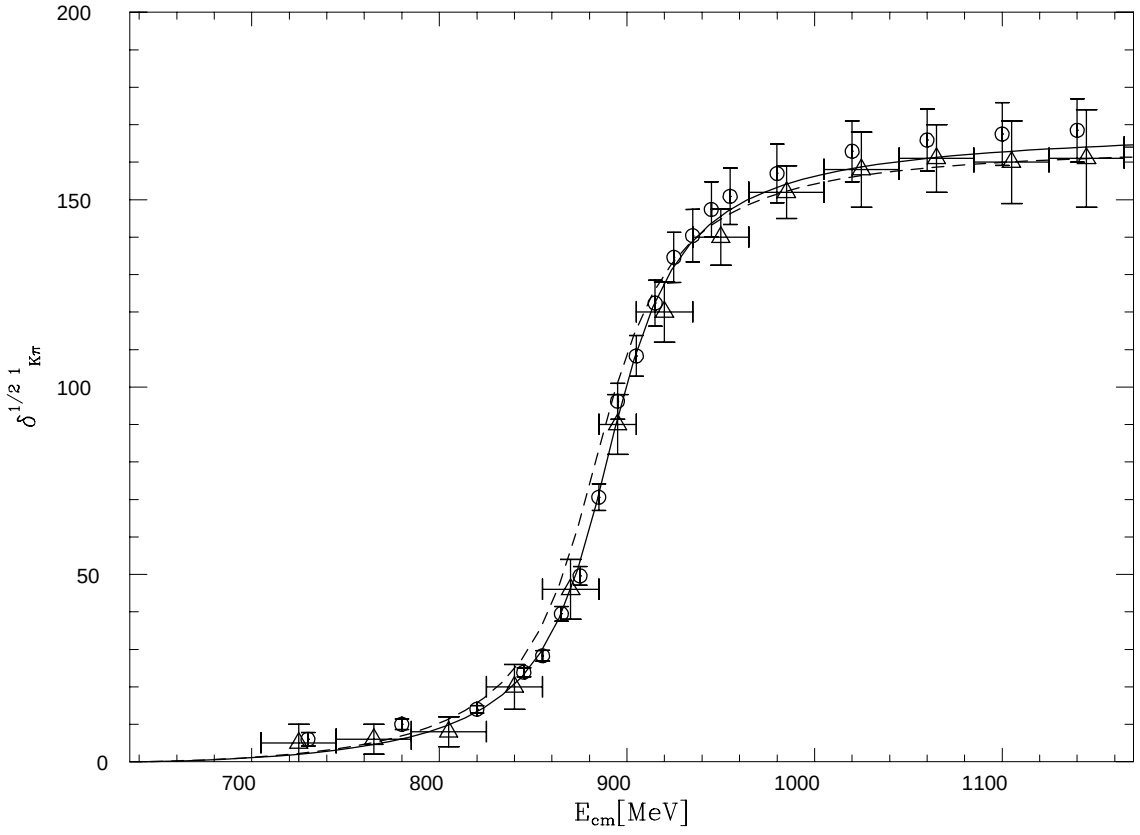

Figure 5.4: P-wave elastic $K\pi$ phase shifts with I=1/2, from threshold up to $\sqrt{s} \leq 1.2$ GeV.The dashed line corresponds to taking $g_v^2 = 1$ and $\tilde{a}^{SL} = 0$. The continuum line corresponds to the simultaneous fit to the ρ and K^* channels, given by eq. (5.61). Data: triangles [68], circles [71]

The subleading constant $\tilde{a}^{SL}$ present in $g_0(s)$, eq. (5.46), should be the same for the $\pi\pi$ and $K\pi$ states because the dependence of the loop represented in Fig. 5.2 on the masses of the intermediate particles is given by eq. (5.46). This point can be used in the opposite sense. That is, if it is not possible to obtain a reasonable good fit after setting $\tilde{a}^{SL}$ to be the same in both channels, some kind of SU(3) breaking is missing.

From eqs. (5.53) and (5.60) we do a simultaneous fit to the experimental P-wave $\pi\pi$ (I=1) and $K\pi$ (I=1/2) phase shifts with g_v^2 and $\tilde{a}^{SL}$ as free parameters using the minimization program MINUIT. In order to make the data from different experiments consistent between each other, a systematic relative error of a 5% is given to each data point if its own error is smaller than this bound. The result of the fit is:

$$\begin{aligned} g_v^2 &= 0.879 \pm 0.016 \\ \tilde{a}^{SL} &= 0.341 \pm 0.042 \end{aligned} \tag{5.61}$$

the errors are just statistical and are obtained by increasing in one unit the χ^2 per degree of freedom, $\chi^2_{d.o.f}$. The $\chi^2_{d.o.f}$ obtained is:

$$\chi^2_{d.o.f} = 0.74 \tag{5.62}$$

with 81 experimental points.

The continuum line corresponds to the fit given by eq. (5.61). We see that the agreement with data is very good. Note also that g_v^2 is very close to unity. To consider the discrepancy with the KSFR result, which refers to the value of the coupling constant, it is better to use g_v which results to be, from eq. (5.61), 0.94. That is, only a 6% of deviation respect to unity.

It is interesting and enlightening to see the value that the regularization scale μ should have in order to generate the ρ pole at 770 MeV when removing $\tilde{a}'^{IL}_{\pi\pi}$ from eq. (5.55) and setting $\tilde{a}^{SL} = 0$. In this way we are taking the regularization scale as a cut-off, as done in the former section for the S-waves. The eq. (5.55), neglecting $4m_\pi^2$ with respect to M_ρ^2, transforms to:

$$\Big[\frac{6f^2}{s-4m_\pi^2} + g_0(s)\Big]^{-1} \tag{5.63}$$

The resulting μ will be around by 0.7 TeV, a value completely senseless [2]. Its natural value is $\mu \simeq 1$ GeV, where typically resonances appear. A similar conclusion about these unrealistic high values of the cut-off was also obtained in [97]. This value of μ makes it manifest that, as we have already seen in this section, the origin of the vectors K^* and ρ is attached to tree level structures, preexisting before unitarization.

For the scalar sector, which we will study in further detail in the next section, we have only to do the following change in eq. (5.63),

$$\frac{6f^2}{s-4m_\pi^2} \longrightarrow \frac{f^2}{s-m_\pi^2/2} \tag{5.64}$$

that is, basically a factor 6 of difference for s around M_ρ^2. This makes that the 'cut-off' needed in the $\pi\pi$ S-wave to get a resonance of the same mass than the ρ is just 1.8 GeV.

[2] Witout neglecting $4m_\pi^2$ compared with M_ρ^2 one has to multiply the quotient $\frac{6f^2}{s-4m_\pi^2}$ in eq. (5.63) by $\frac{M_\rho^2-4m_\pi^2}{M_\rho^2} \simeq 0.87$, as one can check from eq. (5.55). The resulting μ is 0.3 TeV

The change has been drastic due to the logarithmic dependence of the regularization scale in eq. (5.63).

5.4 The scalar sector.

In this section we want to study the S-wave I=0,1 and 1/2 amplitudes. For the partial wave amplitudes with L=0 and I=0 and 1, coupled channels are fundamental in order to get an appropriate description of the physics involved up to $\sqrt{s} \leq 1.3$ GeV. This is an important difference with respect the former vector channels, essentially elastic in the considered energy region. Up to $\sqrt{s} = 1.3$ GeV the most important channels are:

$$\begin{array}{ll} I=0 & \pi\pi(1),\ K\bar{K}(2),\ \eta\eta(3) \\ I=1 & \pi\eta(1),\ K\bar{K}(2) \\ I=1/2 & K\pi(1),\ K\eta(2) \end{array} \tag{5.65}$$

where the number between brackets indicates the index associated to the corresponding channel when using a matrix notation as the one introduced in **section 5.1**.

For the I=0 S-wave, the 4π state becomes increasingly important at energies above $1.2 - 1.3$ GeV, so that, in this channel, we are at the limit of applicability of only two mesons states when $\sqrt{s}$ is close to 1.4 GeV. In the I=1/2 channel, the threshold of the important $K\eta'$ state is also close to 1.4 GeV. Thus, one cannot go higher in energies in a realistic description of the scalar sector without including the $K\eta'$ and 4π states.

Two sets of resonances appear in the former L=0 partial wave amplitudes [19]. A first one, with a mass around 1 GeV, contains the I=0 $f_0(400-1200)$ and $f_0(980)$ and the I=1 $a_0(980)$. A second set appears with a mass around 1.4 GeV as the I=0 $f_0(1370)$ and the $f_0(1500)$, the I=1 $a_0(1450)$ or the I=1/2 $K_0^*(1430)$. As a consequence, one could be tempted to include the exchange of two scalar nonets, with masses around 1 and 1.4 GeV. Before discussing whether this is the case, let us write the symmetric T_0^∞ matrix of tree level amplitudes for the different isospins. This matrix, T_0^∞, is determined, as explained at the end of **section 5.1**, from the lowest order χPT amplitudes, $\mathrm{T}^{(2)}$, and from the exchange of scalar nonets in the s-channel as given by ref. [7], T^R, see also eqs. (2.21) and (2.22) where the corresponding Lagrangians are given. In the following formulas we consider the exchange of only one nonet. If more nonets are needed, they have only to be added in the same way as the first nonet is introduced

I=0

$$\begin{aligned} \mathrm{T}^\infty_{0,11} &= \frac{2s-m_\pi^2}{2f^2} + \frac{3}{2}\frac{(\alpha_1)^2}{M_1^2-s} + \frac{3}{2}\frac{(\beta(0)_1)^2}{M_8^2-s} \\ \mathrm{T}^\infty_{0,12} &= \frac{\sqrt{3}}{4}\frac{s}{f^2} + \sqrt{3}\frac{\alpha_1\alpha_2}{M_1^2-s} + \sqrt{3}\frac{\beta(0)_1\beta(0)_2}{M_8^2-s} \end{aligned}$$

$$
\begin{aligned}
\mathrm{T}^{\infty}_{0,22} &= \frac{3}{4}\frac{s}{f^2} + 2\frac{(\alpha_2)^2}{M_1^2 - s} + 2\frac{(\beta(0)_2)^2}{M_8^2 - s} \\
\mathrm{T}^{\infty}_{0,13} &= -\frac{m_\pi^2}{\sqrt{12}f^2} - \frac{\sqrt{3}}{2}\frac{\alpha_1\alpha_3}{M_1^2 - s} - \frac{\sqrt{3}}{2}\frac{\beta(0)_1\beta(0)_3}{M_8^2 - s} \\
\mathrm{T}^{\infty}_{0,23} &= -\frac{3s - 2m_\eta^2 - 2/3m_\pi^2}{4ff_\eta} - \frac{\alpha_2\alpha_3}{M_1^2 - s} - \frac{\beta(0)_2\beta(0)_3}{M_8^2 - s} \\
\mathrm{T}^{\infty}_{0,33} &= \frac{16m_K^2 - 7m_\pi^2}{18f^2} + \frac{1}{2}\frac{(\alpha_3)^2}{M_1^2 - s} + \frac{1}{2}\frac{(\beta(0)_3)^2}{M_8^2 - s}
\end{aligned}
\tag{5.66}
$$

with M_1 and M_8 the masses of the singlet and octet in the SU(3) limit, m_η is the mass of the η, 547.45 MeV [19], f_η is the decay constant of the η, set to the value $f_\eta = 1.3 f_\pi$ according with the χPT prediction [5], $f_\pi = 92.4$ MeV is the pion decay constant and α_i and $\beta(0)_i$ are given by:

$$
\begin{aligned}
\beta(0)_1 &= \frac{4}{\sqrt{6}f^2}[c_d\frac{s}{2} + (c_m - c_d)m_\pi^2] \\
\beta(0)_2 &= -\frac{\sqrt{2}}{\sqrt{3}f^2}[c_d\frac{s}{2} + (c_m - cd)m_K^2] \\
\beta(0)_3 &= -\frac{4}{\sqrt{6}f^2}[c_d\frac{s}{2} + \frac{4}{3}(2c_m - c_d)m_K^2 - (5c_m - c_d)\frac{m_\pi^2}{3}] \\
\alpha_1 &= \frac{4}{f^2}[\tilde{c}_d\frac{s}{2} + (\tilde{c}_m - \tilde{c}_d)m_\pi^2] \\
\alpha_2 &= \frac{4}{f^2}[\tilde{c}_d\frac{s}{2} + (\tilde{c}_m - \tilde{c}_d)m_K^2] \\
\alpha_3 &= \frac{4}{f^2}[\tilde{c}_d\frac{s}{2} + (\tilde{c}_m - \tilde{c}_d)m_\eta^2]
\end{aligned}
\tag{5.67}
$$

the constants c_d, c_m, $\tilde{c}_d$ and $\tilde{c}_m$ characterize the coupling of a given scalar nonet to the pseudoscalar pairs of pions, kaons and etas as given in [7].

I=1

$$
\begin{aligned}
\mathrm{T}^{\infty}_{0,11} &= \frac{m_\pi^2}{3f^2} + \frac{(\beta(1)_1)^2}{M_8^2 - s} \\
\mathrm{T}^{\infty}_{0,12} &= -\frac{\sqrt{3/2}}{12f^2}(6s - 8m_K^2) - \sqrt{2}\frac{\beta(1)_1\beta(1)_2}{M_8^2 - s} \\
\mathrm{T}^{\infty}_{0,22} &= \frac{s}{4f^2} + 2\frac{(\beta(1)_2)^2}{M_8^2 - s}
\end{aligned}
\tag{5.68}
$$

with the function $\beta(1)_i$ given by:

$$\begin{aligned}\beta(1)_1 &= \frac{\sqrt{2}}{\sqrt{3}f^2}[c_d(s-m_\pi^2-m_\eta^2)+2c_m m_\pi^2] \\ \beta(1)_2 &= \frac{\sqrt{2}}{f^2}[c_d\frac{s}{2}+(c_m-c_d)m_K^2]\end{aligned} \tag{5.69}$$

I=1/2

$$\begin{aligned}\mathrm{T}^{\infty}_{0,11} &= \frac{5s^2-2s(m_\pi^2+m_K^2)-3(m_K^2-m_\pi^2)^2}{8sf_K^2}+\frac{3}{2}\frac{(\beta(1/2)_1)^2}{M_8^2-s} \\ \mathrm{T}^{\infty}_{0,12} &= \frac{-9s^2+2sm_K^2+3sm_\eta^2+7sm_\pi^2-9m_K^4+9m_K^2(m_\pi^2+m_\eta^2)-9m_\pi^2m_\eta^2}{24sf_K^2} \\ &\quad +\sqrt{\frac{3}{2}}\frac{\beta(1/2)_1\beta(1/2)_2}{M_8^2-s} \\ \mathrm{T}^{\infty}_{0,22} &= \frac{-9s^2-9(m_k^2-m_\eta^2)^2+6s(3m_K^2+m_\eta^2)-4sm_\pi^2}{24sf_K^2}+\frac{(\beta(1/2)_2)^2}{M_8^2-s}\end{aligned} \tag{5.70}$$

with f_K the kaon decay constant with the value $f_K = 1.2f_\pi$ according to experiment [98]. The functions $\beta(1/2)_i$ are given by

$$\begin{aligned}\beta(1/2)_1 &= \frac{1}{f_K^2}[c_d s+(c_m-c_d)(m_K^2+m_\pi^2)] \\ \beta(1/2)_2 &= -\frac{1}{\sqrt{6}f_K^2}[c_d s+c_m(5m_K^2-3m_\pi^2)-c_d(m_K^2+m_\eta^2)]\end{aligned} \tag{5.71}$$

Note that the introduction of a nonet implies six new parameters, two masses and four coupling constants, which we fit to the experiment.

According to eq. (5.39), we also need the function $g_0(s)$, given by eqs. (5.46) and (5.48), with its corresponding a^{SL} for the S-wave channels. By SU(3) arguments, the a^{SL} constant can be different for vector and scalar channels. The reason is that a two meson state has different SU(3) wave functions in S- and P-wave, because under the exchange of both mesons the spatial P-wave is antisymmetric while the S-wave is symmetric and the total wave function must be symmetric. That is, the two mesons are in different SU(3) representations.

We have included f_η in the S-wave isoscalar $\mathcal{O}(p^2)$ χPT amplitude for $K\bar{K}\to\eta\eta$ and f_K in the S-wave, I=1/2 tree level amplitudes, to obtain, after the fit, that the a^{SL} constant was the same for all the scalar channels. These changes come from the SU(3) breaking of the octet of (π,K,η) and cannot be taken into account, a priori, in our way of fixing $D_L(s)$ making use of lowest order χPT [5] and the exchange of resonances given by [7].

The fit will be done for the following experimental data: the elastic S-wave $\pi\pi$ phase shifts with I=0, δ_{11}^{00}, the $K\bar{K} \to \pi\pi$, I=L=0 phase shifts, δ_{12}^{00}, the I=L=0 $\frac{1-\eta_{00}^2}{4}$, with η_{00} the inelasticity in that channel, the elastic S-wave, I=1/2 $K\pi$ phase shifts, $\delta_{11}^{\frac{1}{2}0}$ and a distribution of events around the mass of the $a_0(980)$ resonance, corresponding to the central production of $\pi\pi\eta$ in 300 GeV pp collisions [99] for the I=1, L=0 channel.

δ_{11}^{00}

Because results coming from different experimental analyses are not compatible, we have taken as central value for each energy below $\sqrt{s}$ = 1 GeV the mean between the different experimental results [45–48] and [46]. For $\sqrt{s} > 1$ GeV, the mean value comes from [46, 54]. In both cases the error is the maximum between the experimental one and the largest distance of the experimental values to the mean one. This procedure will be the one adopted, when needed, for the rest of the experimental magnitudes included in the fit.

δ_{12}^{00}

For this quantity there are two sets of data below $\sqrt{s} = 1.2$ GeV. Higher in energy both sets converge. One group will be represented by [52] and the other one by [100, 101]. The experimental results from [52] are larger than the data of the other works [100, 101] below 1.2 GeV. We will distinguish between both cases when doing a fit referring it as **high/low** respectively. The change in the value of the fitted parameters will be very small when changing from one set of data to another, so that, this experimental ambiguity will not be relevant for our final values. We will average the experimental data of the second set of works for $\sqrt{s} \leq 1.2$ GeV in the way explained above. When $\sqrt{s} > 1.2$ GeV the average will be done between all the quoted analyses [52, 100, 101].

$\frac{1-\eta_{00}^2}{4}$

There are a series of analyses and experiments about the inelastic cross section $\pi\pi \to K\bar{K}$, which agree between each other in the values for $\frac{1-\eta_{00}^2}{4}$. We have taken the data from [52, 100] as representative for such situation.

The quantity $\frac{1-\eta_{00}^2}{4}$ has been used instead of the inelasticity, η_{00}, because the former is much better measured and all the experiments [52, 100, 101] agree on that quantity.

$\delta_{11}^{\frac{1}{2}0}$

We distinguish between the more recent experiment [72] and the older results [68, 69, 71]. We have averaged the data from the latter analyses up to $\sqrt{s}$ = 1 GeV. Above this energy, in the latter group of experimental works, only [71] offers data. The statistical errors in this latter experiment are very small. We have enlarged them at the level of those in the most recent experiment [72] which would make the different experiments compatible. Thus, the final points used in the fit for this magnitude will be the ones from [72] and the

average between [68, 69, 71] as described above.

I=1, L=0 data.

The experimental data is very scarce for this channel. We will take a distribution of events corresponding to the central production of $\pi\pi\eta$ in 300 GeV pp collisions [99]. We will study the data points around the mass of the $a_0(980)$, where one could think that the energy dependence will be dominated by the exchange of that resonance. We add in an incoherent way with respect the $a_0(980)$ resonance, the same background as in [99]. The $a_0(980)$ contribution is parametrized as:

$$\frac{\mathrm{dN}}{\mathrm{d}E_{cm}} = \mathcal{N}\, p_{\pi\eta}\, |(\mathrm{T}_0)_{12}|^2 \tag{5.72}$$

with $p_{\pi\eta}$ the three momentum of the $\pi\eta$ state in the c.m. corresponding to a total energy E_{cm} and $\mathcal{N}$ is just a normalization constant.

The fit.

Let us now discuss the fits obtained when including: (1) two scalar nonets with masses around 1 and 1.4 GeV or (2) only one nonet with a mass around 1.4 GeV. Of course, the final value for the tree level, 'bare', masses of the octet and singlet will be given by the fit. The fits have been done using the MINUIT minimization program. The output value for the parameters are written with the same precision as given by MINUIT.

The fit that results when two nonets are included and also with the high δ_{12}^{00} data is:

First Nonet (MeV)	Second Nonet (MeV)	
$c_d = 1.80$	$c'_d = 19.51$	$a^{SL} = -.72$
$c_m = 0.66$	$c'_m = 19.61$	$\mathcal{N} = 9.22\,10^{-5}$ MeV^{-2}
$M_8 = 1003 \pm 600$	$M'_8 = 1379$	
$\tilde{c}_d = 20.99$	$\tilde{c}'_d = 0.33$	
$\tilde{c}_m = 8.49$	$\tilde{c}'_m = -2.72$	
$M_1 = 1032$	$M'_1 = 1000 \pm 600$	

$\chi^2_{d.o.f} = 0.97$
188 points (5.73)

A very striking aspect appears when observing the value of the parameters given in eq. (5.73). The value of the constants c_d, c_m and $\tilde{c}'_d$ and $\tilde{c}'_m$ are, at least, one order of magnitude smaller than $\tilde{c}_d$, $\tilde{c}_m$ and c'_d, c'_m respectively. This makes that the first octet and second singlet are phenomenologically irrelevant. Note that their masses are essentially undetermined. This is shown by the need to increase them by 600 MeV in order to make the $\chi^2_{d.o.f}$ to increase by 0.5 units. In this way, they do not originate or participate in the poles corresponding to the physical resonances mentioned at the beginning of the section.

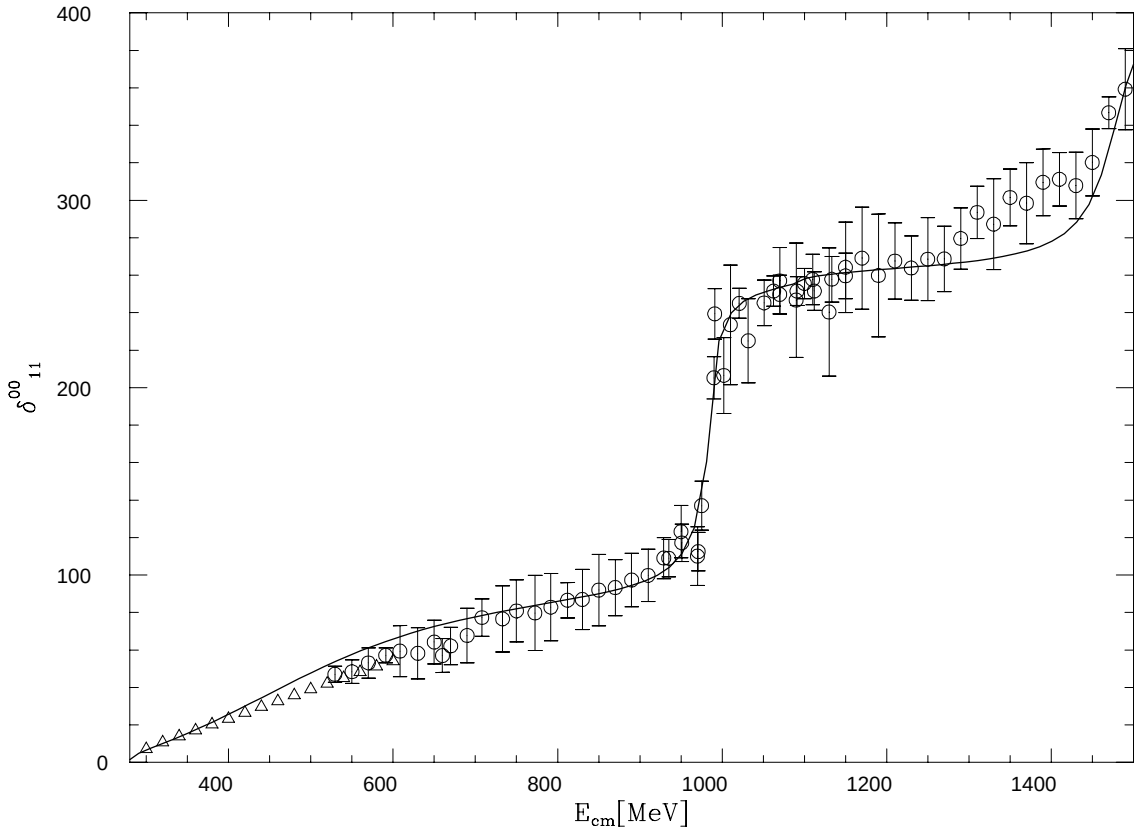

Figure 5.5: Elastic isoscalar $\pi\pi$ phase shifts, δ^{00}_{11}. The circles correspond to the average of [45–48] and [46, 54], as discussed in the δ^{00}_{11} subsection. We have also included the triangle points form [51] to have some data close to threshold, although these points have not been included in the fit because they are given without errors.

They only give rise to poles very close to the real axis, with a width of only a few MeV. These poles manifest themselves as very narrow peaks in the partial waves, which are not observed by experiment.

From the latter discussion we will just introduce a scalar nonet. The resulting values, after a new fit to the data, are:

High δ^{00}_{12}

$$\begin{array}{ll} \text{Nonet (MeV)} & \\ c_d = 19.1^{+2.4}_{-2.1} & a^{SL} = -.75 \pm 0.2 \\ c_m = 15 \pm 30 & \mathcal{N} = (9.4 \pm 4.5)\, 10^{-5}\ \text{MeV}^{-2} \\ M_8 = 1390 \pm 20 & \\ \tilde{c}_d = 20.9^{+1.6}_{-1.0} & \chi^2_{d.o.f} = 1.07 \\ \tilde{c}_m = 10.6^{+4.5}_{-3.5} & 188\ \text{points} \\ M_1 = 1021^{+40}_{-20} & \end{array} \tag{5.74}$$

Low δ_{12}^{00}

$$\begin{array}{ll} \text{Nonet (MeV)} & \\ c_d = 19.18 & a^{SL} = -.74 \\ c_m = 15.25 & \mathcal{N} = 9.43\,10^{-5}\ \text{MeV}^{-2} \\ M_8 = 1390 & \\ \tilde{c}_d = 20.94 & \chi^2_{d.o.f} = 1.21 \\ \tilde{c}_m = 10.64 & 196\ \text{points} \\ M_1 = 1021 & \end{array} \tag{5.75}$$

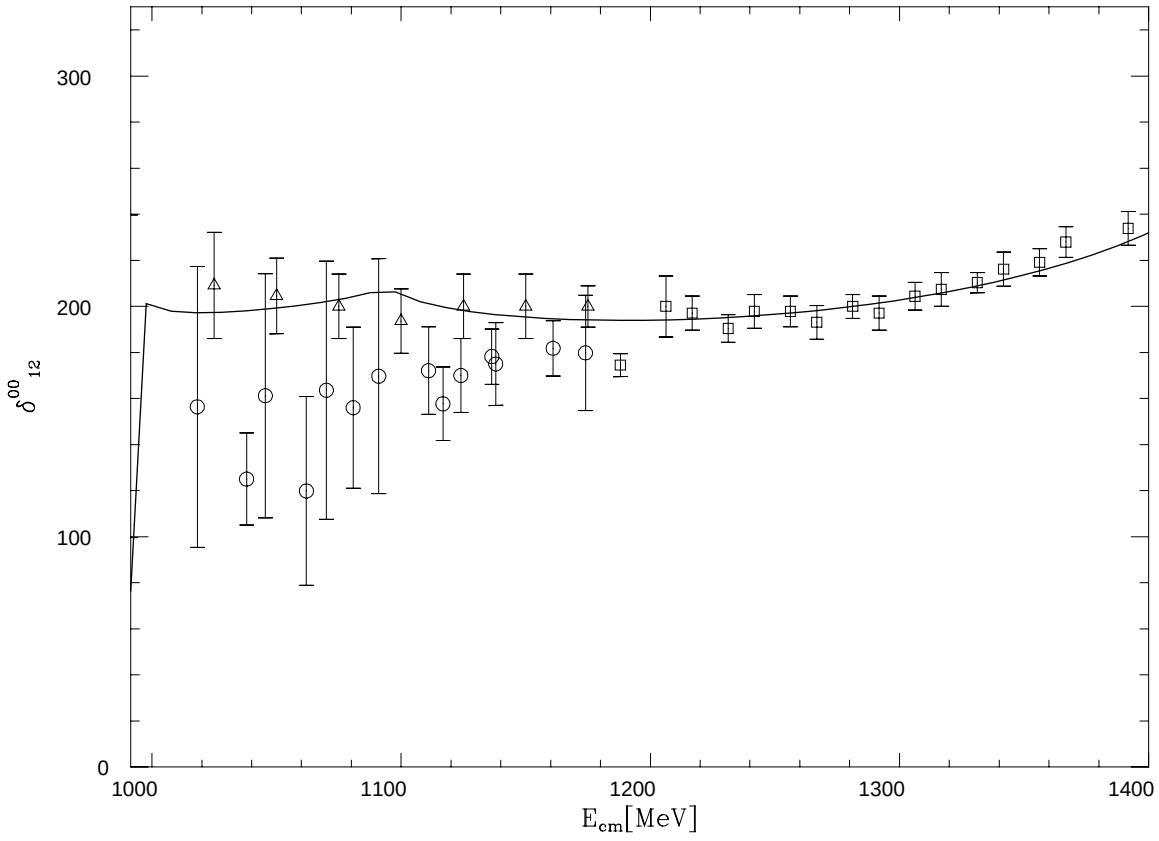

Figure 5.6: S-wave $K\bar{K} \to \pi\pi$ isoscalar phase shifts, δ_{12}^{00}. The triangles points are from [52], circles correspond to the average of [100, 101] and squares to the one of [52, 100, 101].

We have also shown the statistical errors for the parameters of the high δ_{12}^{00} fit obtained by increasing the $\chi^2_{d.o.f}$ by one unit, in order to appreciate the precision in the value of the parameters given by the last fits. The large error on c_m is because this constant, as can be seen from eqs. (5.67), (5.69) and (5.71), enters through the multiplication of squared masses of the lightest pseudoscalars which are much smaller than $s \simeq M_8^2$, around the resonance region of the octet. Thus, its influence in the final value of the amplitudes is

very small. This also happens to $\tilde{c}_m$, although to a lower extension because $M_1 < M_8$. One can see, comparing the last two fits, that the variation in the value of the parameters is very small when changing from one set of data to the other. The resulting fit for the high δ_{12}^{00} data is shown in Figs. 5.5-5.9. The results obtained before also favor the high solution for the δ_{12}^{00} phase shifts because its corresponding $\chi^2_{d.o.f}$ is smaller than the one for the low δ_{12}^{00} solution.

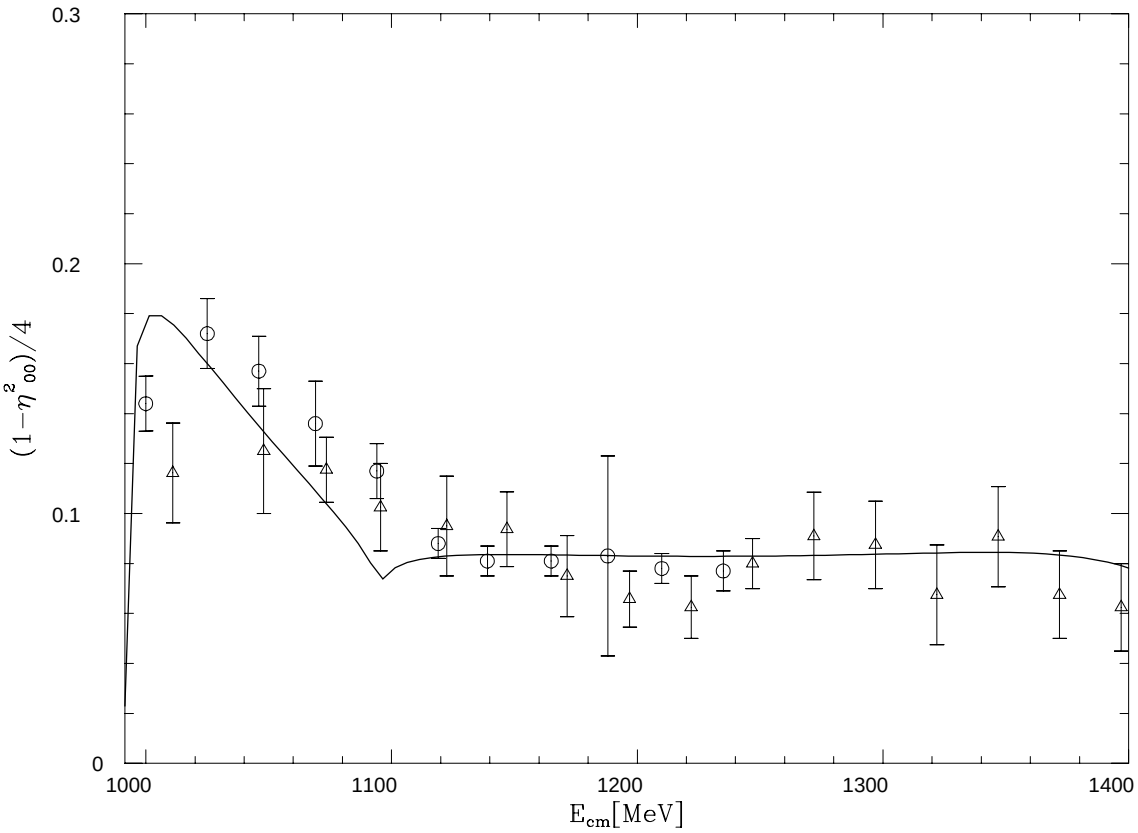

Figure 5.7: $\frac{1-\eta_{00}^2}{4}$ with η_{00} the I=L=0 S-wave inelasticity. Circles [52], triangles [100].

This fit has 8 free parameters, 6 constants from the nonet[3], a^{SL} and the normalization constant $\mathcal{N}$. In our former work [58], see also **section 5.2**, we were able to describe δ_{11}^{00}, δ_{12}^{00} and $\frac{1-\eta_{00}^2}{4}$ up to $\sqrt{s} \leq 1.2$ GeV and a distribution of events around the $a_0(980)$ mass [28], using only 2 free parameters: a cut-off (which plays the role of the regularization scale μ and at the same time generates a concrete value for a^{SL}) and a corresponding normalization constant for the $a_0(980)$ event distribution. In fact, if we remove the resonance contributions in eqs. (5.66) and (5.68) the formalism of ref. [58] follows from the present one. It

[3]If the singlet and the octet introduced form really a nonet is something we cannot say. However, we will denote the global contribution of the introduced octet plus the singlet by using the word nonet as a shortcome. In this way, we also follow the nomenclature of [7], inspired in the U(3) symmetry which holds for $N_c \to \infty$. We will say something more about this issue in the next chapter.

might look surprising that a good fit to the data for $\sqrt{s} < 1.2$ GeV could be obtained in [58] with just one free parameter and a normalization constant for the mass distribution, while here one has needed 7 parameters, apart from the normalization constant. One reason is that now we have pushed the fit up to $\sqrt{s} = 1.4$ GeV, while in [58] only data up $\sqrt{s} = 1.2$ GeV was considered. The fact that new resonances appear around $\sqrt{s} = 1.4$ GeV has forced us to include an octet, which implies 3 new parameters, two couplings and a mass. However, the effect of this octet below $\sqrt{s} = 1.2$ GeV is very small, hence only the singlet appearing with a mass around 1 GeV is relevant for energies below $\sqrt{s} = 1.2$ GeV. The present fit to the data has led us to the inclusion of this singlet resonance in T_0^∞ apart from the lowest order χPT Lagrangian, while in [58] only the latter contribution was considered. The reason that forced us to include now the mentioned singlet is the consideration of the $\eta\eta$ channel in I=0, which was omitted in [58], and is not negligible above 1 GeV, as can be seen in its strong coupling to the $f_0(980)$ resonance that we will obtain below. The $\eta\eta$ channel affects mostly the magnitude $\frac{1-\eta_{00}^2}{4}$. Should one have taken the available data for η_{00} instead of those for $\frac{1-\eta_{00}^2}{4}$, which are measured with better precision from the $\pi\pi \to K\bar{K}$ inelastic cross section, the effect of the $\eta\eta$ channel would be masked by the large errors in η_{00}.

It is quite interesting to recall that an I=0 elementary state around 1 GeV has been predicted from QCD inspired models [8, 102] and has also been advocated in phenomenological analyses [80, 88]. Such state could be associated with the preexisting singlet state that we need. On the ohter hand in [104] making use of QCD sum rules the authors also deduce that the $a_0(980)$ cannot be considered as the first $q\bar{q}$ scalar resonance with I=1. They consider it to be the $a_0(1450)$ as we also conclude in our study. They also claim an I=0 scalar resonance with a mass around 1 GeV.

Resonances.

Let us now concentrate on the resonance content of the fit presented in eq. (5.74). The octet around 1.4 GeV gives rise to eight resonances which appear with masses very close to the physical ones, $f_0(1500)$, $a_0(1450)$ and $K_0^*(1430)$ [19]. Thus, the correlation between tree level resonances, poles and physical resonances is clear around $\sqrt{s} \simeq 1.4$ GeV. However, this correlation is not so clear around 1 GeV. This issue will be the object of the following discussions [4].

From Figs. 5.5 and 5.8, one can easily see two resonances with masses around 1 GeV, the well known $f_0(980)$ and $a_0(980)$ resonances. The first one could be related to the singlet bare state with $M_1 = 1020$ MeV, but for the second we have not bare resonances to associate with, because the tree level resonance was included with a mass around 1.4 GeV and has evolved to the physical $a_0(1450)$. The situation is even more complex, because we

[4] We do not give a detailed study for the resonances with masses around 1.4 GeV because we have not included channels which become increasingly important for energies above $\simeq$ 1.3 GeV as 4π in I=0 or $K\eta'$ for I=1/2. This makes that the widths we obtain from the pole position of the former resonances are systematically smaller than the experimental ones [19]. Thus, a more detailed study, which included all the relevant channels for energies above 1.3 GeV, should be done in order to obtain a better determination of the parameters for this octet around 1.4 GeV. This will be one of the aims in **chapter 6**.

also find in our amplitudes other poles corresponding to the $f_0(400-1200) \equiv \sigma$ and to the $K_0^*(900) \equiv \kappa$. In Table 5.1 the pole positions of the resonances in the second sheet[5] are given and also the modulus of the residues corresponding to the resonance R and channel i, ζ_i^R, given by

$$|\zeta_i^R \zeta_j^R| = \lim_{s \to s_R} |(s - s_R) \mathrm{T}_{ij}| \tag{5.76}$$

where s_R is the complex pole for the resonance R.

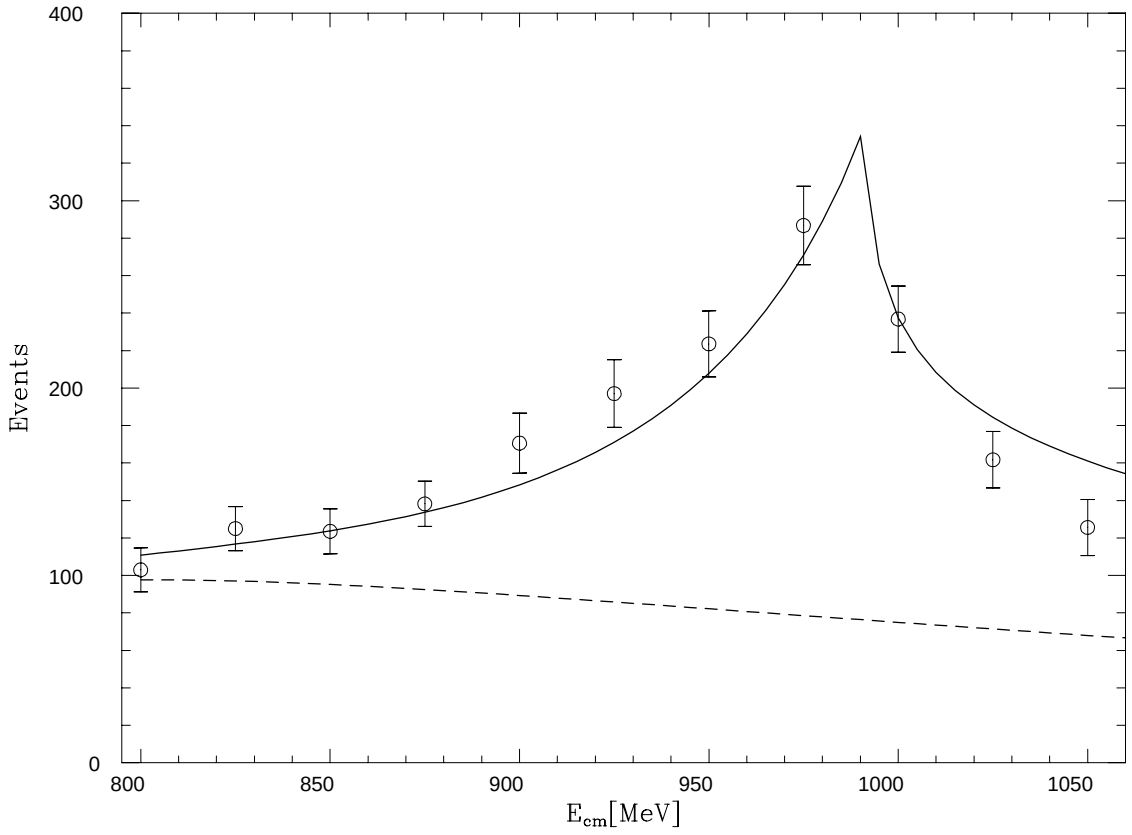

Figure 5.8: Distribution of events around the $a_0(980)$ mass corresponding to the central production $\pi\pi\eta$ in 300 GeV collisions [99]. The abscissa represents the $\pi\eta$ invariant mass, E_{cm}. The dashed line represents the background introduced in the same reference.

While for the $f_0(980)$ one has a preexisting tree level resonance with a mass of 1020 MeV, for the other resonances present in Table 5.1 the situation is rather different. In fact, if we remove the tree level nonet contribution from eqs. (5.66), (5.68) and (5.70) the $a_0(980)$, σ and κ poles still appear as can be seen in Table 5.2. For the $f_0(980)$, in such a situation, one has not a pole but a very strong cusp effect in the opening of the $K\bar{K}$ threshold. In fact, by varying a little the value of a^{SL} one can regenerate also a pole for

[5] I sheet: Im $p_1 > 0$, Im $p_2 > 0$, Im $p_3 > 0$; II sheet: Im $p_1 < 0$, Im $p_2 > 0$, Im $p_3 > 0$

Table 5.1: Pole position and residues for the full amplitude.

$\sqrt{s}_\sigma = 445 + i\,221$ MeV	$\sqrt{s}_{f_0} = 987 + i\,14$ MeV
$\zeta^\sigma_{\pi\pi} = 4.26$ GeV	$\zeta^{f_0}_{K\bar{K}} = 3.63$ GeV
$\frac{\zeta^\sigma_{K\bar{K}}}{\zeta^\sigma_{\pi\pi}} = 0.254$	$\frac{\zeta^{f_0}_{\pi\pi}}{\zeta^{f_0}_{K\bar{K}}} = 0.51$
$\frac{\zeta^\sigma_{\eta\eta}}{\zeta^\sigma_{\pi\pi}} = 0.036$	$\frac{\zeta^{f_0}_{\eta\eta}}{\zeta^{f_0}_{K\bar{K}}} = 1.11$
$\sqrt{s}_{a_0} = 1053.13 + i\,24$ MeV	$\sqrt{s}_\kappa = 779 + i\,330$ MeV
$\zeta^{a_0}_{K\bar{K}} = 5.48$ GeV	$\zeta^\kappa_{K\pi} = 4.99$ GeV
$\frac{\zeta^{a_0}_{\pi\eta}}{\zeta^{a_0}_{K\bar{K}}} = 0.70$	$\frac{\zeta^\kappa_{K\eta}}{\zeta^\kappa_{K\pi}} = 0.62$

Table 5.2: Pole position and residues when the bare resonant contributions are removed

$\sqrt{s}_\sigma = 434 + i\,244$ MeV	$\sqrt{s}_{f_0} =$ cusp effect
$\zeta^\sigma_{\pi\pi} = 4.21$ GeV	$\zeta^{f_0}_{K\bar{K}} = \ldots$
$\frac{\zeta^\sigma_{K\bar{K}}}{\zeta^\sigma_{\pi\pi}} = 0.301$	$\frac{\zeta^{f_0}_{\pi\pi}}{\zeta^{f_0}_{K\bar{K}}} = 0.38$
$\frac{\zeta^\sigma_{\eta\eta}}{\zeta^\sigma_{\pi\pi}} = 0.033$	$\frac{\zeta^{f_0}_{\eta\eta}}{\zeta^{f_0}_{K\bar{K}}} = 1.04$
$\sqrt{s}_{a_0} = 1081.95 + i\,13.3$ MeV	$\sqrt{s}_\kappa = 770 + i\,341$ MeV
$\zeta^{a_0}_{K\bar{K}} = 5.98$ GeV	$\zeta^\kappa_{K\pi} = 4.87$ GeV
$\frac{\zeta^{a_0}_{\pi\eta}}{\zeta^{a_0}_{K\bar{K}}} = 0.74$	$\frac{\zeta^\kappa_{K\eta}}{\zeta^\kappa_{K\pi}} = 0.61$

the $f_0(980)$ from this strong cusp effect. In Table 5.2 we have not given an absolute value for the coupling of the $f_0(980)$ to the $K\bar{K}$ channel because one has not a pole for the given value of a^{SL}. However, the ratios between the different amplitudes are stable around the cusp position. As a result, the physical $f_0(980)$ will have two contributions: one from the bare singlet state with $M_1 = 1020$ MeV and the other one coming from meson-meson scattering, particularly $K\bar{K}$ scattering, generated by the lowest order χPT Lagrangian.

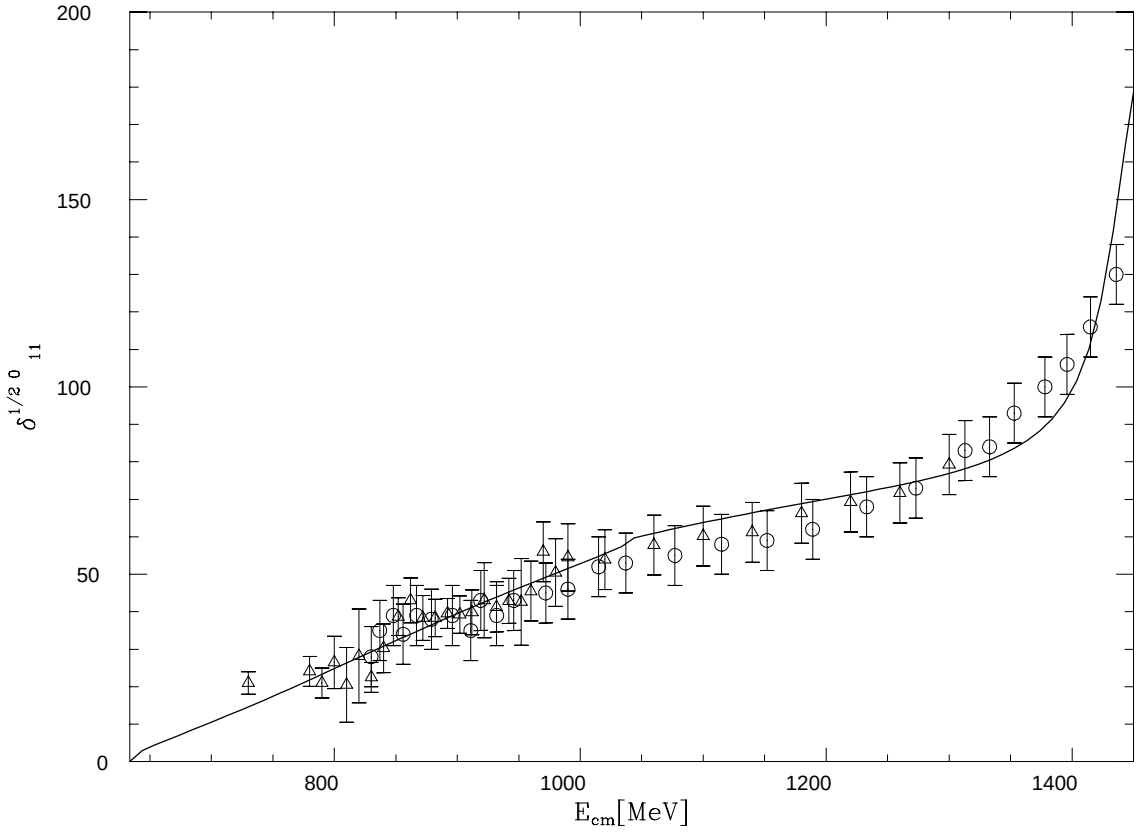

Figure 5.9: S-wave I=1/2 $K\pi$ elastic phase shifts, $\delta_{11}^{1/2\,0}$. The triangles correspond to the average, as described in $\delta_{11}^{1/2\,0}$ subsection, of [68, 69, 71]. Circles correspond to [72].

In eqs. (5.66), (5.68) and (5.70) when the resonant tree level contributions are removed, only the lowest order, $\mathcal{O}(p^2)$, χPT contributions remain. Thus, except for the contribution to the $f_0(980)$ coming from the bare singlet at 1 GeV, the poles present in Table 5.2 originate from a 'pure potential' scattering, following the nomenclature given in [9]. In this way, the source of the dynamics is the lowest order χPT amplitudes. The constant a^{SL} can be interpreted from the need to give a 'range' to this potential so that the loop integrals converge. These meson-meson states are shown in Fig. 5.10 in the chiral limit, setting all the masses of the pseudoscalars to zero and all the $f_P = f$, where P denotes any pseudoscalar meson π, K or η. We see in this last figure a degenerate octet for I=0,1

and 1/2 with a mass around 500 MeV and a singlet in I=0 with 400 MeV of mass. In both cases these meson-meson resonances are very broad.

The situation is very different to that of the former studied vector channels where all the physical resonances, the ρ and K^*, originate from the preexisting tree level resonances. We already saw, at the end of the last section, when comparing the S- and P-wave $\pi\pi$ scattering, that the $\mathcal{O}(p^2)$ χPT amplitude is 6 times larger for L=0 than for L=1 around the resonance energy region. This implies that n-loops in L=1, with the $\mathcal{O}(p^2)$ χPT amplitudes at the vertices, will be suppressed by a factor $\frac{1}{6^{n+1}}$ with respect to L=0. The suppression of loops is expected from large N_c QCD and this is in fact what happens for the vector channels, but for the scalar ones unitarity is unexpectedly large, giving rise to these meson-meson resonances.

As can be seen from eq. (5.39), these meson-meson poles, without tree level resonant contributions, originate from the cancellation between the inverse of the $\mathcal{O}(p^2)$ χPT amplitude and the g_0 function. As a consequence, the following relation between the masses of those resonances with f results

$$M^2 \propto f^2/g_0 \tag{5.77}$$

since g_0 is $\mathcal{O}(1)$ and f^2 is $\mathcal{O}(N_c)$ [90], these masses will grow as N_c. Thus for $N_c \to \infty$ these resonances will go to infinity. This movement can be followed by suppressing the g_0 function by a factor τ from 1 (physical situation) to 0 ($N_c = \infty$). It is then observed how the resonances in Table 5.2, without the preexisting resonant contributions, disappear going to infinity.

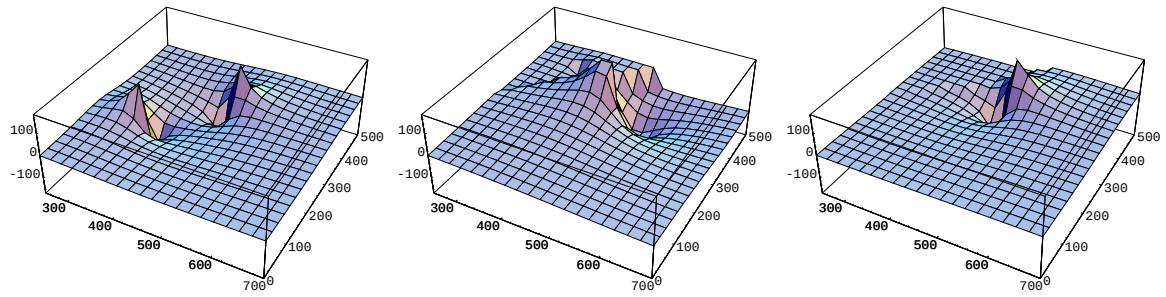

Figure 5.10: **Chiral limit**. From left to right, Figs. 5.10a,b,c respectively. In Fig. 5.10a the poles of T found in the unphysical sheet are shown for I=0. Analogously for I=1/2 and 1 in Figs. 5.10b,c respectively.

5.5 Estimations of the unphysical cut contribution from χPT and the exchange of resonances.

In this last section we estimate the influence of the unphysical cuts for the elastic $\pi\pi$ and $K\pi$ S-waves with I=0 and 1/2 respectively. The unphysical cuts will be approximated

by means of χPT supplied with the exchange of resonances [7] with spin ≤ 1 in the t- and u-channels. The loops are calculated from χPT at $\mathcal{O}(p^4)$ and the exchange of resonances in the crossed channels accounts for a resummation of counterterms up to an infinite order, in the way explained in **section 5.1** after eq. (5.26). The result can be taken directly from ref. [79], where the $\pi\pi \to \pi\pi$ and $K\pi \to K\pi$ amplitudes are calculated up to one loop including explicit resonance fields [7].

In order to extract, from ref. [79], the contribution of the unphysical cuts, which we design by T_{Left}, we have made use of eqs. (3.2), (3.10), (3.13), (3.14) for the $\pi\pi$ scattering and of eqs. (3.6), (3.16), (3.19) and (3.20) for the $K\pi$ one. We calculate the loop contributions at the same regularization scale than in [79], that is, $\mu = M_\rho = 770$ MeV, the same one we have taken in this work. In the following, when we refer to an equation in the form (m.n), it should be understood that this equation is the corresponding one from ref. [79]. The work of [79] contains loops and the exchange of resonances in the s, t and u-channels. The exchange of resonances in the s-channel is also present in our work where the masses and couplings of the scalar resonances, eqs. (5.74), were fitted to data. Obviously the loops and the exchange of resonances in crossed channels, absent in our work, go to T_{Left}. On the other hand, we must also include in T_{Left} a polynomial contribution of $\mathcal{O}(p^4)$ because the loop functions used in [79], J^r_{PQ}, M^r_{PQ} and $\bar{J}_{PQ}$, where P, Q are π, K or η, and our loop functions, $(-)g_0(s)$, differ in a constant. This polynomial contributions can be interpreted as subtraction terms from a dispersion relation of T_{Left}. Since the loops are calculated with ImT at $\mathcal{O}(p^4)$ one needs three subtractions, which fix the order of the subtraction polynomial. Let us explain first the $\pi\pi$ scattering.

From eq. (3.2) one has the expression of the elastic $\pi\pi$ amplitude with I=0 in terms of the amplitude $\mathrm{A}(s,t,u)$, eq. (3.10). Making use of eqs. (3.2) and (3.13) the contribution of the loops in the s-channel is given by

$$\frac{(2s-m_\pi^2)^2}{2f_\pi^4} J^r_{\pi\pi}(s) + \frac{3s^2}{8f_\pi^4} J^r_{KK}(s) + \frac{m_\pi^4}{6f_\pi^4} J^r_{\eta\eta}(s) \tag{5.78}$$

It is straightforward to see that the imaginary part of eq. (5.78) is the one required by unitarity up to $\mathcal{O}(p^4)$ for the I=0 S-wave $\pi\pi$ elastic partial wave with pions, kaons and etas as intermediate states. The squared amplitudes in front of the loop functions are the lowest order χPT amplitudes since loops are calculated at $\mathcal{O}(p^4)$. This is the same kind of result we would obtain for the loop contributions in the s-channel from the expansion of the generalization of eq. (5.39) to coupled channels up to the order considered in eq. (5.78), after dividing eq. (5.78) by a global factor 2 to match with our normalization in eq. (1.41) with $\alpha = 2$. However, as we discussed above we use $(-)g_0(s)_{ii}$ instead of $J^r_{ii}(s)$ in eq. (5.78) in order to evaluate the loop contributions in the s-channel. Hence, we must include in T_{Left} the following expression

$$\frac{(2s-m_\pi^2)^2}{2f_\pi^4}(J^r_{\pi\pi}(s) + g_0(s)_{11}) + \frac{3s^2}{8f_\pi^4}(J^r_{KK}(s) + g_0(s)_{22}) + \frac{m_\pi^4}{6f_\pi^4}(J^r_{\eta\eta}(s) + g_0(s)_{33}) \tag{5.79}$$

The former contribution, together with the exchange of resonances and loops in the

Table 5.3: Influence of the unphysical cuts for the I=L=0 $\pi\pi$ and I=1/2, L=0 $K\pi$ partial waves. The three first columns refer to $\pi\pi$ and the last three to $K\pi$.

$\sqrt{s}$ MeV	$\frac{T_{Left}}{\lvert T_{0,11}\rvert}$ %	$\frac{T_{Left}}{T^{\infty}_{0,11}}$ %	$\sqrt{s}$ MeV	$\frac{T_{Left}}{\lvert T_{0,11}\rvert}$ %	$\frac{T_{Left}}{T^{\infty}_{0,11}}$ %
276	3.7	4.8	634	7.1	8.7
376.	3.5	5.1	684	3.7	4.7
476	4.1	5.7	734	0.3	0.4
576	5.7	6.	784	-2.5	-3.3
676	8.1	6.1	834	-5.7	-7.2
776	11.2	5.6			

crossed channels, after projecting over the S-wave using eq. (1.41) with $\alpha = 2$, define T_{Left} in our approach.

For the I=1/2, L=0 $K\pi$ partial wave one has essentially the same situation than for $\pi\pi$. From eqs. (3.6) and (3.19) one calculates the contribution of loops, which we project over the S-wave. The loops in the s-channel give the corresponding result to eq. (5.78) for the $K\pi$ I=1/2 S-wave. In this case, instead of having the loop function $J^r_{PP}(s)$, one can write it in terms of $\bar{J}_{K\pi}(s)$ and $\bar{J}_{K\eta}(s)$. After taking into account the difference between $\bar{J}_{PQ}(s)$ and our loop functions, one obtains the analog result to eq. (5.79) for $K\pi$. This contribution, together with the projection over the S-wave of loops and the exchange of resonances (eqs. (3.6), (3.20)) in crossed channels, give T_{Left}.

We have not considered the tadpole contributions coming from pseudoscalar loops without flux of energy and the coupling of scalar resonances to the vacuum (Fig. 2.b of [79]) because they are reabsorbed into the residues and positions of the CDD poles and the subtraction constant a_0, eq. (5.24), which we have phenomenologically fixed.

Including explicit resonance fields as done in [79] increases the range of safe applicability of Chiral Symmetry from $\sqrt{s}$ ≈400 MeV, accomplished in χPT, up to $\sqrt{s} \approx 700 - 800$ MeV, as can be seen in [79] when comparing their results with the experimental data.

The results which we obtain for the contribution of T_{Left} in the range of energies of [79] are shown in Table 5.3. In the second and fifth columns we show, respectively, the ratio between T_{Left} and the absolute value of our calculated I, L=0 $\pi\pi$ and I=1/2, L=0 $K\pi$ partial wave amplitudes up to $\sqrt{s} \approx 800$ MeV. In Table 5.3 we also compare T_{Left} with the tree level amplitudes $T^{\infty}_{0,11}$. This ratio is also significative because the procedure which we have followed to arrive to a unitarized amplitude from $T^{\infty}_{0,11}$ would not be much affected by the addition of T_{Left} which is a small correction with respect to $T^{\infty}_{0,11}$. We see that these ratios are rather small. Therefore, this supports our point of view of treating the left hand cut as a perturbation in the range of energies we have considered.

It is worth mentioning that this smallness of the unphysical cuts, as shown in Table 5.3, is a consequence of a cancellation between the contributions to T_{Left} from the loops and the exchange of resonances in crossed channels. In fact, the individual contributions

in the $\pi\pi$ case, for energies around $\sqrt{s} = 600$ MeV, are of the order of 15-20% with respect to $T^{\infty}_{0,11}$.

5.6 Conclusions.

Making use of the N/D method, we have developed the most general structure that an elastic partial wave amplitude has when the unphysical cuts are neglected. After matching this result with lowest order, $\mathcal{O}(p^2)$, χPT [5] and with the exchange of resonances with spin $\leq$1, in a way consistent with chiral symmetry as given in ref. [7], we extend the formalism to handle also coupled channels. Then, $\pi\pi$ and $K\pi(I{=}1/2)$ P-wave amplitudes are described up to $\sqrt{s} = 1.2$ GeV. It is shown that these amplitudes can be given rather accurately in terms of m_π, m_K, f and the masses of the ρ and K^* resonances, when restrictions coming from large N_c QCD and unitarity are considered, in the lines of what was observed in [82].

Next, the scalar sector is studied and good agreement with experiment up to $\sqrt{s} =$ 1.4 GeV is found. An octet and a singlet are included with masses around 1.4 and 1 GeV respectively. The former originates the observed $f_0(1500)$, $a_0(1450)$ and $K_0^*(1430)$ resonances, the latter an important contribution to the physical pole of the $f_0(980)$. Other poles appearing in our amplitudes, the $a_0(980)$, σ, κ and an important contribution to the final $f_0(980)$, originate from meson-meson scattering with the lowest order χPT amplitudes plus the constant a^{SL} as dynamical source. This situation is very different from the one observed in the vector channels where tree level structures dominate the scattering process and a strong suppression of unitarity loops occurs, as indicated at the end of **section 5.4**. As a consequence, the present study supports that a concept like scalar meson dominance, analogous to the well known vector meson one, is not suited at the phenomenological level for the first scalar nonet with a mass $\leq$ 1 GeV.

In the last section we have made some estimations in order to investigate the influence of the unphysical cuts. The results obtained support our picture of treating the unphysical cuts in a perturbative way and then establishing the stability of our conclusions in **sections 5.3** and **5.4** against the corrections coming from cross symmetry.

Chapter 6

S-wave $K\pi$ and $K\eta'$ scattering.

The S-wave I=1/2 and 3/2 amplitudes are studied in this chapter. For the I=1/2 we will consider the channels $K\pi$ and $K\eta'$. In this way, we can go to higher energies than in **chapter 5** and study properly the octet of scalar resonances found there with a bare mass of around 1.4 GeV. Remember that there we did not include the $K\eta'$ channel which, as we will see below, is essential for energies higher than $\sqrt{s} = 1.3$ GeV. In this chapter we also follow the same sign for the T-matrix than in the former one. The material presented in this chapter is based on a recent work [103].

6.1 Inclusion of the η' meson.

In the large N_c limit the $U(1)_A$ anomaly [105, 106, 107] is absent. The massless QCD Lagrangian eq. (2.1) has then a larger $U(3)_L \otimes U(3)_R$ chiral symmetry, and there are nine Goldstone bosons associated with the spontaneous chiral symmetry breaking to the diagonal subgroup $U(3)_V$. These Goldstone excitations can be conveniently collected in the 3×3 unitary matrix

$$\widetilde{U}(\phi) = e^{i\frac{\sqrt{2}}{f}\widetilde{\Phi}} \tag{6.1}$$

with

$$\widetilde{\Phi} = \frac{\eta_1}{\sqrt{3}}\, I_3 + \frac{\vec{\lambda}}{\sqrt{2}}\,\vec{\phi} \tag{6.2}$$

where I_3 is the identity matrix in three dimensions and η_1 is a pseudoscalar singlet. Hence, we see from the former equation than the matrix Φ, introduced in eq. (2.5) and the one used in standard χPT, is modified just by adding a diagonal term proportional to the η_1 meson.

Under the chiral group, $\widetilde{U}(\phi)$ transforms as $\widetilde{U} \to g_R\, \widetilde{U}\, g_L^\dagger$ ($g_{R,L} \in U(3)_{R,L}$). The point is that at lowest order in the chiral expansion, the interactions of the nine Goldstone bosons are described by the same chiral Lagrangians given in eq. (2.7) and eqs. (2.18)-(2.23), with $\widetilde{U}(\phi)$ instead of $U(\phi)$.

Our strategy will be to calculate the tree level amplitudes with the $K\eta'$ channel in large N_c, where the η' is a Goldstone boson. This calculation will be done making use of the lowest order chiral Lagrangians $\mathcal{L}_2$ and of the resonance chiral Lagrangians, eqs. (2.18)-(2.23), to take into account the contributions from the exchange of resonances.

For the $K\pi$ channel we will calculate the same contributions than in the $K\eta'$ one but we will also include the chiral loops calculated at $\mathcal{O}(p^4)$ in ref. [79]. In this way, the elastic $K\pi$ amplitudes will coincide with the χPT amplitudes at $\mathcal{O}(p^4)$ calculated in [43].

Thus, the results we present in this chapter are an extension with respect **chapter 5** for the $K\pi$ $I = 1/2$ scattering, not only because we have included more channels, but also because we will allow for the presence of the unphysical cuts from the exchange of resonances in the crossed channels and also from the chiral loops at $\mathcal{O}(p^4)$.

As we will see immediately below, the η_1 and η_8 mix at $\mathcal{O}(p^4)$ both in the kinetic and mass terms. In this section we will obtain the wave function renormalization leading in large N_c for the pseudoscalars after diagonalizing the kinetic Lagrangian at $\mathcal{O}(p^4)$.

The bilinear terms coming from $\mathcal{L}_2$, eq. (2.7), when including the η_1 meson are:

$$\begin{aligned}\mathcal{L}_2 \;=\; & \frac{1}{2}\,\partial_\mu\pi^0\partial^\mu\pi^0 + \partial_\mu\pi^+\partial^\mu\pi^- + \partial_\mu K^+\partial^\mu K^- \\ & +\partial_\mu K^0\partial^\mu\bar{K}^0 + \frac{1}{2}\,\partial_\mu\eta_8\partial^\mu\eta_8 + \frac{1}{2}\,\partial_\mu\eta_1\partial^\mu\eta_1 \\ & -\frac{1}{2}m_\pi^2\,(\pi^0)^2 - m_\pi^2\,\pi^+\pi^- - m_K^2\,K^+K^- \\ & -m_K^2\,K^0\bar{K}^0 - \frac{1}{2}\left(\frac{4}{3}m_K^2 - \frac{1}{3}m_\pi^2\right)(\eta^8)^2 - \frac{1}{2}\left(\frac{2}{3}m_K^2 + \frac{1}{3}m_\pi^2\right)(\eta_1)^2 \\ & +\frac{8}{\sqrt{18}}\left(m_K^2 - m_\pi^2\right)\eta_8\,\eta_1 + \mathcal{O}(\phi^4)\end{aligned} \tag{6.3}$$

Notice that the η_1 kinetic term decouples at this order and also that the mixing between the η_1 and the η_8 mesons vanishes in the $SU(3)_V$ limit.

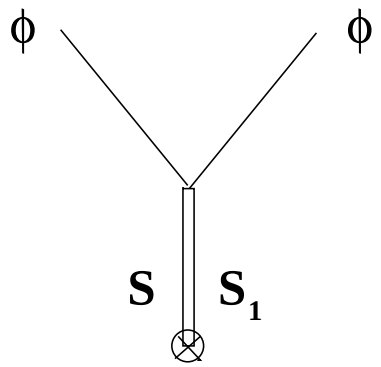

Figure 6.1: Contributions to the bilinear meson terms from the resonance chiral Lagrangians of **section 2.3**.

Apart from the terms coming from $\mathcal{L}_2$ we also consider the contributions from the chiral Lagrangians with resonance fields introduced in **section 2.3**, eqs (2.18)-(2.23). In particular, the scalar resonances (S and $S1$) through the diagram depicted in Fig. 6.1, where they couple to the vacuum, give contributions of $\mathcal{O}(p^4)$ to the former kinetic and mass terms. In writing these contributions we just consider the case with one singlet and one octet of scalar resonances. If more than one nonet is present, one only has to add it in the same way as we have done here for the first one.

$$\begin{aligned}
&\frac{8}{f^2}\,\frac{c_d\,c_m}{M_S^2}\left[m_\pi^2\,\left(\frac{1}{2}\,\partial_\mu\pi^0\partial^\mu\pi^0+\partial_\mu\pi^+\partial^\mu\pi^-\right)+m_K^2\left(\partial_\mu K^+\partial^\mu K^-\right.\right. \qquad (6.4)\\
&\left.\left.+\partial_\mu K^0\partial^\mu\bar{K}^0\right)+\frac{1}{2}\,\left(\frac{4}{3}m_K^2-\frac{1}{3}m_\pi^2\right)\partial_\mu\eta_8\partial^\mu\eta_8+\frac{1}{2}\,\left(\frac{2}{3}m_K^2+\frac{1}{3}m_\pi^2\right)\,\partial_\mu\eta_1\partial^\mu\eta_1\right.\\
&\left.-\frac{4}{\sqrt{18}}\,\left(m_K^2-m_\pi^2\right)\,\partial_\mu\eta_8\partial^\mu\eta_1\right]\\
&-\frac{8}{f^2}\,\frac{c_m^2}{M_S^2}\left[m_\pi^4\,\left(\frac{1}{2}\,(\pi^0)^2+\pi^+\pi^-\right)\right.\\
&\left.+m_K^4\left(K^+\,K^-+K^0\,\bar{K^0}\right)+\frac{1}{2}\,\left(\frac{1}{3}\,m_\pi^4+\frac{2}{3}\,\left(m_K^2-m_\pi^2\right)^2\right)(\eta_8)^2\right.\\
&\left.+\frac{1}{2}\,\left(\frac{2}{3}\,m_\pi^4+\frac{1}{3}\,\left(2\,m_K^2-m_\pi^2\right)^2\right)(\eta_1)^2+\frac{2}{\sqrt{18}}\,\left(m_\pi^4-\left(2\,m_K^2-m_\pi^2\right)^2\right)\eta_1\,\eta_8\right]
\end{aligned}$$

Since we are in large N_c, one has to consider the relations given in eqs. (2.33) of **section 3.3**. This makes that only the former contributions survive. In the χPT language of counterterms L_i, what is happening is that the contributions coming from L_4 and L_6 vanishes since these couplings are subleading in large N_c., see also eq. (2.32).

Together with the former contributions there is another one from the $U(1)_A$ anomaly. The anomaly to lowest order non-trivial in $1/\mathrm{N}_c$, can be taken into account in the effective low-energy theory through the term [108]

$$\mathcal{L}_{U(1)_A}=-\frac{f^2}{4}\frac{a}{N_c}\left(\frac{i}{2}\left[\log(\det\widetilde{U})-\log(\det\widetilde{U}^\dagger)\right]\right)^2 \qquad (6.5)$$

which breaks $U(3)_L\otimes U(3)_R$ but preserves $SU(3)_L\otimes SU(3)_R\otimes U(1)_V$. The parameter a has dimensions of mass squared and, with the factor $1/\mathrm{N}_c$ pulled out, is booked to be $\mathcal{O}(1)$ in the large N_c counting rules. In the presence of the term eq. (6.5), the η_1 field becomes massive even in the chiral limit through a term

$$-\frac{1}{2}\,\frac{3\,a}{N_c}(\eta_1)^2 \qquad (6.6)$$

which should be added to eqs. (6.3) and (6.4). Because the large mass of the η', the effect of the $U(1)_A$ anomaly cannot be treated as a small perturbation and has to be considered

together the lowest order Lagrangian eq. (2.7). It is possible to build a consistent combined expansion in powers of momenta, quark masses and $1/\mathrm{N}_c$, by counting the relative magnitude of these parameters as [109]:

$$\mathcal{M} \sim 1/N_c \sim p^2 \sim \mathcal{O}(\delta) \tag{6.7}$$

Summing up eqs. (6.3), (6.4) and (6.6) we have the kinetic and mass Lagrangian in terms of the fields π, K, η_1 and η_8. We will first diagonalize the kinetic Lagrangian which will provide us with the wave function renormalization of the fields.

The fields π and K remain unmixed both in the kinetic and mass Lagrangian. However they have no the physical normalization since the kinetic terms have a generic factor

$$1 + \frac{c_d\, c_m}{f^2\, M_S^2}\widetilde{m}^2 \neq 1 \tag{6.8}$$

with $\widetilde{m}^2$ a combination of masses of pions and kaons. In this way we have to multiply the pion and kaon fields by a factor in order to obtain the right normalization. This factor is called the **wave function renormalization** and is given by

$$\phi_P = \mathcal{Z}_\phi^{1/2}\, \phi \tag{6.9}$$

where the subindex P means 'physical'. Hence, the wave function renormalization for pions and kaons, from eqs. (6.3) and (6.4),are:

$$\begin{aligned} \mathcal{Z}_\pi^{1/2} &= 1 + \frac{4\, m_\pi^2}{f^2}\, \frac{c_d\, c_m}{M_S^2} \\ \mathcal{Z}_K^{1/2} &= 1 + \frac{4\, m_K^2}{f^2}\, \frac{c_d\, c_m}{M_S^2} \end{aligned} \tag{6.10}$$

where we have made the approximation $\sqrt{1+\epsilon} = 1 + \frac{1}{2}\epsilon + \mathcal{O}(\epsilon^2)$, which is numerically very accurate since $M_S^2 >> m_P^2$ with m_P^2 a pseudoscalar mass squared. In fact, we will work always up to the same order in the calculation of the tree level amplitudes, that is, up to $\frac{(coupling\ constat)^2}{M_R^2}$, with the subindex R indicating an arbitrary resonance. In terms of counterterms this means that we work up to terms linear in the L_i couplings, the resummation to higher orders is done, at the tree level amplitudes, by the inclusion of explicit resonance propagators. Remember the tight relation between the $\mathcal{O}(p^4)$ χPT counterterms and the resonance contributions at $\mathcal{O}(p^4)$ discussed in **section 3.3**.

For the case of the η_1 and η_8 fields the situation is a little more involved since they mix. Making use of a matrix notation, we can write the kinetic term as:

$$\frac{1}{2}\, \partial_\mu \Psi^T\, \mathcal{K}\, \partial^\mu \Psi \tag{6.11}$$

with

$$\Psi = \begin{pmatrix} \eta_8 \\ \eta_1 \end{pmatrix} \tag{6.12}$$

and

$$\mathcal{K} = \begin{pmatrix} 1+\epsilon_8 & \Delta \\ \Delta & 1+\epsilon_1 \end{pmatrix} \equiv \begin{pmatrix} 1+\frac{8}{3\,f^2}\frac{c_d\,c_m}{M_S^2}\,(4\,m_K^2-m_\pi^2) & \frac{32}{3\sqrt{2}\,f^2}\frac{c_d\,c_m}{M_S^2}\,(m_\pi^2-m_K^2) \\ \frac{32}{3\sqrt{2}\,f^2}\frac{c_d\,c_m}{M_S^2}\,(m_\pi^2-m_K^2) & 1+\frac{8}{3\,f^2}\frac{c_d\,c_m}{M_S^2}\,(2\,m_K^2+m_\pi^2) \end{pmatrix} \tag{6.13}$$

We now define the physical Ψ_P field by

$$\Psi_P = \mathcal{Z}_\Psi^{1/2}\Psi \tag{6.14}$$

such that

$$\frac{1}{2}\,\partial_\mu\Psi^T\,\mathcal{K}\,\partial^\mu\Psi = \frac{1}{2}\,\partial_\mu\,\Psi_P^T\,\partial^\mu\,\Psi_P \tag{6.15}$$

which is the correct normalization. Hence, the $\mathcal{Z}_\Psi^{1/2}$ 2×2 matrix must fulfill

$$(\mathcal{Z}_\Psi^{-1/2})^T\,\mathcal{K}\,\mathcal{Z}_\Psi^{-1/2} = I_2 \tag{6.16}$$

with I_2 the 2×2 identity matrix. Up to the order considered one has

$$\mathcal{Z}_\Psi^{-1/2} = \begin{pmatrix} 1-\frac{\epsilon_8}{2} & -\frac{\Delta}{2} \\ -\frac{\Delta}{2} & 1-\frac{\epsilon_1}{2} \end{pmatrix} \tag{6.17}$$

The physical η and η' mesons are obtained from η_8^P and η_1^P contained in Ψ_P after diagonalizing the mass matrix $\mathcal{M}_\Psi$. From eqs. (6.3), (6.4) and (6.6), we can write

$$-\frac{1}{2}\,\Psi^T\,M_\Psi\,\Psi = -\frac{1}{2}\,\Psi_P^T\,(\mathcal{Z}_\Psi^{-1/2})^T\,M_\Psi\,\mathcal{Z}_\Psi^{-1/2}\,\Psi_P = -\frac{1}{2}\,\Psi_P^T\,\mathcal{M}_\Psi\,\Psi_P \tag{6.18}$$

The diagonalization of the mass matrix $\mathcal{M}_\Psi$ introduces a sizeable mixing angle θ_P defined through the relation

$$\begin{pmatrix} \eta \\ \eta' \end{pmatrix} = \begin{pmatrix} \cos\theta_P & -\sin\theta_P \\ \sin\theta_P & \cos\theta_P \end{pmatrix} \begin{pmatrix} \eta_8^P \\ \eta_1^P \end{pmatrix} \tag{6.19}$$

This diagonalization is dominated by the term coming from the $U(1)_A$. Taking the nonet version of the Wess-Zummino-Witten term [21] and [22] one obtains

$$\begin{aligned} \cos\theta_P &= \frac{\sqrt{8}}{3} \\ \sin\theta_P &= -\frac{1}{3} \end{aligned} \tag{6.20}$$

which implies that $\theta_P \approx -20^0$ refs. [110, 109].

We can now calculate the needed matrix elements from $\mathcal{L}_2$ and the resonance Lagrangians given in eqs. (2.18)-(2.23). First one calculates the matrix elements using the bare fields π, K, η_1 and η_8. Then we take into account the wave function renormalization deduced in this section by multiplying the calculated amplitudes by $\prod_\phi \mathcal{Z}_\phi^{-1/2}$, note that in the case of the η_1 and η_8 the wave function renormalization is a matrix. Finally, one has to take into account the rotation given in eq. (6.19).

6.2 Large N_c amplitudes.

The different contributions to the tree level amplitudes are depicted in Figs. 6.2-6.4.

In Fig. 6.2 the lowest order χPT amplitudes from $\mathcal{L}_2$, eq. (2.7), is represented . In Fig. 6.3 the exchange of vector (V) and scalar (S and S_1) resonances is depicted. Of course, this exchange can occur in any of the three channels s, t or u. Finally, for the case of the scalar resonances there are also tadpole-like terms, *i.e.* the scalars can couple to the vacuum. This is represented in Fig. 6.4.

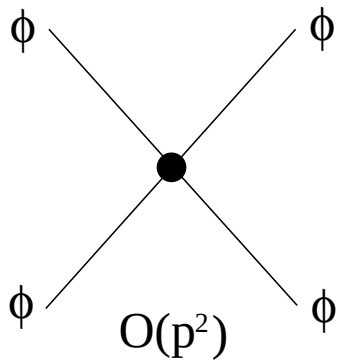

Figure 6.2: $\mathcal{L}_2$ contributions.

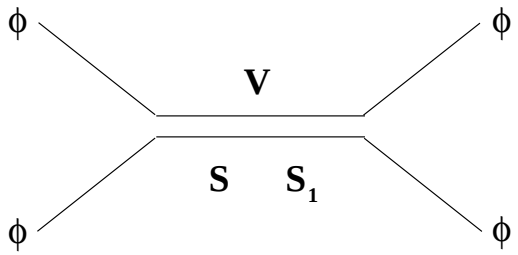

Figure 6.3: V, S and S_1 exchange.

In $\mathcal{L}_2$, the masses from the matrix $\mathcal{M}$ correspond to the bare $\mathcal{O}(p^2)$ masses. These masses are corrected at $\mathcal{O}(p^4)$ in large N_c through terms linear in L_5 and L_8, in terms of the resonance parameters these couplings are given in eq. (2.32). We will express the bare masses of the π and K, $\hat{m}_\pi$ and $\hat{m}_K$ respectively, the ones which appear in $\mathcal{M}$, in terms of the physical ones m_π and m_K. The relations up tp $\mathcal{O}(p^4)$ are [111]:

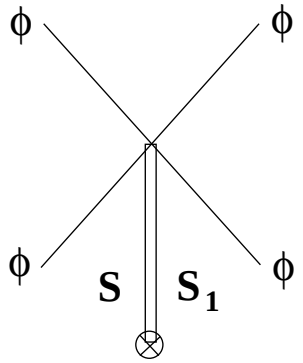

Figure 6.4: Tadpole-like diagram from the coupling of the S and S_1 to the vacuum.

$$m_\pi^2 = \hat{m}_\pi^2 \left[1 + \frac{8\, m_\pi^2}{f^2} \frac{c_m}{M_S^2} (c_m - c_d)\right] \qquad (6.21)$$
$$m_K^2 = \hat{m}_K^2 \left[1 + \frac{8\, m_K^2}{f^2} \frac{c_m}{M_S^2} (c_m - c_d)\right]$$

When expressing the lowest order in terms of the physical masses new terms will appear which sum to the contributions coming from Fig. 6.4.

On the other hand, one has also to consider the wave function renormalization. At leading order in large N_c this wave function renormalization can be reabsorbed to a large extend in the physical decay constants f_π and f_K, which in this limit fulfill:

$$\begin{aligned} f_\pi &= \mathcal{Z}_\pi^{1/2}\, f \\ f_K &= \mathcal{Z}_K^{1/2}\, f \end{aligned} \qquad (6.22)$$

In this way, in the amplitudes with terms of order p^4 and higher, we transform the f constants, which appear in the denominators of the amplitudes, according to the former equation. For instance, for each pion field will appear a $\mathcal{Z}_\pi^{-1/2}$ constant which can be attached to one of the four f. Hence we will write f_π instead of f. The analog for the K fields. This recipe to take into account higher orders is also used in [79].

However, for the lowest order amplitudes, in which only two f appear it is not possible to do the same procedure than before. Typically we will be able to reabsorb in the physical decay constants some of the wave functions renormalization constants but not all. In particular, this will be the case for the η_1 and η_8 for which we have not done such resummations since the wave function renormalization constant is a **matrix**. In these cases there will appear further $\mathcal{O}(p^4)$ contributions which will be summed to the ones coming from Fig. 6.4.

The final tree level amplitudes with definite isospin are given below:

ISOSPIN=3/2

$$\mathbf{T}(\mathbf{K}\pi \to \mathbf{K}\pi)\, f_K^2\, f_\pi^2 =$$

$$\begin{aligned}
& f_K f_\pi \, \frac{m_K^2 + m_\pi^2 - s}{2} - \frac{{c_m}^2 \left(-m_K^2 + m_\pi^2\right)^2}{M_8^2} + \\
& \frac{2\, L_3^V\, M_V^2}{3} \left(\frac{t\ (s-u)}{M_V^2 - t} + \frac{(s-t)\ u - \left(-m_K^2 + m_\pi^2\right)^2}{M_V^2 - u} \right) + \\
& \frac{\left(c_m\ (m_K^2 + m_\pi^2) - c_d\ (m_K^2 + m_\pi^2 - u)\right)^2}{M_8^2 - u} \\
& + \frac{4\ (2\,\widetilde{c}_m\, m_K^2 + \widetilde{c}_d\ (-2\, m_K^2 + t))\ (2\,\widetilde{c}_m\, m_\pi^2 + \widetilde{c}_d\ (-2\, m_\pi^2 + t))}{M_1^2 - t} \\
& - \frac{((2\, c_m\, m_K^2 + c_d\ (-2\, m_K^2 + t))\ (2\, c_m\, m_\pi^2 + c_d\ (-2\, m_\pi^2 + t)))}{3\ (M_8^2 - t)}
\end{aligned} \tag{6.23}$$

ISOSPIN=1/2

$$\mathbf{T}(\mathbf{K}\pi \to \mathbf{K}\pi)\, f_K^2\, f_\pi^2 =$$

$$\begin{aligned}
& f_K f_\pi \, \frac{2\ (m_K^2 + m_\pi^2) + s - 3\, u}{4} - \frac{c_m^2 (-m_K^2 + m_\pi^2)^2}{M_8^2} \\
& - \frac{L_V^3 M_V^2}{3} \left(\frac{4t\,(s-u)}{M_V^2 - t} - \frac{\left(-m_K^2 + m_\pi^2\right)^2 - (s-t)\, u}{M_V^2 - u} \right. \\
& \left. - \frac{3\left(-\left(-m_K^2 + m_\pi^2\right)^2 + s\,(-t+u)\right)}{M_V^2 - s} \right) \\
& + \frac{4\ (2\,\widetilde{c}_m\, m_K^2 + \widetilde{c}_d\ (-2\, m_K^2 + t))\ (2\,\widetilde{c}_m\, m_\pi^2 + \widetilde{c}_d\ (-2\, m_\pi^2 + t))}{M_1^2 - t} \\
& - \frac{((2\, c_m\, m_K^2 + c_d\ (-2\, m_K^2 + t))\ (2\, c_m\, m_\pi^2 + c_d\ (-2\, m_\pi^2 + t)))}{3\ (M_8^2 - t)} \\
& - \frac{\left(c_m\ (m_K^2 + m_\pi^2) - c_d\ (m_K^2 + m_\pi^2 - u)\right)^2}{2\ (M_8^2 - u)} + \frac{3\left((-c_d + c_m)\ (m_K^2 + m_\pi^2) + c_d\, s\right)^2}{2\ (M_8^2 - s)}
\end{aligned} \tag{6.24}$$

$$\mathbf{T}(\mathbf{K}\pi \to \mathbf{K}\eta_{\mathbf{1}}^{\mathbf{P}})\, f_K^2\, f_\pi\, f =$$

$$f_\pi f\, \frac{2\, m_K^2 + m_\pi^2}{3\,\sqrt{2}} \tag{6.25}$$

$$
-\frac{4\sqrt{2}\,{c_m}^2\,(m_K^2-m_\pi^2)^2}{3\,M_8^2}-\frac{\sqrt{2}\,c_d\,c_m\,(m_K^2-m_\pi^2)\,\left(m_{\eta'}^2-m_\pi^2-3\,t\right)}{3\,M_8^2}+
$$

$$
\sqrt{2}\,\frac{\left(-2\,c_m\,m_\pi^2+c_d\,\left(m_{\eta'}^2+m_\pi^2-t\right)\right)\,\left(2\,c_d\,m_K^2-2\,c_m\,m_K^2-c_d\,t\right)}{M_8^2-t}+
$$

$$
\sqrt{2}\,\frac{\left(-2\,c_m\,m_K^2+c_d\,\left(m_{\eta'}^2+m_K^2-u\right)\right)\,\left(-c_m\,(m_K^2+m_\pi^2)+c_d\,(m_K^2+m_\pi^2-u)\right)}{M_8^2-u}+
$$

$$
\sqrt{2}\,\frac{\left(2\,c_m\,m_K^2+c_d\,\left(-m_{\eta'}^2-m_K^2+s\right)\right)\,\left(c_m\,(m_K^2+m_\pi^2)+c_d\,(-m_K^2-m_\pi^2+s)\right)}{M_8^2-s}
$$

$$
\mathbf{T}(\mathbf{K}\pi\to\mathbf{K}\eta_{\mathbf{8}}^{\mathbf{P}})\,f_K^2\,f_\pi\,f=
$$

$$
f_\pi f\,\frac{-3\,m_{\eta'}^2-8\,m_K^2-m_\pi^2+9\,t}{12}
$$

$$
-\frac{c_m^2(m_K^2-m_\pi^2)^2}{3M_8^2}+\frac{c_d c_m\,(m_K^2-m_\pi^2)\,\left(2\,\left(m_{\eta'}^2-m_\pi^2\right)+3\,t\right)}{3M_8^2}
$$

$$
-L_3^V\,M_V^2\,\frac{m_K^4+m_{\eta'}^2\,m_\pi^2-m_K^2\left(m_{\eta'}^2+m_\pi^2\right)+(-s+t)\,u}{M_V^2-u}+
$$

$$
-L_3^V\,M_V^2\,\frac{m_K^4+m_{\eta'}^2\,m_\pi^2-m_K^2\left(m_{\eta'}^2+m_\pi^2\right)+(-u+t)\,s}{M_V^2-s}
$$

$$
\frac{\left(-2\,c_m\,m_\pi^2+c_d\,\left(m_{\eta'}^2+m_\pi^2-t\right)\right)\,\left(2\,c_d\,m_K^2-2\,c_m\,m_K^2-c_d\,t\right)}{M_8^2-t}
$$

$$
-\frac{\left(c_m\,(-5\,m_K^2+3\,m_\pi^2)+c_d\,\left(m_{\eta'}^2+m_K^2-u\right)\right)\,\left(-c_m\,(m_K^2+m_\pi^2)+c_d\,(m_K^2+m_\pi^2-u)\right)}{2\,(M_8^2-u)}
$$

$$
-\frac{\left(c_m\,(-5\,m_K^2+3\,m_\pi^2)+c_d\,\left(m_{\eta'}^2+m_K^2-s\right)\right)\,\left(-c_m\,(m_K^2+m_\pi^2)+c_d\,(m_K^2+m_\pi^2-s)\right)}{2\,(M_8^2-s)}
$$

$$
\mathbf{T}(\mathbf{K}\eta_{\mathbf{1}}^{\mathbf{P}}\to\mathbf{K}\eta_{\mathbf{1}}^{\mathbf{P}})\,f_K^2\,f^2=
$$

$$
f^2\,\frac{2\,m_K^2}{3}-\frac{16\,c_d\,c_m\,(m_K^2-m_\pi^2)^2}{9\,M_8^2}+
$$

$$
\frac{4\,\left(-6\,\widetilde{c}_d\,m_{\eta'}^2+4\,\widetilde{c}_m\,m_K^2+2\,\widetilde{c}_m\,m_\pi^2+3\,\widetilde{c}_d\,t\right)\,\left(2\,\widetilde{c}_m\,m_K^2+\widetilde{c}_d\,(-2\,m_K^2+t)\right)}{3\,(M_1^2-t)}+
$$

$$
\frac{8\,c_m\,(m_K^2-m_\pi^2)\,\left(2\,c_m\,m_K^2+c_d\,(-2\,m_K^2+t)\right)}{9\,(M_8^2-t)}+\frac{4\left(-2\,c_m\,m_K^2+c_d\,\left(m_{\eta'}^2+m_K^2-u\right)\right)^2}{3\,(M_8^2-u)}+
$$

$$
\frac{4\left(-2\,c_m\,m_K^2+c_d\,\left(m_{\eta'}^2+m_K^2-s\right)\right)^2}{3\,(M_8^2-s)}
$$

$$\mathbf{T(K\eta_1^P \to K\eta_8^P)}\, f_K^2\, f^2 =$$

$$\begin{aligned}
& f^2\,\frac{-2\,m_K^2+m_\pi^2}{3\,\sqrt{2}}-\frac{4\,\sqrt{2}\,{c_m}^2\,(m_K^2-m_\pi^2)^2}{3\,M_8^2}+ \\
& \frac{\sqrt{2}\,c_d\,c_m\,\,(m_K^2-m_\pi^2)\,\,(16\,\,(m_K^2-m_\pi^2)+9\,t)}{9\,M_8^2} \\
& -\frac{16\,\sqrt{2}\,\widetilde{c}_m\,\,(m_K^2-m_\pi^2)\,\,(2\,\,(-\widetilde{c}_d+\widetilde{c}_m)\,\,m_K^2+\widetilde{c}_d\,t)}{3\,\,(M_1^2-t)}+ \\
& -\sqrt{2}\,\frac{\left(-6\,c_d\,m_{\eta'}^2+8\,c_m\,m_K^2-2\,c_m\,m_\pi^2+3\,c_d\,t\right)\,\,(2\,c_m\,m_K^2+c_d\,\,(-2\,m_K^2+t))}{9\,\,(M_8^2-t)}+ \\
& -\sqrt{2}\,\frac{\left(-2\,c_m\,m_K^2+c_d\,\,\left(m_{\eta'}^2+m_K^2-u\right)\right)\,\,\left(c_m\,\,(-5\,m_K^2+3\,m_\pi^2)+c_d\,\,\left(m_{\eta'}^2+m_K^2-u\right)\right)}{3\,\,(M_8^2-u)} \\
& -\sqrt{2}\,\frac{\left(2\,c_m\,m_K^2+c_d\,\,\left(-m_{\eta'}^2-m_K^2+s\right)\right)\,\,\left(c_m\,\,(5\,m_K^2-3\,m_\pi^2)+c_d\,\,\left(-m_{\eta'}^2-m_K^2+s\right)\right)}{3\,\,(M_8^2-s)}
\end{aligned} \tag{6.28}$$

$$\mathbf{T(K\eta_8^P \to K\eta_8^P)}\, f_K^2\, f^2 =$$

$$\begin{aligned}
& f^2\,\frac{-6\,m_{\eta'}^2-2\,m_\pi^2+9\,t}{12}+ \\
& \frac{7\,{c_m}^2\,(m_K^2-m_\pi^2)^2}{3\,M_8^2}-\frac{c_d\,c_m\,\,(m_K^2-m_\pi^2)\,\,(32\,m_K^2-32\,m_\pi^2+9\,t)}{9\,M_8^2}+ \\
& 4\,L_3^V\,M_V^2\,\left(\frac{-\left(-m_{\eta'}^2+m_K^2\right)^2+(s-t)\,\,u}{M_V^2-u}+\frac{-\left(-m_{\eta'}^2+m_K^2\right)^2+s\,\,(-t+u)}{M_V^2-s}\right)+ \\
& \frac{4\,\left(-6\,\widetilde{c}_d\,m_{\eta'}^2+8\,\widetilde{c}_m\,m_K^2-2\,\widetilde{c}_m\,m_\pi^2+3\,\widetilde{c}_d\,t\right)\,\,(2\,\widetilde{c}_m\,m_K^2+\widetilde{c}_d\,\,(-2\,m_K^2+t))}{3\,\,(M_1^2-t)}+ \\
& \frac{\left(-6\,c_d\,m_{\eta'}^2+16\,c_m\,m_K^2-10\,c_m\,m_\pi^2+3\,c_d\,t\right)\,\,(2\,c_m\,m_K^2+c_d\,\,(-2\,m_K^2+t))}{9\,\,(M_8^2-t)}+ \\
& \frac{\left(c_m\,\,(-5\,m_K^2+3\,m_\pi^2)+c_d\,\,\left(m_{\eta'}^2+m_K^2-u\right)\right)^2}{6\,(M_8^2-u)}+ \\
& \frac{\left(c_m\,\,(5\,m_K^2-3\,m_\pi^2)+c_d\,\,\left(-m_{\eta'}^2-m_K^2+s\right)\right)^2}{6\,\,(M_8^2-s)}
\end{aligned} \tag{6.29}$$

In the former equation we have maintained the distinction between the S and the S_1 contributions for the direct exchange of such resonances, Fig. 6.3, as we did in **section 5.4**. However, in the numerical results we will always use the large N_c constraints given in eq. (2.33).

The constant L_3^V was given in eq. (2.28) in terms of the parameters describing the octet of vector resonances in the chiral limit. As explained below the former equation, $M_V \approx M_\rho$ and $G_V = \frac{f_\pi}{\sqrt{2}}$ eq. (2.29).

Furthermore, in eqs. (6.23)-(6.29) we have always written $m^2_{\eta'}$ for the square of the four-momenta of the η_1^p and η_8^P fields. We have done this because in the S-wave I=1/2 amplitude we consider the $K\pi$ and $K\eta'$ channels, neglecting the $K\eta$ one. As one can check from the experimental points in Figs. 6.6 and 6.7, the modulus of this amplitude $\left(\eta\, e^{2i\delta_{1/2}} - 1\right)/(2i)$, above the $K\eta$ and below the $K\eta'$ one, is given by $|\sin\delta_{1/2}|$ as in the elastic case with $\eta = 1$.

In the case of the elastic $K\pi$, our amplitudes coincide at $\mathcal{O}(p^4)$ with the calculations done in [79].

We will now consider the restrictions to the values of c_d and c_m imposed by the scalar form factor of $K\pi$ and $K\eta'$ in large N_c.

6.3 Short distance constraints.

We now present a calculation for the scalar $K\pi$, $K\eta'$ and $K\eta$ form factors leading in large N_c counting rules . As in the case of the scattering amplitudes presented in the former section we use $\mathcal{L}_2$ and the chiral resonance Lagrangians eqs. (2.18)-(2.23). However, only the S and S_1 resonances will contribute.

The scalar form factor is defined [112] through the divergence of the vector current $\bar{u}(s)\gamma_\mu s(x)$:

$$\begin{aligned} &< 0|\partial^\mu(\bar{u}(x)\gamma_\mu s(x))|K^-\,\phi^0 >= -i(m_s - m_u) < 0|\bar{u}(x)\,s(x)|K^-\,\phi^0 > \\ &= i(\hat{m}_K^2 - \hat{m}_\pi^2)\,\mathrm{C}_\phi \widetilde{\mathrm{F}}_\phi^S(s) \end{aligned} \tag{6.30}$$

where $u(x)$ and $s(x)$ represent the quarks up and strange respectively, ϕ^0 is a π^0, η or η' meson, C_ϕ is just a number, $\hat{m}_K(\hat{m}_\pi)$ represents the bare mass of the $K(\pi)$ from the lowest order χPT Lagrangian, $\mathcal{L}_2$, eq. (2.7) and $\widetilde{\mathrm{F}}_\phi^S(s)$ is the scalar form factor for the $K\phi^0$ channel. If as in [112] $\mathrm{C}_{\pi^0} = \sqrt{\frac{1}{2}}$, then from explicit calculation or simple game with the Clebsch-Gordan coefficients and eq. (6.19) one obtains $\mathrm{C}_\eta = -\frac{1}{\sqrt{6}}$ and $\mathrm{C}_{\eta'} = \frac{2}{\sqrt{3}}$. Note that the scalar current $\bar{u}s$ is purely I=1/2. It is obtained by doing the functional derivation

$$\frac{\delta\mathcal{L}}{\delta s(x)_{13}} \tag{6.31}$$

with $s(x)$ now referring to the scalar current introduced in eq. (2.1)

In Figs. 6.5 the different diagrams which contribute are shown. Fig. 6.5.a. represents the $\mathcal{L}_2$ contribution. Fig. 6.5.b corresponds to the direct resonance exchange of the S resonances and Fig. 6.5.c. represents a tadpole-like contribution with the resonances S and S_1 coupled to the vacuum. Note that our Lagrangians are given in terms of the fields

η_1 and η_8, so that first we have to calculate in terms of these degree of freedom. Then, these contributions have to be corrected by multiplying by $\prod_\phi \mathcal{Z}_\phi^{-1/2}$ each meson field, in the same way as explained for scattering amplitudes. Finally, making use of eq. (6.19), we will obtain the desired results in terms of the η and η' mesons.

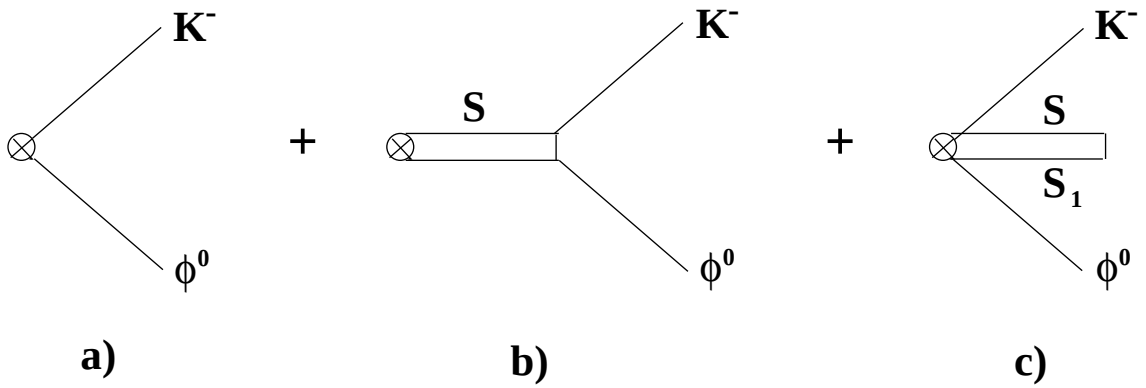

Figure 6.5: Diagrams which contribute to the scalar form factor eq. (6.30). The circle with a cross inside depicts the scalar current. Fig. 6.5.a. represents the $\mathcal{L}_2$ contribution. Fig. 6.5.b corresponds to the direct resonance exchange of the S resonances and Fig. 6.5.c. represents a tadpole-like contribution with the resonances S and S_1 coupled to the vacuum.

On the other hand, the results from the former diagrams are multiplied by a global factor B_0 eq. (2.8). Remember that this factor appears also in the relations between the quark masses and the square of the masses of the pseudoscalars eq. (2.10). But now since the scalar form factor, from eq. (6.30) is multiplied by $m_s - m_u$ we can write

$$B_0\,(m_s - m_u) = \hat{m}_K^2 - \hat{m}_\pi^2 \tag{6.32}$$

this is why this factor appears in eq. (6.30). Expressing the former result in terms of the physical K and π masses, we will have up to $\mathcal{O}(p^4)$:

$$\begin{aligned} \hat{m}_K^2 - \hat{m}_\pi^2 &= \left(m_K^2 - m_\pi^2\right) \frac{\hat{m}_K^2 - \hat{m}_\pi^2}{m_K^2 - m_\pi^2} \\ &= \left(m_K^2 - m_\pi^2\right) \left(1 - \frac{8}{f^2}\frac{m_K^2 + m_\pi^2}{M_S^2}\, c_m\,(c_m - c_d)\right) \end{aligned} \tag{6.33}$$

instead of the final equality in eq. (6.30) we can write

$$< 0|\partial_\mu(\bar{u}(s)\gamma_\mu s(x))|K^-\,\phi^0 >= i\,\left(m_K^2 - m_\pi^2\right)\,\mathrm{C}_\phi\,\mathcal{F}_\phi^S(s) \tag{6.34}$$

with $\mathcal{F}_\phi^S(s) = \left(1 - \frac{8}{f^2}\frac{m_K^2+m_\pi^2}{M_S^2}\, c_m\,(c_m - c_d)\right)\,\widetilde{\mathrm{F}}_\phi^S$.

Taking into account all the former preliminaries given in this section the final results are:

$$
\begin{aligned}
\mathcal{F}^S_{K^-\pi^0}(s) &= 1+\frac{4c_m}{f^2}\left[c_d+(c_m-c_d)\,\frac{m_K^2+m_\pi^2}{M_S^2}\right]\,\frac{s}{M_S^2-s}\\
\mathcal{F}^S_{K^-\eta'}(s) &= (\cos\theta_P-\frac{\sin\theta_P}{\sqrt{8}})\Bigg(1+\frac{\sin\theta_P}{\sqrt{8}}3(m_K^2-m_\pi^2)\frac{4c_m}{f^2}\left[\frac{c_d}{M_S^2}-\frac{c_m}{M_S^2}\left(1+\frac{M_S^2}{M_S^2-s}\right)\right]\\
&+ \frac{4c_m}{f^2}\frac{c_d(s+2m_\pi^2-m_K^2-m_{\eta'}^2-s\frac{2m_\pi^2}{M_S^2})+2c_m(m_K^2-m_\pi^2+s\frac{m_\pi^2}{M_S^2})}{M_S^2-s}\Bigg)\\
\mathcal{F}^S_{K^-\eta}(s) &= \sqrt{8}\sin\theta_P\,3(m_K^2-m_\pi^2)\,\frac{4\,c_m}{f^2}\left[\frac{c_d}{M_S^2}-\frac{c_m}{M_S^2}\left(1+\frac{M_S^2}{M_S^2-s}\right)\right]
\end{aligned}
\tag{6.35}
$$

Imposing that these form factors vanished for $s\to\infty$, one has,

$$
\begin{aligned}
1 &= \sum_i \alpha_i\\
\sum_i \frac{\alpha_i}{M_{S_i}^2} &= \sum_i \frac{\beta_i}{M_{S_i}^2}
\end{aligned}
\tag{6.36}
$$

where M_{S_i} is the mass of the ith resonance and

$$
\begin{aligned}
\alpha_i &= \frac{4\,c_{d,i}\,c_{m,i}}{f^2}\\
\beta_i &= \frac{4\,c_{m,i}^2}{f^2}
\end{aligned}
\tag{6.37}
$$

The $K\pi$ scalar form factor coincides at $\mathcal{O}(p^4)$ with the counterterm part of the calculation done in [112].

In the former equation we have allowed for the presence of more than one octet of scalar resonances which have only to be added in the same way as the first one considered in eqs. (6.35).

Coming back to the case of only one resonance, one has from eq. (6.36) the simple result:

$$
c_d = c_m = f/2 \approx f_\pi/2 = 46.2\ \text{MeV} \tag{6.38}
$$

These kind of relations work very well in the case of the vector channels where there is a proof that the vector pion form factor vanishes at infinity. For this case one also has the requirements [24], as already commented in eq. (2.29):

$$
\begin{aligned}
\sum_i F_{V_i}\,G_{V_i} &= f^2\\
\sum_i \frac{F_{V_i}^2}{M_{V_i}^2}\,(2\,G_{V_i}-F_{V_i}) &= 0
\end{aligned}
\tag{6.39}
$$

where V_i refers to the ith octet of vector resonances with masses M_{V_i}. In the case of only one octet eq. (2.29) is recovered.

As we saw in **section 3.3**, from the values of c_d and c_m given in eq. (6.38) and with a value for the M_S of around 1.2 GeV the scalar contribution to the L_i coefficients is the needed to saturate these $\mathcal{O}(p^4)$ couplings. Hence, it is interesting to see if we are also able to reproduce the $K\pi$ scattering up to energies which embody the first resonance, which is the $K_0^*(1430)$. This resonance appears very close to the $K\eta'$ threshold which is an important channel and then we have to make use of a coupled channel formalism to study properly the I=1/2 S-wave amplitude up to energies around 1.5-1.6 GeV. For the exotic I=3/2 we will consider only the elastic case.

6.4 Unitarization.

The unitarization procedure is basically the one developed in [27], already presented in **section 5.1**. However, we will slightly modify it in order to get the full χPT result at $\mathcal{O}(p^4)$.

In a $\mathcal{O}(p^4)$ χPT calculation there are loops in the crossed channels which give an imaginary part for the partial waves for non-physical values of the s variable. Furthermore, we have also included resonance fields in the t and u-channels. Both contributions give rise to the unphysical cuts not considered in [27], although fair estimations were done about these contributions for the $I = 1/2$ case.

The tree level amplitudes considered in ref. [27] were the $\mathcal{O}(p^2)$ χPT amplitudes, $T^{(2)}$, plus the exchange of resonances in the s-channel included in the same way than here. We called the sum of both contributions T_0^∞, since it is leading in large N_c. We did not include resonances nor loops in crossed channels nor tadpoles since tadpoles are subleading effects in large N_c.

In the sixth row of eq. (3.19) of ref. [79] one can see the square of the lowest order χPT amplitude, see eq. (3.17) of the same reference, times a loop function, $J^r_{K\pi}$ in the s-channel. For the I=1/2 S-wave amplitude one can also arrive to the same kind of result in the s-channel. Writing it in terms of the $\bar{J}_{K\pi}(s)$ function one has:

$$\bar{J}_{K\pi}(s)\left[\frac{1}{8\,f_\pi f_K}\left(5s-2(m_K^2+m_\pi^2)-3\frac{(m_K^2-m_\pi^2)^2}{s}\right)\right]^2 \qquad (6.40)$$
$$-\frac{k(m_\pi^2,m_K^2)}{32}(25s^2+4(m_K^2+m_\pi^2)^2-20\,s\,(m_K^2+m_\pi^2))$$

All these loop functions, which appear in refs. [79, 43] and that are also mentioned here, can be obtained from eqs. (8.8), (8.9) and (8.10) of ref. [111] and also at the end of the Appendix of the same reference.

Coming back to eq. (6.40) one obtains the same type of result, up to $\mathcal{O}(p^4)$, than expanding eq. (5.39) with $-g_0(s)(T^{(2)})^2$. However, the loop function is different. Note that the loop functions need a subtraction constant, see eq. (5.46). In fact one can add

and subtract a constant in $\bar{J}(s)$ in eq. (6.40), and the analog can be done for the I=3/2 in $J^r(s)$. One continues having the square of the lowest order amplitude times a loop function which guarantees the unitary requirement given by eq. (1.26). Thus, one cannot fix the value of the subtraction constant present in $g_0(s)$, making use of the full $\mathcal{O}(p^4)$ χPT result. We will make the following identification for the $g_0(s) \equiv g(s)$ function:

$$\begin{aligned} I &= 3/2 \quad g(s) = -J^r_{\pi K}(s) - \frac{a'_\pi}{16\,\pi^2} \\ I &= 1/2 \quad g_{K\pi}(s) = -\bar{J}_{\pi K}(s) - \frac{a_\pi}{16\,\pi^2} \end{aligned} \tag{6.41}$$

For the $K\eta'$ channel in the I=1/2 we will use the same notation than in eq. (5.46), since there are no full $\mathcal{O}(p^4)$ χPT calculations with this channel. We will denote by a_η the subleading constant present in eq. (5.46) for this channel.

In ref. [79] the loops with energy flux are collected as $T_U^{(4)}$. On the other hand the tadpoles are given by $T_T^{(4)}$. However, since in eqs. (6.23) and (6.24) we have expressed the bare masses and decay couplings in terms of the physical ones, $T_T^{(4)}$ is modified. When taking into account such modifications one has the $T_T^{(4)}$ term given in eq. (3.14) of ref. [43]. In the expression for $T_U^{(4)}$ given in eq. (3.19) of [79] the $K\eta$ channel is included. Since in our unitarization process we are going to discard this channel we have not included the $K\eta$ loops. In any case, we have checked that numerically its influence is negligible.

We design by $\widetilde{T}_U^{(4)}$ to $T_U^{(4)}$ without the unitarity term given by the loop function J^r for I=3/2 and $\bar{J}$ for I=1/2, times the square of the lowest order χPT amplitude. In order to maintain the same $\mathcal{O}(p^4)$ χPT result, we have to add to $\widetilde{T}_U^{(4)} + T_T^{(4)}$ the piece:

$$\begin{aligned} I &= 3/2 \\ &\quad -\frac{a'_\pi}{(4\,\pi)^2}(T^{(2)})^2 \\ I &= 1/2 \\ &\quad -\frac{a_\pi}{(4\,\pi)^2}(T^{(2)})^2 - \frac{k(m_\pi^2, m_K^2)}{32}(25s^2 + 4(m_K^2 + m_\pi^2)^2 - 20\,s\,(m_K^2 + m_\pi^2)) \end{aligned} \tag{6.42}$$

the last term in I=1/2 comes from eq. (6.40). We denote he sum of $\widetilde{T}_U^{(4)} + T_T^{(4)}$ plus the terms in eqs. (6.42) by T_{Left}, since this is the piece we did not consider in ref. [27]. In our notation, the result of [79] is written as:

$$T_0^\infty + T_{Left} - g(s)\,(T^{(2)})^2 \tag{6.43}$$

We can now make an N/D representation of the former amplitude. This representation will contain the unphysical cuts up to order considered in ref. [79], that is, up to one loop calculated at $\mathcal{O}(p^4)$. In matrix formalism:

$$\begin{aligned} N &= T_0^\infty + T_{Left} \\ D &= I + N\,g \\ T &= D^{-1}\cdot N \end{aligned} \tag{6.44}$$

with $g(s)$ a diagonal matrix whose elements are the ones introduced above. Expanding the former result one has:

$$T = N - N\cdot g\cdot N + \mathcal{O}(p^6,\hbar^2) = T_0^\infty + T_{Left} - T^{(2)}\cdot g\cdot T^{(2)} + \mathcal{O}(p^6,\hbar^2) \tag{6.45}$$

reproducing eq. (6.43) up to one loop calculated at $\mathcal{O}(p^4)$. One can also check that up to the same order in the unphysical cuts, the N and D functions satisfy eqs. (5.9) and (5.10):

$$\begin{aligned} \text{Im } D &= N\cdot \text{Im } g \quad s > s_{th} \\ \text{Im } N &= D\cdot \text{Im } T = \text{Im } T_{Left} + \mathcal{O}(p^6,\hbar^2) \quad s \text{ in unphysical cuts} \end{aligned} \tag{6.46}$$

We can reabsorb T_0^∞ in D just by multiplying N and D at the same time by $(T_0^\infty)^{-1}$). In this way, neither their ratio is modified nor their cut structure since T_0^∞ is just a matrix of real rational functions. Then one has

$$\begin{aligned} N &= I + (T_0^\infty)^{-1}\cdot T_{Left} \\ D &= (T_0^\infty)^{-1} + (I + (T_0^\infty)^{-1}\cdot T_{Left})\cdot g(s) \end{aligned} \tag{6.47}$$

In ref. [27] we did not include T_{Left} so that N was the identity eq. (5.24), as happens in the former equation making $T_{Left} = 0$.

In any case eq. (6.44) can also be written as:

$$T = \left[(T_0^\infty + T_{Left})^{-1} + g(s)\right]^{-1} \tag{6.48}$$

setting T_{Left} to zero we recover once again the limit case of eq. (5.24).

6.5 Results for the S-wave I=1/2 scattering.

Making use of the final formulae given in eqs. (6.23)-(6.29) and eq. (6.48), we are going to study the S-wave I=1/2 partial wave amplitude up to around $\sqrt{s} = 1.6$. Up to this energy only one clear resonance appears, the so called $K_0^*(1430)$ [19] and apart of the elastic channel $K\pi$ the other important one is the $K\eta'$ with a threshold of 1.45 GeV. In this way, we will be able to study this resonance which appears around 1.4 GeV in an adequate way. In particular we will see if the values given in eq. (6.38) are consistent with the data coming from the $K\pi$ scattering.

We take the data for the I=1/2 S-wave $K\pi$ phase shifts from the experiments [71] and [72]. The errors are taken to be the size of the dot in Fig. 15 of [72] which corresponds to $\pm 8^0$ for the phase shifts and ± 0.05 for the modulus of the partial wave $\left(\eta_{1/2} e^{2i\delta_{1/2}} - 1\right)/(2\,i)$.

In general we will have as free parameters, once the values for the couplings c_d and c_m have been fixed, the mass of the octet of scalar resonances in the chiral limit M_S and the subleading constants a_π and a'_η. For the pure elastic case with only the $K\pi$ channel the last parameter does not appear.

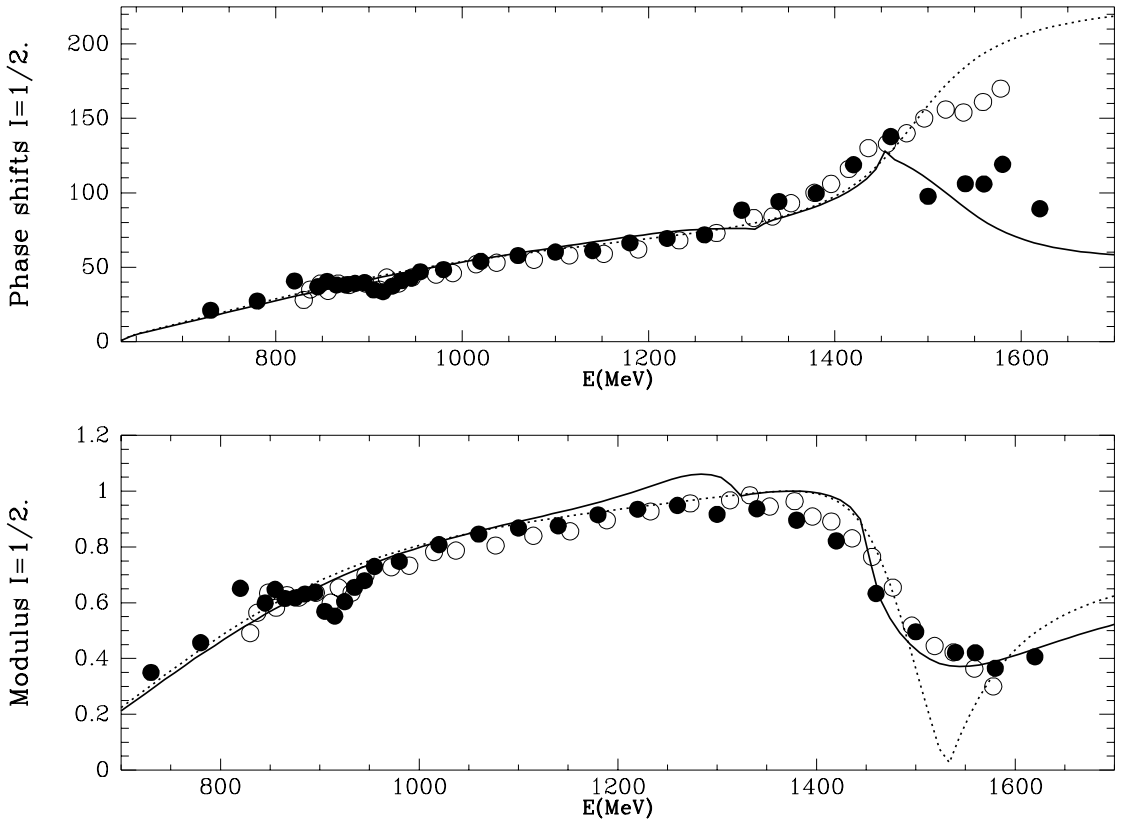

Figure 6.6: The dotted line corresponds to a fit of [72] with only the elastic channel. The continuum line is a fit to the same data but including also the $K\eta'$ channel. Data: Empty circle [72]. Full circle [71].

In Fig. 6.6 we show different curves compared with the data from the solution C of [71](full circle) and [72] (empty circle). In all the curves the couplings constants are given by eq. (6.38). The dotted line corresponds to a fit to the data of [72] with only the elastic channel $K\pi$. The continuum one comes from a fit to the same data but with the $K\eta'$ channel included. It is clear from this figure that the inclusion of the $K\eta'$ channel makes the phase shifts to go down with respect to the elastic case and the data from [72]. However, there is a remarkable agreement with the solution C of [71]. It is worth noting

that in this reference, for energies higher than 1.5 GeV, four solutions are possible, A, B, C and D. The only one which agrees with our curves, once the $K\eta'$ channel is included, is the solution C. It is also worth mentioning that the oscillations in the data of [71] for low energies puts of manifest the presence of large systematic errors in the way to extract the $K\pi$ scattering data from the production mechanism $K^-p \to K^-\pi^+n$. The same technique is also used in [72].

Taking into account the former results we do a fit to the solution C of [71]. Since we are using values for the couplings based in large N_c estimations we will give to the data a 30% of relative error. The resulting fit is:

$$\begin{aligned} M_S &= 1531^{+136}_{107}\ \text{MeV} \\ a_\pi &= 0.096 \pm 0.13 \\ a_{\eta'} &= -2.6974 \pm 0.7 \\ \chi^2_{d.o.f} &= 0.17 \\ \text{Numer of points} &= 66 \end{aligned} \tag{6.49}$$

this fit is telling us that the predictions coming from eq. (6.38) work much better than in a 30% of relative error. In fact, one obtains $\chi^2_{d.o.f}$ smaller than 1 up to a relative error of a 12% in the solution C of [71]. For this particular case the central values of the parameters in eq. (6.49) are the same although the associated errors are reduced. For the mass the error now is ± 50 MeV and for a'_η is ± 0.3. This last fit is represented in Fig. 6.7 by the dotted line where the data of the solution C of [71] is presented with a relative error of a 12%. For comparison the data from [72] is also included. In the same figure by the continuum line we represent the fit to the solution C of [71] but now allowing for a change in a 30% in the couplings constants from the values given in eq. (6.38). The fit is:

$$\begin{aligned} c_d &= 32.003^{+1}\ \text{MeV} \\ c_m &= 52.377^{+8}_{-14}\ \text{MeV} \\ M_S &= 1339^{+54}_{-90}\ \text{MeV} \\ a_\pi &= 0.2466 \pm 0.1 \\ a_{\eta'} &= -1.1078 \pm 0.7 \\ \chi^2_{d.o.f} &= 0.76 \end{aligned} \tag{6.50}$$

In Fig. 6.7 the dashed line represents the former fit but with the couplings put to zero. In this way we see the crucial importance that the presence of the preexisting resonance with a mass around 1.3-1.4 GeV has in order to reproduce the experimental data.

Taking directly the values of eq. (6.50) to calculate the S contribution to the L_i coefficients one has from eqs. (2.32) and (2.33):

$$\begin{aligned} L_5 &= 0.93 \times 10^{-3} \\ L_8 &= 0.76 \times 10^{-3} \end{aligned} \tag{6.51}$$

in good agreement with their experimental values in Table 2.1.

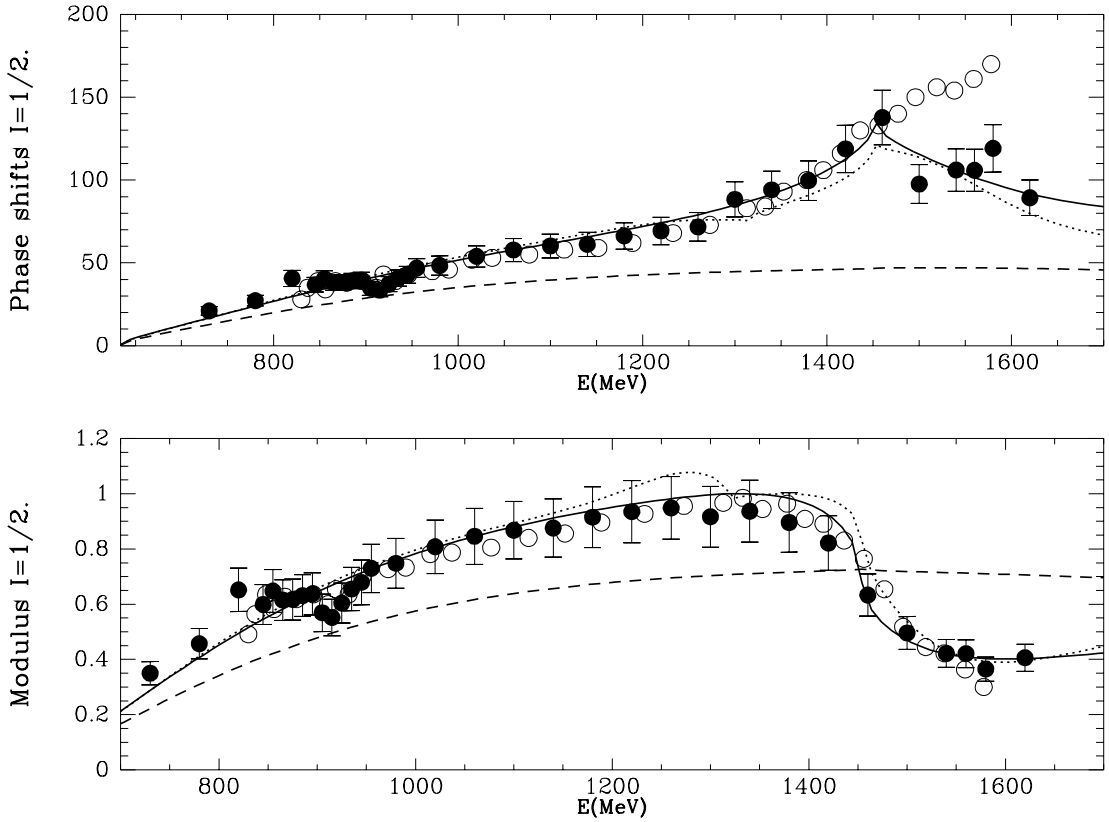

Figure 6.7: The continuum line corresponds to the best fit (6.50) to solution C of [71], the full circles points, allowing for a relative deviation of a 30% from the values in eq. (6.38). The dashed line corresponds to the former fit but with the couplings of the resonance puts to zero. The dotted line is the fit (6.49) to the same data with the values for the couplings in eq. (6.38). The bump in the modulus of the amplitude for this type of line is a consequence of the $K\eta'$ threshold. The data from [72] are depicted by the empty circles.

We see that we are able to reproduce the S-wave I=1/2 scattering making use of the short distance constraints, eq. (6.38) imposed in **section 6.3** when requiring the scalar form factors eq. (6.30) to vanish for $s \to \infty$.

Making use of eq. (2.33) we fix also the parameters for the singlet resonance. We have also fitted these parameters in **section 5.4**. In that section we obtained:

$$\widetilde{c}_d = 20.918^{+1.6}_{-1.0} \quad \widetilde{c}_m = 10.567^{+4.5}_{-3.5} \quad M_{S_1} = 1021.11^{+40}_{-20} \text{ MeV} \tag{6.52}$$

Taking into account the large N_c estimations eq. (6.38) one should have

$$\widetilde{c}_d = \widetilde{c}_m \;\; = \;\; 26.7 \pm 9 \text{ MeV} \tag{6.53}$$

where as usual a $\frac{1}{3}$ of relative error has been allowed from their central values. Both sets of values are compatible when considering the errors. On the other hand, if we take the nonet mass as the average among the masses of the singlet and of the octet we have fitted in this work, one has:

$$M_{nonet} \approx 1200 \text{ MeV} \tag{6.54}$$

this is the value taken for the mass of the nonet in **section 2.3**.

We can also try to find the resonance pole position from the former fits when going to the unphysical sheets. First we consider the resonance region for $\sqrt{s} \approx 1.4 - 1.6$ GeV. The pass from one sheet to the other one can be done following eq. (34) of [58]. This equation can also be deduced by taking into account the analytic expression for $g(s)$ where multivalued logarithms appear. The sheet can be associated with the $i\,2\pi K$ indetermination from the logarithms, and the factor K can be fixed by continuity when passing from one sheet to the oher. At the end one obtains the same result than in eq. (34) of ref. [58].

Changing $g_{K\pi} \to g_{K\pi} + i\,p_{K\pi}/(4\pi\sqrt{s})$, one goes to the II-sheet, which corresponds to changing the sign in the square root defining the three momentum of the lightest threshold, $K\pi$. The poles are:

$$\begin{aligned} \text{Fit (6.49): } & 1603 - i\,73 \text{ MeV} \\ \text{Fit (6.50): } & 1555 - i\,185 \text{ MeV} \end{aligned} \tag{6.55}$$

we see that the mass is more or less the same, however the width changes by a factor 2.

But even more, when going from the second to the third Riemann sheet by changing $g_{K\eta'} \to g_{K\eta'} + i\,p_{K\eta'}/(4\pi\sqrt{s})$ one finds the pole at:

$$\begin{aligned} \text{Fit (6.49): } & 1368 - i\,325 \text{ MeV} \\ \text{Fit (6.50): } & 1233 - i\,358 \text{ MeV} \end{aligned} \tag{6.56}$$

we have seen that this pole is linked to the one in (6.55) by continuously passing from the third to the second Riemann sheets by multiplying by a factor $\lambda \in [0, 1]$ the factor $i\,p_{K\eta'}/(4\pi\sqrt{s})$. Hence, when $\lambda = 0$ we are in the second sheet and when $\lambda = 1$ one is in the third one. The end points of such track are the poles in (6.55) and (6.56). The large variation of the pole position when passing from one sheet to another, means that the η' couples strongly to that resonance, as one also guesses when studying Figs. 6.6 and 6.7. Note that the second and third Riemann sheets are the close ones to the physical sheet since they are reached by continuity when crossing below and above the $K\eta'$ threshold, which is very close to the K_0^* resonance.

If we average the pole positions from eqs. (6.55) and (6.56) one has:

$$1440.75 \pm 148 \ - i\, 235 \pm 113 \text{ MeV} \tag{6.57}$$

However one has to keep in mind the obvious difficulty to characterize the $K_0^*(1430)$ resonance by the position of just one pole because as we have seen the change from the second to third sheet has large influence. In fact, this resonance is a combination of two pole effects, one in the second and another in the third sheet due to the proximity of the $K\eta'$ threshold.

In the PDG [19] the parameters for the $K_0^*(1430)$ come from the fit given in [72] for their data. In this fit they use a simple Breit-Wigner parametrization for the K_0^* resonance and the mass and width are those of the Breit-Wigner. In this way, they disregard the differences that can appear when moving to the final pole position of the resonance, which can be important as we have seeen. They quote:

$$M_R + i\,\frac{\Gamma}{2} = (1429 \pm 4 \pm 5 + i\, 143.5 \pm 5 \pm 10) \text{ MeV} \tag{6.58}$$

In the second sheet there is also another pole corresponding to the κ resonance, already introduced in **chapter 5**. For the values given in (6.55) and in the second sheet (note that this resonance is far away from the $K\eta'$ threshold) one has

$$700 - i\, 323 \text{ MeV} \tag{6.59}$$

in the line of the values given in Table 5.1.

6.6 Results for the I=3/2 $K\pi$ elastic amplitude.

We are going to distinguish data between the sets of experiments [75, 113, 114, 115] and [71]. The differences are very important for low energies around a factor 2-3 as can be seen in Fig. 6.7 for $\sqrt{s} \leq 0.8$ GeV.

Once we have fixed all the values for the scalar resonances, take for instance the fit in eq. (6.50) we proceed to the $I = 3/2$ case where we have only the a'_π eq. (6.41) as free parameter. We have fixed this parameter from the data up to $\sqrt{s} \approx 1$ GeV giving a value of $a'_\pi = 2.5 \pm 0.08$. In Fig. 6.8 the continuum line corresponds to this calculation. Note that for low energies we are in agreement with the data from [75, 113, 114, 115] and not with the one from [71]. This in fact was also the case in Fig. 4.15 of **chapter 4**, where we also discussed this channel making use of the IAM method. For energies higher than 1.2 GeV our results begin to disagree with the trend in the data. Note that in this channel for higher energies there are no resonances or thresholds which dominate the scattering, as in the $I = 1/2$. The latter contributions can be reproduced making use of our techniques. However we go into difficulties when taking into account all the possible soft contributions which appear in the I=3/2 for higher energies.

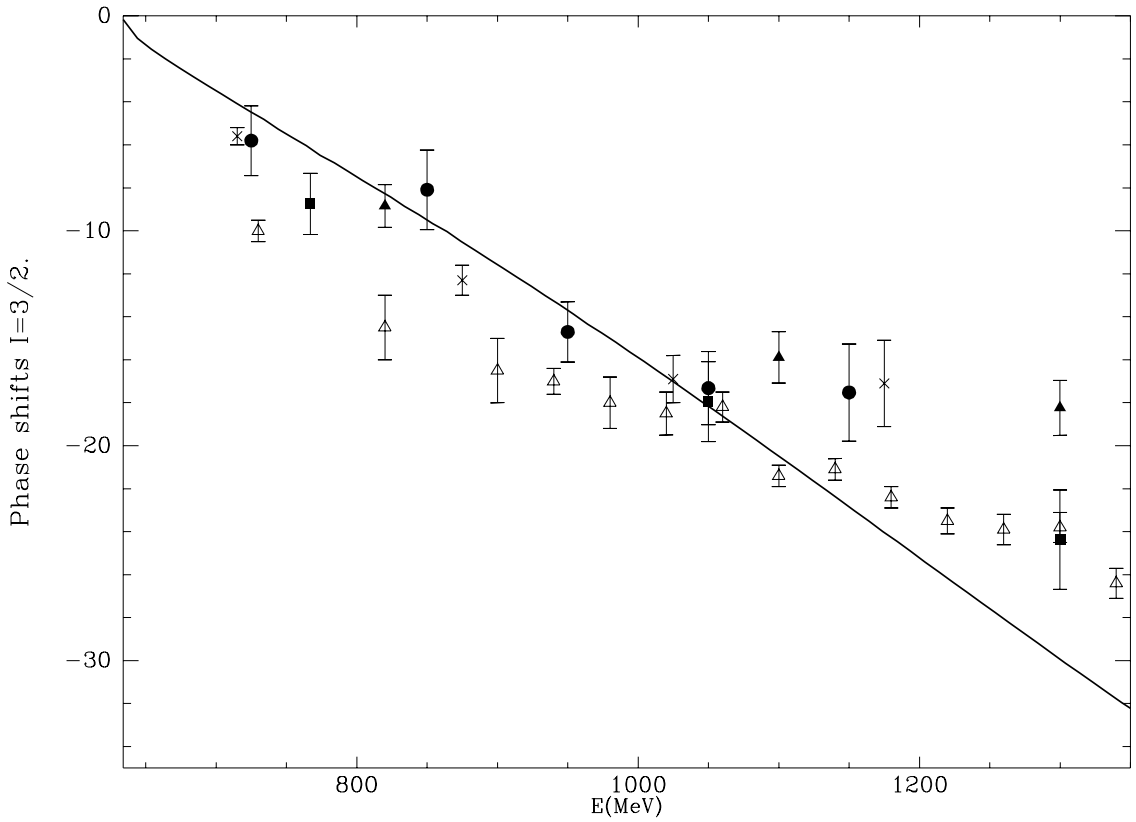

Figure 6.8: Full square: [75]. Full triangle: [113]. Full circle: [114]. Cross: [115]. Empty triangle: [71].

6.7 Conclusions.

In this chapter we have implemented the study of the $K\pi$ channel done in **chapter 5** by allowing the presence of the inelastic threshold $K\eta'$ and contributions coming from the unphysical cuts, which have been included perturbatively. We have discussed the inclusion of the $K\eta'$ channel, which has been done in large N_c limit where the η' is also a Goldstone boson. An extension of the unitarization method of **section 5.1** has also been done in order to take into account the unphysical cuts contributions strictly up to $\mathcal{O}(p^4)$.

We have seen that one is able to understand the I=1/2 and 3/2 scattering with values for the coupling constants c_d and c_m that saturate the L_i coefficients, see eqs. (2.32) and (2.33). The values of these couplings has been fixed in large N_c by requiring that the scalar $K\pi$, $K\eta$ and $K\eta'$ form factors vanish at infinity. These values are $c_d = c_m = f_\pi/2$. The mass of the first scalar nonet has been established to be around 1.2 GeV. With this value for the mass and the former values for the couplings, the contributions to the L_i coefficients given in Table 2.1 are obtained.

In this sense the results of this chapter agree with the conclusions in [7]. However,

in that work the authors consider the first scalar nonet with a mass around 1 Gev and including the $a_0(980)$ resonance. From the results of this chapter and of the former one we can say that this is not the case. The picture is that there is a lighter nonet scalar which embodies the σ, κ, $a_0(980)$ and a strong contribution to the $f_0(980)$ resonance which is of dynamical origin and hence subleading in large N_c. The scalar nonet, leading in this counting and responsible for the saturation of the L_i couplings, is another one. We have determined its mass to be around 1.2 GeV. This nonet embodies an octet formed by the $K_0^*(1430)$, $a_0(1450)$ and the $f_0(1500)$ and a singlet which contributes to the $f_0(980)$ resonance.

Finally, we stress that the situation for the experimental data in these channels has still to be improved both in the $I = 1/2$ and $3/2$ channels, and that an estimation of the associated systematic errors should be wellcome. We only agree with the solution C of [71] for energies higher than 1.5 GeV in the case of the $I = 1/2$ and disagree with this work for low energies in the $I = 3/2$ case. However, we agree with the data from [75, 113, 114, 115] in this latter case. We also disagree with the experimental data from [72] for $\sqrt{s} > 1.5$ GeV.

Chapter 7

Final State Interactions (FSI).

In this chapter we discuss the implementation of the final state¡ interactions(FSI) in several electromagnetic processes involving two mesons in the final state.

7.1 The scalar and vector pion form factors.

The scalar and vector form factors of the pion are defined respectively as

$$\left\langle \pi^a(p')\pi^b(p)\,\mathrm{out}\left|\hat{m}(\bar{u}u+\bar{d}d)\right|0\right\rangle = \delta^{ab}\Gamma(s) \tag{7.1}$$

and

$$\left\langle \pi^i(p')\pi^l(p)\,\mathrm{out}\left|\bar{q}\gamma_\mu\left(\frac{\tau^k}{2}\right)q\right|0\right\rangle = i\,\epsilon^{ikl}(p'-p)_\mu\,F_V(s) \tag{7.2}$$

with $\hat{m}=(m_u+m_d)/2$ and ϵ^{ijk} the total antisymmetric tensor with three indices.

Assuming elastic unitarity (valid up to the $K\overline{K}$ threshold and neglecting multipion states) and making use of the Watson final state theorem [116] the phase of $\Gamma(s)$ and $F_V(s)$ is fixed to be the one of the corresponding partial wave strong amplitude:

$$\begin{aligned}\mathrm{Im}\,\Gamma(s+i\epsilon) &= \tan\delta_0^0\,\mathrm{Re}\Gamma(s)\\ \mathrm{Im}\,F_V(s+i\epsilon) &= \tan\delta_1^1\,\mathrm{Re}F_V(s)\end{aligned} \tag{7.3}$$

The solution of (7.3) is well known and corresponds to the Omnès type [117, 118]:

$$\begin{aligned}\Gamma(s) &= P_0(s)\,\Omega_0(s)\\ F_V(s) &= P_1(s)\,\Omega_1(s)\end{aligned} \tag{7.4}$$

With

$$\Omega_i(s)=\exp\left\{\frac{s^n}{\pi}\int_{4m_\pi^2}^{\infty}\frac{ds'}{s'^n}\,\frac{\delta_i^i(s')}{s'-s-i\epsilon}\right\} \tag{7.5}$$

In (7.4) $P_0(s)$ and $P_1(s)$ are polynomials of degree fixed by the number of subtractions done in $\ln\{\Omega_0(s)\}$ and $\ln\{\Omega_1(s)\}$ minus one, and the zeros of F_V and Γ. For $n = 1$, $P_i(s) = 1$. This follows from the normalization requirement that $\Gamma(0) = F_V(0) = 1$ and the absence of zeros for those quantities.

We will calculate the dispersion integral (7.5) and obtain the pion form factors for both the scalar and vector cases making use of the phase shifts calculated in **section 4.3**. The results are shown in Figs. 7.1 and 7.2. The Omnès solution assumes the phase of the form factor to be that of the scattering amplitude, and that is true exactly only until the first inelastic threshold. The first inelastic threshold is the 4π one. However, as it was already said, its influence, in a first approach, is negligible. The first important inelastic threshold is the $K\bar{K}$ one around 1 GeV. This is essential in $I = L = 0$ but negligible in $I = L = 1$. This inelastic threshold, as discussed above, has been included in our approach and it is responsible for the appearance of the $f_0(980)$ resonance, as it is clearly seen in Figs. 4.5 and 7.2.

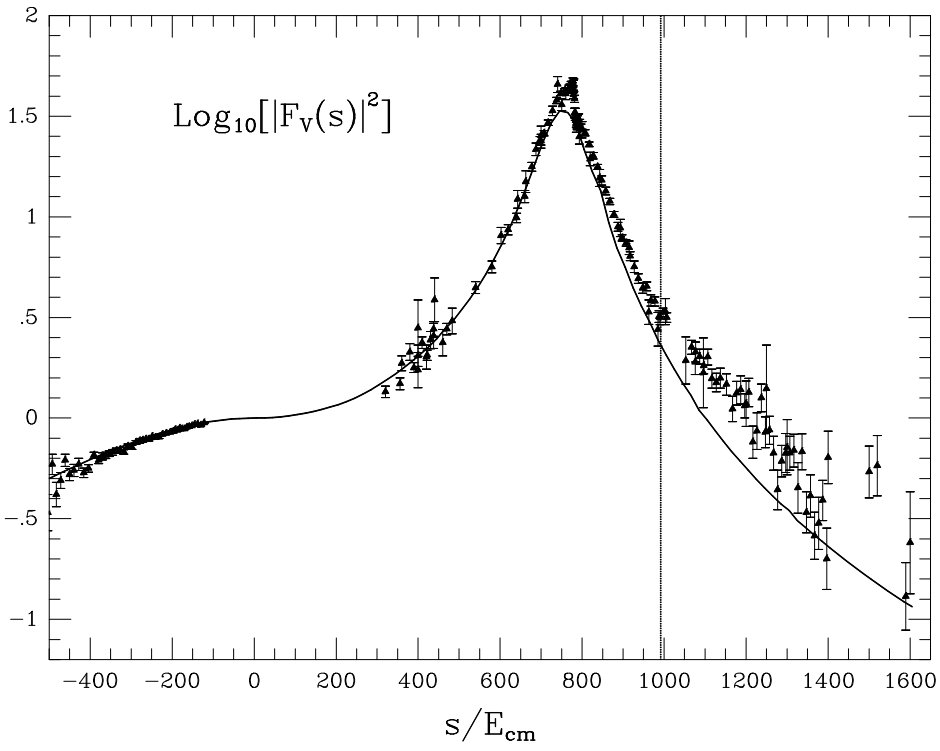

Figure 7.1: Vector pion form factor. The vertical line shows the opening of the $K\overline{K}$ threshold. Data: [119].

We see clearly the appearance in Figs. 7.1 and 7.2 of the $\rho(770)$ and $f_0(980)$ respectively. In the case of the $F_V(s)$ the agreement with existing data is quite satisfactory. Above the $K\bar{K}$ threshold one expects deviations from (7.4) due to the opening of this inelastic channel. However, for the vector form factor we still see a rather good agreement with data and the deviation should be ascribed to the presence of the ρ' resonance above 1.2

GeV. On the other hand, the result obtained for the vector form factor is similar to the one recently obtained in [120] using another phase shift expression, taking into account possible uncertainties coming from orders higher than p^4 in ChPT. For the $I = L = 0$ channel the most dramatic influence of the opening of the $K\bar{K}$ threshold is the appearance of the $f_0(980)$ resonance, what happens a little below $K\bar{K}$ threshold. So that we do not expect large deviations from our results even above the $K\bar{K}$ threshold up to the appearance of new $I = L = 0$, f_0, resonances higher in energy, typically around $\sqrt{s} \sim 1.3$ GeV. In Fig. 7.2 the dashed line represents the scalar form factor unitarizing only with pions to obtain the $\delta_{00,\pi\pi}$ phase shift, in the line of the works [121, 122, 123] and we see a very large influence of the $K\bar{K}$ channel through the f_0 resonance which is even substantial around $|\sqrt{s}| = 500$ MeV.

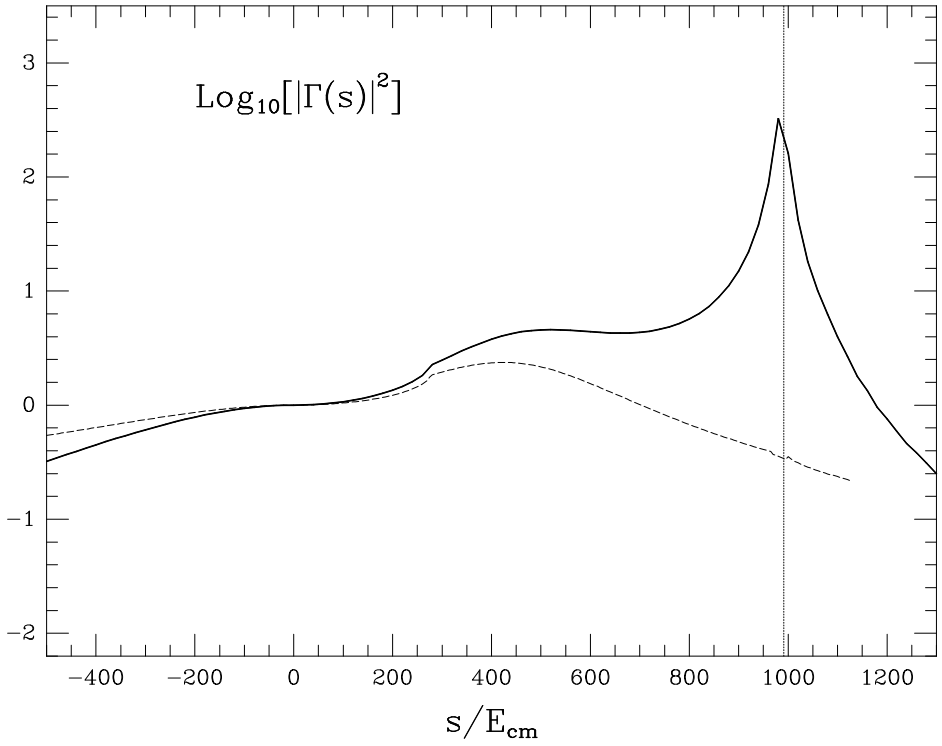

Figure 7.2: Scalar form factor. The dashed curve is the result unitarizing only with pions. The solid line is the full result with both pions and kaons in the intermediate state. The vertical line shows the opening of the $K\overline{K}$ threshold.

7.2 The $\gamma\gamma \rightarrow$meson-meson reaction.

The $\gamma\gamma \rightarrow$ meson-meson reaction provides interesting information concerning the structure of hadrons, their spectroscopy and the meson-meson interactions, given the sensitivity of the reaction to the hadronic final state interactions (FSI) [124]. In this sense, the study of these processes constitute a very interesting test of consistency of our approach for the

scalar sector in ref. [58], see also **section 5.2**. This study was done in ref. [76]. Since the former work was already reported in my master's thesis, I will only give a brief summary in this section.

In that work, we were able of presenting, for first time, a unified theoretical description of the reactions $\gamma\gamma \to \pi^+\pi^-$, $\pi^0\pi^0$, K^+K^-, $K^0\bar{K}^0$, $\pi^0\eta$ up to about $\sqrt{s} = 1.4\ GeV$ reproducing the experimental cross sections and angular distributions, see Fig. 7.6.

For calculating the above processes we correct for FSI the tree level amplitudes coming from Born terms (Fig. 7.3), in the case of the charged channels, and also from the exchange of vector and axial resonances in the crossed channels [125] (Fig. 7.4.).

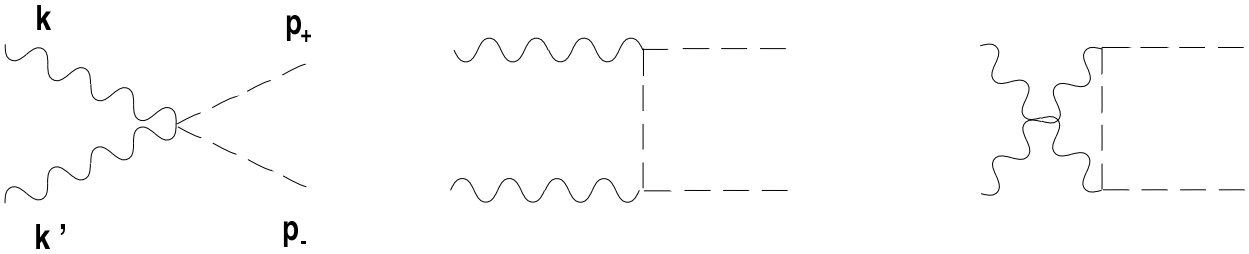

Figure 7.3: Born term amplitude for $\gamma\gamma \to M^+M^-$. k and k' are the momenta of the incoming photons and $p_+(p_-)$ the momentum of the positively(negatively) charged meson.

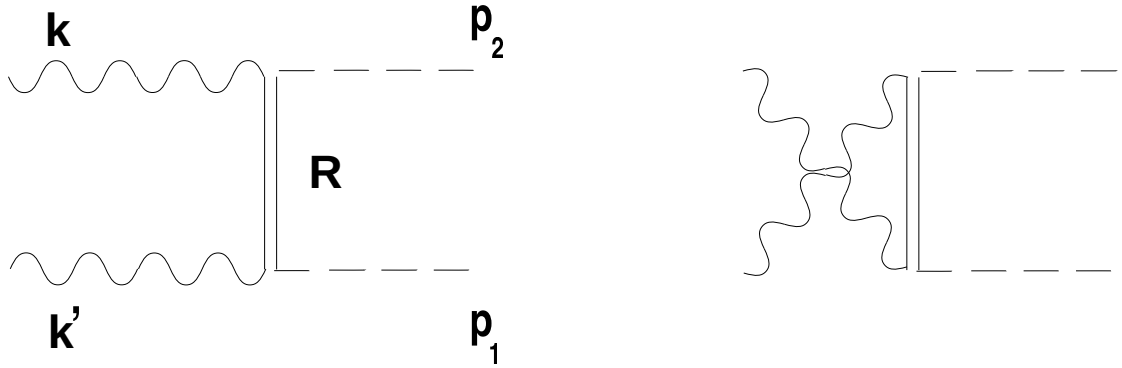

Figure 7.4: Tree level amplitude for $\gamma\gamma \to M_1M_2$ through the exchange of a resonance R(axial or vectorial) in the t,u channels. k and k' are the momenta of the incoming photons and p_1, p_2 are the momenta of the final mesons.

7.2.1 FSI: S-wave.

We first consider the one loop corrections of the tree level amplitudes and then we extend this result to the string of loops represented in Fig. 7.5.

The one loop contribution generated from the Born terms with intermediate charged mesons can be directly taken from the χPT calculations [126, 127] of the $\gamma\gamma \to \pi^0\pi^0$ amplitude at $\mathcal{O}(p^4)$. The important point is that the $\mathcal{O}(p^2)$ χPT amplitude connecting

the charge particles with the $\pi^0\pi^0$ factorizes on-shell outside the loop. We can schematically represent this situation by:

$$\sum_a L(s)_a \, T^{(2)}_{ab}(s) \tag{7.6}$$

where the subindex a represents the pair of intermediate charged mesons, b the final ones and $T^{(2)}$ the on-shell $\mathcal{O}(p^2)$ amplitude.

Our contribution beyond this first loop is to include all meson loops (Fig. 7.5) generated by the coupled channel Lippmann Schwinger equations of **section 5.2**, ref. [58]. We also saw there that the on-shell $\mathcal{O}(p^2)$ χPT amplitudes factorize outside the loop integrals. Thus, the immediate consequence of introducing these loops is to substitute the on-shell $\mathcal{O}(p^2)$ $\pi\pi$ amplitude in eq. (7.6), by our on-shell meson-meson amplitude, $T_{ab}(s)$, evaluated in ref. [58].

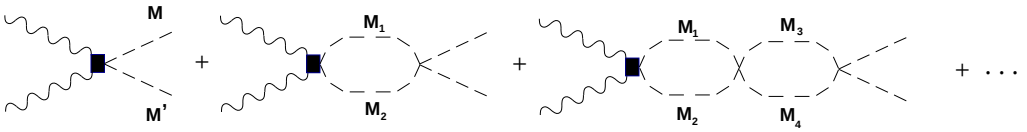

Figure 7.5: Diagrammatic series which gives rise to the FSI from a general $\gamma\gamma \to$M M' vertex, represented by the full square.

A similar procedure can be done to account for the FSI in the case of the tree level diagrams with the exchange of a resonance (vector or axial). As explained in [76] one can justify the accuracy of factorizing the strong amplitude for the loops with crossed exchange of resonances, since this result is correct for $M_R^2 \to \infty$. Because we are dealing with real photons the intermediate axial or vector mesons are always off-shell and the large mass limit is a sensible approximation. The errors were estimated to be below the level of 5% for M_R about 800 MeV.

7.2.2 D-wave contribution.

For the $(2,2)$ component we take the results of ref. [128], obtained using dispersion relations

$$t^{(2,2)}_{BC} = \left[\frac{2}{3}\,\chi^{T=0}_{22}\, e^{i\delta_{20}} + \frac{1}{3}\,\chi^{T=2}_{22}\, e^{i\delta_{22}}\right] t^{(2,2)}_{B} \tag{7.7}$$

For the $\gamma\gamma \to K^+K^-$ reaction the non resonant D-wave contribution is not needed because we are close to $K\bar{K}$ threshold and furthermore the functions χ_{ij} are nearly zero close to the mass of the f_2 and a_2 resonances.

The **resonance contribution** in the $D-$wave coming form the $f_2(1270)$ and $a_2(1320)$ resonances is parametrised in the standard way of a Breit-Wigner as done in ref. [129]. The parameters of these resonances are completely compatible with the ones coming from the Particle Data Group [19]

Once we have corrected for FSI the S- and D-waves, which completely dominate the $\gamma\gamma \to$meson-meson reactions up to the energies considered [76, 128], we compare with several experimental data.

7.2.3 Total and differential cross sections.

The experimental data correspond to total and differential cross sections. As can be seen in Fig. 7.6, the agreement is extraordinary good in all the considered channels. It is worth to say that the results presented are not a fit, they are calculations since the parameters of the axial, vector and tensor resonances were taken from the literature.

It is worth remarking that in the figure corresponding to the $\gamma\gamma \to K^+K^-$ reaction, that the Born term, indicated by the long-dashed line, reduces to the short-dashed line when taking into account the FSI.

7.2.4 Partial decay widths to two photons of the $f_0(980)$ and $a_0(980)$.

We follow the same procedure that in **section 4.4.3** to calculate the partial decay widths of the $f_0(980)$ and $a_0(980)$ in terms of our strong and photo-production amplitudes. From our amplitudes with isospin $I = 1$ and 0, we consider the terms which involve the strong $M\bar{M} \to M\bar{M}$ amplitude. Then, we isolate the part of the $\gamma\gamma \to M\bar{M}$ which proceeds via the resonances a_0 and f_0 respectively. In the vicinity of the resonance the amplitude proceeds as $M\bar{M} \to R \to M\bar{M}$. Hence, we eliminate the $R \to M\bar{M}$ part of the amplitude plus the R propagator and remove the proper isospin Clebsch Gordan coefficients for the final states (1 for $\pi^0\eta$ and $-1/\sqrt{2}$ for K^+K^-) and then we get the coupling of the resonances to the $\gamma\gamma$ channel.

The results are:

$$\Gamma^{\gamma\gamma}_{a_0} = 0.78\ KeV \quad \Gamma^{\gamma\gamma}_{a_0}\frac{\Gamma^{\eta\pi}_{a_0}}{\Gamma^{tot}_{a_0}} = 0.49\ KeV \quad \Gamma^{\gamma\gamma}_{f_0} = 0.20\ KeV \tag{7.8}$$

The calculated width for the $f_0(980)$ is smaller than the average reported in the PDG [19] (0.56 ± 0.11) KeV. In doing this average the PDG refers to the work [128] by Morgan and Pennington where they quote a width of (0.63 ± 0.14) KeV. However, in a recent work by Boglione and Pennington they quote the much more smaller width $(0.28^{+0.09}_{-0.13})$ KeV, [130]. When taking into account the errors, the former result and the ours are compatible.

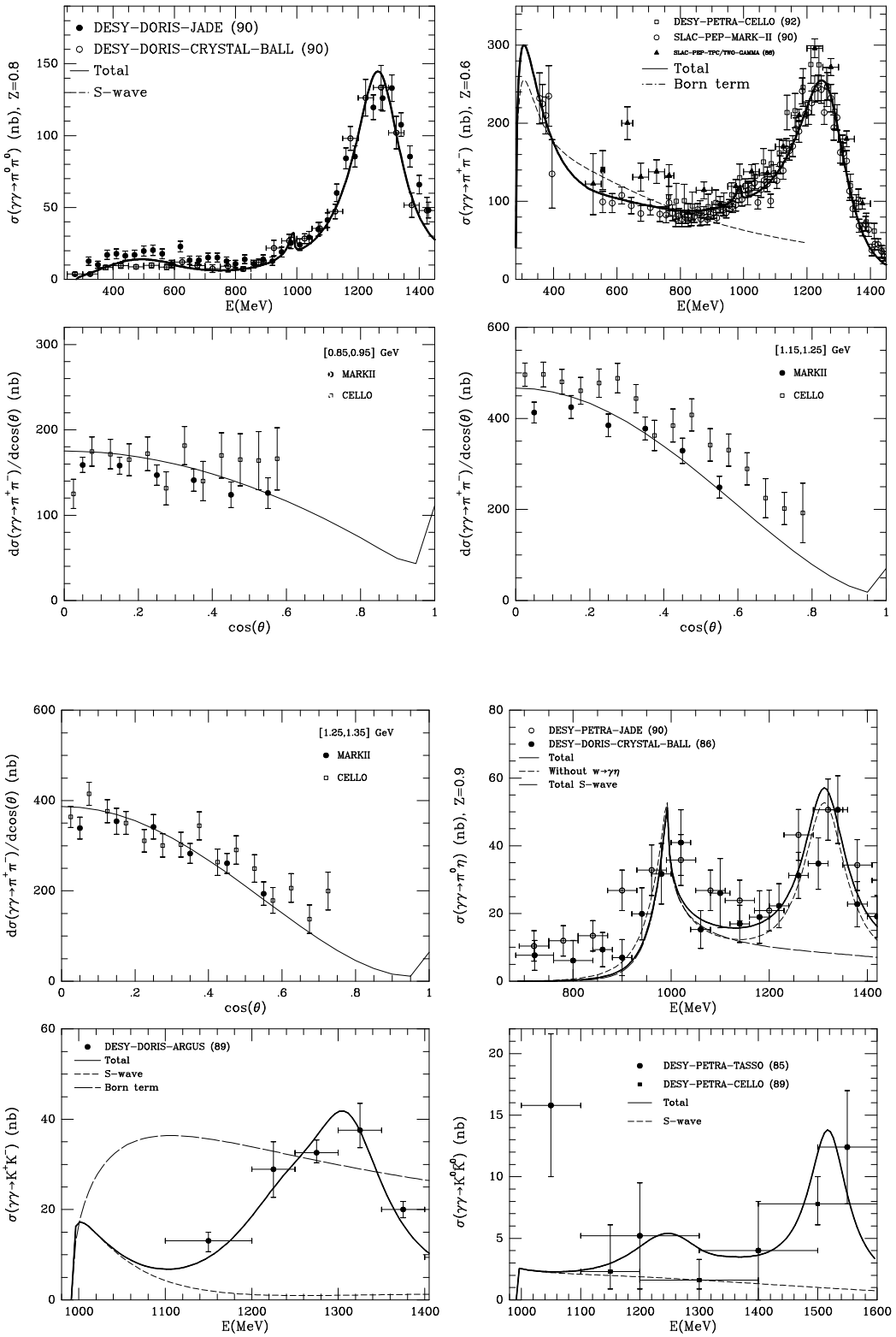

Figure 7.6: Total and differential cross sections for several photoproduction processes. The referenes to the experimental data can be seen in [76].

Our calculation for the second magnitude in eq. (7.8) is larger than the value given in PDG (0.28±0.04±0.1) KeV. However, this value comes from references where a background is introduced in order to fit the data. In our analysis we do not need any background and hence, in a natural way, the strength of the $a_0(980)$ to two photons is increased.

7.2.5 Conclusions

1) The resonance $f_0(980)$ shows up weakly in $\gamma\gamma \to \pi^0\pi^0$ and barely in $\gamma\gamma \to \pi^+\pi^-$.

2) In order to explain the angular distributions of the $\gamma\gamma \to \pi^+\pi^-$ reaction we did not need the hypothetical $f_0(1100)$ broad resonance suggested in other works [128]. This also solves the puzzle of why it did not show up in the $\gamma\gamma \to \pi^0\pi^0$ channel. Furthermore, such resonance does not appear in the theoretical work of ref. [58], while the $f_0(980)$ showed up clearly as a pole of the T matrix in $I = 0$.

3) The resonance a_0 shows up clearly in the $\gamma\gamma \to \pi^0\eta$ channel and we reproduce the experimental results without the need of an extra background from a hypothetical $a_0(1100 - 1300)$ resonance suggested in ref. [124].

4) We have found an explanation to the needed drastic reduction of the Born term in the $\gamma\gamma \to K^+K^-$ reaction in terms of final state interaction of the K^+K^- system.

7.3 The $\phi \to \gamma K^0\bar{K}^0$ decay.

The study of the process $\phi \to \gamma K^0\bar{K}^0$ is an interesting subject since it provides a background to the reaction $\phi \to K^0\bar{K}^0$. This latter process has been proposed as a way to study CP violating decays to measure the small ratio ϵ'/ϵ [131], but since this implies seeking for very small effects a BR($\phi \to \gamma K^0\bar{K}^0$)$\geq 10^{-6}$ will limit the scope of these perspectives. There are several calculations of this quantity [128–131]. In [136] it is estimated for a *non resonant* decay process without including the f_0 and a_0 resonances. The issue is revisited in [137]. In this section we will follow the work done in [138].

Here, a different way to treat the scalar meson-meson sector, and its related $f_0(980)$ and $a_0(980)$ resonances, is proposed. For this we use a recent approach [58] to the S-wave meson-meson interaction for isospin 0 and 1 which reproduces the experimental data for those processes up to about 1.2 GeV and generates dynamically the a_0 and f_0 resonances. In this way, we will consider their interference and the energy dependence of their widths and coupling constants to the $K\bar{K}$ system. Furthermore, other possible contributions, non resonant, are also taken into account. The ideas and amplitudes exposed there were used in [76] for the $\gamma\gamma \to \pi\pi$, $K\bar{K}$ and $\pi^0\eta$ processes and a good agreement with the experiment was obtained.

As in former works [127–131] we consider the process $\phi \to \gamma K^0\bar{K}^0$ through an intermediate K^+K^- loop which couples strongly to the ϕ and the scalar resonances, see Fig.7.7.

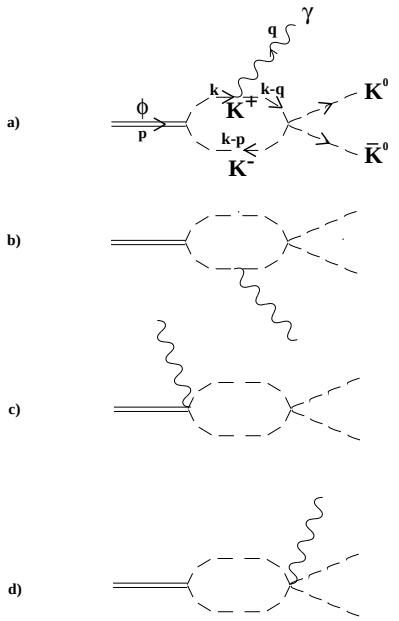

Figure 7.7: The loop radiation (a,b) and contact (c) contributions.

For calculating this loop contributions we use the minimal coupling to make the interaction between the ϕ and the K^+K^- mesons gauge invariant, then we have

$$H_{int} = (eA_\mu + g_\phi \phi_\mu) i(K^+ \partial^\mu K^- - \partial^\mu K^+ K^-) - 2e g_\phi A^\mu \phi_\mu K^+ K^- \tag{7.9}$$

Where g_ϕ is the coupling constant between the ϕ and the K^+K^- system.

An essential ingredient to evaluate the loop in Fig. 7.7 is the strong amplitude connecting K^+K^- with $K^0\bar{K}^0$. As we said before we will use the amplitude calculated in [58]. This implies the sum of an infinite series of diagrams which is represented in Fig.7.8 for the diagram of Fig. 7.7.a, and the analogue corresponding to Figs. 7.7b,c.

This series gives rise to the needed corrections due to final state interactions and in fact, from the vertex connecting the K^+K^- with the $K^0\bar{K}^0$, this series is the same one that in [58] gives rise to the S-wave strong amplitude $K^+K^- \to K^0\bar{K}^0$. In this approach the vertex between the loops correspond to the lowest order chiral perturbation theory [4, 5], χPT. Note that an analogous series before the loop with the emission of the photon is absorbed in the infinite series of diagrams contained in the ϕ resonance propagator.

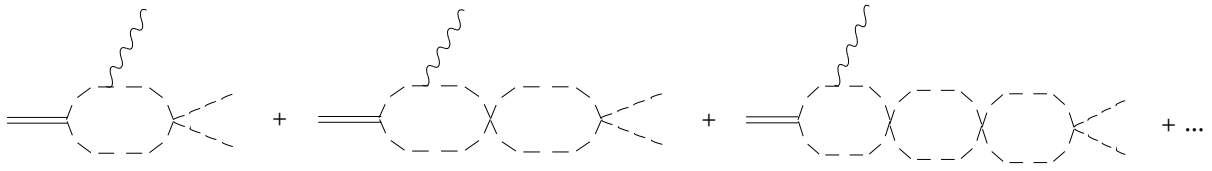

Figure 7.8: Diagrammatic series which gives rise to the FSI from a general loop of Fig. 7.7.

First of all, let us see that the strong amplitude connecting K^+K^- with $K^0\bar{K}^0$ calculated in the way shown in Fig. 7.8 [58] must factorize out of the integral.

For this consider the diagrams in Fig. 7.7 but with the $\mathcal{O}(p^2)$ χPT amplitude connecting the kaons. This amplitude is given by

$$< K^0\bar{K}^0|t|K^+K^- >= \frac{1}{2}[t_{I=0} - t_{I=1}] = -\frac{1}{4f^2}[s + \frac{4m_K^2 - \sum_i p_i^2}{3}] \tag{7.10}$$

where f is the pion decay constant, $f \simeq 93\ MeV$, I refers to the isospin channel of the amplitude and the subindex i runs from 1 to 4 and refers to any of the four kaons involved in the strong interaction. If the particle is on-shell then $p_i^2 = m_K^2$. In our case $p_{K^0}^2 = p_{\bar{K}^0}^2 = m_K^2$ so we have

$$-\frac{1}{4f^2}[s + \frac{(m_K^2 - p_{K^+}^2) + (m_K^2 - p_{K^-}^2)}{3}] \tag{7.11}$$

The important point for the sequel is that the off-shell part, which should be kept inside the loop integration, will not contribute.

In order to see this, note that, due to gauge invariance, the physical amplitude for $\phi \to \gamma K^0\bar{K}^0$ has the form

$$M(\phi(p) \to \gamma(q)K^0\bar{K}^0) = [g^{\mu\nu}(p\cdot q) - p^\mu q^\nu]\epsilon_\mu^\gamma \epsilon_\nu^\phi H(p\cdot q, Q^2, q\cdot Q) \tag{7.12}$$

where ϵ_μ^γ and ϵ_ν^ϕ are the polarisation vectors of the photon and the ϕ, $Q = p_{K^0} + p_{\bar{K}^0}$ and H is an arbitrary scalar function. In the calculation of this loop contribution the problem is the presence of divergences in the loops represented in Fig. 7.7. Following refs. [132, 133, 134] we will take into account the contribution of $p^\mu q^\nu$ of Figs. 7.7.a,b, since Fig. 7.7.c,d does not give such type of terms. Then, by gauge invariance, see formula (7.12), the coefficient for $(p\cdot q)g^{\mu\nu}$ is also fixed. In fact, as in ref. [132, 133, 134, 137] it is shown, the $p^\mu q^\nu$ contribution will be finite since the off shell part of the strong amplitudes do not contribute, as we argue below, and then we are in the same situation than in the latter references. On the other hand, depending on the renormalization scheme chosen, additional tadpole like terms can appear [139]. However, they do not contribute to the $p^\mu\, q^\nu$ structure and hence can be ignored.

Take the diagrams of Figs. 7.7.a,b. These diagrams give the same contribution and this is the reason for the factor 2 in front of the following integral accounting for both contributions.

$$\begin{aligned} M' = \epsilon_\mu^\gamma \epsilon_\nu^\phi \tfrac{2eg_\phi}{i} \int \tfrac{d^4k}{(2\pi)^4} \tfrac{(2k_\nu - p_\nu)(2k_\mu - q_\mu)}{(k^2 - m_K^2 + i\epsilon)((k-q)^2 - m_K^2 + i\epsilon)((k-p)^2 - m_K^2 + i\epsilon)} \\ \cdot \tfrac{-1}{4f^2}[Q^2 + \tfrac{(m_K^2 - p_{K^+}^2) + (m_K^2 - p_{K^-}^2)}{3}] \end{aligned} \tag{7.13}$$

The momentum for each particle in the loop is indicated in Fig. 7.7.a and so we have that $p_{K^+} = k - q$, $p_{K^-} = k - p$. Concentrating in the off-shell part of the strong amplitude, we have the integral

$$\int \frac{d^4k}{(2\pi)^4} \frac{(2k_\nu - p_\nu)(2k_\mu - q_\mu)}{(k^2 - m_K^2 + i\epsilon)((k-q)^2 - m_K^2 + i\epsilon)((k-p)^2 - m_K^2 + i\epsilon)} \cdot [(k-q)^2 - m_K^2 + (k-p)^2 - m_K^2] =$$
$$\int \frac{d^4k}{(2\pi)^4} \frac{(2k_\nu - p_\nu)(2k_\mu - q_\mu)}{(k^2 - m_K^2 + i\epsilon)((k-p)^2 - m_K^2 + i\epsilon)} + \int \frac{d^4k}{(2\pi)^4} \frac{(2k_\nu - p_\nu)(2k_\mu - q_\mu)}{(k^2 - m_K^2 + i\epsilon)((k-q)^2 - m_K^2 + i\epsilon)} \tag{7.14}$$

Taking into account that

$$\epsilon_\mu^\phi \cdot p^\mu = 0 \; ; \; \epsilon_\nu^\gamma \cdot q^\nu = 0 \;\; (Feynman\ gauge) \tag{7.15}$$

then we only have

$$\int \frac{d^4k}{(2\pi)^4} \frac{4k_\mu k_\nu}{(k^2 - m_K^2 + i\epsilon)((k-p)^2 - m_K^2 + i\epsilon)} + \int \frac{d^4k}{(2\pi)^4} \frac{4k_\mu k_\nu}{(k^2 - m_K^2 + i\epsilon)((k-q)^2 - m_K^2 + i\epsilon)} \tag{7.16}$$

The above integrals do not give contribution to $q^\mu p^\nu$ since in each integral there is only one of the two vectors q or p. In this way we see that the strong amplitude $\mathcal{O}(p^2)$ factorizes out on-shell in (7.12). Note that the important point in the former argumentation is the form of the off-shell part of the S-wave strong amplitude at $\mathcal{O}(p^2)$ and this is common to any other S-wave meson-meson amplitude at this order, as one can see in [58].

Next we want to sum all the infinite series represented in Fig. 7.8. The intermediate loops also contain $\pi\pi$ for $I = 0$ and $\pi^0\eta$ for $I = 1$, since in ref. [58] coupled channel Lippmann-Schwinger equations were used with $\pi\pi$, $K\bar{K}$ in $I = 0$ and $\pi^0\eta$, $K\bar{K}$ in $I = 1$. In ref. [58] it is shown that the meson-meson amplitude factorizes on-shell outside the loop integrals and since we have also here the $\mathcal{O}(p^2)$ strong amplitude factorizing we are then in the same situation as in [58] and we can substitute the $\mathcal{O}(p^2)$ strong amplitude by the one calculated to all orders in this reference. This result is an exact consequence of the approach used in [58]. Similar ideas were also used in [76] to include the corrections coming from the final state interaction in $\gamma\gamma \to$meson-meson giving rise to a very good agreement with the experimental results. Then to all orders in the approach of [58] we have the amplitude

$$t_S = \frac{1}{2}[t_{I=0} - t_{I=1}] \tag{7.17}$$

Note that the amplitude obtained in [58] contains also the resonances $f_0(980)$ and $a_0(980)$ which are generated dynamically.

Then we have for the amplitude $\phi(p) \to \gamma(q) K^0 \bar{K}^0$

$$M = \epsilon_\mu^\gamma \epsilon_\nu^\phi \frac{2eg_\phi}{i} t_S \int \frac{d^4k}{(2\pi)^4} \frac{(2k_\nu - p_\nu)(2k_\mu - q_\mu)}{(k^2 - m_K^2 + i\epsilon)((k-q)^2 - m_K^2 + i\epsilon)((k-p)^2 - m_K^2 + i\epsilon)} \tag{7.18}$$

This integral has been evaluated in [132] using dimensional regularization and confirmed in [137], with the result

$$M = \frac{eg_\phi}{2\pi^2 i m_K^2} I(a,b) \, [(p\cdot q)(\epsilon_\gamma \cdot \epsilon_\phi) - (p\cdot\epsilon_\gamma)(q\cdot\epsilon_\phi)] t_S \tag{7.19}$$

with $a = M_\phi^2/m_K^2$ and $b = Q^2/m_K^2$

$$I(a,b) = \frac{1}{2(a-b)} - \frac{2}{(a-b)^2}(f(\frac{1}{b}) - f(\frac{1}{a})) + \frac{a}{(a-b)^2}(g(\frac{1}{b}) - g(\frac{1}{a})) \tag{7.20}$$

where

$$f(x) = \begin{cases} -(arcsin(\frac{1}{2\sqrt{x}}))^2 & x > \frac{1}{4} \\ \frac{1}{4}[ln(\frac{\eta_+}{\eta_-}) - i\pi]^2 & x < \frac{1}{4} \end{cases}$$

$$g(x) = \begin{cases} (4x-1)^{\frac{1}{2}} arcsin(\frac{1}{2\sqrt{x}}) & x > \frac{1}{4} \\ \frac{1}{2}(1-4x)^{\frac{1}{2}}[ln(\frac{\eta_+}{\eta_-}) - i\pi] & x < \frac{1}{4} \end{cases} \tag{7.21}$$

$$\eta_\pm = \frac{1}{2x}(1 \pm (1-4x)^{\frac{1}{2}})$$

After summing over the final polarisations of the photon, averaging over the ones of the ϕ and taking into account the phase space for three particles [19] one obtains

$$\Gamma(\phi \to \gamma K^0 \bar{K^0}) = \int \frac{dm_{12}^2 dQ^2}{(2\pi)^3 192 M_\phi^3} |e g_\phi \frac{I(a,b)}{2\pi^2 m_K^2}|^2 (M_\phi^2 - Q^2)^2 |t_S|^2 \tag{7.22}$$

where $m_{12}^2 = (q + p_{K^0})^2$.

Taking $\frac{g_\phi^2}{4\pi} = 1.66$ from its width to K^+K^-, $M_\phi = 1019.41\ MeV$, $\Gamma(\phi) = 4.43\ MeV$, BR($\phi \to K^0\bar{K^0}$) $= 0.34$ and using the mass of the K^0 for the phase space considerations, ref. [19], one gets

$$\begin{aligned} \Gamma(\phi \to \gamma K^0 \bar{K^0}) &= 2.22 \times 10^{-7}\, MeV \\ BR(\phi \to \gamma K^0 \bar{K^0}) &= 0.50 \times 10^{-7} \\ \frac{\Gamma(\phi \to \gamma K^0 \bar{K^0})}{\Gamma(\phi \to K^0 \bar{K^0})} &= 1.47 \times 10^{-7} \end{aligned} \tag{7.23}$$

The uncertainties coming from the range of the possible values for the cut-off give a relative error around 20%.

Taking only into account the $I = 0$ contribution

$$\begin{aligned} \Gamma(\phi \to \gamma K^0 \bar{K^0}) &= 8.43 \times 10^{-7}\, MeV \\ BR(\phi \to \gamma K^0 \bar{K^0}) &= 1.90 \times 10^{-7} \\ \frac{\Gamma(\phi \to \gamma K^0 \bar{K^0})}{\Gamma(\phi \to K^0 \bar{K^0})} &= 5.58 \times 10^{-7} \end{aligned} \tag{7.24}$$

and with only the $I = 1$

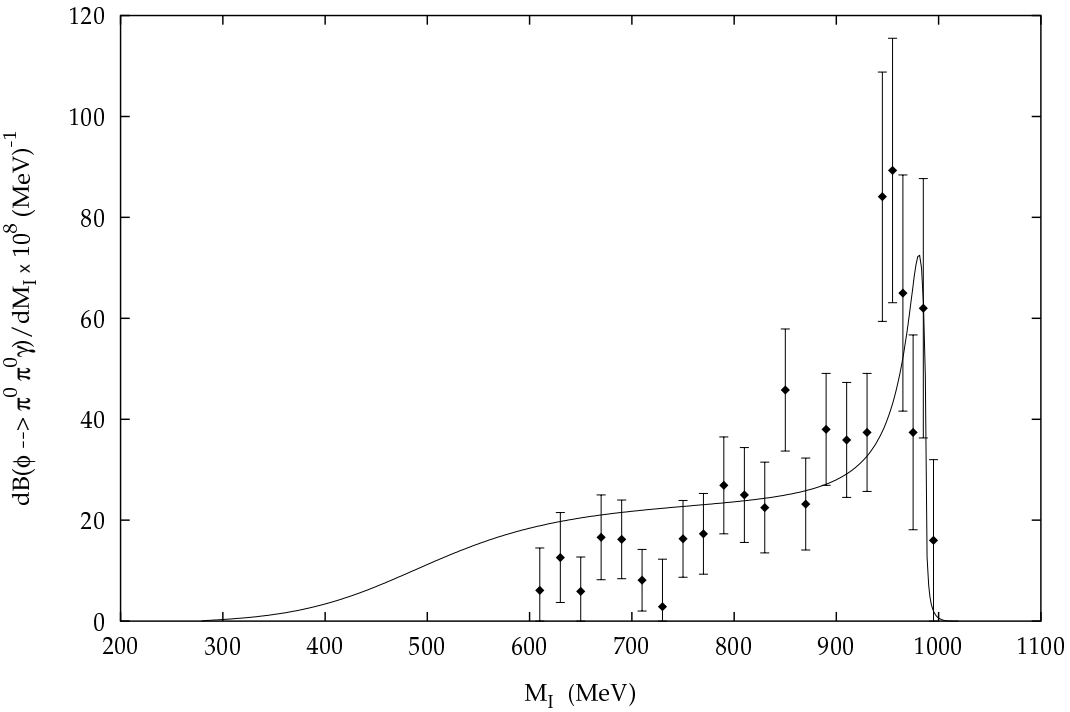

Figure 7.9: Distribution dB/dM_I for the decay $\phi \to \pi^0\pi^0\gamma$, with M_I the invariant mass of the $\pi^0\pi^0$ system. The data points are from [141] and only statistical errors are shown. The systematic errors are similar to the statistical ones [141]. The distribution for $\phi \to \pi^+\pi^-\gamma$ is twice the results plotted there.

$$\begin{aligned} \Gamma(\phi \to \gamma K^0 \bar{K}^0) &= \quad 2.03 \times 10^{-7}\, MeV \\ BR(\phi \to \gamma K^0 \bar{K}^0) &= \quad 4.58 \times 10^{-8} \\ \tfrac{\Gamma(\phi \to \gamma K^0 \bar{K}^0)}{\Gamma(\phi \to K^0 \bar{K}^0)} &= \quad 1.35 \times 10^{-7} \end{aligned} \tag{7.25}$$

We see that the process is dominated by the $I = 0$ contribution and that the interference between both isospin channels is destructive.

From the former results we see that the $\phi \to \gamma K^0 \bar{K}^0$ background will **not** be too significant for the purpose of testing CP violating decays from the $\phi \to K^0 \bar{K}^0$ process at DAΦNE in the lines of what was expected in [137]. All these calculations have been done in a way that both the resonant and non-resonant contributions are considered at the same time and taking into account also the different isospin channels.

Finally, I would like to comment the recent calculations for the decay $\phi \to \gamma\pi^0\pi^0$ done in [140] following the approach developed in this section. The calculation was done just before the group from Novosibirsk [141] published their data. The agreement is extraordinary as can be seen in the Fig. 7.9 taken from [140].

Chapter 8

Final Conclusions.

In this work we have presented two methods of resummation of the chiral series resulting from χPT [4, 5] or from the χPT amplitudes plus the resonance chiral Lagrangians [7]. In both cases one obtains a unitary amplitude to all orders in the chiral expansion although cross symmetry is obtained perturbatively.

The first method is the Inverse Amplitude Method [25], developed in **chapter 4**. Our original contribution has been to extended this formalism to the coupled channel case [26]. In this way, the IAM originally restricted to the elastic scattering, could also be applied to study several S-waves amplitudes for which the coupled channels are very important, for instance the $K\bar{K}$ coupled to $\pi\pi(\pi\eta)$ for the I=0(1). The method has proved to be very successful from the phenomenological point of view up to $\sqrt{s} \simeq 1.2$ GeV. This success can be understood through VMD for the vector channels and from the great importance that the unitarization of the lowest χPT amplitudes has for the scalar channels. The method also reproduces the resonances which appear in the scattering of two mesons, namely, ρ, K^*, $f_0(980)$, $a_0(980)$, σ, κ and an octet contribution to the ϕ meson.

The other approach is based in the use of the N/D method. In this way, the unitarization of the lowest order chiral amplitudes from $\mathcal{L}_2$ and the exchange of resonances from ref. [7] was accomplished. This method is specially suited to address the spectroscopic problem of differentiating between meson-meson versus elementary resonances. In this way, we concluded that the σ, $a_0(980)$ and κ, together with a strong contribution to the $f_0(980)$, are meson-meson resonances, while a singlet contribution to the $f_0(980)$ and an octet around 1.4 GeV ($a_0(1450)$, $K_0^*(1430)$ and $f_0(1500)$) are elementary resonances, not meson-meson ones. This latter nonet would be the responsible of the saturation of the χPT counterterms at $\mathcal{O}(p^4)$ [7]. In fact, the lightest meson-meson nonet disappears in the large N_c limit.

On the other hand, in **chapter 6**, we were able to fix in large N_c the values of the couplings for the scalar nonet from the vanishing at infinity of the scalar $K\pi$, $K\eta$ and $K\eta'$ form factors. In this way the saturation of the L_i χPT counterterms at $\mathcal{O}(p^4)$ is obtained for a mass of around 1.2 GeV for this nonet. We also saw that with these values one is able to obtain a good description of the $K\pi$ I=1/2, 3/2 S-waves up to energies around 1.6 GeV. To accomplish this, the $K\eta'$ channel was introduced in large N_c, where the η' is also

a Goldstone boson, making use of the lowest order chiral Lagrangians [5, 7].

Finally, in **chapter 7** we studied several electromagnetic processes corrected from FSI. We used an Omnès resummation for the scalar and vector $\pi\pi$ form factors. For the $\gamma\gamma \to$ meson-meson and the decays of the ϕ meson we make use of a resummation of loops in the s-channel, which is based in the factorization of the lowest order chiral amplitudes in the loops involved in the production mechanisms of the mesons.

We hope in the future to apply these techniques to other scenarios apart from the meson-meson scattering, as for instance, meson-baryon or baryon-baryon scattering.

Appendix A

Relation between cut-off and dimensional renormalization.

In this appendix we are showing the relationship between our regularization scheme and dimensional regularization, which is the usual one when dealing with χPT.

A.1 Analytical formula for $G(s)$ with a cut-off regularization.

In the general case with different masses, M_1 and M_2

$$\begin{aligned} G(s) &= \frac{1}{32\pi^2}\Bigg[-\frac{\Delta}{s}\log\frac{M_1^2}{M_2^2} + \frac{\nu}{s}\left\{ \log\frac{s-\Delta+\nu\sqrt{1+\frac{M_1^2}{q_{max}^2}}}{-s+\Delta+\nu\sqrt{1+\frac{M_1^2}{q_{max}^2}}} + \log\frac{s+\Delta+\nu\sqrt{1+\frac{M_2^2}{q_{max}^2}}}{-s-\Delta+\nu\sqrt{1+\frac{M_2^2}{q_{max}^2}}} \right\} \\ &+2\frac{\Delta}{s}\log\frac{1+\sqrt{1+\frac{M_2^2}{q_{max}^2}}}{1+\sqrt{1+\frac{M_2^2}{q_{max}^2}}} - 2\log\left[\left(1+\sqrt{1+\frac{M_1^2}{q_{max}^2}}\right)\left(1+\sqrt{1+\frac{M_2^2}{q_{max}^2}}\right)\right] \\ &+\log\frac{M_1^2\,M_2^2}{q_{max}^4}\Bigg] \end{aligned} \tag{A.1}$$

where $\nu = \sqrt{(s-(M_1+M_2)^2)(s-(M_1-M_2)^2)}$ and $\Delta = M_1^2 - M_2^2$. In the case of equal masses, $M_1 = M_2 = m$, the above formula reduces to

$$G(s) = \frac{1}{(4\pi)^2}\left[\sigma\log\frac{\sigma\sqrt{1+\frac{m^2}{q_{max}^2}}+1}{\sigma\sqrt{1+\frac{m^2}{q_{max}^2}}-1} - 2\log\left\{\frac{q_{max}}{m}\left(1+\sqrt{1+\frac{m^2}{q_{max}^2}}\right)\right\}\right] \tag{A.2}$$

where now, $\sigma = \sqrt{1-4m^2/s}$.

The numerical evaluation of the principal part of eq. (4.36) is also performed as an additional check.

A.2 Relation between the cut-off and the dimensional regularization scale.

In order to obtain the relationship between the cut-off and the renormalization scale μ let us consider, for the sake of simplicity, the case with equal masses (the same result is obtained with different masses but the formulas are more cumbersome). As far as we are going to compare the same function calculated in different ways, let us denote by $G^C(s)$ the $G(s)$ calculated with a cut-off regularization and $G^D(s)$ the one calculated with dimensional regularization. In this latter case we have

$$G^D(s) = \frac{1}{(4\pi)^2}\left[\frac{1}{\hat{\epsilon}} - 2 + \log\, m^2 + \sigma \log\frac{\sigma+1}{\sigma-1}\right] \tag{A.3}$$

where $1/\hat{\epsilon} = 1/\epsilon - \log(4\pi) + \gamma$ with $D = 4 + 2\epsilon$.

The scale μ in $G^D(s)$ appears through the inclusion of the L_i [5] at $\mathcal{O}(p^4)$

$$L_i = L_i^r(\mu) + \Gamma_i \lambda \tag{A.4}$$

where $L_i^r(\mu)$ is the renormalized value of L_i at the μ scale, Γ_i is just a number and

$$\lambda = \frac{1}{32\pi^2}\left[\frac{1}{\hat{\epsilon}} + \log\mu^2 - 1\right] \tag{A.5}$$

The $\log\mu^2$, and its companion $\frac{1}{\hat{\epsilon}} - 1$, are incorporated in $G^D(s)$ so that at the end one has a logarithm of the dimensionless quantity m^2/μ^2. In this way we rewrite $G^D(s)$ as:

$$G^D(s) = \frac{1}{(4\pi)^2}\left[-1 + \log\frac{m^2}{\mu^2} + \sigma\log\frac{\sigma+1}{\sigma-1}\right] \tag{A.6}$$

We expand eq. (A.2) in powers of m^2/q_{max}^2 to compare with the cut-off regularization, as follows

$$\begin{aligned} G^C(s) &= \frac{1}{(4\pi)^2}\left[-2\log\frac{2q_{max}}{m} + \sigma\log\frac{\sigma+1}{\sigma-1} + \mathcal{O}\left(\frac{m^2}{q_{max}^2}\right)\right] \\ &= \frac{1}{(4\pi)^2}\left[-1 + \log\, e + \log\frac{m^2}{4\,q_{max}^2} + \sigma\log\frac{\sigma+1}{\sigma-1} + \mathcal{O}\left(\frac{m^2}{q_{max}^2}\right)\right] \\ &= \frac{1}{(4\pi)^2}\left[-1 + \log\frac{m^2\, e}{4q_{max}^2} + \sigma\log\frac{\sigma+1}{\sigma-1} + \mathcal{O}\left(\frac{m^2}{q_{max}^2}\right)\right] \end{aligned} \tag{A.7}$$

Then comparing eqs. (A.6) and (A.7) one has:

$$\mu = \frac{2\, q_{max}}{\sqrt{e}} \simeq 1.2\, q_{max} \tag{A.8}$$

Hence, to our cut-off $q_{max} \simeq 1$ GeV would correspond a $\mu = 1.2$ GeV dimensional regularization scale. In Table II, we have listed the values of the $\hat{L}_i$ parameters and those of standard χPT scaled to $\mu = 1.2$ GeV. As it is explained in the text, in our fit we have neglected the crossed channel diagrams and we have treated tadpoles differently. The effect of these contributions is effectively reabsorbed in our $\hat{L}_i$ parameters, hence some differences between the $\hat{L}_i$ and L_i parameters should be expected and this is indeed the case as can be seen in Table II. Note that, even if we had used the complete $\mathcal{O}(p^4)$ χPT calculations, these parameters could be different, since they have been obtained from a fit over a much wider range of energies than it is used in χPT and higher order contributions have been included.

Finally, note that the terms $\mathcal{O}(m^2/q^2_{max})$ in eq. (A.7) yield $\mathcal{O}(p^6)$, or higher, contributions and that is why they are not included in $G^D(s)$.

It is also worth stressing that the relationship of eq. (A.8) is independent of the physical process and channel since the function $G(s)$ appears in all them in the same way.

Appendix B

T_2 and T_4^P Amplitudes.

We have used the following formulae in our calculations.

Masses and decay constants

$$\begin{aligned} f_\pi &= f\left[1+\frac{4m_\pi^2}{f^2}(L_5+L_4)+\frac{8m_K^2}{f^2}L_4\right] \\ f_K &= f\left[1+\frac{4m_K^2}{f^2}(L_5+2L_4)+\frac{4m_\pi^2}{f^2}L_4\right] \\ f_\eta &= f\left[1+\frac{4m_\eta^2}{f^2}L_5+\frac{8m_K^2+4m_\pi^2}{f^2}L_4\right] \end{aligned} \tag{B.1}$$

$$\begin{aligned} m_\pi^2 &= \hat{m}_\pi^2\left[1+\frac{8m_\pi^2}{f^2}(2L_6+2\,L_8-L_4-L_5)+\frac{16m_K^2}{f^2}(2L_6-L_4)\right] \\ m_K^2 &= \hat{m}_K^2\left[1+\frac{16m_K^2}{f^2}(2L_6+L_8-L_4-\frac{1}{2}L_5)+\frac{8m_\pi^2}{f^2}(2L_6-L_4)\right] \end{aligned} \tag{B.2}$$

$\pi\pi \to \pi\pi$ scattering

The definite isospin amplitudes $T^{(I)}$ are obtained from just one amplitude T:

$$\begin{aligned} T^{(0)}(s,t,u) &= 3T(s,t,u)+T(t,s,u)+T(u,t,s) \\ T^{(1)}(s,t,u) &= T(t,s,u)-T(u,t,s) \\ T^{(2)}(s,t,u) &= T(t,s,u)+T(u,t,s) \end{aligned} \tag{B.3}$$

where $T = T_2 + T_4$ is given by:

$$\begin{aligned} T_2 &= \frac{m_\pi^2 - s}{f_\pi^2} \\ T_4 &= -\frac{4}{f_\pi^4}\left\{(2L_1+L_3)(s-2m_\pi^2)^2 + L_2\left[(t-2m_\pi^2)^2+(u-2m_\pi^2)^2\right]\right. \\ &\qquad \left. +2(2L_4+L_5)m_\pi^2(s-2m_\pi^2) + 4(2L_6+L_8)m_\pi^4\right\} \end{aligned} \tag{B.4}$$

which have been obtained at tree level from $\mathcal{L}_2$ and $\mathcal{L}_4$, respectively.

$K\pi \to K\pi$ scattering

Using crossing symmetry, we can write the $I = 1/2$ amplitude in terms of that with $I = 3/2$, as

$$T^{(1/2)}(s,t,u) = \frac{3}{2}T^{(3/2)}(u,t,s) - \frac{1}{2}T^{(3/2)}(s,t,u) \tag{B.5}$$

where

$$\begin{aligned} T_2^{(3/2)} &= \frac{s-(m_\pi^2+m_K^2)}{2f_\pi f_K} \\ T_4^{(3/2)} &= -\frac{2}{f_\pi^2 f_K^2}\left\{(4L_1+L_3)(t-2m_\pi^2)(t-2m_K^2) + 2L_2(m_\pi^2+m_K^2-s)^2\right. \\ &+ (2L_2+L_3)(m_\pi^2+m_K^2-u)^2 + 4L_4\left[(m_\pi^2+m_K^2)t - 4m_\pi^2 m_K^2\right] \\ &+ \left. L_5\left[(m_\pi^2+m_K^2)(m_\pi^2+m_K^2-s) - 4m_\pi^2m_K^2\right] + 8m_\pi^2m_K^2(2L_6+L_8)\right\} \end{aligned} \tag{B.6}$$

once more, they have been obtained, respectively, from $\mathcal{L}_2$ and $\mathcal{L}_4$ at tree level.

$K\overline{K} \to K\overline{K}$ scattering

The definite isospin amplitudes can be written just in terms of two:

$$\begin{aligned} T^{(0)}(s,t,u) &= T^{+-+-}(s,t,u) + T^{\bar{0}0+-}(s,t,u) \\ T^{(1)}(s,t,u) &= T^{+-+-}(s,t,u) - T^{\bar{0}0+-}(s,t,u) \end{aligned} \tag{B.7}$$

where T^{+-+-} is the amplitude for $K^+K^- \to K^+K^-$, whose respective $\mathcal{O}(p^2)$ and $\mathcal{O}(p^4)$ contributions are

$$\begin{aligned} T_2^{+-+-}(s,t,u) &= \frac{u-2m_K^2}{f_K^2} \\ T_4^{+-+-}(s,t,u) &= -\frac{4}{f_K^4}\left\{2L_2(u-2m_K^2)^2 + (2L_1+L_2+L_3)\left[(s-2m_K^2)^2+(t-2m_K^2)^2\right]\right. \\ &\qquad \left. -2u\,m_K^2(2L_4+L_5) + 8m_K^4(2L_6+L_8)\right\} \end{aligned} \tag{B.8}$$

whereas $T^{\bar{0}0+-}$ is the amplitude for $\overline{K}^0 K^0 \to K^+ K^-$, which is given by

$$\begin{aligned} T_2^{\bar{0}0+-}(s,t,u) &= \frac{u-2m_K^2}{2f_K^2} \qquad \text{(B.9)} \\ T_4^{\bar{0}0+-}(s,t,u) &= -\frac{2}{f_K^4}\left\{(4L_1+L_3)(s-2m_K^2)^2+(2L_2+L_3)(t-2m_K^2)^2+2L_2(u-2m_K^2)^2\right. \\ &\quad \left. -2um_K^2L_5-8L_4m_K^2(2m_K^2-s)+8m_K^4(2L_6+L_8)\right\} \end{aligned}$$

$\pi\pi \to K\overline{K}$ scattering

Again, we can use crossing symmetry to obtain, from $K\pi \to K\pi$, the definite isospin amplitudes T_I of this process:

$$\begin{aligned} T^{(0)} &= \sqrt{\frac{3}{2}}\left(T^{(3/2)}(u,s,t)+T^{(3/2)}(t,s,u)\right) \qquad \text{(B.10)} \\ T^{(1)} &= T^{(3/2)}(u,s,t)-T^{(3/2)}(t,s,u) \end{aligned}$$

$K\eta \to K\eta$ scattering

This process is pure $I = 1/2$. We obtain the following contributions to the amplitude:

$$T_2(s,t,u) = \frac{6m_\eta^2+2m_\pi^2-9t}{12f_\eta f_K} \qquad \text{(B.11)}$$

$$\begin{aligned} T_4(s,t,u) &= -\frac{1}{3f_K^2f_\eta^2}\{2(t-2m_K^2)(t-2m_\eta^2)(12L_1+5L_3)+[(u-m_\eta^2-m_K^2)^2 \qquad \text{(B.12)} \\ &\quad +(s-m_\eta^2-m_K^2)^2](12L_2+L_3)+2(t-2m_K^2)[11m_K^2(2L_4+L_5) \\ &\quad -m_\pi^2(L_4+3L_5)]+4m_K^4\left[3(2L_4+L_5)+32(L_6+L_7+L_8)\right] \\ &\quad +2(t-2m_\eta^2)[9m_K^2(2L_4+L_5)+m_\pi^2(3L_4-L_5)]+4m_\pi^4(16L_7+8L_8-L_5) \\ &\quad +6L_5m_\eta^4-t[m_K^2(24L_4+7L_5)+2m_\pi^2(6L_4-L_5)+9L_5m_\eta^2] \\ &\quad +6m_\eta^2m_K^2(4L_4+L_5)+2m_\eta^2m_\pi^2(6L_4+L_5) \\ &\quad +2\ m_K^2m_\pi^2\left[6L_4+L_5-8(2L_6+7L_8+12L_7)\right]\} \end{aligned}$$

$K\eta \to K\pi$ scattering

The $I = 1/2$ amplitude can be obtained as follows:

$$T^{(1/2)}(s,t,u) = \sqrt{\frac{3}{2}}T_{\overline{K}^0\eta\to K^-\pi^+}(s,t,u) \qquad \text{(B.13)}$$

The $\mathcal{O}(p^2)$ and $\mathcal{O}(p^4)$ contributions to $\overline{K}^0\eta \to K^-\pi^+$ are

$$
\begin{aligned}
T_2(s,t,u) &= \frac{\sqrt{6}\left[8m_K^2+3m_\eta^2+m_\pi^2-9t\right]}{36f_Kf_\eta} && \text{(B.14)}\\
T_4(s,t,u) &= -\frac{\sqrt{2/3}}{3f_K^2f_\eta^2}\left\{3L_3\left[2(t-m_\pi^2-m_\eta^2)(t-2m_K^2)-(s-m_K^2-m_\pi^2)(s-m_K^2-m_\eta^2)\right.\right.\\
&- \left.(u-m_K^2-m_\pi^2)(u-m_K^2-m_\eta^2)\right]+L_5\left[(t+m_\pi^2-m_\eta^2)(7m_K^2-5m_\pi^2)\right.\\
&+ \left.4m_K^2(3t-3m_\pi^2-m_\eta^2)+2(t-2m_K^2)(m_K^2+m_\pi^2)+4(m_\pi^4-m_K^4)\right]\\
&+ \left.+16(2L_7+L_8)(m_\pi^4-2m_K^4+m_K^2m_\pi^2)\right\}
\end{aligned}
$$

$\eta\pi \to \eta\pi$

This channel is pure $I=1$ isospin. The amplitude is given by

$$
\begin{aligned}
T_2(s,t,u) &= \frac{-m_\pi^2}{3f_\eta f_\pi} && \text{(B.15)}\\
T_4(s,t,u) &= -\frac{4}{3f_K^2f_\eta^2}\{(t-2m_\pi^2)(t-2m_\eta^2)(6L_1+L_3)+4t\,L_4(m_\pi^2+2m_K^2)\\
&+ (3L_2+L_3)\left[(s-m_\pi^2-m_\eta^2)^2+(u-m_\pi^2-m_\eta^2)^2\right]\\
&+ m_\pi^4(4L_4-L_5-8L_6+32L_7+12L_8)-16m_K^2m_\pi^2(L_4-2L_6+2L_7)\\
&- 3m_\pi^2m_\eta^2(4L_4+L_5)\} && \text{(B.16)}
\end{aligned}
$$

Appendix C

N/D in coupled channels.

In this appendix we make use of a matrix formalism to deal with several coupled channels. In analogy with the elastic case, eq. (5.7), let us define the matrix T'_L as

$$\mathrm{T}'_L(s) = p^{-L}\mathrm{T}_L(s)p^{-L} \tag{C.1}$$

with p a diagonal matrix which elements are $p_{ij} = p_i\delta_{ij}$ where p_i is the modulus of the CM momentum of the channel i, $p_i = \dfrac{\lambda^{1/2}(s, m_{1i}^2, m_{2i}^2)}{2\sqrt{s}}$, with m_{1i} and m_{2i} the masses of the two mesons in channel i.

From the beginning we neglect the unphysical cuts. As a consequence $\mathrm{T}_L(s)_{ij}$ will be proportional to $p_i^L p_j^L$. This makes that $\mathrm{T}_L(s)_{ij}$, apart from the right hand cut coming from unitarity (above the thresholds for channels i and j, s_{th}^i and s_{th}^j respectively), will have another cut for odd L between s_{th}^i and s_{th}^j due to the square roots present in p_i and p_j. In this way, T'_L will be free of this cut and will have only the right hand cut coming from unitarity. Thus it will satisfy

$$\mathrm{Im}\ \mathrm{T}'^{-1}_L(s) = -p^L\rho(s)p^L = -\rho(s)p^{2L} \tag{C.2}$$

where $\rho(s)$ is a diagonal matrix defined by

$$\rho(s) = -\frac{p}{8\pi\sqrt{s}}\theta(s) \tag{C.3}$$

with $\theta(s)$ another diagonal matrix such that $\theta(s)_{ii}$=1 above the threshold of channel i and 0 below it.

We write T'_L as a quotient of two matrices, N_L and D_L making use of the coupled channel version of the N/D method [94]

$$\mathrm{T}'_L = \mathrm{D}'^{-1}_L\mathrm{N}'_L \tag{C.4}$$

We can always take N'_L free of poles and also containing all the zeros of T'_L. In such a case N'_L will be just a matrix of polynomials, we then write

$$\mathrm{N}'_L = \mathrm{Q}_{n-L-1} \tag{C.5}$$

with Q_{n-L-1} a matrix of polynomials of maximum degree $n-L-1$.

In this way, from eq. (C.2) and (C.4) one has

$$\mathrm{Im}\ \mathrm{D}'_L(s) = -\mathrm{N}'_L(s)\rho(s)p^{2L} \tag{C.6}$$

and making a dispersion relation for D'_L one has

$$\mathrm{D}'_L(s) = -\frac{(s-s_0)^n}{\pi}\int_0^\infty ds' \frac{\mathrm{Q}_{n-L-1}(s')\rho(s')p^{2L}(s')}{(s'-s)(s'-s_0)^n} + \mathrm{P}_{n-1} \tag{C.7}$$

with P_{n-1} a matrix of polynomials of maximum degree $n-1$.

Because N'_L is just a matrix of polynomials, it can be reabsorbed in D'_L to give rise to a new $\widetilde{\mathrm{D}}'_L$ which will fulfill eq. (C.6) but with $\widetilde{\mathrm{N}}'_L = 1$. In this way

$$\begin{aligned}
\mathrm{T}'_L &= \widetilde{\mathrm{D}}'^{-1}_L \\
\widetilde{\mathrm{N}}'_L &= 1 \\
\widetilde{\mathrm{D}}'_L &= -\frac{(s-s_0)^L+1}{\pi}\int_0^\infty \frac{\rho(s')p^{2L}(s')}{(s'-s)(s'-s_0)^{L+1}} + \mathrm{R}(s)
\end{aligned} \tag{C.8}$$

with $\mathrm{R}(s)$ a matrix of rational functions whose poles will contain the zeros of T'_L. This fact is in clear analogy with the role played by the CDD poles included in **Section 5.1** for the elastic case.

Bibliography

[1] H. Fritzsch and M. Gell-Mann, Proc. XVI Int. Conf. on High Energy Physics, eds. J. D. Jackson and A. Roberts, Fermilab, 1972, Vol. 2, 135; H. Fritzsch, M. Gell-Mann and H. Leutwyler, Phys. Lett. **B47** (1973) 365.

[2] G. F. Chew, High Energy Physics, Les Houches, 1965, eds. C. de Witt and M. Jacob (Gordon and Breach), p. 189.

[3] G. t'Hooft, in Recent Developments in Gauge Theories. Eds. G. t'Hooft et al. (Plenum, New York), 1980; Y. Frishman, A. Schwimmer, T. Banks and S. Yankielowicz, Nucl. Phys. **B177** (1981) 157; S. Coleman and B. Grossman, Nucl. Phys. **B203** (1982) 205; J. Preskill and S. Weinberg, Phys. Rev. **D24** (1981) 1059.

[4] S. Weinberg, Physica A **96** (1979) 327.

[5] J. Gasser and H. Leutwyler, Ann. Phys. NY **158** (1984) 142; J. Gasser and H. Leutwyler, Nucl. Phys. **B250** (1985) 465, 517, 539.

[6] A. Manohar and H. Georgi, Nucl. Phys. **B234** (1984) 189.

[7] G. Ecker, J. Gasser, A. Pich and E. de Rafael, Nucl. Phys. **B321** (1989) 311.

[8] S. Peris, M. Perrottet and E. de Rafael, J. High Energy Physics **9805** (1998) 11.

[9] G. F. Chew and S. Mandelstam, Phys. Rev. **119** (1960) 467.

[10] R. Omnès and M. Froissart, Mandelstam Theory and Regge Poles, W. A. Benjamin, Inc., 1963.

[11] A. D. Martin and T. D. Spearman, Elementary Particle Theory, John Willey, 1970.

[12] G. F. Chew, S-Matrix Theory of Strong Interactions, W. A. Benjamin, 1961.

[13] S. Mandelstam, Phys. Rev. **112** (1958) 1344.

[14] R. E. Cutkosky, Rev. of Mod. Phys. **33** (1961) 448.

[15] A. Pich, Rep. Prog. Phys. **58** (1995) 563.

[16] J. Goldstone, Nuovo Cimento **19** (1961) 154.

[17] M. Gell-Mann, Phys. Rev. **125** (1962) 1067.

[18] S. Okubo, Prog. Theor. Phys. **27** (1962) 949.

[19] C. Caso et al., The European Physical Journal **C3** (1998) 1.

[20] N. H. Fuchs, H. Sazdjian and J. Stern, Phys. Lett. **B269** (1991) 183; J. Stern, H. Sazdjian and N. H. Fucks, Phys. Rev. **D47** (1993) 3814; M. Knecht, B. Moussallam, J. Stern and N. H. Fuchs, Nucl. Phys. **B457** (1995) 513.

[21] J. Wess and B. Zumino, Phys. Rev. **163** (1967) 1727; J. Wess and B. Zumino, Phys. Lett. **B37** (1971) 95.

[22] E. Witten, Ann. Phys. NY **128** (1980) 363; E. Witten, Nucl. Phys. **B223** (1983) 422.

[23] S. Weinberg, Phys. Rev. Lett. **18** (1967) 507.

[24] G. Ecker, J. Gasser, H. Leutwyler, A. Pich and E. de Rafael, Phys. Lett. **B223** (1989) 425.

[25] T. N. Truong, Phys. Rev. Lett. **61** (1998) 2526; *ibid.* **67** (1991) 2260; A. Dobado, M. J. Herrero and T. N. Truong, Phys. Lett. **B235** (1990) 134; A. Dobado and J. R. Peláez, Phys. Rev. **D47** (1993) 4883; *ibid.* Phys. Rev. **D56** (1997) 3057.

[26] J. A. Oller, E. Oset and J. R. Peláez, Phys. Rev. Lett. **80** (1998) 3452.

[27] J. A. Oller and E. Oset, to be published in Phys. Rev. **D**, hep-ph/9809337.

[28] S. M. Flatté, Phys. Lett. **B63** (1976) 224.

[29] K. Kawarabayashi and M. Suzuki, Phys. Rev. Lett. **16** (1996) 255; Rizuddin and Fayyazuddin, Phys. Rev. **147** (1966) 1071.

[30] S. Weinberg, Phys. Rev. **137** (1965) 672.

[31] N. A. Tornqvist, Phys. Rev. Lett. **49** (1982) 624; M. Roos and N. A. Tornqvist, Phys. Rev. Lett. **76** (1996) 1575.

[32] M. Boglione and M. R. Pennington, Phys. Rev. Lett. **79** (1997) 1998.

[33] T. Applequist and C. Bernard, Phys. Rev. **D22** (1980) 200; A. C. Longhitano, Nucl. Phys. **B188** (1981) 118.

[34] H. Leutwyler, Phys. Rev. **D49** (1994) 3033; H. Leutwyler, Helv. Phys. Acta **70** (1997) 275; S. C. Zhang, Science **275** (1997) 1089; C. P. Burgess and A. Lutken, Phys. Rev. **B57** (1998) 8642.

[35] J. V. Steele, H. Yamagishi and I. Zahed, Nucl. Phys. **A615** (1997) 305; M. R. Pennington and J. Portolés, Phys. Lett. **B344** (1995) 399.

[36] A. Dobado, M. J. Herrero and T. N. Truong, Phys. Lett. **B235** (1990) 129; A. Dobado, M. J. Herrero and J. Terrón, Z. Phys. **C50** (1991) 205; *ibid.* **C50** (1991) 465; J. R. Peláez, Phys. Rev. **D55** (1997) 4193.

[37] J. Weinstein and N. Isgur, Phys. Rev. Lett. **48** (1982) 659; J. Weinstein and N. Isgur, Phys. Rev. **D27** (1983) 588; *ibid.* Phys. Rev. **D41** (1990) 2236.

[38] G. Jansen, B. C. Pearce, K. Holinde and J. Speth, Phys. Rev. **D52** (1995) 2690.

[39] J. L. Basdevant, Fortschr. Phys. **20** (1972) 283.

[40] M. Boglione and M. R. Pennigton, Z. Phys. **C75** (1997) 113; T. Hannah, Phys. Rev. **D59** (1999) 57502.

[41] L. V. Dung and T. N. Truong, hep-ph/9607378.

[42] F. Guerrero and J. A. Oller, Nucl. Phys. **B57** (1999) 459.

[43] V. Bernard, N. Kaiser and U. G. Meissner, Nucl. Phys. **B357** (1991) 129.

[44] G. Passarino and M. Veltman, Nucl. Phys. **B160** (1979) 151.

[45] D. B. Kaplan and A. V. Manohar, Phys. Rev. Lett. **56** (1986) 2004.

[46] R. Kaminski, L. Lesniak and K. Rybicki, Z. Phys. **C74** (1997) 79.

[47] B. Hyams et al., Nucl. Phys. **B64** (1973) 134.

[48] P. Estabrooks et al., AIP Conf. Proc. 13 (1973) 37.

[49] G. Grayer et al., Proc. 3rd Philadelphia Conf. on Experimental Meson Spectroscopy, Philadelphia, 1972 (AIP, NY, 1972) pag. 5.

[50] S. D. Protopopescu and M. Alson-Granjost, Phys. Rev. **D7** (1973) 1279.

[51] C. D. Frogatt and J. L. Petersen, Nucl. Phys. **B129** (1977) 113.

[52] D. Cohen et al., Phys. Rev. **D22** (1980) 2595.

[53] A. D. Martin and E. N. Ozmuth, Nucl. Phys. **B158** (1979) 520.

[54] W. Ochs, University of Munich thesis, 1974.

[55] L. Rosselet et al., Phys. Rev. **D15** (1977) 574.

[56] A. Schenk, Nucl. Phys. **B363** (1991) 97.

[57] J. A. Oller, E. Oset and J. R. Peláez, Phys. Rev. **D59** (1999) 74001.

[58] J. A. Oller and E. Oset, Nucl. Phys. **A620** (1997) 438; *erratum* hep-ph/9710554.

[59] J. Charap, Phys. Rev. **D2**(1970) 1115; I. S. Gerstein, R. Jackiw, B. W. Lee and S. Weinberg, Phys. Rev. **D3** (1971) 2486, J. Honerkamp, Nucl. Phys. **B36** (1972) 130.

[60] L. Tararu, Phys. Rev. **D12** (1975) 3351.

[61] G. Grayer et al., in Experimental Meson Spectroscopy, edited by A. H. Rosenfeld and K. W. Lai, AIP Conf. Proc. 8 (AIP, New York, 1972) p. 117.

[62] G. Grayer etl al., Paper No.768 Contributed to the 16th Int. Conf. on High Energy Physics, Batavia, 1972.

[63] G. Grayer et al., Nucl. Phys. **B75** (1974) 189.

[64] W. Manner, Contribution to the 4th Int. Conf. on Experimental Meson Spectroscopy, Boston, Massachusetts, USA, April 1974 and CERN preprint.

[65] S. J. Lindenbaum and R. S. Longacre, Phys. Lett. **B274** (1992) 492.

[66] P. Estabrooks and A. D. Martin, Nucl. Phys. **B79** (1974) 301.

[67] Amsterdam, CERN, Nijmegen-Oxford Collaboration, J. B. Gay et al., Phys. Lett. **B63** (1976) 220.

[68] R. Mercer et al., Nucl. Phys. **B32** (1971) 381.

[69] H. H. Bingham et al., Nucl. Phys. **B41** (1972) 1.

[70] S. L. Baker et al., Nucl. Phys. **B99** (1975) 211.

[71] P. Estabrooks et al., Nucl. Phys. **B133** (1978) 490.

[72] D. Aston et al., Nucl. Phys. **B296** (1988) 493.

[73] S. Ishida et al, Prog. Theor. Phys. **98** (1997) 621.

[74] R. L. Jaffe, Phys. Rev. **D15** (1977) 267; *ibid*. **D15** (1977) 281.

[75] D. Linglin et al., Nucl. Phys. **B57** (1973) 64.

[76] J. A. Oller and E. Oset, Nucl. Phys. **A629** (1997) 739.

[77] E. Oset and A. Ramos, Nucl. Phys. **A635** (1998) 99.

[78] P. Schuck, W. Norenberg and G. Chanfray, Z. Phys. **A330** (1988) 119; H. C. Chiang, E. Oset and M. J. Vicente, Nucl. Phys. **A644** (1998) 77.

[79] V. Bernard, N. Kaiser and U. G. Meissner, Nucl. Phys. **B364** (1991) 283.

[80] K. L. Au, D. Morgan and M. R. Pennington, Phys. Rev. **D35** (1987) 1633.

[81] N. N. Achasov and G. N. Shestakov, Phys. Rev. **D49** (1994) 5779.

[82] F. Guerrero and A. Pich, Phys. Lett. **B412** (1997) 382.

[83] For general revies about the issue: L. Montanet, Rep. Prog. Phys. **46** (1983) 337; F. Close, Rep. Prog. Phys. **51** (1988) 833; M. R. Pennington, Nucl. Phys. **B21** (Proc. Suppl.) (1991) 37.

[84] D. Morgan, Phys. Lett. **B51** (1974) 71.

[85] N. N. Achasov, S. A. Debyanin and G. N. Shestakov, Z. Phys. **C22** (1984) 53; N. N. Achasov, S. A. Devyanin and G. N. Shestakov, Phys. Lett. **B96** (1980) 168; N. N. Achasov, S. A. Devyanin and G. N. Shestakov, Phys. Scripta **27** (1983) 330.

[86] R. L. Jaffe, Phys. Lett. **41** (1975) 267; D. Robson, Nucl. Phys. **B130** (1977) 328.

[87] T. Barnes, in Proceedings of the Fourth Workshop on Polarized Targets Materials and Techniques, Bad Honned, Germany, 1984, edited by W. Meyer (Bonn Univeristy, Bonn, 1984); J.F. Donoghue, in Hadron Spectroscopy-1985, Proceedings of the International Conference, College Park, Maryland, edited by S. Oneda, AIP Conf. Proc. No. 132 (AIP, New York, 1985), p. 460; also, Close [83].

[88] D. Morgan and M.R. Pennington, Phys. Rev. **D48** (1993) 1185; D. Morgan and M.R. Pennignton, Phys. Lett. **B258** (1991) 444; D. Morgan and M.R. Pennington, Phys. Rev. **D48** (1993) 1185, 5422.

[89] B. S. Zou and D. V. Bugg, Phys. Rev. **D48** (1993) R3948.

[90] E. Witten, Nucl. Phys. **B160** (1979) 57.

[91] L. Castillejo, R. H. Dalitz and F. J. Dyson, Phys. Rev. **101** (1956) 453.

[92] G. F. Chew and S. C. Frautschi, Phys. Rev. **124** (1961) 264.

[93] M. S. Chanowitz, M. Golden and H. Georgi, Phys. Rev. **D36** (1987) 1490.

[94] J. D. Bjorken, Phys. Rev. Lett. **4** (1960) 473.

[95] N. Kaiser, P. B. Siegel and W. Weise, Nucl. Phys. **A594** (1995) 325; N. Kaiser, T. Waas and W. Weise, Nucl. Phys. **A612** (1997) 297.

[96] J. Nieves and E. Ruiz Arriola, nucl-th/9807035. To be published in Phys. Lett. **B**.

[97] H. Leutwyler, Nucl. Phys. **B7A** (Proc. Suppl.) (1989) 42.

[98] H. Leutwyler and M. Roos, Z. Phys. **C25** (1984) 91.

[99] T. A. Armstrong et al., Z. Phys. **C52** (1991) 389.

[100] A. Etkin et al., Phys. Rev. **D28** (1982) 1786.

[101] W. Wetzel et al., Nucl. Phys. **B115** (1976) 208; V. A. Polychronakos et al., Phys. Rev. **D19** (1979) 1317; G. Costa et al., Nucl. Phys. **B175** (1980) 402.

[102] A. A. Andrianov, D. Espriu and R. Tarrach, Nucl. Phys. **B533** (1998) 429.

[103] M. Jamin, J. A. Oller and A. Pich, in preparation.

[104] V. Elias, A. H. Fariborz, Fang Shi and T. G. Steele, Nucl. Phys. **A633** (1998) 279.

[105] S. L. Adler, Phys. Rev. **177** (1969) 2426.

[106] J. S. Bell and R. Jackiw, Nuovo Cimento **A60** (1969) 47.

[107] S. L. Adler and W. A. Bardeen, Phys. Rev. **182** (1969) 1517.

[108] P. Di Vecchia and G. Veneziano, Nucl. Phys. **B171** (1980) 253; E. Witten, Ann. Phys. NY **128** (1980) 363; C. Rosenzweig, J. Schechter and G. Trahern, Phys. Rev. **D21** (1980) 3388.

[109] P. Herrera-Siklódy, J. I. Latorre, P. Pascual and J. Taron, Nucl. Phys. **B497** (1997) 345; Phys. Lett. **B419** (1998) 326.

[110] H. Leutwyler, Phys. Lett. **B374** (1996) 163. Nucl. Phys. **B497** (1997) 345; Phys. Lett. **B419** (1998) 326.

[111] See the first of the Nucl. Phys. **B** papers in [5].

[112] See the second of the Nucl. Phys. **B** papers in [5].

[113] Y. Cho et al., Phys. Lett. **B32** (1970) 409.

[114] A. M. Bakker et al., Nucl. Phys. **B24** (1970) 211.

[115] B. Jongejans et al., Nucl. Phys. **B67** (1973) 381.

[116] K. M. Watson, Phys. Rev. **95** (1955) 228.

[117] N. I. Muskhelishivili, Singular Integral Equations (Noordhoof, Groningen, 1953).

[118] R. Omnès, Nuovo Cimento **8** (1958) 316.

[119] L. M. Barkov, Nucl. Phys. **B256** (1985) 365.

[120] F. Guerrero, Phys. Rev. **D57** (1998) 4136.

[121] See the Phys. Rev. Lett. papers by Truong in [25].

[122] L. Beldjoudi and T. N. Truong, hep-ph/9403348.

[123] T. Hannah, Phys. Rev. **D55** (1997) 5613.

[124] M. R. Pennington, The Second DAPHNE Physics Handbook (1995) Vol. II, pag. 531; M. Feindt and J. Harjes, Nucl. Phys. **B21** (Proc. Suppl.) (1991) 61.

[125] P. Ko, Phys. Rev. **D41** (1990) 1531; J. F. Donoghue and B. R. Holstein, Phys. Rev. **D48** (1993) 137; J. F. Donoghue, B. R. Holstein and D. Wyler, Phys. Rev. **D47** (1993) 2089.

[126] J. Bijnens and F. Cornet, Nucl. Phys. **B296** (1988) 557.

[127] J. F. Donoghue, B. K. Holstein and Y. C. Lin, Phys. Rev. **D37** (1988) 2423.

[128] D. Morgan and M. R. Pennington, Z. Phys. **C37** (1988) 431.

[129] H. Albrecht et al., Z. Phys. **C48** (1989) 183.

[130] M. Boglione and M. R. Pennington, hep-ph/9812258.

[131] I. Dunietz, J. Hauser and J. L. Rosner, Phys. Rev. **D35** (1987) 2166.

[132] J. Lucio and J. Pestiau, Phys. Rev. **D42** (1990) 3253; *ibid.* **D43** (1991) 2447.

[133] S. Nussinov and T. N. Truong, Phys. Rev. Lett. **63** (1989) 1349.

[134] S. Nussinov and T. N. Truong, Phys. Rev. Lett. **63** (1989) 2003.

[135] N. N. Achasov and V. N. Ivachenko, Nucl. Phys. **B315** (1989) 465.

[136] N. Paver and Riazuddin, Phys. Lett. **B246** (1990) 240.

[137] F. E.Close, N. Isgur, S. Kumano, Nucl. Phys. **B389** (1993) 513.

[138] J. A. Oller, Phys. Lett. **B426** (1998) 7.

[139] A. Bramon, A. Grau and G. Pancheri, Phys. Lett. **B289** (1992) 97.

[140] E. Marco, S. Hirenzaki, E. Oset and H. Toki, hep-ph/9903217.

[141] M. N. Achasov et al., Phys. Lett. **B440** (1998) 442.